

Performance of Structures and Equipment  
in Base-Isolated Medical Facilities  
Subjected to Severe Earthquake Motions

2011

Sachi FURUKAWA





# TABLE OF CONTENTS

## CHAPTER 1 INTRODUCTION

1.1	Background	1-1
1.2	Objective	1-2
1.3	Organization	1-3
	REFERENCES	
	LIST OF PUBLICATIONS	

## CHAPTER 2 REVIEW OF PREVIOUS RESEARCH

2.1	Introduction	2-1
2.2	Isolation systems in Japan	2-1
	2.2.1 Design practice	2-1
	2.2.2 Construction statistics	2-2
2.3	Concerned ground motions for base-isolated buildings	2-5
	2.3.1 Long-period and long-duration ground motion	2-5
	2.3.2 Vertical ground motion	2-6
2.4	Acceleration records of base-isolated buildings for past earthquake	2-7
	2.4.1 Horizontal response	2-7
	2.4.2 Vertical response	2-9
2.5	Vertical performance of base-isolated buildings	2-9
	2.5.1 Vertical response characteristics of base-isolated buildings	2-10
	2.5.2 Design practice of base-isolated buildings for vertical response	2-15
2.6	Damage reports of hospitals for past earthquakes	2-15
2.7	Summary and conclusions of Chapter 2	2-17
	REFERENCES	

## CHAPTER 3 FULL-SCALE SHAKING TABLE TEST OF BASE-ISOLATED MEDICAL FACILITY

3.1	Introduction	3-1
3.2	Design and fabrication of test specimen	3-2
3.3	Design of base isolation devises	3-4
3.4	Arrangement of furniture and medical equipment	3-6
3.5	Measurement	3-9
3.6	Ground motions	3-10



3.7	Loading program	3-13
3.8	Overview of shaking table tests	3-15
3.8.1	Natural frequency and damping ratio	3-15
3.8.2	Maximum floor responses	3-17

REFERENCES

**CHAPTER 4 STRUCTURAL RESPONSES OF THE BASE-ISOLATED SYSTEM FOR HORIZONTAL MOTIONS**

4.1	Introduction	4-1
4.2	Performance of base isolation	4-1
4.3	Performance of base-isolated system	4-3
4.3.1	Near-fault ground motion	4-3
4.3.2	Long-period and long-duration ground motion	4-5
4.4	Types of isolators	4-6
4.5	Effect of stiffness degradation of superstructure	4-9
4.6	Summary and conclusions of Chapter 4	4-11

REFERENCES

**CHAPTER 5 STRUCTURAL RESPONSES OF THE BASE-ISOLATED SYSTEM FOR VERTICAL MOTIONS**

5.1	Introduction	5-1
5.2	Input ground motions	5-2
5.3	Vertical floor acceleration responses of base-isolated system	5-3
5.4	Dynamic response characteristics of base-isolated system	5-5
5.4.1	Response amplification	5-5
5.4.2	Natural frequency and damping ratio	5-8
5.4.3	Mode shape	5-9
5.5	Analytical study of vertical modes	5-12
5.5.1	Modeling description	5-12
5.5.2	Estimation of vertical dynamic configurations	5-16
5.5.3	Identifications of modes and damping ratio	5-16
5.6	Comparison of vertical responses between the base-isolated and fixed-base systems against ground motion	5-19
5.7	Shift of vertical dynamic response characteristics for larger response amplitude	5-21
5.7.1	Vertical acceleration response amplifications	5-21
5.7.2	Shift of vertical natural frequencies and damping ratios	5-22

5.8	Damping ratio in the vertical direction	5-23
5.9	Axial force sustained by base isolators	5-24
5.10	Summary and conclusions of Chapter 5	5-26

REFERENCES

**CHAPTER 6 MEDICAL EQUIPMENT BEHAVIOR FOR HORIZONTAL MOTIONS**

6.1	Introduction	6-1
6.2	Contents installed in the facility	6-1
6.3	Performance of medical equipment for horizontal ground motions	6-3
6.3.1	Near-fault ground motions	6-5
6.3.2	Long-period and long-duration ground motions	6-6
6.4	Effect of measures	6-12
6.4.1	Effect of measures	6-12
6.4.2	Effect of locking casters	6-13
6.5	Summary and conclusions of Chapter 6	6-15

REFERENCES

**CHAPTER 7 MEDICAL EQUIPMENT BEHAVIOR FOR VERTICAL MOTIONS**

7.1	Introduction	7-1
7.2	Notable vertical response of equipment	7-1
7.2.1	Suspended item	7-3
7.2.2	Equipment with eccentricity	7-4
7.2.3	Operating table	7-5
7.2.4	Patient bed	7-7
7.2.5	Incubator	7-9
7.2.6	Others	7-11
7.3	Supplemental shaking table test of equipment	7-11
7.3.1	Dynamic properties of equipment	7-12
7.3.2	Operating table and patient bed	7-13
7.4	Summary and conclusions of Chapter 7	7-20

REFERENCES

## **CHAPTER 8 VERTICAL DYNAMIC RESPONSE CHARACTERISTICS OF BASE-ISOLATED BUILDINGS**

8.1	Introduction	8-1
8.2	Development of generic lump mass model for vertical vibration examination of base-isolated buildings	8-2
8.2.1	Three representative modes of base-isolated buildings	8-3
8.2.2	3DOF lump mass model	8-4
8.3	Supporting factors for 3DOF model	8-6
8.3.1	Supporting factor for column	8-6
8.3.2	Supporting factors for slab	8-7
8.4	Verification of 3DOF model	8-11
8.4.1	Model description	8-12
8.4.2	Verification of 3DOF model	8-13
8.5	First vertical floor response amplification of base-isolated buildings	8-16
8.5.1	Model description	8-16
8.5.2	Vertical floor response amplification of base-isolated buildings	8-17
8.5.3	First mode contribution	8-25
8.6	Summary and conclusions of Chapter 8	8-28

### **REFERENCES**

## **CHAPTER 9 SUMMARY AND CONCLUSIONS**

### **ACKNOWLEDGMENT**

# CHAPTER 1

## INTRODUCTION

### 1.1 Background

Japan is one of the countries that have applied isolation system to buildings most extensively. Since 1983 when the first base-isolated building was completed, the number of base-isolated buildings has increased, especially after the Hyogo-ken Nanbu earthquake (or Kobe earthquake) in 1995, and has reached around 2,500 in the last three decades [1-1]. This rapid increase is conspicuous when it is compared with the number of applications in the U.S., which is still only about 100 [1-2]. The large number of applications in Japan is primarily because of the following reasons: (1) the approval process of the base-isolated buildings in Japan is straightforward, compared with that in the U.S.; (2) large construction companies in Japan make efforts to develop and market this new technology; (3) Japanese high seismicity encourages people to invest more money on their assets to ensure not only their structural safety but also high-level performance to the extent that the contents of buildings are also protected and service can be continued during earthquakes without any intermission [1-2, 3]. The significance of business continuity was re-recognized after the 1995 Kobe earthquake, in the aftermath of which the service of some important facilities was suspended, causing serious delay in controlling the disorders. This experience accentuated the application of the isolation system since it has been considered as one of the most advanced technologies for the mitigation of the acceleration-related damages. The well-developed design approval process also helps its smooth applications [1-2, 4]. Recently, about half of the isolation applications are to residential apartments in Japan. This statistic shows how much this system has prevailed in this country.

The medical facility is also one of the facilities that prefer to adopt the isolation system. Currently, about 12 % of the isolated buildings in Japan are medical facilities. The number is equivalent to 300 buildings [1-1]. This is because the medical facility is one of the most important facilities that are required to keep providing service on an emergency period after disaster. Facilities with conventional structural systems suffered in the past earthquakes, not only because of the structural damages but also because of the interior and infrastructure damages, resulted in delay or suspension of some of their services. In the 1995 Kobe earthquake, hospitals constructed after the implementation of the Standard for Earthquake Resistant Design (1980) were verified at least

for structural safety, which was the minimum requirement of Standard Law [1-5 to 7]. However, their medical performance was significantly damaged mostly due to (1) the damage to infrastructure (water, gas, electricity and sewerage system), (2) interruption of communication service, (3) lack of staff, and (4) interior damage of the facility [1-9]. The base isolation system has been adopted by newly-constructed hospitals with high expectation that will mitigate (4) interior damages of the facility, and about 300 hospitals have been base-isolated by 2009 in Japan.

The technology of the base isolation system has matured, but not all concerns have been resolved: its actual performance has not been fully verified for very large earthquakes, and the performance against some types of ground motions, such as the long-period pulse, long-period and long-duration ground motion, and the vertical ground motion occurred from near-fault earthquakes, is not well understood. The long-period and long-duration ground motion is newly recognized in the last decade as the type of ground motion that may cause problems for high-rise and isolated buildings [1-10]. Since Japanese major metropolitan areas, where most high-rise and isolated buildings are located, has a high likelihood of encountering this type of ground motion in the next few decades [1-11, 12], verification of the performance of current buildings is an urgent task to determine whether upgrading measures are required or not. Research on high-rise buildings for long-period and long-duration ground motions can be found elsewhere [1-13 to 17]. Long-lasting and resonated vibrations may damage the performance of the isolation system, may cause inferior performance of the contents of the building, and may increase the possibility of pounding against surrounding retaining walls. The damages related to the long-period pulse are similar to those caused by the long-period and long-duration ground motion. The vertical ground motion has been another major concern for the isolation systems for many years. Since horizontal vibration is greatly reduced thanks to the isolation, the effect of vertical ground motion becomes more conspicuous for isolated buildings. Some research is available that examines the performance of isolators under vertical excitations [1-18 to 20]. However, almost no data is available to disclose the actual performance of the building contents such as medical equipment against vertical motions. In addition, evaluating the vertical dynamic response characteristics of base-isolated buildings is also important since it determines the amplitude of vertical floor accelerations, which is considered as an indicator to assess the performance of the building contents, and that of the axial force exerted on the isolators. Some research observed the vertical dynamic response characteristics of base-isolated buildings based on actual earthquake records [1-21 to 25]. However, no comprehensive research is present that generalizes the vertical dynamic response characteristics of base-isolated buildings.

## **1.2 Objective**

Considering the high demand on the performance of isolated buildings, it is more than worthwhile to examine the effects of ground motions on the performance of structures and contents before their

disadvantages are revealed by future earthquakes. This dissertation aims at the verification of the seismic performance of base-isolated buildings and the assessment of the capability of base-isolated medical facilities to maintain function against large earthquakes, i.e., long-period and long-duration ground motion and near-fault ground motion with large vertical motions. Since almost no data was available to observe the intrinsic factors causing interior damages, a full-scale shaking table test was conducted for the base-isolated specimen, whose interior was furnished and equipped with medical appliances following the actual medical practices. The performance and resulting damages to the structure's contents were observed, and seen to be related to major structural responses such as the maximum floor accelerations, velocities and absolute displacements. Those findings were supported by separately conducted supplemental shaking table tests for some typical medical appliances. Structural performance of the base-isolated specimen was also observed for both the horizontal and vertical responses. The damages related to pounding against the surrounding retaining wall [1-26] were outside of interest of this dissertation. Generalized vertical dynamic response characteristics of base-isolated buildings were also comprehensively observed.

In summary, the following three issues are the focus of this dissertation:

- (1) Examining the dynamic response and related damages of base-isolated buildings against the long-period and long-duration ground motion and vertical ground motion.
- (2) Evaluating the performance of the contents of base-isolated medical facilities.
- (3) Developing a generic model to capture the general relationship between the vertical dynamic response characteristics and the configuration of the base-isolated building.

The first two were examined mainly based on a full-scale shaking table test and associated component tests, and the last was carried out by numerical parametric study.

### **1.3 Organization**

This dissertation consists of nine chapters. Except Chapter 1 for introduction, Chapter 2 for reviewing the previous research and Chapter 9 for a summary and conclusions, five out of the remaining six chapters deal with the full-scale shaking table test of a base-isolated medical facility. The series of shaking table tests was conducted twice: one was the series of shaking table tests conducted from December 2008 to January 2009, and the other was the series of shaking table tests in the fall of 2010. The first series of the test was to observe the performance of a base-isolated medical facility against large earthquakes (mainly horizontal motions). The second series of test aimed at the verification of the capability of various countermeasures to improve the performance of building contents, and at observing the performance of the base-isolated system against vertical motions. The same superstructure and base isolation systems were used for both tests. In addition, the same superstructure was tested in the fixed-base condition for comparison purposes. Chapter 3

explains the setting of shaking table test, Chapters 4 and 5 discuss the structural responses in the horizontal and vertical direction, respectively, and Chapters 6 and 7 discuss the interior performance of the medical facility for the horizontal and vertical motions. Chapter 8 generalizes the vertical dynamic response characteristics of the base-isolated buildings with respect to various combinations of major components. The major contents and discussion presented in each chapter are as follows:

Chapter 1 describes the backgrounds and objectives, and shows the entire organization of this dissertation.

Chapter 2 summarizes the previous research related to this dissertation topic. The contents of this chapter are: (1) design practices and application of isolation systems in Japan; (2) the characteristics of two types of ground motions that would significantly influence base-isolated buildings, that is the long-period and long-duration ground motion and the vertical ground motion, (3) recorded responses of base-isolated buildings of past earthquakes; (4) vertical response characteristics of base-isolated buildings estimated based on past earthquake records; and (5) damages of hospitals observed from past earthquakes.

Chapter 3 introduces the setting of the full-scale shaking table test. The configuration of the specimen, including the structural components, adopted isolation systems (the natural rubber bearing accompanied by a U-shaped steel damper and the high-damping rubber bearing) and interior setting as the medical facility, are described. A total of 700 sensors were used for measurements, six ground motions including three near-fault or short-period ground motions and three long-period and long-duration ground motions were adopted. 11 and 24 shakings were conducted for the first and second series of the tests, respectively, for all three systems: the base-isolated systems with the natural rubber bearing accompanied by a U-shaped steel damper, the system with the high-damping rubber bearing, and the corresponding fixed-base system.

Chapter 4 examines the horizontal structural response of the base-isolated system, focusing on (1) stability performance of the base isolation layer for repeated shaking, especially for the long-period and long-duration ground motion; (2) horizontal responses with respect to the type of ground motion, i.e., the near-fault and long-period long-duration ground motion; (3) comparison of the performance for different base isolation systems; and (4) the effects of stiffness degradation of the superstructure on the structural performance of the base-isolated and fixed-base systems. Since the specimen was continuously damaged during the shaking table tests of the fixed-base system in the first series of test, the stiffness of the superstructure of the second series of test was about quarter of that of the first series of tests.

Chapter 5 examines the vertical structural response of the base-isolated system: (1) vertical floor acceleration responses and their amplitude distribution throughout the superstructure; (2) vertical dynamic response characteristics (natural frequency and damping ratio), and (3) axial force exerted on isolators. The response amplifications in the base isolation layer, columns, and slabs were main focuses. The effects of inserting the base isolation layer on the shift of vertical dynamic response characteristics of the fixed-base systems (or the superstructure) to the base-isolated systems were

examined in more detail by associated finite element analysis. In addition, the shift of the vertical dynamic response characteristics for larger response amplitudes was also examined.

Chapter 6 examines the performance of the medical facility's contents for horizontal ground motions based on the full-scale shaking table tests. The performance of building contents, the dislocation distances of furniture and medical equipment, was described for different types of ground motions. Those performances were related to the response amplitudes such as the floor accelerations, velocities, and absolute floor displacements. The effectiveness of measures to reduce the damages observed in the first series of tests was also evaluated based on the results of the second series of the tests.

Chapter 7 examines the performance of the medical facility's contents for vertical ground motions. Notable responses of furniture and equipment were observed. The observation mostly focused on the acceleration amplifications in the vertical direction through the equipment, and on whether the patient or the furniture themselves jump or not. Those phenomena were related to the corresponding vertical floor accelerations. These results were strengthened by the supplemental shaking table test conducted for seven selected pieces of equipment, obtaining the vertical dynamic response characteristics of various types of medical appliances.

Chapter 8 tries to generalize the vertical dynamic response characteristics of the base-isolated buildings with respect to various combinations of major components. The vertical response of the base-isolated building was decoupled into three modes, i.e., the mode that was related to the base isolation layer, the mode related to columns, and the mode related to slabs. The three degrees of freedom model was introduced, which has a capability to represent the first mode response of the base-isolated building as the combinations of the three modes. Parametric study was conducted to observe the relationship of the response amplifications and the contribution of the first mode as a whole system with the various combinations of the first natural frequencies of the three modes.

Chapter 9 summarizes major findings and conclusions of this dissertation.

## REFERENCES

- [1-1] Tanaka Y., Fukuwa N., Tobita, J., and Mori M., Present Situation of Isolation Building in Japan Base on Establishing a Database on Technical Evaluation Sheet, The 13<sup>th</sup> Japan Earthquake Engineering Symposium, Japan Association for Earthquake Engineering, 2010, pp.569 – 576 (Japanese).
- [1-2] Becker T.C., Furukawa S., Mahin S.A. and Nakashima M., Comparison of US and Japanese Codes and Practices for Seismically Isolated Buildings, Structures Congress, Structural Engineering Institute of ASCE, 2010.
- [1-3] James M. Kelly, Base Isolation: Origins and Development, NISEE, website: [nisee.berkeley.edu/lessons/kelly.html](http://nisee.berkeley.edu/lessons/kelly.html) (valid on 04/01/2011).
- [1-4] Otani S. and Kani N., Japanese state of practice in design of seismically isolated buildings,



- 4<sup>th</sup> US-Japan workshop on performance-based earthquake engineering methodology for reinforced concrete building structures, Toba, Japan 2002.
- [1-5] Building Standard Law of Japan, the Ministry of Construction, Japan, 1950 implemented, 2008 latest revised (Japanese).
- [1-6] Enforcement Ordinate of Construction Standard Law, the Ministry of Construction, Japan, 1950 implemented, 2011 latest revised (Japanese).
- [1-7] Structural provisions for building structures – 2007 Edition, the Ministry of Construction and Building Research Institute, 2007 (Japanese).
- [1-8] Report of Investigation of Hospital Damages for Southern Hyogo Prefecture earthquake, Japan Institute of Healthcare Architecture, March, 1996 (Japanese).
- [1-9] Kakehi A., Symposium (1) What Happened to Buildings and Equipment of Hospitals at The Great Hanshin-Awaji Earthquake: To Buildings-1, Journal of Medical Instrument, Vol.38, June, 1996, pp.281-288 (Japanese).
- [1-10] Structural Response and Performance for Long Period Seismic Ground Motions, AIJ, 2007 (Japanese).
- [1-11] Machizuki K., Kaname K., Kawabe H., Irikura K., Seismic Activities along the Nankai Trough. Bull. Earthq. Res. Inst. Univ. Tokyo, Vol. 78, 2003, pp.185-195.
- [1-12] The Headquarters for Earthquake Research Promotion:  
<http://www.jishin.go.jp/main/index.html>
- [1-13] Nakagawa Y., Kaname K., Kawabe H., Irikura K. Damage prediction of long-period structures during subduction earthquakes-Part 2: Long-period ground motion prediction in the Osaka basin for future Nankai Earthquakes, The 14<sup>th</sup> World Conference on Earthquake Engineering, Beijing, China, October 2008.
- [1-14] Kawabe H., Kaname,K., Irikura K. Damage prediction of long-period structures during subduction earthquakes-Part 1: Long-period ground motion prediction in the Osaka basin for future Nankai Earthquakes, P The 14<sup>th</sup> World Conference on Earthquake Engineering, Beijing, China, October 2008.
- [1-15] Chung Y., Nagae T., Fukuyama K., Kajiwara K., Inoue T., Hitak, T. and Nakashima M. Seismic resistance capacity of high-rise buildings subjected to long-period ground motions – E-Defense shaking table test,” The 14<sup>th</sup> World Conference on Earthquake Engineering, Beijing, China, October 2008.
- [1-16] Chung Y., Nagae T., Hitaka T., and Nakashima M. Seismic resistance capacity of high-rise buildings subjected to long-period ground motions: E-Defense shaking table test. Journal of Structural Engineering, ASCE, Vol., 2010 (available online).
- [1-17] Ji X., Kajiwara K., Nagae T., Enokida R., and Nakashima M., A substructure shaking table test for reproduction of earthquake responses of high-rise buildings, Earthquake Engineering and Structural Dynamics, Vol. 38, 2009, pp. 1381-1399.
- [1-18] Umino R, Mifune Y., Matuda S., and Asano K., Dynamic Behavior of Base Isolation Systems Considering Vertical Earthquake Motion Component, Proceedings of the Annual Conference on Architectural Institute of Japan, September 1997, paper ID:21326

(Japanese).

- [1-19] Pan P., Safety and Functionality of Base-isolated Building Structures Subjected to Vertical Ground Motions, Ph.D. dissertation, Kyoto University, 2004
- [1-20] Gordon P. Warn and Andrew S. Whittaker, Vertical Earthquake Loads on Seismic Isolation Systems in Bridges, Journal of Structural Engineering, November, 2008, pp.1696 – 1704.
- [1-21] Morishita T., Sito Y., Yoshida T., and Ryujin H., Properties of Vibration through Earthquake Observation on a Base Isolated Building, Summaries of Technical Papers of Annual Meeting, AIJ, Hokkaido, paper ID: 21147, 2004 (Japanese).
- [1-22] Shinohara T., Uru M., Nakayama K., and Kondo T., Study on the Response Characteristics of Base-Isolated Structures for Vertical Earthquake Motion Part-1 and 2, Proceedings of the Annual Conference on Architectural Institute of Japan, September 1998, paper ID:21320 – 21321 (Japanese).
- [1-23] Kondo T., Uru M., Nakayama K., and, Hashimura H., Study on the Response Characteristics of Base-Isolated Structures for Vertical Earthquake Motion Part-3 to 5, Proceedings of the Annual Conference on Architectural Institute of Japan, September 1999, paper ID:21322 – 21324 (Japanese).
- [1-24] Kondo T., Uru M., and, Hashimura H., Study on the Response Characteristics of Base-Isolated Structures for Vertical Earthquake Motion Part-6 and 8, Proceedings of the Annual Conference on Architectural Institute of Japan, September 2000, paper ID:21267 – 21269 (Japanese).
- [1-25] Nobata A., Teramura A., and Yasui Y., Vertical Resposne Characteristic of Base-Isolated Building Based on Observed Earthquake Records, Report of Obayashi Corporation Technical Research Institute, No.56, 1998, pp.23-28.
- [1-26] Sano T., Katsumata H., Miwada G., Komaki J., Sata K., Takiyama N., and Hayashi Y., Esperiments of Collision to Retaining Wall with Real Scale Base-Isolated Building, Part I to IV, Proceedings of the Annual Conference on Architectural Institute of Japan, September 2010, paper ID:21214 – 21217 (Japanese).

## LIST OF PUBLICATIONS

*Journal papers (full papers reviewed by multiple reviewers and published in recognized journals):*

- [1] Sato E., Sakai H., Inoue T., Fukuyama K., Kajiwara K., Kakehi A., Kobayashi K., Kamada T., **Furukawa S.**, Nakashima M., Full-Scale Shaking Table Tests for Assessment of Functionality in Medical Facility Against Earhquake, Journal of Structural and Construction Engineering, Vol.75, No.650, 2010.
- [2] Sato E., **Furukawa S.**, Kakehi A, and Nakashima M., Full-scale shaking table test for exmanination of safety and functionality of base-isolated medical facilities, Earthquake

***Conference papers (abstracts reviewed by multiple reviewers and presented in international conference):***

- [1] **Furukawa S.**, Goel S. C., Chao S., Seismic Evaluation of Eccentrically Braced Steel Frames Designed by Performance-Based Plastic Design, Proceedings of 14<sup>th</sup> World Conference on Earthquake Engineering, 2008.10, ID: 05-01-0385.
- [2] Becker T.C., **Furukawa S.**, Mahin S.A. and Nakashima M., Comparison of US and Japanese Codes and Practices for Seismically Isolated Buildings, Structures Congress, Structural Engineering Institute of ASCE, 2010.
- [3] Sato E., Kajiwarra K., **Furukawa S.** (presenter), Ji X., and Nakashima M., Full-scale shaking table test of a hospital made of a base-isolated four-story concrete structure, 9<sup>th</sup> US National and 10<sup>th</sup> Canadian Conference on Earthquake Engineering, paper ID:303, July,2010.

***Technical papers presented at domestic conference***

- [1] **Furukawa S.**, Sato E., Ji X., Sakai H., Fukuyama K., Inoue T., and Nakashima M., Research Project on Assessment of Functionality in Medical and Telecommunication Facilities, Part 3: Response Behavior of Aseismic and Seismic Isolation Structures against Short Period Earthquake, Proceedings of the Annual Conference on Architectural Institute of Japan, September 2009, paper ID:21489 (Japanese).
- [2] Sato E., Sakai H., **Furukawa S.**, Fukuyama K., and Inoue T., Research Project on Assessment of Functionality in Medical and Telecommunication Facilities, Part 4: Response Behavior of Aseismic and Seismic Isolation Structures against Long Period Earthquake, Proceedings of the Annual Conference on Architectural Institute of Japan, September 2009, paper ID:21490 (Japanese).
- [3] Ikeda S., Shimano Y., Kashima K., Ishikawa Y., Sato E., Nagae T., **Furukawa S.**, and Fukuyama K., Research Project on Assessment of Functionality in Medical and Telecommunication Facilities, Part 13: Comparison between Results of Table Tests and Results of Numerical Analysis, Proceedings of the Annual Conference on Architectural Institute of Japan, September 2009, paper ID:21495 (Japanese).
- [4] Shimano Y., Ikeda S., Kashima K., Ishikawa Y., Sato E., Nagae T., **Furukawa S.**, and Fukuyama K., Research Project on Assessment of Functionality in Medical and Telecommunication Facilities, Part 14: Study for Results of Table Tests and Results of Numerical Analysis, Proceedings of the Annual Conference on Architectural Institute of Japan, September 2009, paper ID:21496 (Japanese).
- [5] Sato E., Sakai H., Inoue T., **Furukawa S.**, Fukuyama K., Kobayashi K., Kakehi A., and Nakashima M., Research Project on Assessment of Functionality in Medical and Telecommunication Facilities, Part 17: Response of Medical Appliances (Bed) by Full-scale Shaking Table Test, Proceedings of the Annual Conference on Architectural

Institute of Japan, September 2010, paper ID:21037 (Japanese).

- [6] Ikeda S., Shimano Y., Kashima K., Ishikawa Y., Sato E., Nagae T., **Furukawa S.**, and Fukuyama K., Research Project on Assessment of Functionality in Medical and Telecommunication Facilities, Part 18: Analysis of Differences between Results of Table Tests and Results of Numerical Analyses, Proceedings of the Annual Conference on Architectural Institute of Japan, September 2010, paper ID:21038 (Japanese).
- [7] **Furukawa S.**, Sato E., and Nakashima M., 3DOF Lump Mass Model for Examination of Vertical Floor Acceleration of Base-Isolated Building, Proceedings of the Annual Conference on Architectural Institute of Japan, September 2010, paper ID:21128 (Japanese).
- [8] Inoue T., Sato E., Sakai H., Fukuyama K., Nakahsima M., **Furukawa S.**, Kobayashi K., Kosuge R., and Takehi A., Research Project on Assessment of Functionality in Medical and Telecommunication Facilities, Part 21: Outline of Full-scale Shaking Table Test for Improvement of Functional Maintenance in Medical Facility, Proceedings of the Annual Conference on Architectural Institute of Japan, September 2011, (process to publication) (Japanese).
- [9] Sato E., Sakai H., Inoue T., Fukuyama K., **Furukawa S.**, Nakahsima M., Kobayashi K., Kosuge R., and Takehi A., Research Project on Assessment of Functionality in Medical and Telecommunication Facilities, Part 22: Results of Full-scale Shaking Table Tests for Improvement of Functional Maintenance in Medical Facility, Proceedings of the Annual Conference on Architectural Institute of Japan, September 2011, (process to publication) (Japanese).
- [10] **Furukawa S.**, Sato E., Sakai H., Shi Y, Fukuyama K., Inoue T., Nakahsima M., , Research Project on Assessment of Functionality in Medical and Telecommunication Facilities, Part 23: Vertical Dynamic Response Characteristics of Base-isolated System against Vertical ground motions, Proceedings of the Annual Conference on Architectural Institute of Japan, September 2011, (process to publication) (Japanese).
- [11] Hora H., Sato E., Sakai H., Fukuyama K., Nakahsima M., **Furukawa S.**, Kobayashi K., Takehi A., Research Project on Assessment of Functionality in Medical and Telecommunication Facilities, Part 25: Full-scale Shaking Table Test of 2-Dimensional Isolation Floor to Improve Functional Maintenance in Medical Facility, Proceedings of the Annual Conference on Architectural Institute of Japan, September 2011, (process to publication) (Japanese).



## **CHAPTER 2**

### **REVIEW OF PREVIOUS RESEARCH**

#### **2.1 Introduction**

This chapter describes the present state of the application of the base isolation and summarizes past research related to this dissertation topic, i.e., the verification of seismic performance of base-isolated buildings and the assessment of functional maintenance capability of base-isolated medical facilities against large earthquakes. The contents of this chapter are as follows: (1) design practices and application of isolation systems in Japan; (2) the characteristics of two types of ground motions that may degrade the performance of base-isolated buildings, that is the long-period and long-duration ground motion and the vertical ground motion, (3) recorded responses of base-isolated buildings from past earthquakes, (4) vertical response characteristics of base-isolated buildings estimated based on past earthquake records, and (5) reported damages of hospitals observed from past earthquakes.

#### **2.2 Isolation systems in Japan**

##### ***2.2.1 Design practice***

Currently, two design procedures are adopted into codes for isolated buildings (including base- and mid-isolated buildings). One procedure requires the peer review and the approval of the Ministry of Construction, which is considered as the highest level design verification procedure in Japan [2-1, 2-2]. The other provides an alternative simpler design procedure that requires no peer review nor the approval of the Ministry of Construction [2-3, 2-4].

The design guidelines for isolated buildings were originally developed following that the guidelines applied for high-rise buildings, which have been implemented since the 1970s for buildings taller than 60 m. Construction approval by the Ministry of Construction is required through peer review via a committee specializing in isolated buildings. In this process, isolated buildings are recommended to be designed for multiple levels of performance. The standard (minimum) performance levels are as follows [2-5]:

L-1: Damage of systems has to be limited to a minor repairable level. Wind and seismic loads that would occur more than once during the building life cycle are considered for this level. A 50 year return period for wind load and PGV equal to 0.25 m/s for seismic loads are recommended.

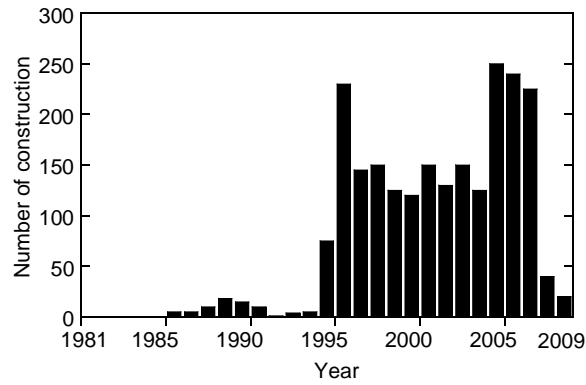
L-2: Structural safety has to be maintained. Wind and seismic loads with the maximum intensity that would occur at the concerned site or that would possibly occur in the future are considered for this level. A 500 year return period for wind load and PGV equal to 0.50 m/s for seismic loads are recommended.

Most buildings are likely to be designed for higher performance levels by specifying more detailed performance levels and minimizing the acceptable damage level [2-6]. Time history analysis has to be conducted to verify the specified performance. A sufficient number of ground motions have to be selected, which are categorized into two groups [2-7]. One group is considered as standard design ground motions such as El Centro 1940 (Imperial Valley), Taft 1952 (Kern County), and Hachinohe 1968 (Tokachi-oki). The other group is what must be considered for the specific local site. Recorded accelerograms in the vicinity of the building site or synthetic ground motions yielded following Notification No. 1461 of the Ministry of Construction (2000) are commonly accepted. Ground motions synthesized by the designated committee have been provided in some locales such as the Sannomaru wave of Nagoya city, which is one of the strongest synthesized long-period and long-duration ground motions, and the Yokohama wave of Yokohama city. Commonly, at least six ground motions (three from the standard waves, and the other three from site specific waves) are recommended.

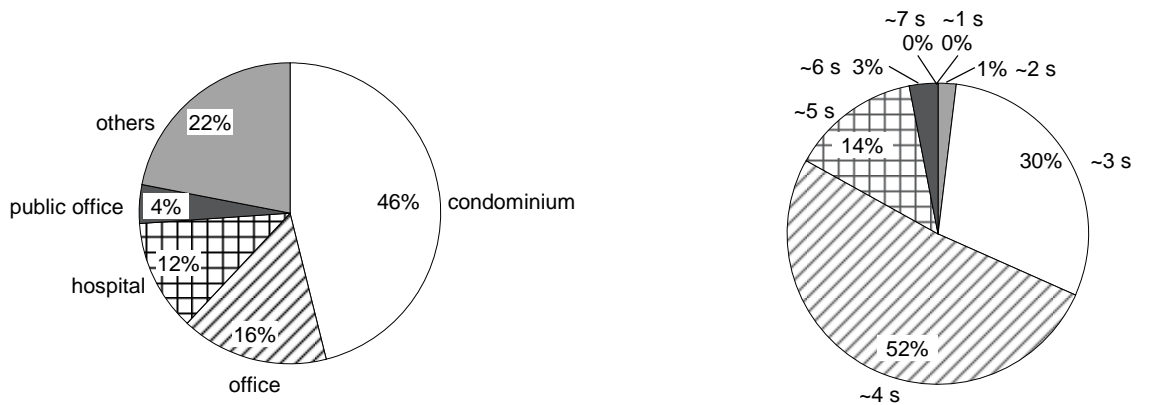
In 2000, Notification No. 2009 of the Ministry of Construction began to be enforced. This allows us to design isolated buildings by an equivalent linear method (based on the capacity spectra design methodology). According to this Notification, buildings not greater than 60 m, not mid-story isolated, and constructed on firm soil with no possibility of liquefaction are exempt from the Ministry approval procedure. The L-2 seismic load is considered, which is the same intensity adopted in the calculation of the ultimate lateral strength of ordinal buildings [2-2].

## ***2.2.2 Construction statistics***

Since the implementation of Notification No. 2009, the number of isolated buildings which do not obtain the approval of the Ministry of Construction has increased. Therefore, it has become difficult to carry out a statistical survey on the constructed isolated buildings. Tanaka [2-9] constructed a comprehensive database based on (1) electrical data provided by the Japan Society of Seismic Isolation (JSSI) [2-10]; (2) information from the journal “MENSIN” published by JSSI [2-11]; (3) the “Building Letter” published by the Building Center of Japan [2-13]; and (4) the Books for the Approval of Construction Method provided by the Ministry of Construction [2-14]. This subsection describes the construction statistics of isolated buildings mostly based on the data provided by Tanaka [2-9]. Since some delay is present in issuing those data, the data of the most recent two years are incomplete in the following statistics.

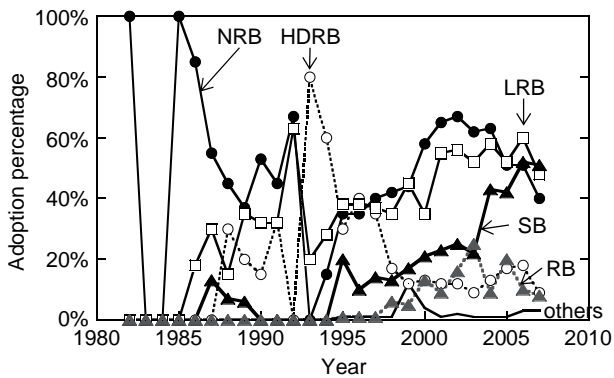


(a) Number of buildings

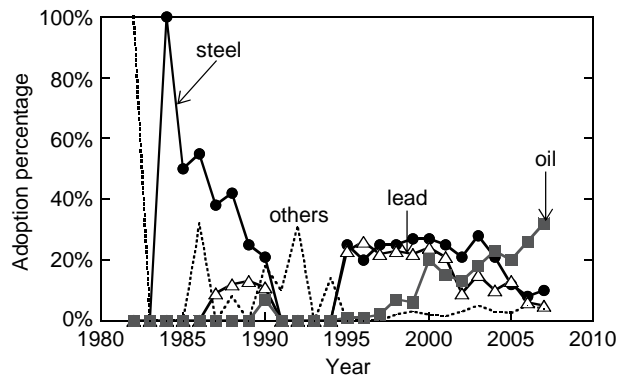


(b) Types of facility

(c) Natural period (Level 2)



(d) Types of isolator



(e) Types of damper

(Note) all figures are reproduced based on figures in Tanaka [2-9]

Figure 2-1 Construction statistics of base-isolated buildings

**Number of isolated buildings**

The chronological development of the isolated buildings is shown in Figure 2-1(a). In the figure, the number of private houses is excluded. The number of isolated buildings in Japan increased rapidly after the Hyogo-ken Nanbu earthquake (Kobe earthquake) in 1995. The construction number per year before 1995 remained less than ten, but increased drastically to 150 buildings per year afterward. The damages of the Kobe earthquake helped owners to realize that the minimum



standard of structural safety (life safety) was not enough and higher levels of seismic performance were needed to protect their assets. The isolation system has been appreciated as a choice for upgrading the building's performance to the extent that not only is almost no damage expected for the structure but it also enables the facility to continue to provide service during and after the earthquake without any critical intermission. The rapid prevalence was also accentuated by intensive research and positive marketing by major construction companies [2-8]. The implementation of Notification No. 2009 of the Ministry of Construction in 2,000 has also helped the wide application of isolation systems. Recently, the total number of constructions has reached 2,500. Most seismically isolated buildings are concentrated in the three major metropolitan areas [2-9].

### **Usage and building height**

The types of facilities that adopt the base isolation system consist of condominiums, offices, medical facilities and public offices. Figure 2-1(b) shows the occupancy ratio for each of them. Currently, half of the seismically isolated buildings in Japan are condominium buildings. The application of the system to medical facilities is also popular, and is the source of 12% of the applications. The drastic increase of its application to condominium buildings in the late 1990s also led to an increase in the height of the building. The height reached 60 m in the late 1990s, and about 20 buildings (all of them are apartments except one office) with a height of above 100 m have been constructed.

### **Natural period**

Statistics of the natural period at the Level 2 displacement are shown in Figure 2-1(c). About half of buildings have the natural periods between 3 to 4 s, and 96 % fall between 2 to 5 s. It is commonly recommended that the natural period of the base isolation layer with the rigid-body assumption of the superstructure is better by at least three times that of the superstructure with the fixed-base condition [2-5]. The ratio of the natural period of the base isolation layer that is determined by the equivalent stiffness at the maximum response deformation to that of the superstructure is less than five in about half of the buildings, and 5% were found to be less than three [2-9].

### **Types of isolators and dampers**

Figures 2-1 (d) and (e) show the adoption ratios of various types of isolators and dampers in chronological order. Isolators that are commonly adopted are categorized into five types: (1) natural rubber bearing (NRB), (2) high-damping rubber bearing (HDRB), (3) lead rubber bearing (LRB), (4) slider bearing (SB), and (5) roller bearing (RB). The first three are rubber bearings composed of laminated rubber layers, inner steel plates and flange plates at both ends. NRB behaves in a linear way, while HDRB and LRB behave non-linearly since they are accompanied by damping. The latter two are mechanical bearings that isolate the building by low friction. SB has a sliding plate coated by a low-friction material such as Fluoropolymers, and the RB is

composed of ball bearings sandwiched by steel plates. Detailed characteristics and properties of each type of bearing can be found elsewhere [2-6, 2-14].

From Figure 2-1(d), rubber bearings (NRB+U, HDRB and LRB) were dominant by the mid 1990s. Afterward, HDRB has gradually lost its market, being replaced by mechanical bearings (SB and RB). The growing popularity in mechanical bearings in the late 1990s may contribute to increasing demands on the elongation of the natural period since taller buildings have become increasingly common since the late 1990s. Steel dampers occupied the largest share in the first decade, and lead dampers became similarly popular in the 1990s. Recently, the share of oil dampers has increased gradually.

## **2.3 Concerned ground motions for base-isolated buildings**

Three types of ground motions seriously affect the performance of base-isolated buildings in both safety and functionality. They are (1) the long-period and long-duration ground motion, (2) the vertical ground motion generated by the near-fault ground motion, and (3) the long period pulse. Since (1) may overlap with the problem caused by (3), only the first two ground motions are considered in this dissertation.

### ***2.3.1 Long-period and long-duration ground motion***

Subduction zone earthquakes generate long-period ground motions on land, especially in the basin areas where large cities such as Tokyo, Nagaya and Osaka are located. Their predominant periods range from two to ten seconds, and the duration of primary motion extends over several minutes. The dominant period of the natural response of the local soil is estimated to be longer than 5 s for the Kanto plains, 2 to 4 s for the Nobi plains, and 2 to 5 s for the Osaka plains [2-9]. It is notable that these natural periods are similar to those of high-rise buildings and overlap with those of isolated buildings (Figure 2-1(c)), most of which are located in these metropolitan areas.

Long-period and long-duration ground motions had not been recognized for many years. The 1985 Mexico City earthquake was the first event of this type of ground motions were recognized and caused significant damage [2-15]. In Japan, this type of ground motion was recognized at the 1968 Tokachi-oki earthquake, but had not been taken seriously until the Tokachi-oki earthquake occurring in 2003, in which fire from an oil tank occurred due to sloshing [2-16, 17]. It was the first time in this country that many long-period and long-duration ground motions with a dominant period of longer than 10 s were recored at major basin areas by the nation-wide networks of seismic recording (K-net, and Kik-net). Research has been conducted in the field of seismology to provide the expected ground motions for design purposes, and in the field of structural engineering to examine the structural performance of constructed high-rise buildings, isolated buildings, and infrastructure [2-16 to 21]. By 2010, no large acceleration has been recorded for long-period and

long-duration ground motions. However, it is expected that major Japanese cities will encounter this type of ground motion in a near future [2-16, 17].

The long-period and long-duration ground motions have been considered in designs as a local site wave, which is not required for consideration if the building is designed based on the Notification of 2009.

### 2.3.2 Vertical ground motion

Since vertical ground motion is commonly considered to be secondary in design, no design spectrum or comprehensive design methodology has been established in Japan. Conveniently, half to two thirds the amplification of the required horizontal loads have been adopted in design in this direction [2-6].

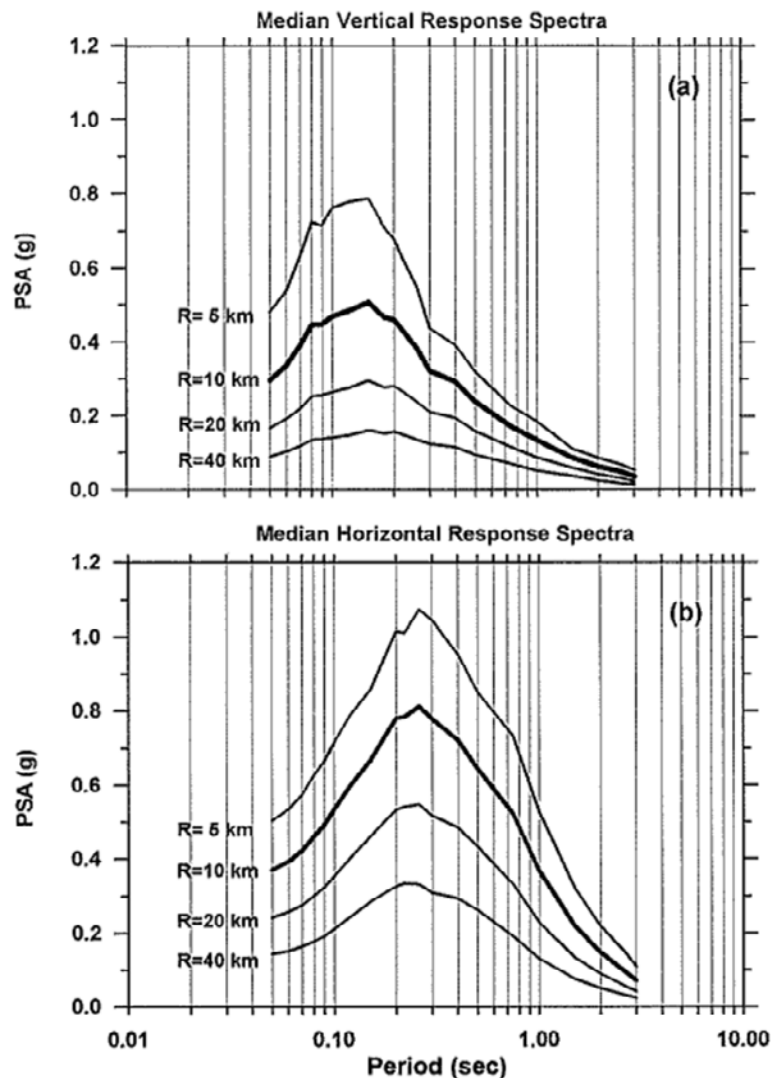


Figure 2-2 Distance-dependent response spectra for 5% damping for different distances of 5, 10, 20, 40 km from the epicenter (exerted from Bozorgnia [2-22])

Niazi and Bozorgnia [2-22 to 25] provided vertical response spectra, analyzing free-field

vertical motion of over 700 accelerograms from 12 earthquakes recorded on the SMART-1 array in Taiwan, 159 response spectra of the motions recorded during the 1989 Loma Prieta, California earthquake, and 123 response spectra of the motions recorded during the Northridge earthquake. The main findings summarized by Bozorgnia [2-22] are as follows:

- (1) The main characteristics of the vertical-to-horizontal (V/H) spectral ratio are approximately similar for all these earthquakes.
- (2) The V/H spectral ratio is a function of period and site-to-source distance.
- (3) Vertical acceleration spectra have peaks in a period range of about 5 to 10 Hz. For the horizontal motion the spectral peaks fall in a frequency range of 3.3 to 5 Hz.

Figure 2-2 shows the distance-dependent response spectra for 5% damping for various distances of 5 to 40 km from the epicenter, the original figure of which can be found in Bozorgnia [2-22]. Bozorgnia [2-24] also indicated that PGA of the vertical motions may exceed that of the horizontal motions at sites close to an epicenter for the frequency range higher than 10 Hz. They suggested that a commonly adopted method that constructs the vertical response spectra by scaling the horizontal spectra by two-thirds neglected their characteristics of period- and distance-dependency. It is also suggested that there was a low possibility that the vertical component of ground motions was mitigated due to the non-linear characteristics of the soil, such as liquefaction as it is propagated by P wave [2-26, 27]. Therefore, the response spectra of Figure 2-2 (a) are applicable to all soil conditions.

## **2.4 Acceleration records of base-isolated buildings for past earthquake**

### ***2.4.1 Horizontal response***

Quite a few earthquake responses of base-isolated buildings have been recorded. The 1994 Northridge earthquake was the first large earthquake in which the responses of base-isolated buildings had been recorded. The hospital building of California State University was located about 36 km from the epicenter. The building was an eight-story concentrically-braced steel frame with a base isolation layer composed of 68 LRBs and 81 NRBs. PGA equal to  $3.59 \text{ m/s}^2$  at the foundation level was reduced to  $1.28 \text{ m/s}^2$  on the first floor and  $2.01 \text{ m/s}^2$  on the roof. No conspicuous damage was reported [2-28]. In Japan, there was a record of an even larger earthquake event, which was recorded at a nursing home building in Ojiya city, Niigata Prefecture, closely located to the epicenter of the Niigata Prefecture Chuetsu earthquake, 2004 [2-14]. The building was a 5 story reinforced concrete structure, isolated by 18 rubber bearings and 21 elastic sliding bearings. PGA equal to  $7.40 \text{ m/s}^2$  in the direction of North to South (NS),  $8.08 \text{ m/s}^2$  in the direction of East to West (EW), and  $4.87 \text{ m/s}^2$  in the direction of up to down (UD) were recorded at

the basement level, which were reduced by one quarter in the horizontal direction but were increased by 1.5 times in the vertical direction with respect to the first floor. Markings in dust on the sliding plates suggested that the maximum displacement of the bearings was about 150 mm. Figure 2-3 shows the acceleration records (a) at the basement and (b) at the first floor, which excerpted from Higashino et.al. [2-14]. Some of the recorded accelerations are summarized in the form of amplification ratios in Table 2-1 [2-14, 2-29 to 32]. It is notable that most of horizontal accelerations were reduced by isolation layers. For the horizontal response, Higashino et.al [2-14] concluded that the base isolation system works more efficiently for larger ground motions based on 20 records obtained from five earthquakes, all of which, except one (Building I), were categorized into short-period ground motions.

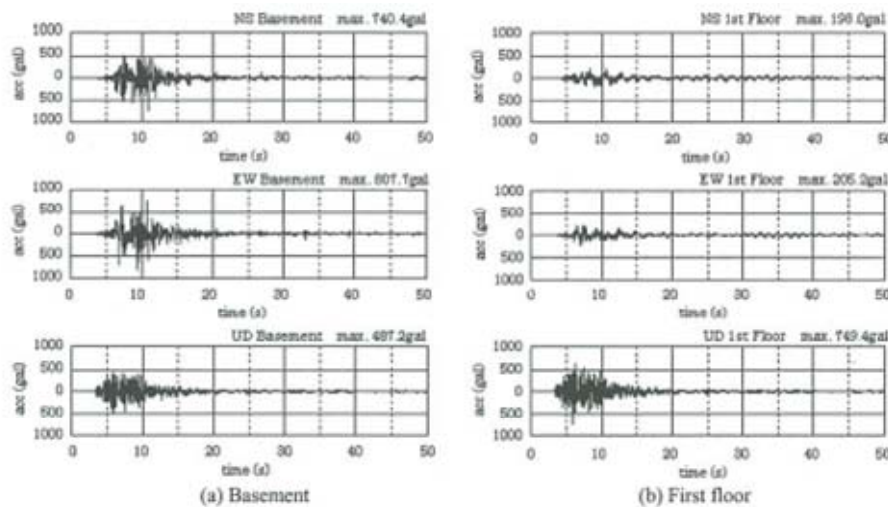


Figure 2-3 Acceleration records of the nursing home building (Building A in Table 2-1) located in the Niigata Prefecture (Niigata Prefecture Chuetsu earthquake), excerpted from Higashino [2-14]

Table 2-1 Acceleration amplification of base-isolated buildings obtained from earthquake records (based on data provided by reference [2-14])

Building	facility type	configuration	Acc. amp			
			NS 1st / Base	EW 1st / Base	UD 1st / Base	Top / Base
A <sup>*1)</sup>	Nursing home building	5 story RC	0.27	0.25	1.54	
B <sup>*2)</sup>	Government office building	9 story SRC	0.45	0.42	1.11	2.40
C <sup>*2)</sup>	Hospital building	3 story RC	0.73	0.86	1.46	
D <sup>*3)</sup>	Computer service building	2 story RC				5.11
E <sup>*3)</sup>	Office building	18 story	0.66	0.79	1.03	2.20
F <sup>*4)</sup>	Post and Telecommunication building	6 story SRC	0.22	0.35	0.91	1.77
G <sup>*4)</sup>	Office building	3 story RC	0.54	0.95	1.15	1.44
H <sup>*5)</sup>	Hospital building	4 story RC	0.32	0.72	1.09	1.57
I <sup>*2)</sup>	Condominium building	20 story RC	1.37			

\*1) The Niigata Prefecture Chuetsu earthquake, 2004

- \*2) The Tokachi-oki earthquake, 2003
- \*3) The Miyagi-ken-oki earthquake, 2003
- \*4) The Hyogoken-nanbu earthquake, 1995
- \*5) The Northridge earthquake, 1994

Table 2-1 shows one exception in that the acceleration amplitude in the horizontal direction was increased by 1.37 times. Building I was a 20 story condominium building with a height of 64.2 m located at Sapporo [2-32]. The natural period for the 50% shear stain of rubber bearings was about 3.0 s. Since the dominant periods of ground motion recorded at the foundation were about 3 to 4 s when the building encountered the 2003 Tokachi-oki earthquake, the building amplified the input acceleration through the base isolation layer and also the superstructure. The acceleration amplification from the foundation to the roof was 1.67 times. The maximum displacement of the base isolation layer reached 90 mm in the NS direction even though PGA was only 0.40 m/s<sup>2</sup>. This record indicates that the performance of base-isolated buildings may deteriorate when encountering a larger long-period and long-duration ground motion.

### ***2.4.2 Vertical response***

There are also a number of vertical responses recorded from base-isolated buildings. In Table 2-1, it is notable that vertical accelerations were amplified in almost all cases. Vertical accelerations were amplified through the base isolation layer to the first floor by 0.9 to 1.6 times what it was. The acceleration amplifications of the top floor to the input varied between 1.4 and 5.2. These amplifications in the vertical direction were conspicuous compared with that of the horizontal responses were reduced in most cases. A larger range in the vertical acceleration amplifications is thought to be due to the differences in the building configurations, input ground motions, and soil contribution to dissipating energy. In addition, the difference in the contribution of floor vibration also played a significant role since the locations of the installed accelerometer was not necessarily similar among all recorded buildings. Some might have been located at the center of the slab, while others were located close to the columns. Since the rigid-diaphragm assumption does not appear to be valid in the vertical direction, the location of accelerometers should affect the floor acceleration amplitudes.

## **2.5 Vertical performance of base-isolated buildings**

In practical design, a vertical response is considered primarily in terms of its contribution to the axial force exerted on the bearings. A simplified design method which does not consider the effect of the slab vibrations has been used to estimate the forces. However, estimation of vertical acceleration amplitudes on the floor is also essential to examine the performance of building

contents since the floor acceleration is one of the most important indicators to control the building's functionality. Contribution of vertical responses becomes more significant for base-isolated buildings since vertical motion remains to be amplified, while horizontal responses are reduced. In this section, research that studied the fundamental vertical dynamic response characteristics of base-isolated buildings and current design practice for the vertical response are introduced.

### 2.5.1 Vertical response characteristics of base-isolated buildings

A detailed study was conducted for the vertical response characteristics of buildings, including base-isolated buildings. Bozorgnia [2-22] examined response records of the 1994 Northridge earthquake for twelve selected buildings. The buildings were located within a distance range of about 8 to 71 km from the causative fault of the Northridge earthquake and included various types of structural systems: four steel buildings, five concrete buildings (including a parking structure), and three base-isolated buildings. The superstructures of the base-isolated buildings were braced steel frames in two cases (two and seven stories) and concrete frames for the rest (eight stories). The notable findings mentioned are as follows.

- (1) The lowest vertical natural frequency ranges from 3.9 to 13.3 (3.9 to 13.3 Hz for four steel buildings, 4.3 to 10 Hz for four reinforced concrete buildings excluding one parking structure, and 6.1 to 10.5 Hz for three base-isolated buildings).
- (2) Those identified natural frequencies were likely to correspond to high vertical spectral accelerations (Figure 2-2(a)).

Table 2-2 Vertical response characteristics of base-isolated buildings estimated by earthquake records (Morishita [2-35], Shinohara et.al [2-36 to 38], and Nobata et al. [2-39])

Build. configuration	Acc. amp		Natural freq. [Hz] base isolation	Natural frequency [Hz] (damping ratio)				
	1st / Base	Roof / Base		1st	2nd	3rd	4th	
Morishita [2-34] I 4 story (2 × 2 span)	-	-	14 - 16 <sup>*1)</sup>	14 - 16 (5 - 12%)				
Shinohara et.al [2-35 to 37] i -	-	-	14.3	(20% )				
	ii 4 story (4 × 5 span)	-	14.3	11.1 (20% )				
A 5 story (1 × 6 span)	1.3	1.7	15	5.5 (2.0%)	7.9 (5.0%)	13.6 (1%)	20.4 (5.0%)	
Nobata et al. [2-38] B 6 story with BF (3 × 5 span) <sup>*2)</sup>	1.3	1.8	13					
	C 1 sotry (3 × 7 span)	1.9	-	13	13.6 (2.0%)			
	D 3 story with BF (3 × 4 span) <sup>*2)</sup>	1.8	-	6 <sup>*3)</sup>	6.4 (1.3%)	6.8 (6.6)		

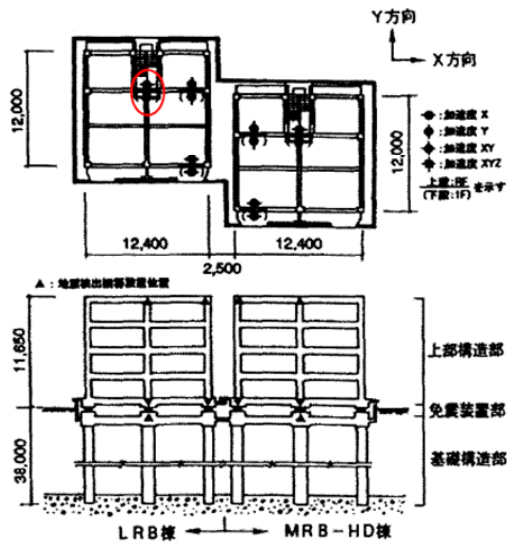
\*1) No value is available but Morishita [2-35] mentions that he confirmed the estimated natural frequency was close to

the design value.

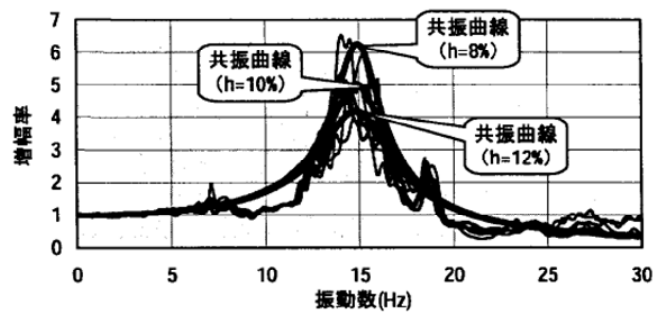
\*2) The number of stories includes the basement. The base isolation layer was below the basement floor.

\*3) The stiffness of the base isolation layer was intentionally reduced to filter traffic-related vibrations.

The coincident of vertical frequency range of buildings with the plateau of the vertical acceleration response spectrum is also pointed out by Papazoglou A. J. et al. [2-33]. They also estimated the range of vertical natural frequencies for four- to ten-story RC buildings to be 8.3 to 25.0 Hz, while Papaleontious [2-34] estimated those of steel buildings to be 4.0 to 6.25 Hz.

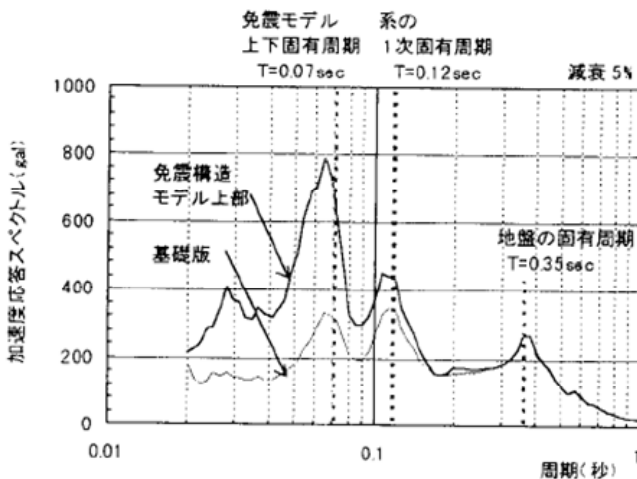


(a) Building configuration

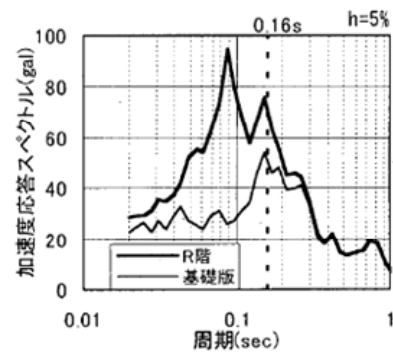


(b) Response amplification (above / below the base isolation layer)

Figure 2-4 Response amplification of a base-isolated building (Example 1: Morishita [2-35])



(a) Acceleration response spectra (at roof and base) for a building (no configuration available)



(b) Acceleration response spectra (at roof and base) for the four-story building

Figure 2-5 Response amplification of a base-isolated building (Example 2: Shinohara et.al [2-36 to 38])

Some studies tried to obtain the vertical damping of base-isolated buildings in addition to the first natural frequency. Table 2-2 summarizes the major properties for seven base-isolated



buildings provided by Morishita [2-35], Shinohara et.al [2-36 to 38], and Nobata et al. [2-39] such as the building configuration, acceleration amplifications, vertical natural frequencies, and corresponding damping ratio estimated by earthquake records. In the table, natural frequencies estimated based on the vertical stiffness of the base isolation layer with the rigid-body assumption for the superstructure are also shown, if available. The superstructures of all seven buildings were made of reinforced concrete.

Morishita [2-35] analyzed vertical acceleration records of a base-isolated building obtained from eight earthquakes (M 4.3 to 7.0) with the largest PGA equal to  $0.47 \text{ m/s}^2$ . The building was a four-story reinforced structure with a two-bay by two-bay floor and jointed with the other building having a similar configuration, as shown in Figure 2-4(a). The isolation layer had 10 LRBs. The response amplification obtained by transfer function of the accelerations of above to below the base isolation layer showed that a clear single mode dominated the vertical response (Figure 2-4(b)). Estimated vertical first natural frequency ranged 14 to 16 Hz, and corresponding damping ratio was estimated as ranging from 5% to 12%. Morishita [2-35] also mentioned the estimated vertical first natural frequency was close to the natural frequency calculated based on the assumption of the rigid-body superstructure.

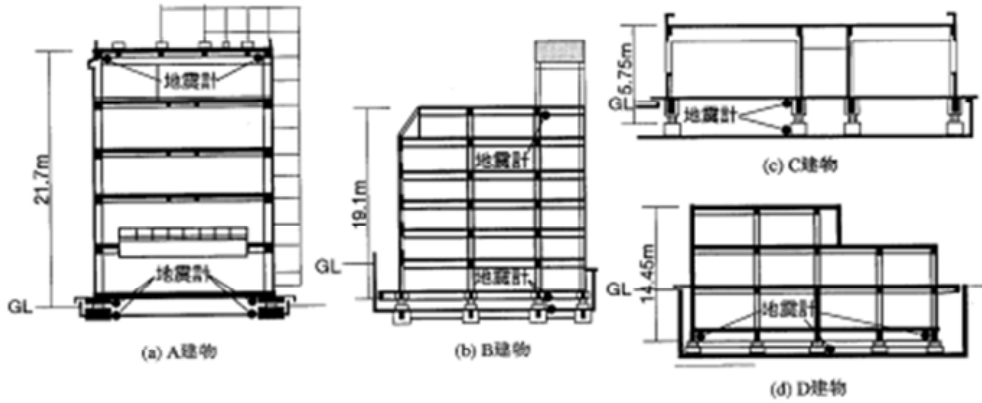
Shinohara et al. [2-36 to 38] examined response records obtained from two different base-isolated buildings, focusing on the contribution of soil to damping. The total damping ratios were estimated to be about 20% for both buildings based on the formula, which enabled the estimation of the damping ratio of the total system including the soil and the superstructure [2-40]. No configuration for one building and no information about the components of the isolation layer was available. The natural frequency of the four-story building with a 4-bay by 5-bay floor was 11.1 Hz (0.09 s), which was estimated by earthquake records (M5.1,  $\text{PGA} = 0.32 \text{ m/s}^2$ ), while the natural frequency of the base isolation layer estimated in the design was 14.3 Hz (0.07 s) with the rigid-body assumption for the superstructure. Figure 2-5 shows the acceleration response spectra of the accelerations at the roof and base for both buildings. Shinohara et al. [2-36 to 38] suggested that the vertical floor acceleration responses can be reproduced by the concentrated story mass model with a damping ratio of 20%.

Nobata et al. [2-39] provided a detailed examination of the vertical response characteristics of four base-isolated buildings using earthquake records obtained over decades. Accelerometers were installed close to beam-column connections to eliminate the floor vibration contribution. Figure 2-6 shows the building configurations and the averaged response amplification of selected 10 earthquake records with relatively larger amplitudes ( $\text{PGA}$  of less than  $0.5 \text{ m/s}^2$ ) for each base-isolated building (Building A to D). Building D had base isolators with relatively soft vertical stiffness to reduce the effect of traffic-related vibration. All buildings were supported by NRBs accompanied by steel dampers. Building A had friction dampers, Building B had oil dampers, and Building C had viscos dampers. Building D had viscos dampers in the vertical direction. Their major findings are summarized as follows:

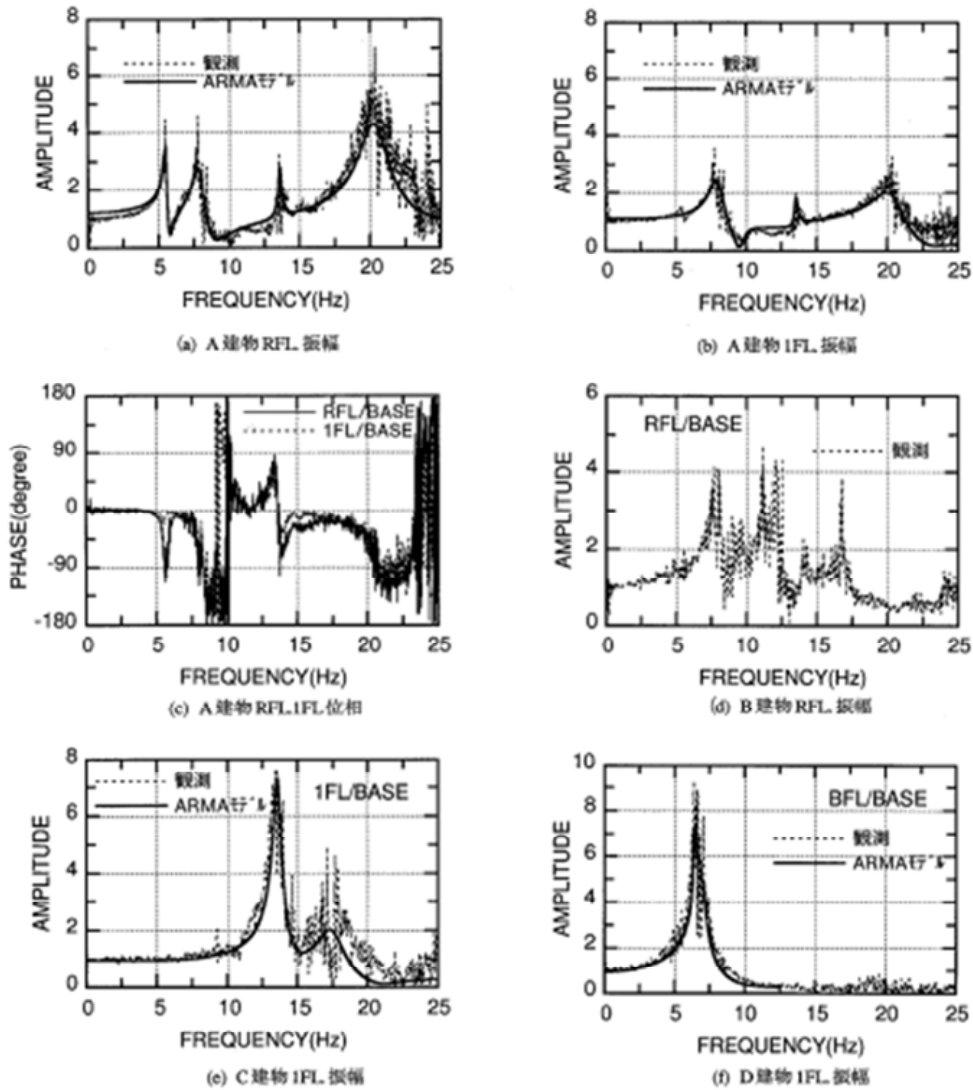
- (1) The acceleration amplification by the base isolation layer (first story relative to the base) and

also toward the roof ranged from 1 to 2, which is similar to the acceleration amplifications of high-rise buildings recorded in past earthquakes [2-41].

- (2) The vertical first natural frequencies ranged from 5.5 to 13.6 Hz for low- to mid-rise buildings.
- (3) The vertical first mode damping ratios were about 1% to 2%.



(a) Building configurations



(b) Magnitude and phase of the transfer functions of acceleration responses of Buildings A (first and roof), B (roof), C and D (first) with respect to the base acceleration  
 Figure 2-6 Response amplification of base-isolated building (Example 3; Nobata et al. [2-39])

- (4) The vertical first natural frequencies tended to be below those estimated based on the rigid-body assumption of the superstructure.
- (5) Vertical motions input to buildings tended to be smaller than those recorded on the free field by about 0.6.

It is also mentioned that the vertical first natural frequency of the base-isolated buildings may be controlled by the natural frequency of the slabs, if the building had longer spans as Building A did. It was confirmed that the several peaks of the response amplitude obtained by a transfer function appeared close to the natural frequency of the slab of each story in Building A. The vertical natural frequencies of the slabs were 8.6, 14.5, 8.9, 8.4, 8.5, and 5.3 Hz from the first to top stories, while the estimated natural frequencies of the buildings were 5.5, 7.9, 13.6 and 20.4 Hz. Since Building A had a longer span slab, the slab response dominated the whole system response. On the other hand, it was also notable that the response of Buildings C and D was dominated by the single mode response of the base isolation layer. In conclusion, Nobata et al. [2-39] suggested that suitable models for the vertical response had to be chosen based on respective building configurations.

In summary, the above findings can be summarized as follows:

- (1) The vertical first natural frequencies ranged from 5.5 to 16 Hz for low- to mid-rise buildings (less than ten stories) including the reinforced concrete and steel braced frame as the superstructure [2-22, 35, 36, 38]. It ranged from 11 to 16 Hz for the common reinforced buildings, while it was reduced to 5 to 10 Hz when the superstructure had longer spans, was constructed from the steel frame, or had a softer base isolation layer. Their range overlapped the plateau range (5 to 10 Hz) of the vertical response spectrum [2-22]. No data about high-rise base-isolated buildings or the buildings, whose isolation layer was composed of sliding bearings, was available.
- (2) The acceleration amplification caused by the base isolation layer ranged from 1.0 to 2.0 [2-39].
- (3) The vertical first natural frequency of the base-isolated buildings became significantly smaller than those estimated based on the assumption of a rigid-body superstructure in some cases, while they were relatively close to each other in other cases. For the former cases, the vertical response had multiple modes, and the vertical first natural frequency may be controlled by that of the slab. In the latter case, the vertical response tended to be dominated by a single mode [2-36, 2-38].
- (4) Models to estimate the vertical responses should be chosen based on respective building configurations [2-39].

To the knowledge of the author, little comprehensive research is available on the contribution of the floor vibration to the vertical response and the amplitude of floor accelerations which may be related to functionality [2-42]. Recommendation for the Design of Base Isolated Buildings [2-6]

suggests that the acceleration amplification of beams with respect to columns becomes 1.1 to 4.0.

### ***2.5.2 Design practice of base-isolated buildings for vertical response***

In Japanese design, vertical ground motions are considered by conducting time history analysis to examine the contribution of the vertical responses to the axial forces exerted into the base isolators. The vertical components of the standard ground motion are typically used with their amplitudes adjusted so that the ratio of vertical to horizontal PGA becomes the same as that of the original records. Typically, the concentrated story mass lump mass model, which is the same as the horizontal analysis, is used. This simplification is supported by Kitamura [2-43]. Kitamura [2-43] indicates that the concentrated story mass model tends to provide a conservative estimation of acceleration responses at columns and axial forces exerted into the base isolators since the existence of floors helps reduce the possibility of the vertical response being dominated by a single mode. This simplification of analytical modeling for vertical response, however, has some concerns and limitations: (1) a shift of natural frequency resulting from the rigid floor assumption may cause significant difference in the response amplitude; (2) contribution of floor vibrations to reduce responses may be minimized when a single mode dominates response; and (3) neglecting the slab contribution to the response amplification may underestimate the force exerted into the isolators. In addition, this model has no capability to assess the floor acceleration responses.

## **2.6 Damage reports of hospitals for past earthquakes**

Medical facilities are required to maintain their service for an emergency period after disasters. Therefore, the adoption of the base isolation system has been popular for such facilities. In this section, notable damages to hospitals (mainly fixed-base buildings) from past earthquakes are summarized.

In Japan, seismic damage reports on medical appliances started from the 1964 Niigata earthquake and the 1968 Tokachi-oki earthquake [2-44]. Later, the importance to maintaining operational condition of hospital buildings and infrastructure were also recognized at the 1978 Miyagi-oki earthquake [2-44]. Their significance was emphasized in the 1995 Kobe earthquakes, which caused more than 6,000 casualties and 43,000 injuries. In the earthquake, hospitals constructed after the implementation of Standard for Earthquake Resistant Design (1980) were verified at least for their structural safety, which was the minimum requirement of Standard Law [2-1, 2]. However, their medical performance significantly deteriorated mostly due to (1) the damage to infrastructure (water, gas, electricity and sewage systems), (2) interruption of communication services, (3) lack of staff, and (4) interior damage to facilities [2-45]. In this dissertation, (4) interior damage is examined further.

Major interior damages can be summarized as follows [4-45 to 48]:

- (1) Residual displacement of nonstructural components such as partition and virus-proof walls of operating rooms, which impeded conducting operations
- (2) Watering by sprinklers
- (3) Fall-off of suspended ceilings, and breaking of window glass
- (4) Damages to plumbing systems
- (5) Overturning and excessive sliding of furniture, medical appliances, and computers
- (6) Scattering of objects fallen from shelves

Even though overturning and excessive sliding of appliances was commonly reported, there were not many medical appliances seriously functionally damaged by physical impact. The major reason for the interruption of the operation of medical appliances was primarily due to the cutting off of the water supply and electricity. Scattered objects such as medicine and medical sheets also interrupted service. In some hospitals, it was reported that objects covered the floor of the acute care unit and service was impossible. It was also reported that clasps supporting shelves anchored to walls did not work. The dislocations of CT scans were also reported up to a maximum distance of 1 m. In addition, many hospital staff suggested in questionnaires that casters were effective at preventing appliances from falling and protecting their contents. However, at the same time, it was also reported that sliding caster-supported appliances caused pounding on walls or other objects, causing damages to both the appliances and their contents.

It is obvious that performance control of equipment is essential to maintain the functionality of the building. Especially for hospitals, these damages would cause severe interruption of medical service, which is mostly required right after earthquakes, and over-turning or excessive dislocation of equipment may cause injury and result in delay of resuming the service. A comprehensive recommendation of seismic design for nonstructural components is provided by AIJ [2-49], and some other supplemental instructions are also available for some medical appliances [2-50]. Among many options, the isolation system is considered one of the most efficient solutions for mitigating the damages of nonstructural components and equipment. Significant reduction of floor accelerations can be expected so that the excessive response of nonstructural components and the initiation of movement of free-standing objects can be prevented if objects have sufficient friction. With these advantages, many hospitals have adopted the base isolation systems. As of 2010, no inferior performance of base-isolated buildings has been reported [2-14, 30, 51, 52]. It was, however, reported that people felt fear during earthquakes ( $PGV=0.47$  m/s) because of large displacement amplitudes lasting nearly for one minute [2-52]. No reduction of vertical vibrations was also a concern even though no critical damage was observed.

## 2.7 Summary and conclusions of Chapter 2

This chapter reviews design practices of base-isolated buildings and research related to the dissertation topic: the verification of seismic performance of base-isolated buildings and the assessment of the capability of base-isolated medical facilities to maintain functionality against large earthquakes. The major contents are summarized as follows:

- (1) The adoption ratio of isolation systems for medical facilities shows high expectations for the performance of the systems.
- (2) Earthquake records of base-isolated buildings show their effectiveness at reducing horizontal acceleration responses. However, their efficiency may deteriorate for the long-period and long-duration ground motion and for the vertical ground motion.
- (3) The vertical first natural frequencies ranged from 5 to 16 Hz for low- to mid-rise buildings including the reinforced concrete and steel braced frame as the superstructure. It ranges from 11 to 16 Hz for the common reinforced buildings with rubber bearings, while it is reduced to 5 to 10 Hz when the superstructure had longer spans, was constructed using the steel frame, or had a softer base isolation layer. Their range is overlapped by the plateau range (5 to 10 Hz) of the vertical response spectrum.
- (4) Damping ratios of the first mode in the vertical direction were estimated as 1% to 2%, if the soil effect was not considered. It increased to 20% once the soil contribution was considered.
- (5) Vertical response of base-isolated buildings may be dominated by a single mode while multiple modes may dominate if the building has longer spans.
- (6) There is little research on the contribution to vertical response amplification by floors and vertical floor accelerations, factors which is thought to be related to functionality.
- (7) Disorder of facility equipment caused great difficulty for the continuity of medical service. Major damages observed were violent movements of appliances and equipment, scattered contents, break down of nonstructural components.
- (8) No significant damage has been reported for base-isolated buildings from past earthquakes.

## REFERENCES

- [2-1] Building Standard Law of Japan, the Ministry of Construction, Japan, 1950 implemented, 2008 latest revised (Japanese).
- [2-2] Enforcement Ordinate of Construction Standard Law, the Ministry of Construction, Japan, 1950 implemented, 2011 latest revised (Japanese).
- [2-3] Structural provisions for building structures – 2007 Edition, the Ministry of Construction and Building Research Institute, 2007 (Japanese).
- [2-4] Otani S. and Kani N., Japanese state of practice in design of seismically isolated buildings, 4<sup>th</sup> US-Japan workshop on performance-based earthquake engineering methodology for reinforced concrete building structures, Toba, Japan 2002.

- [2-5] Design Methods for Response Controlled Structures, Japan Structural Consultants Association, Shokokusha, 2000 (Japanese).
- [2-6] Recommendation for the Design of Base Isolated Buildings, AIJ, 2001 (Japanese).
- [2-7] Pan, P., Zamfirescu, D., Nakashima, M., Nkayasu, N. and Kashiwa, H., Base-isolation design practice in Japan: Introduction to the Post-Kobe approach, Journal of Earthquake Engineering, Vol. 9, No. 1, January 2005, pp.147-171.
- [2-8] James M. Kelly, Base Isolation: Origins and Development, NISEE, website: [nisee.berkeley.edu/lessons/kelly.html](http://nisee.berkeley.edu/lessons/kelly.html) (valid on 04/01/2011).
- [2-9] Tanaka Y., Fukuwa N., Tobita, J., and Mori M., Present Situation of Isolation Building in Japan Base on Establishing a Database on Technical Evaluation Sheet, The 13th Japan Earthquake Engineering Symposium, Japan Association for Earthquake Engineering, 2010, pp.569 – 576 (Japanese).
- [2-10] the Japan Society of Seismic Isolation: [www.jssi.or.jp](http://www.jssi.or.jp)
- [2-11] MENSIN, the Japan Society of Seismic Isolation (Japanese).
- [2-12] Building Letter, the Building Center of Japan (Japanese).
- [2-13] the Books for the Approval of Construction Method, the Ministry of Construction (Japanese).
- [2-14] Higashino M., and Okamoto S., Response Control and Seismic Isolation of Buildings, Taylor & Francis, 2006.
- [2-15] Esteva L., The Mexico Earthquake of September 19, 1985 – Consequences, Lessons, and Impact on Research and Practice, Earthquake Spectra, Vol. 4, No. 3, pp.413-426.
- [2-16] Structural Response and Performance for Long Period Seismic Ground Motions, AIJ, 2007 (Japanese).
- [2-17] The Headquarters for Earthquake Research Promotion: <http://www.jishin.go.jp/main/index.html>
- [2-18] Nakagawa, Y., Kaname, K., Kawabe, H., Irikura, K. Damage prediction of long-period structures during subduction earthquakes-Part 2: Long-period ground motion prediction in the Osaka basin for future Nankai Earthquakes, The 14th World Conference on Earthquake Engineering, Beijing, China, October 2008.
- [2-19] Kawabe, H., Kaname, K., Irikura, K. Damage prediction of long-period structures during subduction earthquakes-Part 1: Long-period ground motion prediction in the Osaka basin for future Nankai Earthquakes, P The 14th World Conference on Earthquake Engineering, Beijing, China, October 2008.
- [2-20] Chung, Y., Nagae, T., Fukuyama, K., Kajiwara, K., Inoue, T., Hitaka, T. and Nakashima, M. Seismic resistance capacity of high-rise buildings subjected to long-period ground motions – E-Defense shaking table test,” The 14th World Conference on Earthquake Engineering, Beijing, China, October 2008.
- [2-21] Chung, Y., Nagae T., Hitaka T., and Nakashima M. Seismic resistance capacity of high-rise buildings subjected to long-period ground motions: E-Defense shaking table test. Journal of Structural Engineering, ASCE, Vol., 2010 (available online).

- [2-22] Bozorgnia Y., Mahin S. A., and Gerald Brady, Vertical Response of Twelve Structures Recorded during the Northridge Earthquake, *Earthquake Spectra*, Vol.41, No.3, 1998.
- [2-23] Bozorgnia Y., Niazi M., and Campbell K. W., 1995b, Characteristics of free-field vertical ground motion during the Northridge earthquake, *Earthquake Spectra*, 11, pp. 515-525.
- [2-24] Bozorgnia Y., Campbell W. K., and Niazi M., Observed Spectral Characteristics of Vertical Ground Motion Recorded During Worldwide Earthquake from 1957 to 1995, *Proceedings of 12<sup>th</sup> World Conference on Earthquake Engineering*, 2000, paper ID: 2671.
- [2-25] Bozorgnia Y., and Niazi M., 1993, Distance scaling and horizontal response spectra of the Loma Prieta earthquake, *Earthquake Engineering and Structural Dynamics*, 22, pp. 695-707.
- [2-26] Ohta T., et al., Distance Attenuation of Strong Ground Motion During the Hyogoken Nanbu Earthquake and Characteristics of Spectra, *Proceedings of the Annual Conference on Architectural Institute of Japan*, August, 1995, paper ID: 21077.
- [2-27] Nigannaduiyb B., and Pecger A., Kiwer-frequency transfer of seismic energy by superficial soil deposits and soft rocks, *Earthquake Engineering and Structural Dynamics*, Vol.12, pp.537-564, 1984.
- [2-28] Nagarajaiah, S. and Sun, X. Response of base-isolated USC hospital building in Northridge earthquake, *Journal of Structural Engineering*, ASCE Vol. 126, No. 10, October, 2000, pp.1177-1186.
- [2-29] Suzuki Y. et al., "Behaviors of a base-isolated building in Kushiro City for the Tokachi-oki Earthquake in 2003 Part 1. Earthquake observation records," *Proceedings of the Annual Conference on Architectural Institute of Japan*, August 2004, pp.279-280 (Japanese).
- [2-30] Terada, H, et al., Record of the Tohachi-oki Earthquake in 2003 at Base Isolated Hospital in Kushiro-City Part 2: Analysis of the record and Questionnaire, *Proceedings of the Annual Conference on Architectural Institute of Japan*, August 2004, pp.271-272 (Japanese).
- [2-31] Kashima T., Fujita H., et al., Seismic Response of the Kushira National Government Building during the 2003 of Tokachi Earthquake Part 1: Analysis of the Strong Motion Record, *Proceedings of the Annual Conference on Architectural Institute of Japan*, August 2004, paper ID: 21133 (Japanese).
- [2-32] Yamada T. et al., "Earthquake Response of Base Isolated Building on Off-Takachi Earthquake 2003," *Proceedings of the Annual Conference on Architectural Institute of Japan*, August 2004, pp.285-286, paper ID: 21143 (Japanese).
- [2-33] Papazoglow A. J. and Elnashai A. S., Analytical and Field Evidence of the Damaging Effect of Vertical Earthquake Ground Motion, *Earthquake Engineering and Structural Dynamics*, Vol.25, pp.1109-1137, 1996.
- [2-34] Papaleontious C. and Roesset J. M., Effect of vertical accelerations on seismic response of frames, in T. Moan et al., (eds), *Structural Dynamics – EURO DYN '93*, Balkema, Rotterdam, 1993, pp. 19 – 26.
- [2-35] Morishita T., Sito Y., Yoshida T., and Ryujin H., Properties of Vibration through



- Earthquake Observation on a Base Isolated Building, Summaries of Technical Papers of Annual Meeting, AIJ, Hokkaido, paper ID: 21147, 2004 (Japanese).
- [2-36] Shinohara T., Uru M., Nakayama K., and Kondo T., Study on the Response Characteristics of Base-Isolated Structures for Vertical Earthquake Motion Part-1 and 2, Proceedings of the Annual Conference on Architectural Institute of Japan, September 1998, paper ID:21320 – 21321 (Japanese).
- [2-37] Kondo T., Uru M., Nakayama K., and, Hashimura H., Study on the Response Characteristics of Base-Isolated Structures for Vertical Earthquake Motion Part-3 to 5, Proceedings of the Annual Conference on Architectural Institute of Japan, September 1999, paper ID:21322 – 21324 (Japanese).
- [2-38] Kondo T., Uru M., and, Hashimura H., Study on the Response Characteristics of Base-Isolated Structures for Vertical Earthquake Motion Part-6 and 8, Proceedings of the Annual Conference on Architectural Institute of Japan, September 2000, paper ID:21267 – 21269 (Japanese).
- [2-39] Nobata A., Teramura A., and Yasui Y., Vertical Resposne Characteristic of Base-Isolated Building Based on Observed Earthquake Records, Report of Obayashi Corporation Technical Research Institute, No.56, 1998, pp.23-28.
- [2-40] Tajimi H., Structural Dynamics, Corona-sha
- [2-41] Konoue N., et al., Vertical Amplitude Characteristic of Building by Studying on Earthquake Observation Records, Proceedings of the Annual Conference on Architectural Institute of Japan, October 1989, paper ID:2169 (Japanese).
- [2-42] Pan P., Safety and Functionality of Base-isolated Building Structures Subjected to Vertical Ground Motions, Ph.D. dissertation, Kyoto University, 2004
- [2-43] Kitamura H., an Observation of Vertical Vibration Response on Base Isolated Buildings, C-1, III, Summaries of Technical Papers of Annual Meeting, AIJ, pp.817-818 (Japanese).
- [2-44] Report of Medical Function Maintenance for Earthquakes in Metropolitan Areas, National Institute of Public Health, 1984 (Japanese).
- [2-45] Kakehi A., Symposium (1) What Happened to Buildings and Equipment of Hospitals at The Great Hanshin-Awaji Earthquake: To Buildings-1, Journal of Medical Instrument, Vol.38, June, 1996, pp.281-288 (Japanese).
- [2-46] Watanabe T., et.al, Symposium: Earthquake and Medical Appliances –How Experiences of Hanshin-Awaji earthquake changes Design–, Japanese Journal of Medical Instrumentation, Vol.67, No.2, 1197, pp.49-81 (Japanese).
- [2-47] Report of Investigation of Hospital Damages for Southern Hyogo Prefecture earthquake, Japan Institute of Healthcare Architecture, March, 1996 (Japanese).
- [2-48] Report of Medical Damages due to Hanshin-Awaji earthquake, National Institute of Public Health, 1995 (Japanese).
- [2-49] Recommendations for Aseismic Design and Construction of Nonstrucutral Elements, Japan Institute of Architecture, 2003 (Japanese).
- [2-50] Current Trend Report of Seismic Application of Medical Radiological Equipment, Japan

Industries Association of Radiological Systems, 1998 (Japanese).

- [2-51] Izawa K., Terada H., and Onishi Y., Record of the Tokachi-oki Earthquake in 2003 at Base Isolated Hospital in Kushira-City. Part 1 Summary of Building and record, Proceedings of the Annual Conference on Architectural Institute of Japan, August, 2004, paper ID: 21135 (Japanese).
- [2-52] Terada H., Izawa K., and Onishi Y., Record of the Tokachi-oki Earthquake in 2003 at Base Isolated Hospital in Kushira-City. Part 2 Analysis of the record and Questionnaire, Proceedings of the Annual Conference on Architectural Institute of Japan, August, 2004, paper ID: 21136 (Japanese).



# CHAPTER 3

## FULL-SCALE SHAKING TABLE TEST OF BASE-ISOLATED MEDICAL FACILITY

### 3.1 Introduction

Full-scale shaking table tests were conducted on the E-Defense shaking table to examine a base-isolated system not only for the structural performance but also for the operability and functionality during strong earthquakes. A specimen was designed as a medical facility, in which major nonstructural components and plumbing system were installed, and rooms were furnished and equipped with medical equipment to simulate an actual medical facility. The series of shaking table tests were divided into two parts: one was the series of shaking conducted from December 2008 to January 2009, and the other was the series of shaking in the fall of 2010. The purpose of the first series of test (designated Test I) was to observe the performance of a base-isolated medical facility against large earthquakes. Equipment inside the specimen was arranged based on the current medical practices. The second series of tests (designated Test II) aimed at the verification of the capability of various countermeasures to improve the performance. The performance of a base-isolated system against vertical motions was also tested in Test II. The same superstructure and base isolation systems were used for both Tests I and II. The room arrangement of medical facilities and the layout of furniture and medical appliances in each room were also basically the same as Tests I and II. A fixed-base system was also tested using the same superstructure to facilitate the comparison between the base-isolated and fixed-base systems. Figure 3-1 shows the overview of this series of full-scaled shaking table tests.

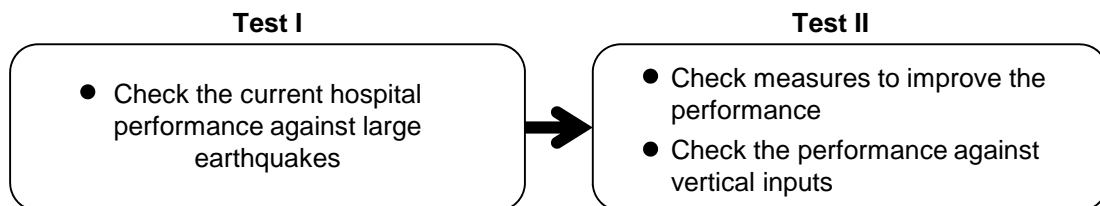


Figure 3-1 Overview of shaking table tests

This chapter summarizes the overview of the full-scale shaking table tests and presents the

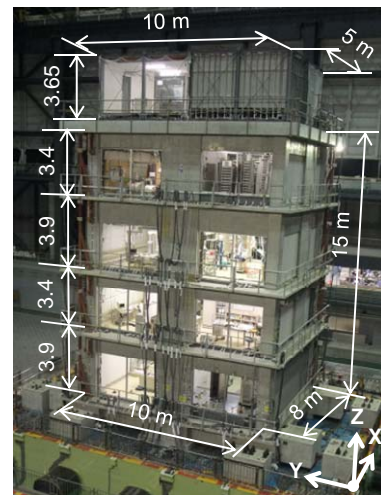
design of the specimen, the arrangement of interiors as a medical facility, measurements, and the types and orders of input ground motions.

### 3.2 Design and fabrication of test specimen

Figure 3-2 shows the base-isolated hospital specimen prepared for the test. The concrete blocks surround the structure, representing the retaining walls. The specimen used for Tests I and II was almost the same with the exception that two rooftop water tanks (132 kN for the total weight) installed on the specimen in Test I were replaced by a penthouse (167 kN) in Test II. This additional room on the roof at Test II (Figure 3-2(b)) was constructed to examine the effectiveness of floor isolation systems, which were adopted to improve the interior performance of the facility of the fixed-base system. Performance of the floor isolation systems are out of scope of this paper. The global axis was assigned so that X-axis was oriented to the transverse direction, Y-axis to the longitudinal direction, and Z-axis to the upward direction, as shown in Figure 3-2(b).



(a) Specimen for Test I (2008 to 2009)



(b) Specimen for Test II (2010)

Figure 3-2 Specimen overview

Because a fixed-base system was also tested using the same superstructure, as shown in Figure 3-3, the superstructure was designed as a fixed-base system following current Japanese seismic code [3-1]. According to Japanese seismic design practice, both the elastic stiffness and maximum strength required for the superstructure are nearly the same for the base-isolated and fixed-base cases when the superstructure is low-rise and made of RC with walls. Therefore, it was justified to use the same superstructure for both cases. A design base shear of 0.3 was adopted, which was 1.5 times the code-specified design base shear of 0.2 in Japan to avoid excessive damage. This was primarily because the design base shear was commonly increased for important facilities. This design scheme

is similar to the concept of the importance factor adopted in IBC (ICC 2003) [3-2]: an importance factor of 1.5 for hospital buildings in California [3-3]. This intentional increase also ensured that excessive damage due to continuous shaking was avoided.

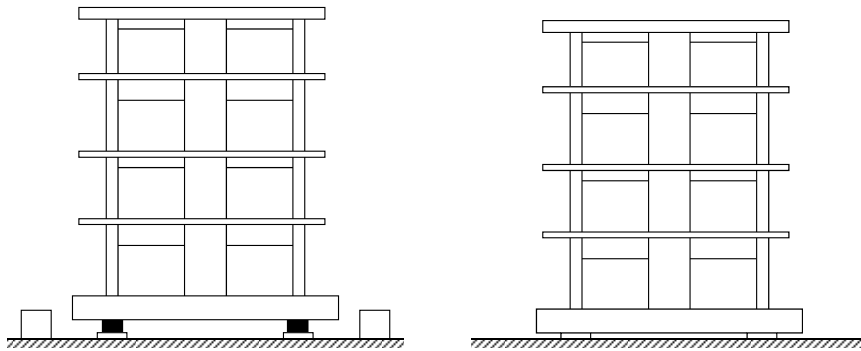
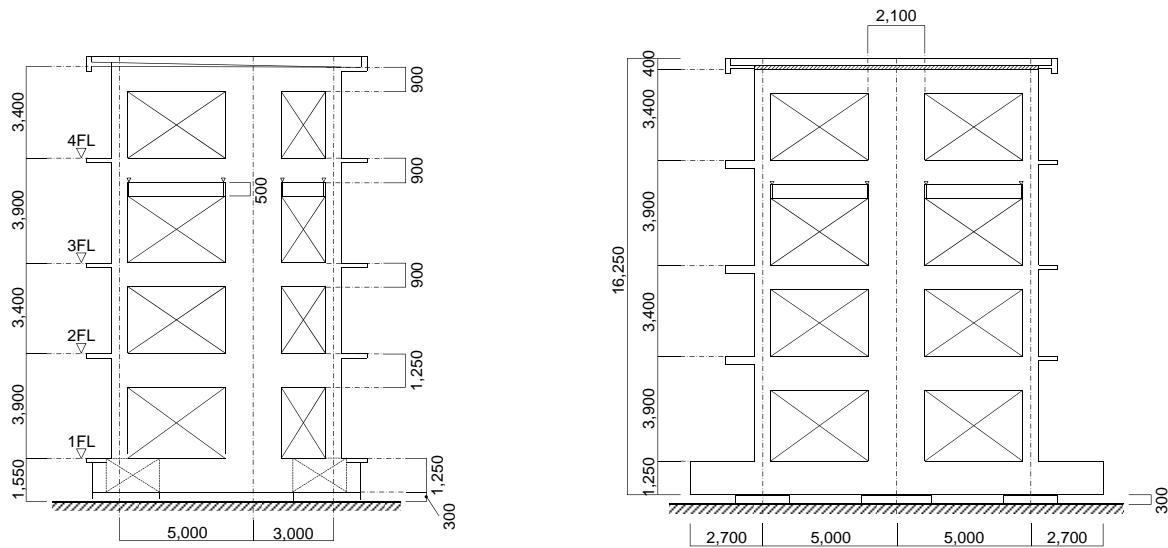
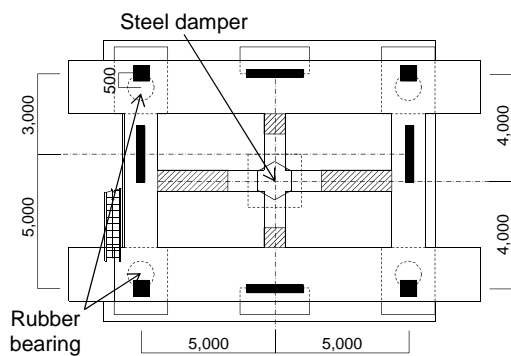


Figure 3-3 Base-isolated system and fixed-base system

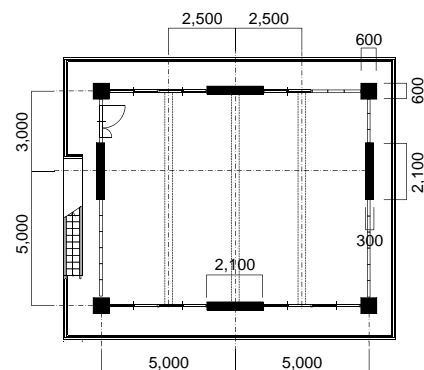


(a) X-Z elevation (fixed-base case)

(b) Y-Z elevation (fixed-base case)



(c) Base floor plan and base isolators arrangement



(d) Second to fourth floor plan

Figure 3-4 Specimen plan

The superstructure was a four-story RC structure with an 8 m by 10 m floor plan and 15 m in total

height. The second and fourth stories had 3.4 m in height, while the height of the first and third stories was increased to 3.9 m since a room for large medical appliances and an operating room, requiring increased space in height, was arranged on these floors. The total weight of the specimen was about 7,450 kN in Test I (7,470 kN in Test II), about 40% of which was the weight of the base floor. This total weight was measured when the specimen was lifted by cranes to set it on the shaking table. Figure 3-4 shows the elevations and plans of the specimen. Columns with sections of 600 mm by 600 mm were arranged at the four corners and shear walls with the section of 2.1 m by 300 mm were arranged in each bay (Figure 3-4 (d)). These shear walls were technically defined as ‘column-shear walls’ since they were designed to sustain both gravity and horizontal loads. The size of beams was 250 mm by 1,250 mm for the second floor and 250 mm by 900 mm for the upper floors (Figure 3-4 (a) and (b)). The second to roof floors had three girders in the transverse direction with the section of 300 mm by 750 mm (Figure 3-4 (d)). The base floor was stiffened with beams large enough to avoid excessive deformation when the specimen was lifted by cranes (Figure 3-5) to set it down on the shaking table. The size of the longitudinal base beams was 1,250 mm by 1,250 mm, that of transverse base beams was 2,000 mm by 1,250 mm, and the size of the girders was 800 mm by 1,250 mm. The thickness of the floor slabs was 150 mm. Concrete with specified concrete strength  $F_C$  of 30 N/mm<sup>2</sup> was used for the base floor, and concrete with specific strength  $F_C$  of 24 N/mm<sup>2</sup> was used for the rest. Reinforcement followed the prescriptions of current Japanese seismic design code [3-1]. The first natural period of the superstructure was 0.24 s in both directions, measured by white noise waves before the series of shaking table test in Test I started.



Figure 3-5 Lifting the specimen to set on the shaking table

### 3.3 Design of base isolation devises

Two isolation systems commonly used in Japan were chosen. One system was rubber bearings combined with dampers, in which the bearings exhibit linear behavior, while the damper dissipates energy by hysteresis. In this test, natural rubber bearings with a parallel U-shaped steel damper (designated as NRB+U hereinafter) were adopted (Figure 3-6(a) and (b)). The other was high-damping rubber bearings (designated as HDRB), in which the bearing itself dissipates energy

(Figure 3-6(c)). The same isolation systems were used for both Tests I and II. The layout of the base isolators is shown in Figure 3-4(c). If the superstructure was assumed to be rigid, the period of NRB+U was estimated as 2.56 s and the period of HDRB was 2.41 s, with respect to the secant stiffness measured for the bearing displacement of 300 mm. The major properties of the base isolators are shown in Table 3-1.



(a) U-shaped steel damper



(b) Natural rubber bearing (NRB)



(c) High damping rubber bearing (HDRB)

Figure 3-6 Base isolation system

Table 3-1 Fundamental mechanical and material properties of base isolation devices

isolator	NRB	HDRB
Diameter [mm]	1,000	750
Sectional area of rubber [mm <sup>2</sup> ]	7,854	4,416
Height of devices [mm]	565	376.9
Thickness of rubber [mm]	285	200
Total height of steel plate	4.4	3.1
Primary shape factor $S_1^{(*1)}$	37.31	36.75
Secondary shape factor $S_2^{(*2)}$	3.51	3.75
Shear modulus of rubber	0.29	0.62
Shear stiffness [kN/m]	$0.81 \times 10^3$	$1.37 \times 10^3^{(*3)}$
Equivalent damping ratio		$0.24^{(*3)}$
Vertical modulus [kN/m]	$2,200 \times 10^3$	$3,090 \times 10^3$

U-shaped steel damper	
Number of rods	6
Thickness of rods [mm]	40
Yield strength [kN]	348
Yield displacement [mm]	27.9
Initial stiffness [kN/m]	12,500
Second stiffness [kN/m]	216

(\*1) Primary shape factor defined as sectional area divided by circumferential area of each rubber layer

(\*2) Secondary shape factor defined as diameter divided by total height of rubber

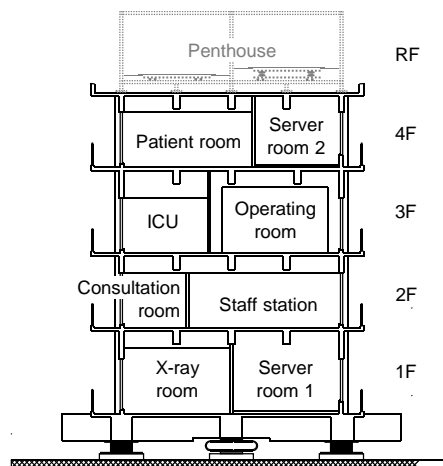
(\*3) Shear stiffness and equivalent damping ratio estimated for 200 mm displacement



### 3.4 Arrangement of furniture and medical equipment

The functions of respective floors were arranged following the current design practice: rooms equipped with heavy medical appliances, such as CT scan, were located in lower floors, while rooms that must be virus-free, such as an operating room and an intensive care unit (ICU), were arranged in upper floors. After consultation with designers experienced in hospital planning, the following arrangements were adopted in this test: an X-ray room and a server room were arranged in the first floor; a consultation room, a staff station, and a dialysis room were arranged in the second floor; an ICU and an operating room were arranged in the third floor; and a patient room and another server room were arranged in the fourth (top) floor. Figure 3-7 shows the room arrangement adopted in the test.

All furniture items, medical appliances, and service equipment units were placed following actual hospital practice. Figure 3-8 to 3-9 show the arrangement of items for all floors when Test II was conducted. Nonstructural components were also installed, including a virus-proof wall of the operating room, plumbing (Figure 3-8(a-2)), medical plumbing, sprinklers, lights, air conditioner, and hanging-type sliding doors. Two rooftop tanks were installed and filled with water to 2/3 of their capacity for Test I: they were replaced by a penthouse (Figure 3-2) in Test II. All rooms were furnished and equipped with medical appliances as shown in photos of Figure 3-8 and 3-9. In the figures, furniture and medical appliances drawn by dotted lines were those newly added in Test II. Bars, which were also drawn in dotted lines, were attached to walls as a measure to improve the performance of the medical facility in Test II. A notable characteristic of furniture and medical equipment used in hospitals is that most of them are supported by casters at the bottom so that they are mobile. Whether the casters of each appliance were locked or unlocked was determined following the advice of medical experts. Details of furniture and appliances, and their setting condition are described in Chapter 6. Some appliances, i.e., dialyzers, a high-oxygen pressure unit, and an IT network that connected the server rooms arranged in different floors, were tested under operational conditions. In both Test I and II, the power cords of most appliances were not plugged in.



(note) A penthouse on the roof was installed in Test II

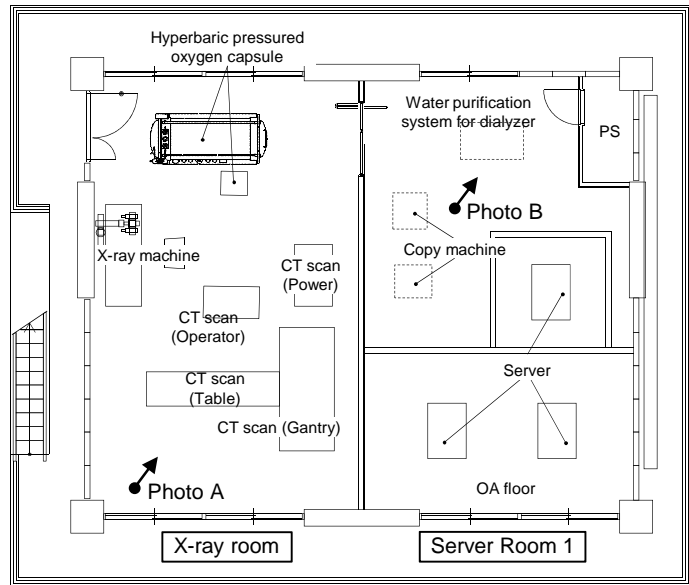
Figure 3-7 Room arrangement as a medical facility



(a-1) X-ray room (Photo A)



(a-2) Plumbing (Photo B)



(a-3) First floor plan

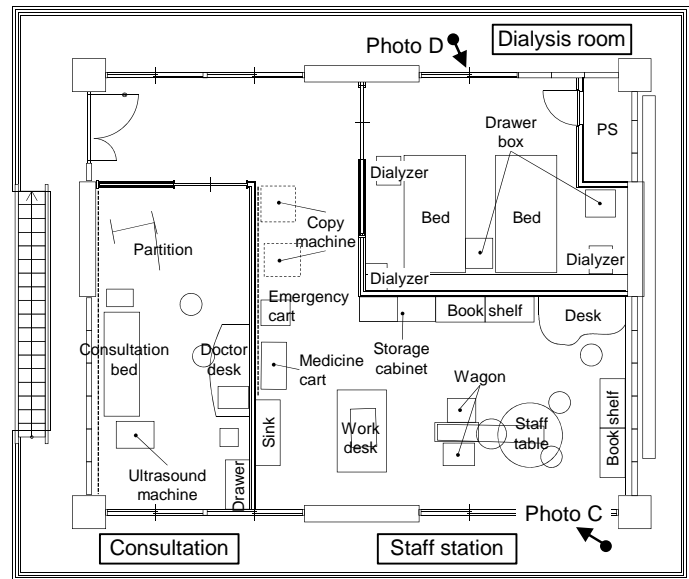
(a) First floor



(b-1) Staff room (Photo C)



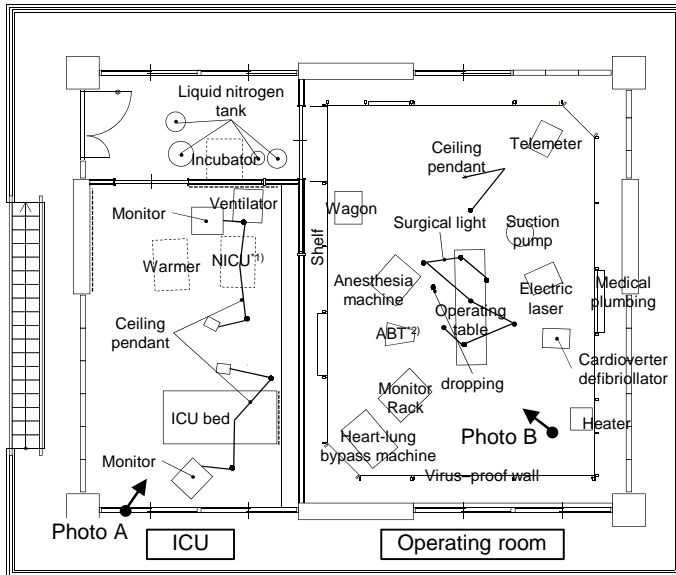
(b-2) Dialysis room (Photo D)



(b-3) Second floor plan

(b) Second floor

Figure 3-8 Arrangement of furniture and medical equipment (First and second floors)



(\*1) NICU: Neotatal Intensive Care Unit  
 (\*2) ABT: Autologous blood transfusion machine

(a-1) Third floor plan

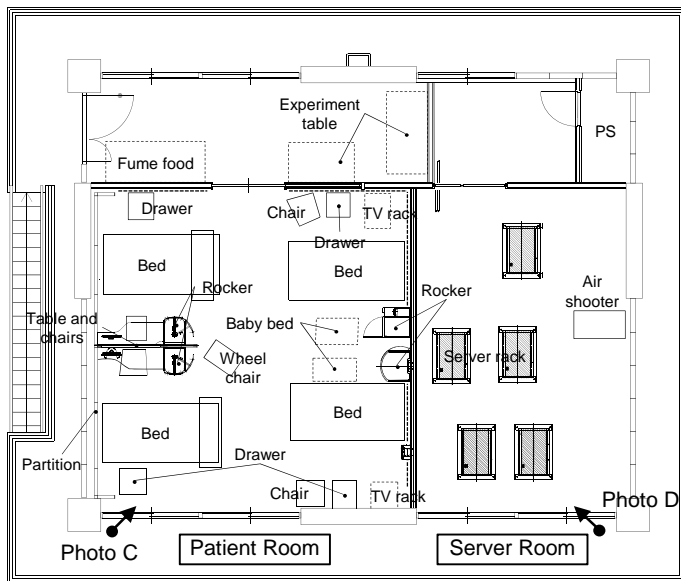
(a) Third floor



(a-2) ICU (Photo A)



(a-3) Operating room (Photo B)



(b-1) Fourth floor plan

(b) Fourth floor



(b-2) Patient room (Photo C)



(b-3) Server room (Photo D)

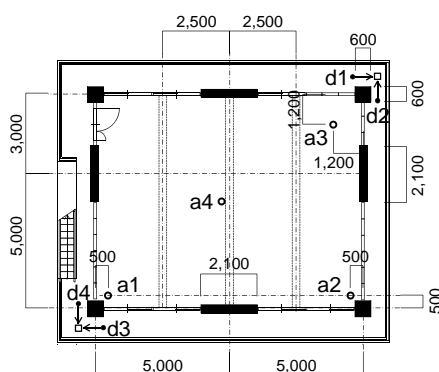
Figure 3-9 Arrangement of furniture and medical equipment (Third and fourth floors)

### 3.5 Measurement

A total of 700 channels were used for measuring the responses; 170 channels for measuring the structural responses, such as the displacements of the base isolation layers and inter-story drifts, and 530 channels (mostly accelerometers) for examining the responses of furniture items and medical appliances. In addition, about 50 CCD (Charge Coupled Device) cameras were installed inside the rooms to record the furniture's behavior in the rooms. The number of channels was increased in Test II since about 50 additional accelerometers were installed to measure the vertical responses of the floor and appliances.

The location of installed accelerometers and laser transducers are shown in Figure 3-10(a). a1 to a4 are accelerometers to measure floor accelerations, and d1 to d4 are to measure story displacements. Story displacements were obtained by measuring the difference in displacement between two points: one belonging to the concerned floor and the other belonging to the floor upper to the concerned floor. Steel frames were constructed at two diagonal corners of each floor (Figure 3-10(b)) to settle the laser transducers and their targets. This measurement method was able to estimate only the element displacement of the vertical components but the story displacement, because this method had no capability to consider the contribution of the column end rotation to the story displacement [3-4]. Strain gauges were also attached to rebar of the walls, columns and beams located the first and second floors. For all shakings, response data are measured in units of 1,000 Hz.

The residual conditions in the inside of the rooms were recorded after every shaking. Several research members, some of them belonging to the providers of medical appliances and furniture installed in the specimen, checked the damages to major nonstructural components, plumbing, sprinkler and other equipment in accordance with the check sheet, as shown in Figure 3-11(a). The residual displacements of all furniture and medical appliances were also plotted (Figure 3-11(b)). After data collection, all appliances and items were returned to their respective initial positions.



(a) location of measurements



(b) Frame to measure story displacements

Figure 3-10 Arrangement of measurements to record structural responses



in Japanese design practice for the level 2 design in which limited damage is accepted. The vertical motion of El Centro was scaled up to 1.5 times

so that the corresponding PGV became 0.14 m/s. JMA Kobe is one of the strongest records obtained from the 1995 Kobe earthquake, with PGV scaled at 0.60 m/s, 0.64 m/s and 0.31 m/s in the NS, EW and UD directions, respectively. This was 80% that of the original record in the amplitude. This scaling was adopted intentionally to avoid excessive structural damage so that the test specimen could be used for many times of shaking. Yokohama is the synthesized ground motion obtained by the simulation of a hypothetical Kanto earthquake, which is expected to hit the Japan's capital, Tokyo. This ground motion is also classified as the near-fault or short-period ground motion. Nishishinjuku and Sanrizuka are modified ground motions, which recorded at Nishishinjuku (Tokyo) and Sanrizuka (Chiba) when Ibaraki-ken-oki earthquake (M5.0) occurred in May, 2008, by scaling up the moment magnitude to M7.3. The Ibaraki-ken-oki earthquake occurred on an ocean ridge of the coast of Ibaraki, and it reached Sanrizuka and Nishishinjuku, located about 110 km and 160 km away from the epicenter, as the long-period and long-duration ground motions. Sanrizuka is characterized by a long pulse with a dominant period of 1.0 s at the beginning of the wave. Sannomaru is one of the strongest synthesized long-period and long-duration ground motions. Its dominant frequencies are 2.5 to 3.0 s, which match the natural periods of the base-isolated buildings, i.e., 2.4 to 2.6 s. The direction of input ground motions were so oriented that the NS component corresponded to the longitudinal direction (Y direction), and the EW component corresponded to the transverse direction (X direction).

Among all motions, Yokohama and Sannomaru do not have the vertical motion (Figure 3-12). El Centro and JMA Kobe were adopted to examine the vertical response of structures and building's contents.

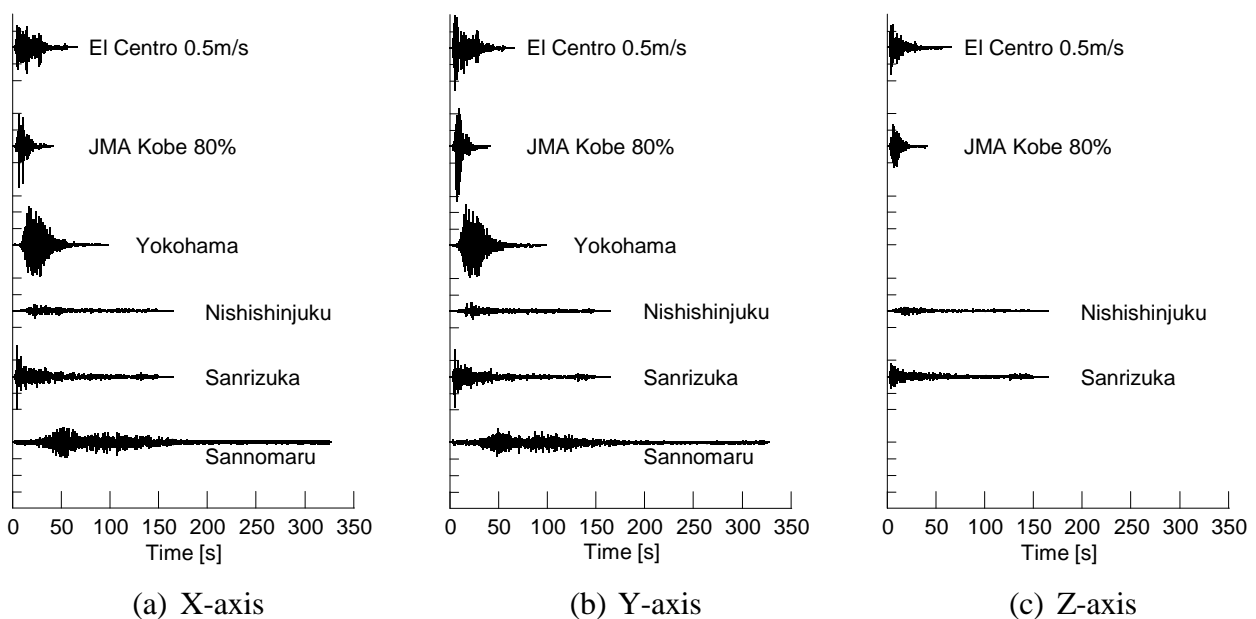
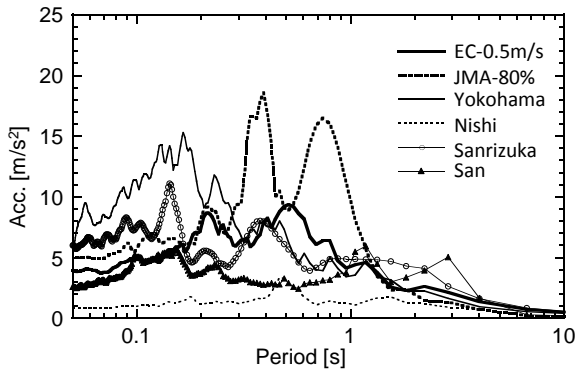
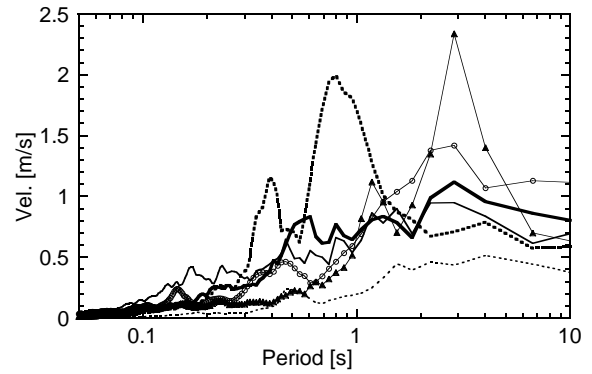


Figure 3-12 Acceleration time history of input ground motions

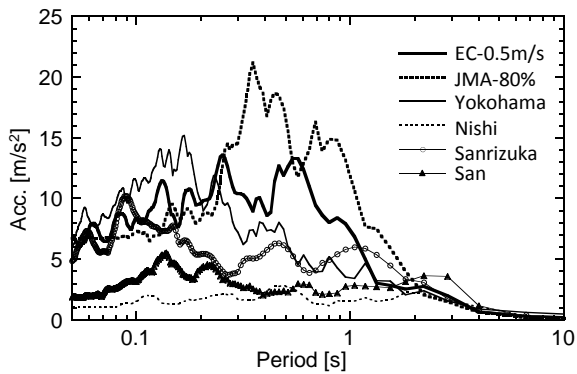


(a-1) Acceleration response spectra

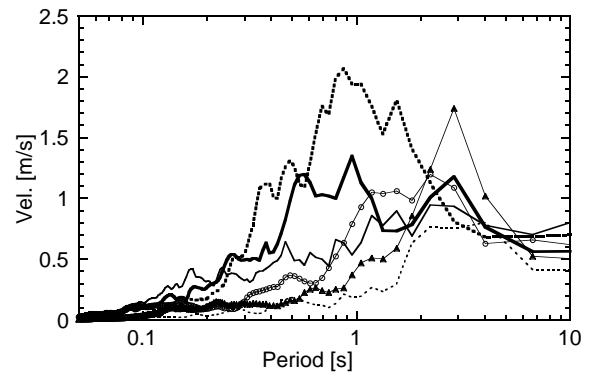


(a-2) Velocity response spectra

(a) X-axis

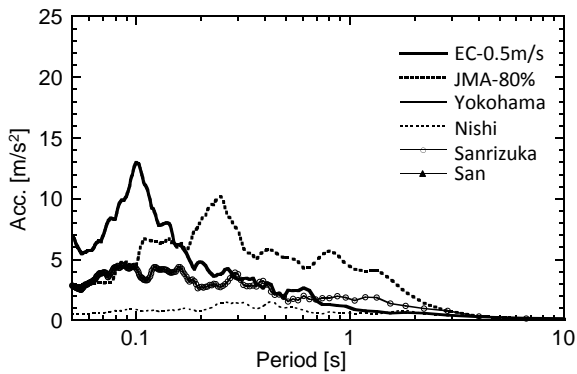


(b-1) Acceleration response spectra

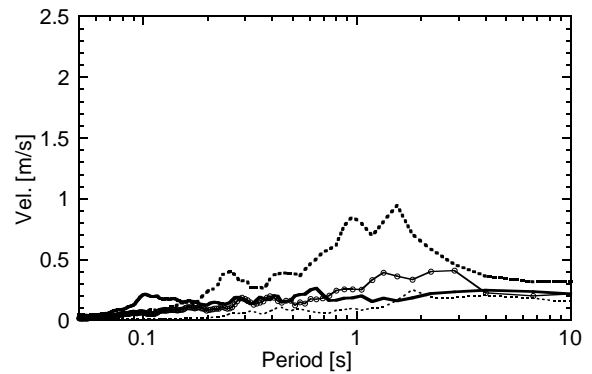


(b-2) Velocity response spectra

(b) Y-axis



(c-1) Acceleration response spectra



(c-2) Velocity response spectra

(c) Z-axis

Figure 3-13 Response spectra of input ground motions

Table 3-2 PGA and PGV of input ground motions

Direction	ground motion types	PGA [ $\text{m/s}^2$ ]			PGV [ $\text{m/s}$ ]		
		X-axis	Y-axis	Z-axis	X-axis	Y-axis	Z-axis
El Centro	short-period	3.14	5.10	3.08	0.57	0.48	0.14
JMA Kobe	short-period	4.94	6.54	2.66	0.61	0.64	0.31
Yokohama	short-period	4.67	4.87		0.61	0.49	
Nishishinjuku	long-period	0.79	1.02	0.49	0.27	0.3	0.07
Sanrizuka	long-period	4.02	3.69	1.52	0.76	0.48	0.17
Sannomaru	long-period	1.86	1.66		0.49	0.49	

### 3.7 Loading program

Table 3-3 shows the shaking order of each series of shakings. All tests were conducted on the E-Defense shaking table, which has a table dimension of 15 m by 20 m and can accommodate a specimen up to 12 MN in weight. Details of this facility are presented elsewhere [3-5, 3-6]. The series of the tests began with the two base-isolated systems, NRB+U and HDRB, and then the superstructure was securely anchored to the shaking table and the fixed-base system was tested. Eleven major shakings were conducted in Test I, and twenty-two shakings in Test II. Both the near-fault and long-period ground motions were input to all the types of systems and for Tests I and II. The same ground motions but different combinations of components such as XY, Z and XYZ were input in Test II to examine the effect of vertical inputs.

A white noise wave was input to measure the natural frequency of the specimen at each stage. In Test I, a Gaussian white noise wave was designed as a wave with a pass band of 0.2 to 30, a root mean square (RMS) amplitude of  $0.14 \text{ m/s}^2$  in the X direction and  $0.15 \text{ m/s}^2$  in the Y direction and the duration of 250 s. This white noise wave was input separately to each horizontal direction to measure the shift of the horizontal natural frequency of the specimen when the fixed-base system was tested. No white noise was input to the base-isolated systems in Test I. A white noise wave used in Test II was a Gaussian white noise wave with a pass band of 0.2 to 50, a root mean square (RMS) amplitude of  $0.13 \text{ m/s}^2$ , and the duration of 60 s. In test II, white noise was input to all three directions including the vertical direction for all systems. The input amplitude was doubled for the fixed-base system to obtain clearer response amplifications in Test II. Table 3-3 shows when and in which directions each white noise was input, with the inputs numbered thus: (I-i) to (I-v) for Test I and (II-i) to (II-x) for Test II.



Table 3-3 Sequence of shaking table test and adopted input ground motion

Type of Structure	Shaking Number	Ground Motion	Directions	Max. Acc. [m/s <sup>2</sup> ]			
				X	Y	Z	
Shaking Table Test #1 (December, 2008 - January, 2009)							
Base-isolated NRB+U	1	El Centro <sup>(*1)</sup>	X,Y	3.14	5.11		
	2	JMA Kobe <sup>(*2)</sup>	X,Y,Z	4.93	6.54	2.66	
	3	Sannomaru	X,Y	1.86	1.66		
Base-isolated HDRB	4	El Centro	X,Y	3.14	5.11		
	5	JMA Kobe	X,Y	4.93	6.54		
	6	JMA Kobe	X,Y,Z	4.93	6.54	2.66	White noise Number
Fixed-base	7	Sannomaru	X,Y	1.86	1.66		← (I-i) x, y
	8	Sannomaru	X,Y	1.86	1.66		← (I-ii) x, y
	9	Yohohama	X,Y	4.79	4.99		← (I-iii) x, y
	10	El Centro	X,Y	3.14	5.11		← (I-iv) x, y
	11	JMA Kobe	X,Y,Z	4.93	6.54	2.66	← (I-v) x, y
Shaking Table Test #2 (September - October, 2010)							
Base-isolated NRB+U	1	JMA Kobe	Z			2.66	← (II-i) x, y, z
	2	El Centro	X,Y	3.14	5.11		
	3	JMA Kobe	X,Y,Z	4.93	6.54	2.66	
	4	Sanrizuka	X,Y,Z	4.02	3.70	1.52	
	5	JMA Kobe	X,Y	4.93	6.54		
	6	Sannomaru	X,Y	1.86	1.66		
Base-isolated HDRB	7	JMA Kobe	Z			2.66	← (II-ii) x, y, z
	8	Yohohama	X,Y	4.79	4.99		
	9	El Centro	X,Y	3.14	5.11		
	10	El Centro	X,Y,Z	3.14	5.11	3.08	
	11	JMA Kobe	X,Y	4.93	6.54		
	12	JMA Kobe	X,Y,Z	4.93	6.54	2.66	
	13	Nishishinjuku	X,Y,Z	0.79	1.02	0.43	
	14	Sannomaru <sup>(*3)</sup>	X,Y	1.49	1.33		← (II-iii) x, y, z
Fixed-base	15	Sannomaru	X,Y	1.86	1.66		← (II-iv) x, y, z
	16	Sanrizuka	X,Y,Z	4.02	3.70	1.52	← (II-v) x, y, z
	17	Yokohama	X,Y	4.79	4.99		← (II-vi) x, y, z
	18	El Centro	X,Y	3.14	5.11		← (II-vii) x, y, z
	19	JMA Kobe	Z			2.66	
	20	JMA Kobe	X,Y,Z	4.93	6.54	2.66	← (II-viii) x, y, z
	21	JMA Kobe <sup>(*4)</sup>	X,Y,Z	1.73	2.29	0.93	← (II-ix) x, y, z
	22	JMA Kobe	X,Y	4.93	6.54		← (II-x) x, y, z

(\*1) El Centro with PGV = 0.5 m/s

(\*2) JMA Kobe with 80% in scaled magnitude

(\*3) Sannomaru with 80% in scaled magnitude

(\*4) JMA Kobe with PGV = 0.2 m/s (0.28% in scaled magnitude)

## 3.8 Overview of shaking table tests

### 3.8.1 Natural frequency and damping ratio

Since the same specimen was shaken many times, including eleven major shakings as the fixed-base system, the stiffness of the specimen was reduced significantly from the initial condition. The magnitude of the stiffness reduction was kept measuring as the shift of the natural frequency by white noise wave. Table 3-4 shows the sequence of the natural frequencies for three directions of the superstructure at each stage throughout the series of shaking table tests from the beginning of Test I toward the end of the Test II (Table 3-3). In the vertical direction, the lowest two dominant frequencies are listed in the table. The vertical damping ratios are also shown in Table 3-4. The natural frequencies of the first to third modes for the horizontal directions and the first mode for the vertical direction are plotted in Figure 3-14 (a), which converted into the residual ratios to the initial natural frequencies in Figure 3-14 (b). The first vertical natural frequencies of NRB+U and HDRB are also plotted in the figure. No uniaxial white noise wave was input to the base-isolated system, nor to the vertical direction throughout Test I. To estimate the vertical natural frequency and damping ratio of the specimen in Test I, six-axial random waves, which were always input before major shakings to optimize the shaking table control, were substantially used. Those vertical responses yielded fairly smooth response amplifications enough to estimate reasonable dynamic properties for base-isolated systems. For a fixed-base system, however, the response amplifications obtained from those random waves was too random to obtain a certain values. Therefore, the center values of 17 Hz with the error width of 1~2 Hz of the first peak was adopted as the initial natural frequency of the first mode in the vertical direction. The response amplifications obtained by six-axial random wave in Test I are shown in Figure 3-15 for the base-isolated and fixed-base systems. The difference in the order for the estimated natural frequencies between tests I ( $10^{-2}$ ) and II ( $10^{-1}$ ) is because of the difference in the time duration of the white noise wave used in both test series, 250 s for Test I while 60 s for Test II.

The first natural period of the superstructure was 0.24 s (4.2 Hz) in both directions when Test I started. The natural period increased significantly when the shaking table tests were conducted for the fixed-base system. Cracks apparently increased after Yokohama for the fixed-base system in Test I (white noise (I-iii)), which also can be seen in Figure 3-14(a) as the shift of the horizontal natural frequencies. Some rebars also yielded at this moment. At the end of Test I, most major components at lower stories had minor cracks with the width of less than 0.2 mm with some exception propagated from the top end of the slits inserted at third floor beam's ends (Figure 3-4 (a) and (b)), where it reached more than 1 mm. After the completion of Test I, the overall damage had not progressed to a fatal level. Some major cracks were filled with epoxy, and the deformed U-shaped steel damper was replaced before Test II. When Test II started, the first natural period of the superstructure was elongated by 1.5 to 1.6 times from the initial period, which became 0.39 s (2.1 Hz) in the transverse direction (X axis) and 0.35 s (2.5 Hz) in the longitudinal direction (Y axis). Damages were also propagated throughout Test II. Some small concrete tips started to drop when

El Centro XY was input (before white noise (II-vii)) in Test II. After all of the shaking finished, no components were in fatal condition but some cracks reached a few mm in width. The final natural periods were 0.60 s (1.7 Hz) and 0.57 s (1.8 Hz) for the X and Y-axis, which were 2.5 and 2.4 times longer than the initial values. Even though significant large elongations in the natural periods were observed, the maximum drift of the first floor remained 0.62% so that the specimen tolerated all shakings without any critical damage.

Table 3-4 Natural frequencies and damping ratios measured by a white noise wave

Test #	system	axis mode	X				Y				Z			
			1	2	3	4	1	2	3	4	1	2	$h_1$	$h_2$
Test I	NRB+U										11.6 <sup>(*)</sup>	23.7 <sup>(*)</sup>	4.2% <sup>(*)</sup>	
	HDRB										12.1 <sup>(*)</sup>	24.0 <sup>(*)</sup>	3.0% <sup>(*)</sup>	
	Fixed-base	(i)	4.20	16.60	30.76	41.80	4.20	15.82	31.15	42.38	17.0 <sup>(*)</sup>	27.5 <sup>(*)</sup>		
		(ii)	4.10	16.50	30.47	41.50	4.10	15.63	30.66	41.41				
		(iii)	3.32	13.72	27.03	36.08	3.49	13.65	25.88	37.84				
		(iv)	3.20	13.13	24.46	34.47	3.17	12.82	24.59	35.72				
(v)	2.71	9.91	21.36	30.96	2.71	9.91	21.61	32.25						
Test II	NRB+U	(i)	2.5				2.8				10.6	19.2	2.5%	3.0%
	HDRB	(ii)	2.4				2.6				10.7	19.4	2.9%	3.9%
	Fixed-base	(iii)	2.1	8.4	16.0	23.6	2.5	10.9	22.4	27.3	13.6	19.6	6.0%	8.0%
		(iv)	2.1	8.1	16.1	23.0	2.3	9.8	21.1	26.4	13.6	18.9	4.8%	5.0%
		(v)	2.1	7.8	16.0	22.4	2.2	9.7	20.7	26.4	13.3	18.8	4.0%	4.5%
		(vi)	2.0	7.5	15.1	22.4	2.1	9.0	19.8	25.7	13.5	18.8	3.0%	4.0%
		(vii)	1.8	6.9	14.2	20.9	1.9	7.4	14.7	23.1	12.5	18.0	6.0%	4.5%
		(viii)	1.7	6.6	12.9	19.8	1.8	7.0	14.7	22.4	11.0	17.7	4.0%	5.0%
		(ix)	1.7	6.5	12.9	19.4	1.8	6.8	14.3	22.4	11.4	17.7	6.0%	3.5%
		(x)	1.7	6.5	12.9	19.8	1.8	6.8	14.3	22.4	11.5	17.7	7.5%	5.0%

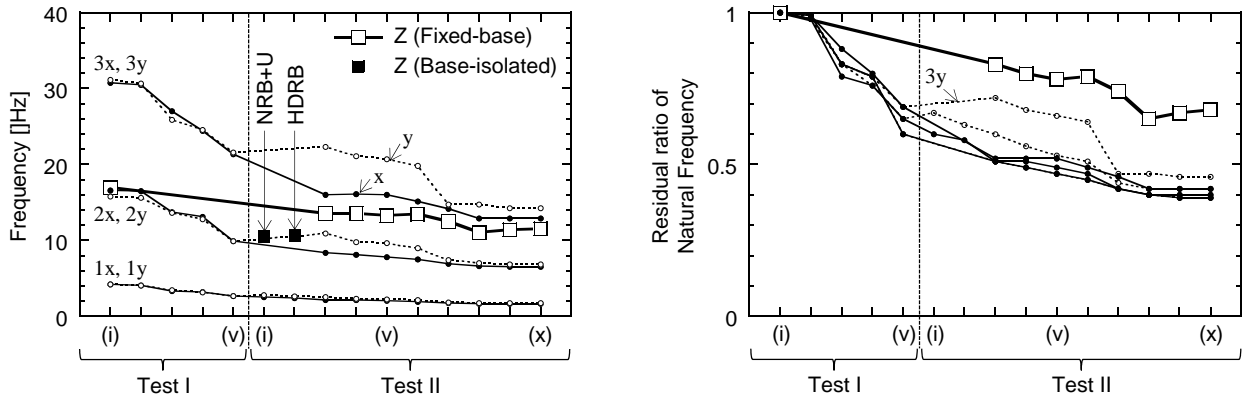
(\*1) Values estimated by six-axial random waves.

(note) Damping ratios with parenthesis are uncertain estimated values.

From Table 3-4 and Figure 3-14, the following findings are notable for the natural frequency sequence of the superstructure throughout Test I and II:

- (1) The residual percentage of the natural frequencies in X and Y-axes, with respect to every one of the experienced ground motions, were similar to each other for all modes.
- (2) The overall declining sequence of the natural frequencies in horizontal directions and vertical direction were similar but with a different reduction ratio. These ratio of the end of the shaking table tests (white noise number II-x) to the initial (white noise number I-i) was 0.4 ~ 0.44 for horizontal directions, while it increased to 0.6 ~ 0.63 for the vertical direction. The reason why the reduction ratio in the vertical natural frequency remained lower than in the horizontal natural frequencies may be because of the difference in the contribution of columns' damage to the measured natural frequencies. The columns had already been pressured axially

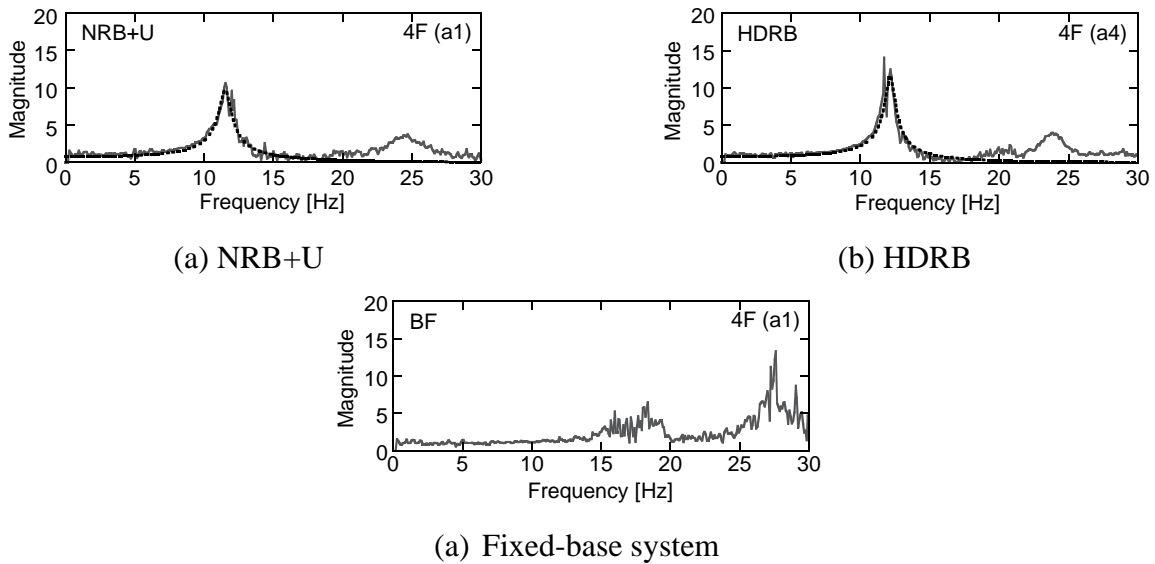
by self-weight, maybe canceling the contribution of column damages at some extent to reduce the vertical natural frequency, considering that the amplitude of a white noise wave was low. The maximum input acceleration was less than  $1.0 \text{ m/s}^2$ .



(a) Transient of the natural frequencies

(b) Residual ratio of the natural frequencies

Figure 3-14 Transient of the natural frequencies of the superstructure



(a) NRB+U

(b) HDRB

(c) Fixed-base system

Figure 3-15 Transfer function of the fourth floor responses recorded in Test I

### 3.8.2 Maximum floor responses

Table 3-5 and 3-6 summarizes the maximum absolute floor acceleration, and velocities recorded at each floor, and the maximum displacements of the base isolation layer measured in Tests I and II, respectively. Responses for all types of structural systems are shown in the tables: the base-isolated systems (NRB+U and HDRB) and the fixed-base system. Since the results of Test I were selected particularly to observe the horizontal responses, these for the near-fault ground motion and the long-period long-duration ground motion are summarized in Table 3-5. JMA Kobe XYZ was selected as the former, and Sannomaru as the latter. The results of Test II were used to examine the vertical responses so that the responses for the ground motions with vertical

motions are selected to be listed in Table 3-6, which are JMA Kobe XYZ, JMA Kobe Z, and El Centro XYZ. All recorded acceleration data was filtered by 50 Hz lowpass filter by Fourier transformation. The locations of accelerometers attached to the respective floors, which is the same as Figure 3-10(a), are re-plotted in Figure 3-16. Three directional accelerations were measured at all four locations. The horizontal acceleration recorded at **a1** and **a3** were averaged to obtain the X and Y axes responses of the floors. Vertical responses recorded at the corner and the center are chosen to observe the out-of-plane vibration of the floors: **a1**, which was located close to the column, and **a4**, which was located close to the center. The velocities listed in tables were estimated by the integration of accelerations with a high-pass filter of 0.05 Hz. In Table 3-6, columns titled 'Z1' and 'Z4' correspond to the vertical responses recorded at **a1** and **a4**, respectively.

Table 3-5 Maximum responses (Test I)

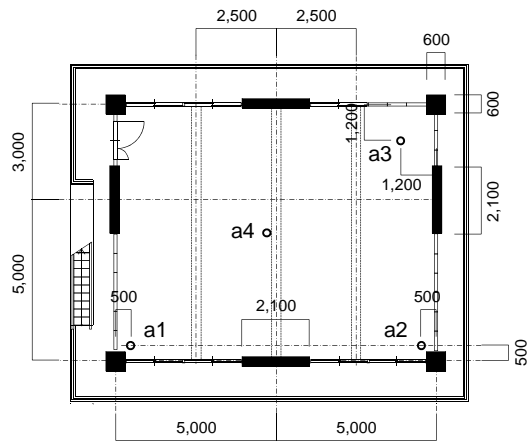


Figure 3-16 Location of accelerometers measuring floor responses

wave	JMA Kobe XYZ (I-2)			Sannomaru (I-3)			
	direction	X	Y	Z	X	Y	Z
Base-isolated System (NRB+U)	Abs. Acc [m/s <sup>2</sup> ]						
	RF	2.38	2.61	4.82	2.33	2.03	0.17
	4F	2.00	2.45	5.07	2.54	2.10	0.25
	3F	1.27	1.79	4.93	2.48	2.08	0.12
	2F	1.50	1.98	4.78	2.46	2.04	0.12
	1F	1.70	2.15	4.60	2.44	2.03	0.12
	T	5.88	6.80	4.82	2.09	1.61	0.29
Base-isolated System (HDRB)	Abs. Vel. [m/s]						
	RF	0.40	0.64	0.29	1.03	0.82	0.02
	4F	0.41	0.67	0.32	1.10	0.86	0.02
	3F	0.40	0.66	0.31	1.09	0.86	0.01
	2F	0.39	0.65	0.31	1.08	0.85	0.01
	1F	0.38	0.64	0.30	1.07	0.85	0.01
	T	0.57	0.60	0.28	0.44	0.45	0.00
mm BI	112	206		409	321		
wave	JMA Kobe XYZ (I-6)			Sannomaru (I-7)			
	direction	X	Y	Z	X	Y	Z
Base-isolated System (HDRB)	Abs. Acc [m/s <sup>2</sup> ]						
	RF	2.02	2.47	6.03	5.39	1.97	2.68
	4F	1.86	2.24	6.26	5.06	2.05	7.41
	3F	1.46	1.84	5.74	5.07	2.05	2.08
	2F	1.40	1.94	5.36	5.41	2.03	1.49
	1F	1.49	1.99	5.06	6.03	2.03	1.78
	T	6.00	6.96	6.03	2.00	1.62	1.07
Base-isolated System (HDRB)	Abs. Vel. [m/s]						
	RF	0.35	0.54	0.28	0.87	0.71	0.02
	4F	0.36	0.57	0.30	0.89	0.75	0.05
	3F	0.35	0.56	0.30	0.86	0.75	0.02
	2F	0.33	0.56	0.30	0.87	0.74	0.01
	1F	0.33	0.56	0.29	0.89	0.74	0.02
	T	0.61	0.60	0.29	0.44	0.45	0.01
mm BI	104	187		284	264		
wave	JMA Kobe XYZ (I-11)			Sannomaru (I-8)			
	direction	X	Y	Z	X	Y	Z
Fixed-base System	Abs. Acc [m/s <sup>2</sup> ]						
	RF	15.56	19.71	13.10	2.52	2.54	0.21
	4F	13.43	13.81	13.02	2.32	2.14	0.48
	3F	15.37	21.49	10.47	1.88	1.65	0.16
	2F	13.04	20.32	6.83	1.83	1.51	0.13
	1F	11.05	17.99	5.37	1.98	1.43	0.12
	T	7.50	11.25	13.10	1.93	1.43	0.10
Fixed-base System	Abs. Vel. [m/s]						
	RF	1.07	1.11	0.38	0.45	0.43	0.01
	4F	1.01	1.08	6.81	0.47	0.45	0.02
	3F	0.72	0.92	0.35	0.46	0.45	0.00
	2F	0.57	0.75	0.32	0.45	0.44	0.01
	1F	0.57	0.73	0.29	0.45	0.44	0.00
	T	0.56	0.60	0.29	0.44	0.45	0.00

Table 3-6 Maximum responses (Test II)

	wave	JMA Kobe Z (II-1)				JMA Kobe XYZ (II-3)				El Centro XYZ				
	direction	X	Y	Z1 <sup>(*1)</sup>	Z4 <sup>(*2)</sup>	X	Y	Z1	Z4	X	Y	Z1	Z4	
Base-isolated System (NRB+U)	Abs. Acc [m/s <sup>2</sup> ]	RF	-	-	- <sup>(*3)</sup>	9.14	3.17	3.48	8.05	22.36				
		4F	0.58	0.48	4.03	8.51	1.89	2.58	6.57	18.64				
		3F	0.24	0.29	4.02	7.14	1.59	2.67	6.59	14.51				
		2F	0.45	0.35	3.87	5.79	1.45	2.45	5.90	11.43				
		1F	0.38	0.31	3.75	4.84	1.64	2.05	5.49	11.50				
		T	0.25	0.17	3.37		6.20	7.38	3.69					
		RF	-	-	- <sup>(*3)</sup>	0.35	0.45	0.74	0.31	0.38				
		4F	0.03	0.01	0.32	0.35	0.43	0.71	0.31	0.37				
		3F	0.02	0.01	0.32	0.35	0.42	0.68	0.31	0.36				
		2F	0.02	0.01	0.32	0.35	0.39	0.65	0.30	0.33				
		1F	0.03	0.01	0.32	0.32	0.39	0.64	0.30	0.31				
		T	0.01	0.00	0.30		0.56	0.61	0.29					
mm	BI	5	2			114	206							
Base-isolated System (HDRB)	Abs. Acc [m/s <sup>2</sup> ]	RF	0.54	0.45	4.21	7.88	2.75	2.29	7.85	17.82	2.42	2.67	18.66	41.03
		4F	0.62	0.38	3.93	8.77	2.33	2.46	6.52	16.84	2.35	2.17	15.11	37.78
		3F	0.21	0.26	3.89	8.00	1.59	2.11	6.22	13.69	3.08	2.51	9.30	29.04
		2F	0.58	0.28	3.78	5.59	1.46	1.81	5.89	9.68	2.82	1.96	9.70	25.38
		1F	0.35	0.35	3.66	4.86	1.62	1.67	5.31	9.42	1.70	1.70	7.05	21.86
		T	0.21	0.14	3.40		5.91	7.36	3.62	0.00	4.36	5.09	4.80	0.00
		RF	0.04	0.02	0.32	0.34	0.42	0.62	0.33	0.38	0.73	0.41	0.25	0.52
		4F	0.03	0.02	0.31	0.34	0.40	0.60	0.32	0.39	0.71	0.39	0.21	0.54
		3F	0.02	0.01	0.31	0.34	0.37	0.57	0.31	0.38	0.70	0.38	0.20	0.43
		2F	0.02	0.01	0.31	0.34	0.36	0.54	0.30	0.35	0.67	0.38	0.19	0.35
		1F	0.02	0.01	0.31	0.31	0.36	0.54	0.30	0.31	0.67	0.39	0.18	0.27
		T	0.01	0.00	0.30		0.57	0.60	0.29		0.50	0.44	0.14	
mm	BI	3	1			111	188			175	180			
Fixed-base System	Abs. Acc [m/s <sup>2</sup> ]	RF	0.54	0.23	3.90	7.93	13.94	19.13	8.72	11.22	5.83	8.49	2.18	2.78
		4F	0.54	0.39	3.65	7.54	10.52	15.63	8.08	12.83	5.10	6.21	2.18	3.07
		3F	0.33	0.29	3.52	5.63	8.52	12.78	6.70	13.50	3.98	4.52	2.36	3.80
		2F	0.42	0.34	3.28	3.96	7.68	9.16	5.69	9.44	3.13	3.17	1.69	2.05
		1F	0.27	0.20	3.19	3.63	6.42	6.77	4.47	4.13	2.10	2.75	1.08	1.18
		T	0.11	0.12	3.37	0.00	6.05	6.84	3.88	0.00	2.06	2.75	1.13	0.00
		RF	0.03	0.01	0.31	0.32	1.09	1.70	0.40	0.49	0.63	0.73	0.17	0.19
		4F	0.02	0.01	0.30	0.31	0.95	1.45	0.37	0.46	0.57	0.60	0.15	0.17
		3F	0.02	0.01	0.30	0.31	0.73	1.05	0.34	0.44	0.46	0.39	0.15	0.16
		2F	0.01	0.01	0.30	0.31	0.54	0.74	0.32	0.37	0.35	0.29	0.14	0.15
		1F	0.01	0.00	0.30	0.29	0.49	0.52	0.29	0.29	0.27	0.26	0.12	0.12
		T	0.01	0.00	0.30		0.50	0.52	0.28		0.27	0.26	0.12	

(\*1) Z1: vertical response recorded at a1(Figure 3-14)

(\*2) Z4: vertical response recorded at a4(Figure 3-14)

(\*3) No accelerometer was install at the corner of the roof.

(\*4) Bottom row of base-isolated systems shows the maximum displacement of the base isolation layer [mm]

## REFERENCES

- [3-1] Building Center of Japan, Structural provisions for building structures – 2007 Edition. (2007), Tokyo (Japanese).
- [3-2] International Building Code, International Code Council (ICC), Birmingham, AL., 2003.
- [3-3] California Building Code, California Building Standards Commission, 2007.
- [3-4] Ikeda S., Shimano Y., Kashima K., Ishikawa Y., Sato E., Nagae T., Furukawa S., and Fukuyama K., Research Project on Assessment of Functionality in Medical and Telecommunication Facilities, Part 18: Analysis of Differences between Results of Table Tests and Results of Numerical Analyses, Proceedings of the Annual Conference on Architectural Institute of Japan, September 2010, paper ID:21038 (Japanese).
- [3-5] Ogawa, N., Ohtani, K., Katayama, T., Shibata, H. Construction of a three-dimensional, large-scale shaking table and development of core technology, Philosophical Transactions of the Royal Society, No.359, September 2001, pp.1725-1751.
- [3-6] Nakashima, M. Roles of large structural testing for the advancement of earthquake engineering, The Fourteenth World Conference on Earthquake Engineering, Beijing, China, October 2008.





# **CHAPTER 4**

## **STRUCTURAL RESPONSES OF THE BASE-ISOLATED SYSTEM FOR HORIZONTAL MOTIONS**

### **4.1 Introduction**

Floor responses are relevant to the damage of building contents and nonstructural components. The required strength to anchor medical appliances to floors or ceilings is determined based on the expected floor accelerations during earthquakes with sufficient safety factors [4-1, 4-2]. Floor accelerations also determine the initiation of the movement of objects placed on a floor, and the possibility of overturning the determination of whose possibility is accompanied by velocity [4-3, 4-4]. The story drift greatly influences the damage magnitude of some nonstructural components such as doors and plumbing. This chapter examines the structural responses of the base-isolated systems with a focus on the horizontal responses obtained from the series of the full-scaled shaking table tests. Structural responses are described with respect to the type of ground motion, i.e., near-fault and long-period long-duration, and the type of base isolation system, i.e., NRB+U and HDRB. The vertical responses will be detailed in Chapter 5. Responses are compared to those of the fixed-base system to highlight the dynamic characteristics of the base-isolated system.

Horizontal responses of the base-isolated systems are examined, focusing on (1) stability performance of the base isolation layer for repeated shaking, especially for the long-duration ground motion, (2) horizontal responses with respect to the type of ground motion, i.e., near-fault and long-period long-duration, (3) comparison of the performance between the two base isolation systems, i.e., NRB+U and HDRB, and (4) the effect of stiffness degradation of the superstructure, which was examined by comparing the responses recorded in Tests I and II.

### **4.2 Performance of base isolation**

The base isolation layers of the two base isolation systems were sufficiently stable throughout the shaking. Figure 4-1 shows hysteresis loops of the horizontal force versus displacement in the X-axis for all five shakings of NRB+U in Test II (II-i to II-v). Horizontal forces were estimated as

the product of the floor mass and floor acceleration. The dotted lines show a bilinear relation used in the design of the specimen. Figure 4-2 shows the cumulative displacement of the base isolation layer.

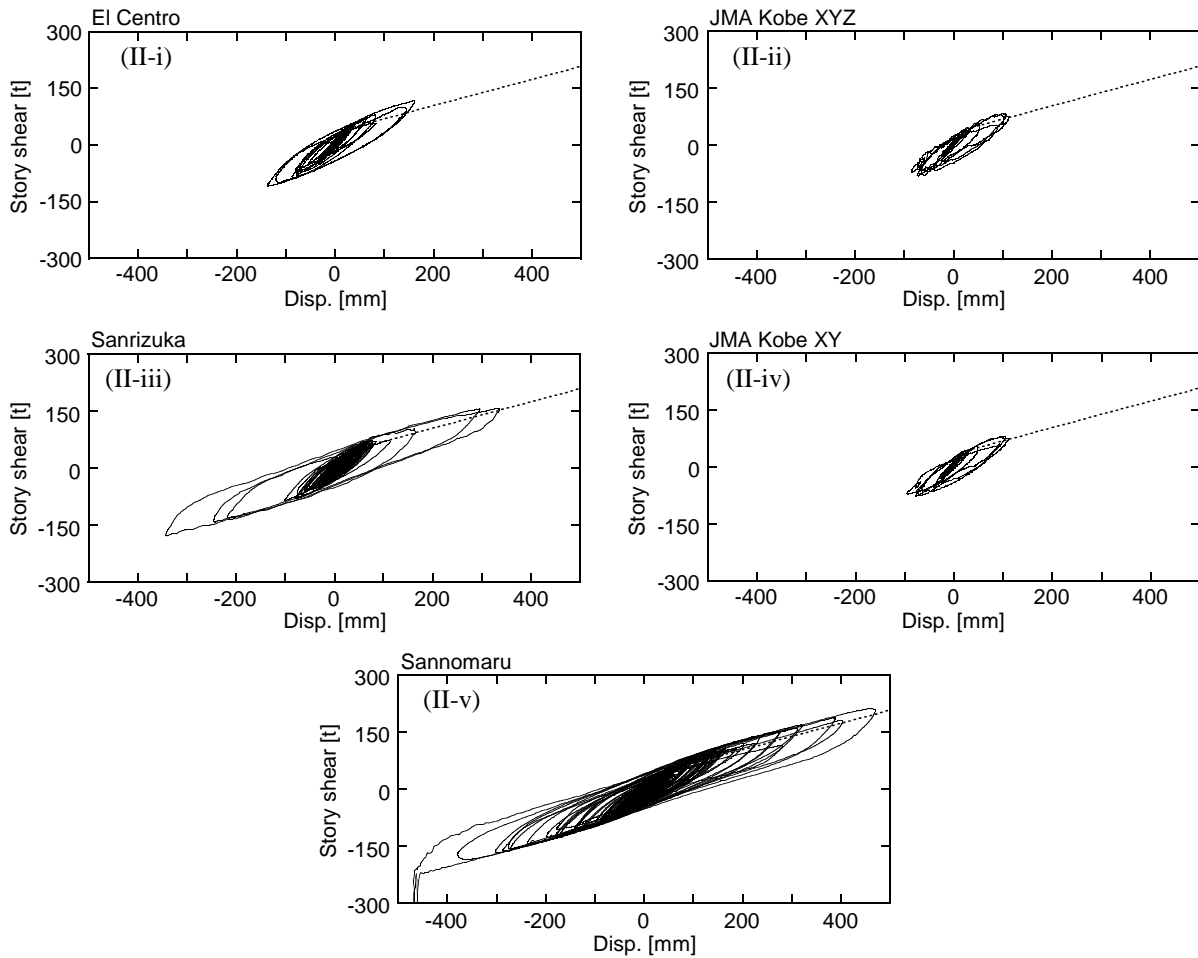


Figure 4-1 Performance of the base isolation layer (NRB+U, Test II)

In NRB+U, the stability of the base isolation layer depends mainly on that of the U-shaped steel damper [4-6]. NRB+U in Test II was shaken three times by the near-fault ground motions, which were JMA Kobe XY and XYZ, and El Centro XY, and two times by the long-period long-duration ground motions, which were Sanrizuka and Sannomaru. The absolute maximum displacements of the base isolation layer were 187 mm, 230 mm, and 222 mm for El Centro XY, JMA Kobe XYZ, and JMA Kobe XY, while these were 454 mm and 486 mm for Sanrizuka and Sannomaru. This indicates significantly larger responses obtained for the long-period ground motion. The disparities between two types were about 1:2. As shown in Figure 4-1, the bearings sustained large cyclic displacements many times during the long-period ground motions that lasted for about 150 to 300 s. The cumulative displacements reached about 19.5 m for Sanrizuka and 46 m for Sannomaru, while those experienced in El Centro and JMA Kobe were smaller than 5 m. It is notable that the restoring force behavior remained very stable throughout the shaking, meaning that the bearings did not exhibit major deterioration after such extent of cumulative displacements. The hysteresis loops

of JMA Kobe before and after Sanrizuka (II-iii) were almost identical with the similar maximum displacements of 230 mm and 222 mm. In addition, the second stiffness remained unchanged throughout the series of shaking. In summary, the U-shaped steel damper performed very well without any rupture even though it experienced cumulative deformation of about 81 m (Figure 4-2). Figure 4-3 shows two photos of the damper after Sannomaru.

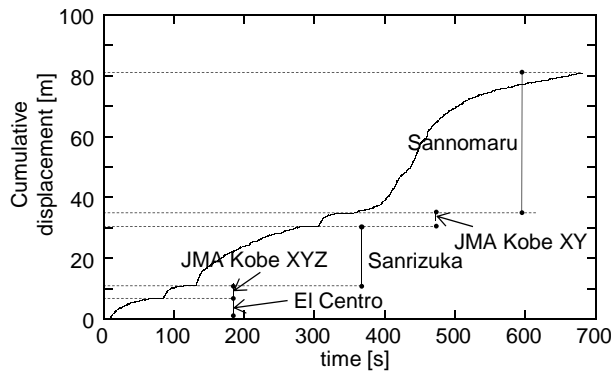


Figure 4-2 Cumulative displacement of the base isolation layer (NRB+U, Test II)



Figure 4-3 U-shaped steel damper after all shakings (Test II)

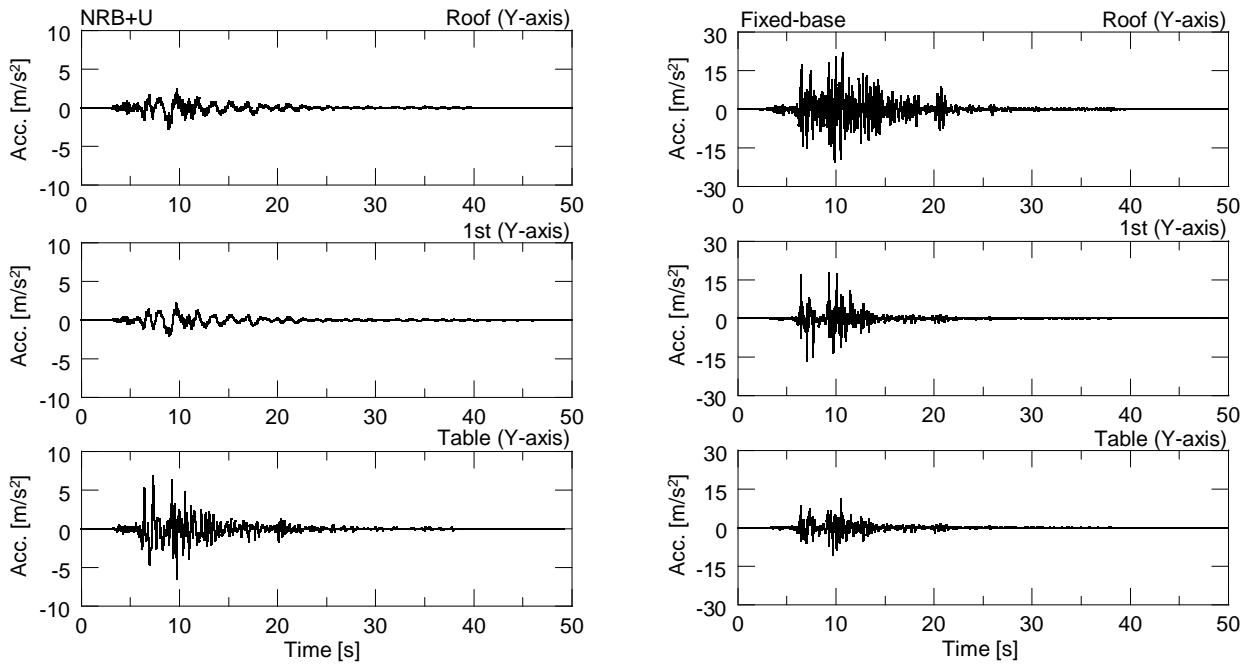
## 4.3 Performance of base-isolated system

### 4.3.1 Near-fault ground motion

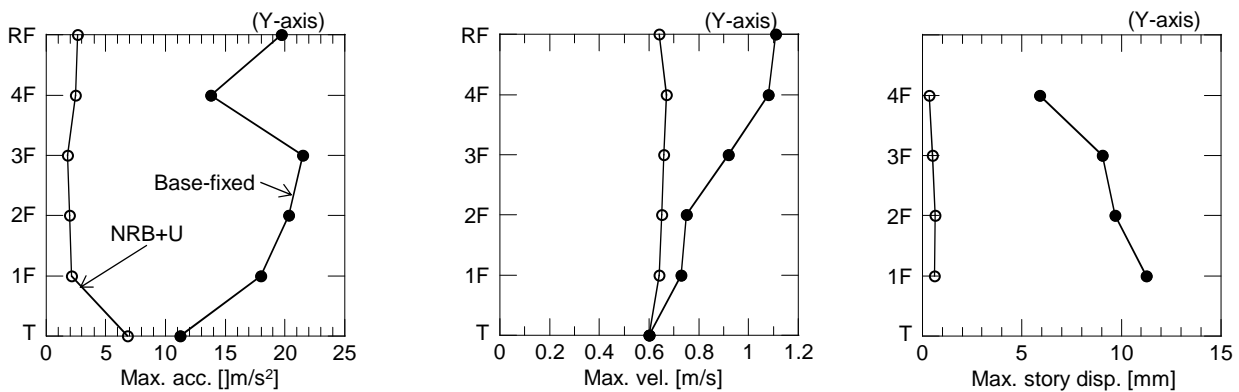
Figure 4-4(a) shows the floor acceleration time histories in the Y axis for JMA Kobe XYZ for the fixed-base and base-isolated systems (NRB+U) in Test I. Among El Centro, Yokohama, and JMA Kobe, all classified as the near-fault ground motion, JMA Kobe generated the largest floor responses. Note that the vertical full scales are different for different structural types;  $10 \text{ m/s}^2$  for the base-isolated system and  $30 \text{ m/s}^2$  for the fixed-base system. Figure 4-4(b) plots the absolute maximum of the floor accelerations, velocities and story displacements of the superstructure.

In the fixed-base system, the maximum input acceleration of  $11.3 \text{ m/s}^2$  was amplified by 1.8 times to the roof maximum acceleration of  $19.7 \text{ m/s}^2$ . In the base-isolated system, the high frequency vibrations contained in the input ground motion were successfully eliminated by the base isolation

layer. The base isolation layer elongated the dominant period of the superstructure response to 2 to 3 s. The maximum input acceleration of  $6.80 \text{ m/s}^2$  was reduced by 0.38 times to the roof maximum acceleration of  $2.61 \text{ m/s}^2$ . The first floor's maximum acceleration was 0.32 times smaller than the maximum input acceleration, while the amplification along the height of the superstructure was not greater than 20%. The difference in maximum floor acceleration by a factor of 7.5 observed between the fixed-base and base-isolated systems is very significant for the near-fault ground motion.



(a) Acceleration time histories of NRB+U and the fixed-base system



(b-1) Maximum acceleration

(b-2) Maximum velocity

(b-3) Maximum story displacement

Figure 4-4 Dynamic responses for JMA Kobe

Because the base-isolation system vibrates with a longer period to reduce the acceleration input to the superstructure, it tends to increase the floor velocity. The floor velocities of the base-isolated system for JMA Kobe, however, remained smaller than those of the fixed-base system. The maximum velocity at the roof of the fixed-base system was  $1.11 \text{ m/s}^2$  while that of the base-isolated

system was  $0.64 \text{ m/s}^2$ . The difference between them is 1.7 to 1, the ratio of which becomes smaller than the difference in maximum floor acceleration, i.e., 7.5 to 1.

Large floor accelerations of the fixed-base system increased the story displacements. The difference in the first story displacement between the two systems was 19 to 1. The maximum story displacement of the fixed-base system, however, remained less than 0.3 % in story drift, which was sufficiently smaller than the level 1 design criteria of 0.5%. Cracks propagated for all structural components every after major shaking for the fixed-base system. Some minor cracks reached 1.0 mm in gap after Test I. These cracks propagated from the tips of slits inserted to the both ends of fourth floor's beams to reduce the effective height of the beams from 1,250 mm to 900 mm. Most of these gaps, however, were less than 0.2 mm.

Because the floor accelerations were significantly reduced to not greater than  $3.0 \text{ m/s}^2$  for the base-isolated system, no furniture responded violently, while most free-standing items were dislocated and many articles stored on shelves or placed on tables fell down for the fixed-base system.

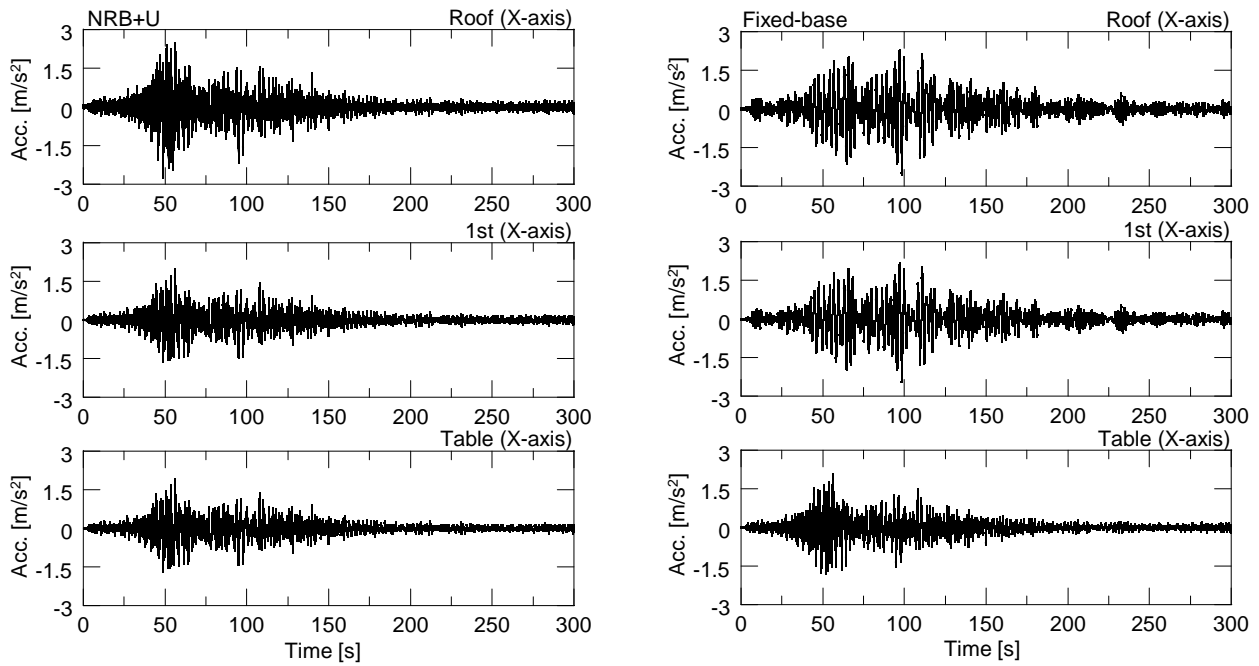
### ***4.3.2 Long-period and long-duration ground motion***

Figure 4-5(a) shows the acceleration time histories (in the X axis) obtained from Sannomaru. Figure 4-5(b) shows the maximum floor accelerations, velocities, and story displacement at all stories. In the fixed-base system, the maximum input acceleration of  $1.93 \text{ m/s}^2$  was amplified to the roof maximum acceleration of  $2.52 \text{ m/s}^2$ , which was 1.3 times the maximum input acceleration. As compared to the case when subjected to JMA Kobe, the amplification from the input to the roof acceleration is significantly smaller, 1.3 (Sannomaru) versus 1.8 (JMA Kobe), and most notable are very small accelerations in the roof acceleration,  $2.52 \text{ m/s}^2$  (Snnnomaru) versus  $15.6 \text{ m/s}^2$  (JMA Kobe). The long-period ground motion whose dominant period is in a range of 2 to 3 s did not promote the response of the fixed-base system whose natural period is not larger than 0.35 s.

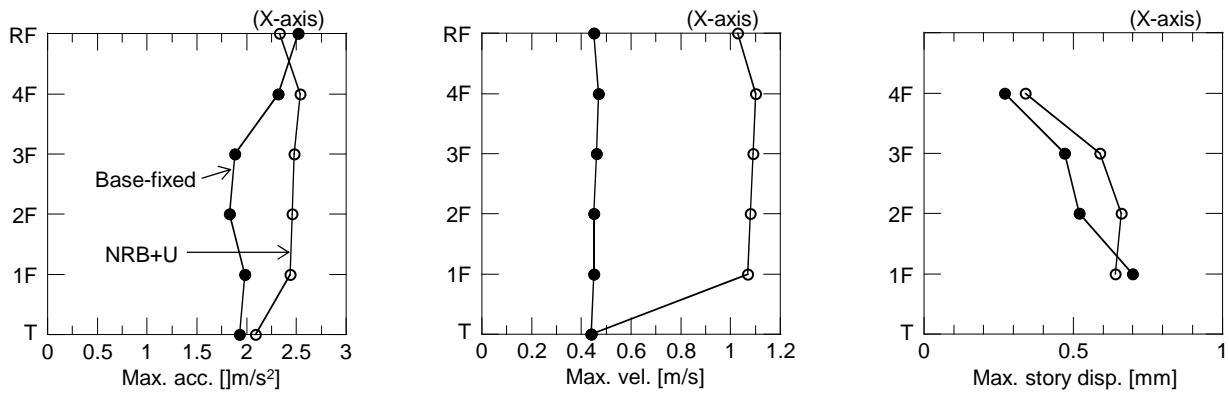
In the base-isolated system, the maximum displacement of 409 mm, which was twice as large as that of JMA Kobe, was recorded at the base isolation layer. The maximum acceleration increases by 1.1 times from the input of  $2.10 \text{ m/s}^2$  to the roof response of  $2.33 \text{ m/s}^2$ . The amplification of acceleration responses was also lessened by the base isolation, but the degree of response reduction was lowered compared to the case for the near-fault motion, in which the response was reduced to 0.32 times. This was primarily because resonance occurred in the long-period ground motion. However, the degree of the acceleration response amplification remained only 1.1 times, because the superstructure was stiff enough to be considered as a rigid body. All amplification was attributed by the base isolation layer. Although the floor acceleration responses remained relatively small, which happened to be close to those of the fixed-base system, the velocity responses were notably large as shown in Figure 4-5(b-2). In Sannomaru, the maximum roof velocity was 0.45 m/s for the fixed-base system, while it reached 1.03 m/s for the base-isolated system. This velocity is nearly twice as large as that obtained for JMA Kobe, i.e., 0.64 m/s (Figure 4-4(b-2)).

Because floor accelerations were much less than those for the near-fault ground motions, no significant damage to building's contents was observed for the fixed-base system. For the

base-isolated system, however, primarily because of significantly large displacement, many mobile furniture items and medical appliances sustained large movement and accompanying damage, whose details will be described in Chapter 6.



(a) Acceleration time histories of NRB+U and the fixed-base system



(b-1) Maximum acceleration

(b-2) Maximum velocity

(b-3) Maximum story displacement

Figure 4-5 Dynamic responses for JMA Kobe

## 4.4 Types of isolators

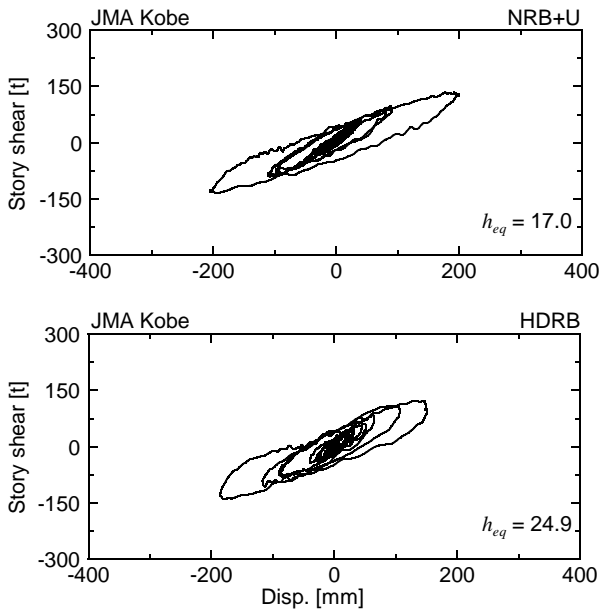
The two base-isolated systems were similar to each other in overall performance because the equivalent elastic natural periods of NRB+U and HDRB were set to be close to each other, i.e., 2.56 s for NRB+U and 2.41 s for HDRB with respect to the secant stiffness estimated for the bearing

displacement of 300 mm. But their energy dissipation mechanisms are different. In NRB+U, a U-shaped steel damper dissipates energy by means of hysteresis, while high-damping rubber bearings dissipate energy in itself, in a similar way to the dissipation caused by viscos damping. Hence, the shape of the hysteresis loops of these two base isolation systems was different. NRB+U behaves more in a bilinear relation, while the hysteresis loop of high-damping rubber bearings is commonly modeled by a modified bilinear manner since the tangent stiffness is shear-displacement dependent [4-5]. This section compares the performances of the two base-isolated systems using the results obtained in Test I.

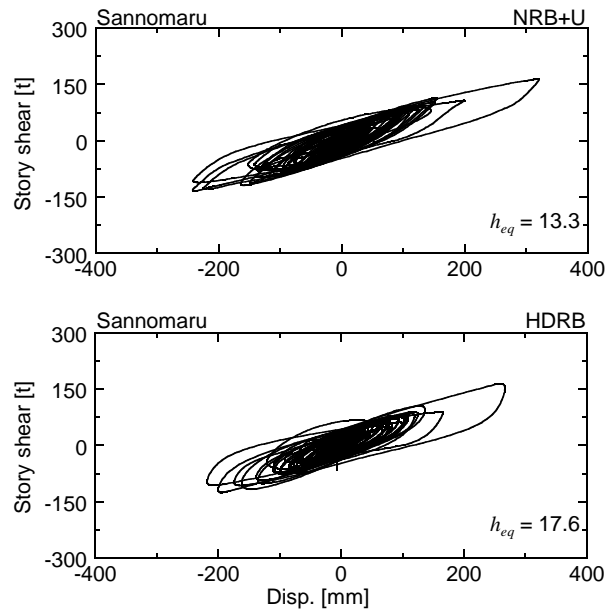
Responses are compared between NRB+U and HDRB in Figure 4-6 for JMA Kobe XYZ and Sannomaru. In the figures, (a) shows the hysteresis loops of the base isolation layer, and (b) and (c) plot the maximum accelerations, velocities, and story drifts for both ground motions. The maximum displacements, secant stiffness and equivalent damping ratios ( $h_{eq}$ ) of the base isolation layer estimated by hysteresis loops (Figure 4-6(a)) are summarized in Table 4-1. The secant stiffness was estimated with respect to the maximum displacement of the base isolation layer, and equivalent damping ratio was estimated with respect to the largest hysteresis cycle.

The secant stiffness and the equivalent damping ratio of the base isolation layer of HDRB were always larger than those of NRB+U for both types of ground motions. The disparity in the secant stiffness between HDRB (2,100 kN/m) and NRB+U (1,640 kN/m) was 1.28, and the disparity in the equivalent damping ratio between HDRB (24.9%) and NRB+U (17.0%) was 1.46 for JMA Kobe. Those disparities became small for Sannomaru. The disparity in the secant stiffness between HDRB (1,460 kN/m) and NRB+U (1,200 kN/m) became 1.22, and the disparity in the equivalent damping ratio between HDRB (17.6%) and NRB+U (13.3%) became 1.32. The reduction ratio from JMA Kobe to Sannomaru in the secant stiffness was 0.73 for NRB+U and 0.70 for HDRB, and that in the equivalent damping ratio was 0.78 for NRB+U, and 0.71 for HDRB. With this clear difference in the horizontal dynamic response characteristics of two base isolation systems, however, the maximum displacement of the base isolation layer of both systems became close for JMA Kobe; 223 mm for NRB+U and 201 mm for HDRB (the disparity ratio was equivalent to 1.1). On the other hand, for Sannomaru, the differences in stiffnesses and damping ratios were represented by a larger disparity in the displacement of the base isolation layer; the displacement of NRB+U reached 409 mm, while it remained 311 mm for HDRB, the disparity ratio of which became 1.32. In summary, the disparity in horizontal stiffness and damping ratio of the base isolation layer tended to more influence the case when the displacement of the base isolation layer became larger such as Sannomaru, while little effect was observed for JMA Kobe.



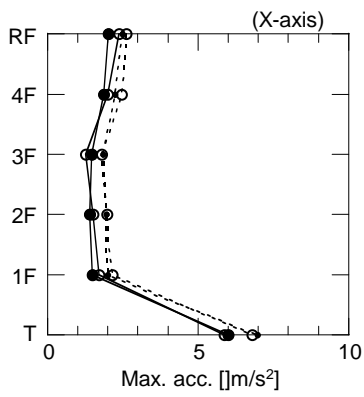


(a-1) JMA Kobe

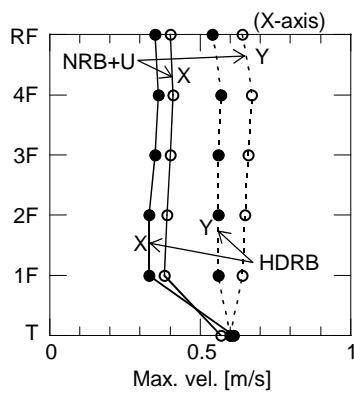


(a-2) Sannomaru

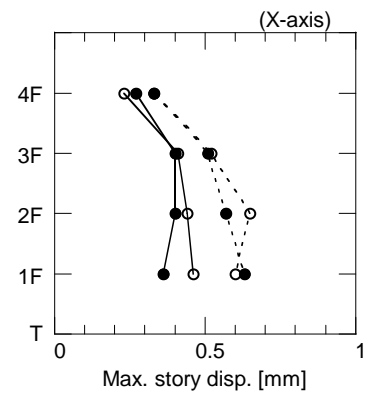
(a) Acceleration time histories of NRB+U and the fixed-base system



(b-1) Maximum acceleration

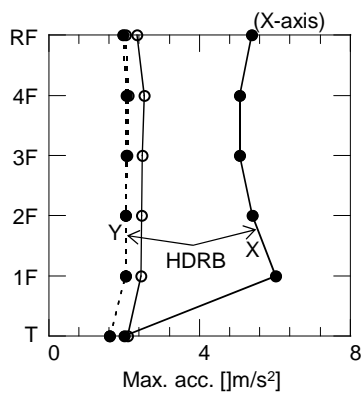


(b-2) Maximum velocity

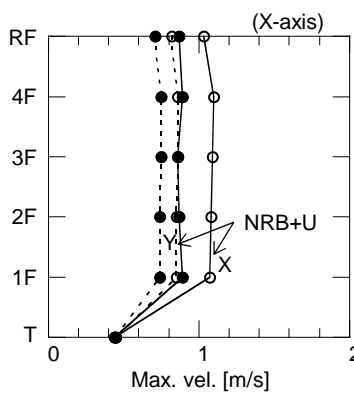


(b-3) Maximum story displacement

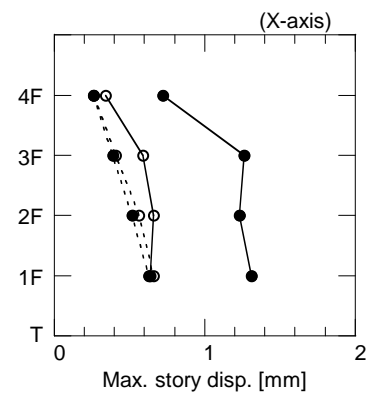
(b) Maximum responses for JMA Kobe



(c-1) Maximum acceleration



(c-2) Maximum velocity



(c-1) Maximum story displacement

(c) Maximum responses for Sannomaru

Figure 4-6 Dynamic responses for JMA Kobe

Table 4-1 Equivalent stiffness and damping ratio of the base isolation layer

axis		JMA Kobe		Sannomaru	
		NRB+U	HDRB	NRB+U	HDRB
Disp. of base isolation layer [mm]	X	112	104	409	284
	Y	206	187	321	264
	absolute	223	201	409	319
secant stiffness per isolater [kN/m]	estimated <sup>(*1)</sup>	1,640	2,100	1,200	1,470
Equivalent damping ratio	estimated <sup>(*1)</sup>	17.0%	24.9%	13.3%	17.6%

(\*1) Estimated by hysteresis loop of the base isolation layer shown in Figure 4-6(a)

Even though the shapes of hysteresis loops and the maximum displacement of the base isolation layer were significantly different, it is notable that the maximum accelerations and story drifts of the superstructure were similar between NRB+U and HDRB for both types of ground motions (Figure 4-6(b-1), (b-3), (c-1), and (c-3)). One exception is the X-axis responses of HDRB for Sannomaru, which experienced pounding against the surrounding concrete blocks anchored to the table. Difference in velocities became slightly larger; the maximum for NRB+U was 0.67 m/s, while that for HDRB was 0.57 m/s for JMA Kobe (Figure 4-6(b-2)). The difference became even larger for Sannomaru: 1.07 m/s for NRB+U and 0.89 m/s for HDRB (Figure 4-6(c-2)). In summary, when two base-isolated systems with the different isolation systems but with the relatively close natural periods (2.56 s for NRB+U and 2.41 s for HDRB with respect to the secant stiffness estimated for the bearing displacement of 300 mm) were compared, the acceleration responses and story displacements of the superstructure were stable regardless of the differences in the displacement magnitude and the shapes of hysteresis loops of the base isolation layer, while the velocity responses were affected by the displacement amplitude of the base isolation layer.

Even though the floor accelerations were similar to each other, the displacement amplitude of movement of mobile furniture and medical appliances became smaller for HDRB than NRB+U, when Sannomaru was input. This was primarily because of the smaller absolute floor displacement in HDRB.

## 4.5 Effect of stiffness degradation of superstructure

Because the shaking table tests were conducted many times for the same specimen, cracks were propagated in the superstructure when the fixed-base system was tested. Accordingly, the natural frequencies of the superstructure were gradually reduced from the beginning of Test I to the end of Test II. The initial first natural frequencies of the superstructure were 4.2 Hz for both directions when the tests of the base-isolated systems were conducted in Test I. When the test of the base-isolated system in Test II started, the natural frequencies were decreased to 2.54 Hz for the X

axis and 2.83 Hz for the Y axis, because tests of the fixed-base system in Test I were conducted in between (Table 3-3). The reduction ratios of 0.60 and 0.68 for each axis were equivalent to the reduction by one quarter in stiffness. If the stiffness of the base isolation layer is represented by the natural frequency with the assumption of the superstructure as a rigid body, the ratio between the natural frequencies of the superstructure and that of the base isolation layer was 10.5 in Test I. The ratios were reduced to 6.4 and 7.1 for the X and Y axes in Test II. These ratios were still much larger than the recommended minimum frequency ratio of the superstructure to the base isolation layer of 3.0 [4-7]. However, it may have caused the inferior performance of structures and building contents in Test II to Test I. The results obtained from Tests I and II are compared in detail with respect to the type of structure, i.e., base-isolated versus fixed-base, and the type of ground motion, i.e., near-fault versus long-period. NRB+U was chosen to represent of the base-isolated system.

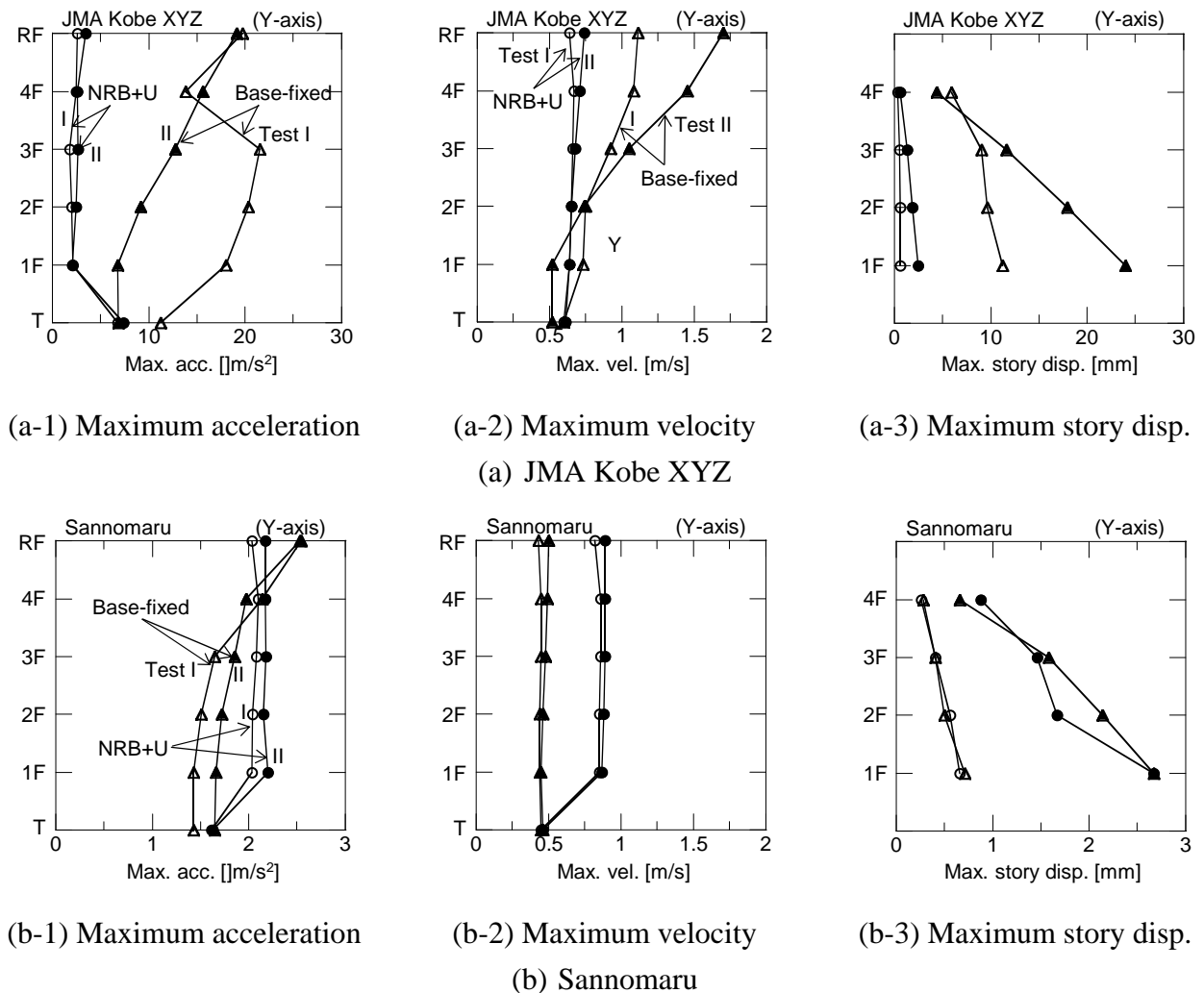


Figure 4-7 Maximum response comparison between Test I and II

Figure 4-7 shows the maximum floor accelerations, velocities, and story displacements of both systems for JMA Kobe and Sannomaru. It was notable that floor accelerations of the fixed-base system for JMA Kobe were significantly reduced from Test I to II for most of the floors. This is

not because the effect of the stiffness was reduced but because unexpected slips occurred between the superstructure and the foundation blocks anchored to the table. These slips caused pulsive responses in Test I, increasing the maximum floor accelerations. The accelerations recorded at the upper floors for both Tests I and II remained to be close since the effect of slips had been damped by the lower stories. In other major shakings, floor accelerations were confirmed to be relatively similar between Test I and II. This is likely because the major structural components had already yielded in Test I. Floor velocities increased by 1.34 and 1.59 for the fourth floor and the roof from Test I since the natural period was elongated by a factor of two. The effect of stiffness degradation was also exhibited by the increase in the story displacements up to 2.13 times, which was recorded at the first story. On the other hand, little changes in floor accelerations and velocities were observed between Test I and II for NRB+U when JMA Kobe was input, even though the significant increase by a factor of four was observed for the story displacements. When Sannomaru was input, the differences between Tests I and II were almost negligible for both systems, as compared with the responses for JMA Kobe.

The above observations indicate that the horizontal response of the base-isolated system was relatively stable for the change in natural frequencies of the superstructure, while that of the fixed-base system was more sensitive to those changes. Significant increase in floor velocities was observed for the fixed-base system when JMA Kobe was input, while floor accelerations remained relatively similar. This increase in floor velocities resulted in severe rocking of slender furniture placed at the fourth floor in Test II, whose intensity was milder in Test I.

## **4.6 Summary and conclusions of Chapter 4**

This chapter describes the horizontal responses of the base-isolated system based on the results of the full-scaled shaking table tests. The responses of two types of structural systems (the base-isolated system and the fixed-base system) for two types of ground motions (near-fault ground motion and long-period and long-duration ground motion) are compared. In addition, the performance of two different base-isolation systems (NRB+U and HDRB) are also compared. Major findings are summarized as follows:

- (1) The performance of the base isolation systems was satisfactory for both the near-fault and long-period and long-duration ground motions. The maximum horizontal displacements of the base isolation layer were twice as large in the long-period and long-duration ground motion (486 mm in the long-period ground motion named Sannomaru and 230 mm in the near fault ground motion named JMA Kobe). Also notable was a significant difference in cumulative horizontal displacement, i.e., 46 m in Sannomaru and less than 5 m in JMA Kobe. This large difference (by a factor of ten) was due to a combined effect of resonance of the base-isolated system with Sannomaru and the long duration of 300 s in Sannomaru. Despite such large

displacements, the base-isolated system remained stable, and the U-shaped steel damper eventually sustained 81 m of cumulative displacement without any significant stiffness degradation.

- (2) The fixed-base system sustained the whole series of shaking table tests, including seven major shakings as the fixed-base system (El Centro, JMA Kobe, Yokohama), without any critical damage.
- (3) In the base-isolated system (NRB+U) when subjected to JMA Kobe, the floor accelerations were significantly reduced; the maximum floor acceleration ( $2.61 \text{ m/s}^2$ ) was 0.38 times the input maximum acceleration ( $6.80 \text{ m/s}^2$ ), and 0.13 times the maximum floor acceleration recorded in the counterpart fixed-base system ( $19.7 \text{ m/s}^2$ ). The maximum floor velocity was also smaller in the base-isolated system ( $0.62 \text{ m/s}$ ) than was in the fixed-base system ( $1.00 \text{ m/s}$ ), but the difference was not as large as the difference of the maximum floor acceleration.
- (4) In the base-isolated system when subjected to Sannomaru, the maximum floor acceleration was not reduced; instead, it ( $2.30 \text{ m/s}^2$ ) increased to 1.1 times the input maximum acceleration ( $2.10 \text{ m/s}^2$ ). The corresponding fixed-base system sustained the roof maximum acceleration of  $2.52 \text{ m/s}^2$ , which was still larger than that obtained from the base-isolated system, but the disparity (1.1) was much smaller than the case for JMA Kobe (a disparity of 7.5). Notable was the large floor velocity observed in the base-isolated system, i.e.,  $1.0 \text{ m/s}$  in the maximum floor velocity, which was twice the maximum floor velocity observed in the fixed-base system ( $0.5 \text{ m/s}$ ).
- (5) The maximum displacements of the base isolation layer were similar between NRB+U (223 mm) and HDRB (201 mm) for JMA Kobe, even though the estimated horizontal secant stiffnesses and damping ratios of HDRB were larger than NRB+U. Their differences in response characteristics were clearly represented in the long-period and long-duration ground motion; the maximum became 409 mm for NRB+U and 319 mm for HDRB for Sannomaru.
- (6) When two base-isolated systems with the different isolation systems but with the relatively close natural periods (2.56 s for NRB+U and 2.41 s for HDRB with respect to the secant stiffness estimated for the bearing displacement of 300 mm) are compared, the acceleration responses and story displacements of the superstructure were stable regardless of the differences in the displacement amplitude and the way of dissipating energy by the base isolation layer, while the velocity responses were affected by the displacement amplitude of the base isolation layer.
- (7) The stiffness reduction by one quarter of the superstructure had little effect on the performance stability of the base-isolated systems. Floor accelerations and velocities remained unchanged while story displacements were increased by four times from Test I to Test II. For the fixed-base system, the significant increases in velocities by 1.3 and 1.6 times for the X and Y-axis from Test I were observed because of the elongation of the natural period by more than 1.5 in the superstructure. Floor accelerations of the fixed-base system remained relatively unchanged because the major components had been already yielded in the test of the fixed-base system of Test I.

## REFERENCES

- [4-1] Recommendations for Aseismic Design and Construction of Nonstructural Elements, Japan Institute of Architecture, 2003 (Japanese).
- [4-2] Current Trend Report of Seismic Application of Medical Radiological Equipment, Japan Industries Association of Radiological Systems, 1998 (Japanese).
- [4-3] Structural Response and Performance for Long Period Seismic Ground Motions, AIJ, 2007 (Japanese).
- [4-4] Kaneko M., Method to Estimate Overturning Ratios of Furniture During Earthquakes, Journal of Structure and Construction Engineering, AIJ, No.551, 61-68, Jan., 2002
- [4-5] Fujita T., Suzuki S., and Fujita S., High Damping Rubber Bearings for Seismic Isolation of Buildings First Report: Hysteretic Restoring Force Characteristics and Analytical Models), Journal of Japan Society of Mechanical Engineers, The Japan Society of Mechanical Engineers, Vol.56, No.523, March, 1990
- [4-6] Suzuki K., Watanabe A., and Saeki E., Development of U-shaped Steel Damper for Seismic Isolation System, Nippon Steel Technical Report, Vol.382, 2005
- [4-7] Design Methods for Response Controlled Structures; Architectural Institute of Japan, September 2001.



# **CHAPTER 5**

## **STRUCTURAL RESPONSES OF THE BASE-ISOLATED SYSTEM FOR VERTICAL MOTIONS**

### **5.1 Introduction**

Vertical responses under vertical excitations are one of the most concerning issues for base-isolated systems. The specimen has horizontal natural periods of 2.46 s and 2.34 s for NRB+U and HDRB with respect to the secant stiffness measured for a bearing displacement of 200 mm, while it becomes 0.058 s (17.1 Hz) and 0.049 (20.3 Hz) for the vertical natural period (frequency), assuming the superstructure as a rigid body. These vertical natural frequencies of the base isolation layer were found to be close to the first vertical natural frequency of the superstructure of 12 Hz (the fixed-base condition in Test II), while the horizontal natural periods were sufficiently longer than the natural period of the superstructure by ten times for Test I and seven times for Test II. As a result, the base-isolated system behaved significantly differently in the vertical direction compared with its performance in the horizontal direction, which was described in the previous chapter.

This chapter described the vertical response characteristics of the base-isolated system based on the shaking table tests results. Discussions are mainly based on the results of Test II, in which measurements and input waves were rearranged for the purpose of observing these characteristics. The following subjects are the focus of this chapter: (1) vertical floor acceleration responses and its amplitude distribution throughout the superstructure, (2) vertical dynamic response characteristics (natural frequency and damping ratio), and (3) axial force exerted on isolators. Vertical dynamic response characteristics are compared with those of the fixed-base system, and the effect of inserting the base isolation layer under the superstructure on the shift of the vertical dynamic response characteristics are examined by conducting finite element analysis. In addition, the shift of the vertical dynamic response characteristics are examined with respect to the response amplitudes. Note that NRB+U was tested without the penthouse, and the penthouse (the weight of 167 kN) was placed on the roof before the test of HDRB began. Therefore, the vibration characteristics of the roof floor were different between two base-isolated systems.



## 5.2 Input ground motions

Among six input waves used for the series of tests, two recorded ground motions were used to examine the vertical response characteristics of the base-isolated system. One was JMA Kobe, and the other was El Centro. Those waves were scaled so that PGAs of JMA Kobe became  $4.94 \text{ m/s}^2$ ,  $6.54 \text{ m/s}^2$  and  $2.66 \text{ m/s}^2$  for the X, Y and Z directions, respectively, while those of El Centro became  $3.14 \text{ m/s}^2$ ,  $5.10 \text{ m/s}^2$  and  $3.08 \text{ m/s}^2$ . More detailed information about these scaling factors for input waves, PGV, and those acceleration time histories can be found in Chapter 3. Figure 5-1 shows the pseudo acceleration spectra for the vertical wave of JMA Kobe and El Centro for 5% damping with respect to frequency Hz. In this chapter for convenience, frequencies, instead of periods, are used to express a cyclic vibration speed as its relative magnitude is directly related to the corresponding stiffness. The vertical wave of JMA Kobe has a peak acceleration response of 4.1 Hz and holds a frequency range of lower than 13 Hz, while that of El Centro has a peak of 10.1 Hz and contains larger amplitude of waves for a higher frequency range than that of JMA Kobe.

JMA Kobe with the vertical motion only (designated JMA Kobe Z), horizontal motions only (designated JMA Kobe XY) and motions in all directions (designated JMA Kobe XYZ) were used as input for all types of structural systems in Test II to clarify the effect of the vertical input. El Centro with three directional inputs (designated El Centro XYZ) was only input to HDRB.

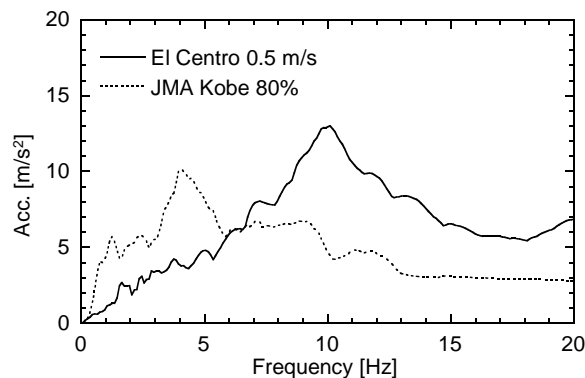
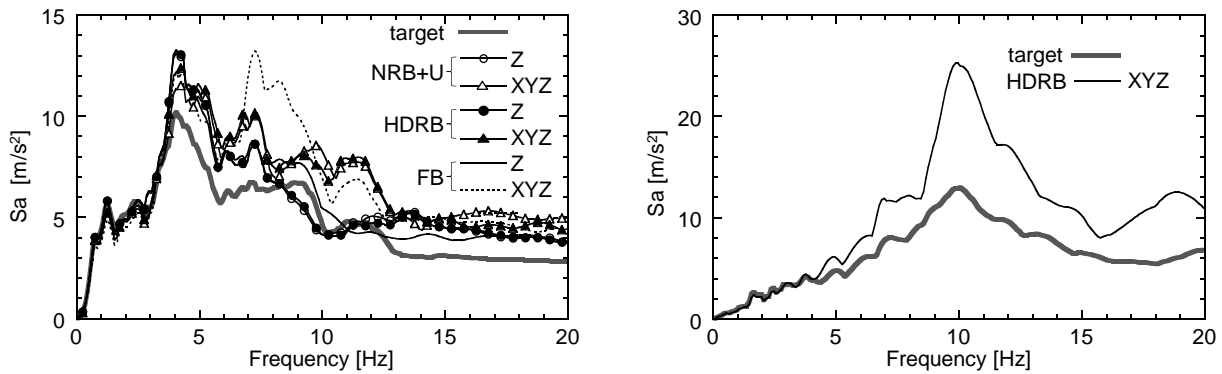


Figure 5-1 Z direction pseudo acceleration response spectra

Figure 5-2 shows the pseudo acceleration response spectra for 5 % damping of the vertical acceleration response recorded on the shaking table when JMA Kobe (Figure 5-2(a)) and El Centro (Figure 5-2(b)) were input. The input accelerations were reproduced up to 4 Hz but the reproduction quality for the higher frequency range was poor. This error was the result of the input waves been optimized based on trial inputs for calibration with a target of only 30 % the full scale in amplitude in order to avoid excessive damage of the specimen. In addition, there was difficulty in control of the shaking table for the vertical direction movement especially for the higher frequency ranges. Large errors around 10 Hz for El Centro vertical input was found to be the result of the resonance between the input wave and a base-isolated system, as the vertical first natural frequency of HDRB was 10.7 Hz, while the vertical wave of El Centro has its clear

dominant frequency of 10.1 Hz. As shown in Figure 5-2(a), the reproduced waves for JMA Kobe Z were reasonably close among all systems. The waves when JMA Kobe XYZ was input into two base-isolated systems were also almost identical but for that of the fixed-base system. Therefore, the comparable combination of vertical responses between different systems was limited to those against JMA Kobe Z.



FB: fixed-base

(a) JMA Kobe

(b) El Centro

Figure 5-2 Pseudo acceleration response spectra of reproduced vertical input waves compared with the target

### 5.3 Vertical floor acceleration responses of base-isolated system

Vertical floor acceleration responses are compared with the horizontal floor acceleration responses when three-dimensional ground motions were input to the base-isolated system. The floor acceleration response time histories of the base-isolated system of HDRB against JMA Kobe XYZ are shown in Figure 5-3 for the accelerations recorded on the table, first floor and roof for X and Z axes. The accelerations recorded at the corner (a1) and the center (a4) are shown in Figure 5-3 to demonstrate the effect of in-plane and out-of-plane vibration of the floor. The definitions of a1 and a4 are shown in Figure 3-14. The absolute maximum accelerations for all floors are shown in Table 3-6, and are re-plotted in Figure 5-4. Figure 5-4(a) shows the maximum absolute acceleration responses for X-axis recorded at the corner. Figure 5-4(b) shows the maximum absolute accelerations for Z-axis, recorded at the corner (a1) and the center (a4). All plots recorded at the corner were connected by lines from the bottom while the plots of the center were connected with the plot of the corner of the same floor.

In Figure 5-3, it is notable that the dominant period of the input acceleration was significantly elongated to 2 to 3 s, and successfully reduced the input acceleration of  $5.91 \text{ m/s}^2$  by 0.47 times the roof maximum acceleration of  $2.75 \text{ m/s}^2$ . The difference in acceleration recorded at the corner and the center of the X axis remained less than 5 %, which shows the assumption of rigid diaphragm for in-plane deformation to be reasonable. On the other hand, high frequencies in the input wave

remained unchanged or were amplified through the specimen in the vertical direction. The vertical input acceleration for JMA Kobe XYZ with the maximum of  $3.62 \text{ m/s}^2$  was amplified by 2.2 through columns to the roof corner, and further it was amplified by 2.3 to the center of the floor. Eventually, the maximum floor acceleration at the roof center reached  $17.82 \text{ m/s}^2$ , which was five times larger than the input. The disparity between horizontal and vertical responses at the roof center became 1:6.5, which was significantly large compared to those of the fixed-base system of 2.3:1 and 2.8:1 for X and Y directions, as shown in Table 3-6. This large vertical amplification of acceleration response was mainly contributed to by the floor vibration, whose amplification ratio of the floors from the corner to the center was 1.8, 1.6, 2.2, 2.6 and 2.3 from the first floor to the roof. Those values were greater than the amplification through the base isolation layer of 1.5 and that of the columns of 1.5, which is defined as the ratio of the maximum acceleration of the roof corner to that of the first floor's corner. For velocity responses, the maximum input velocity of  $0.29 \text{ m/s}$  was amplified by 1.5 times to the roof center of  $0.38 \text{ m/s}$ , which was significantly smaller amplification compared to acceleration amplification. Similar characteristics can be observed for NRB+U against JMA Kobe XYZ, as shown in Table 3-6.

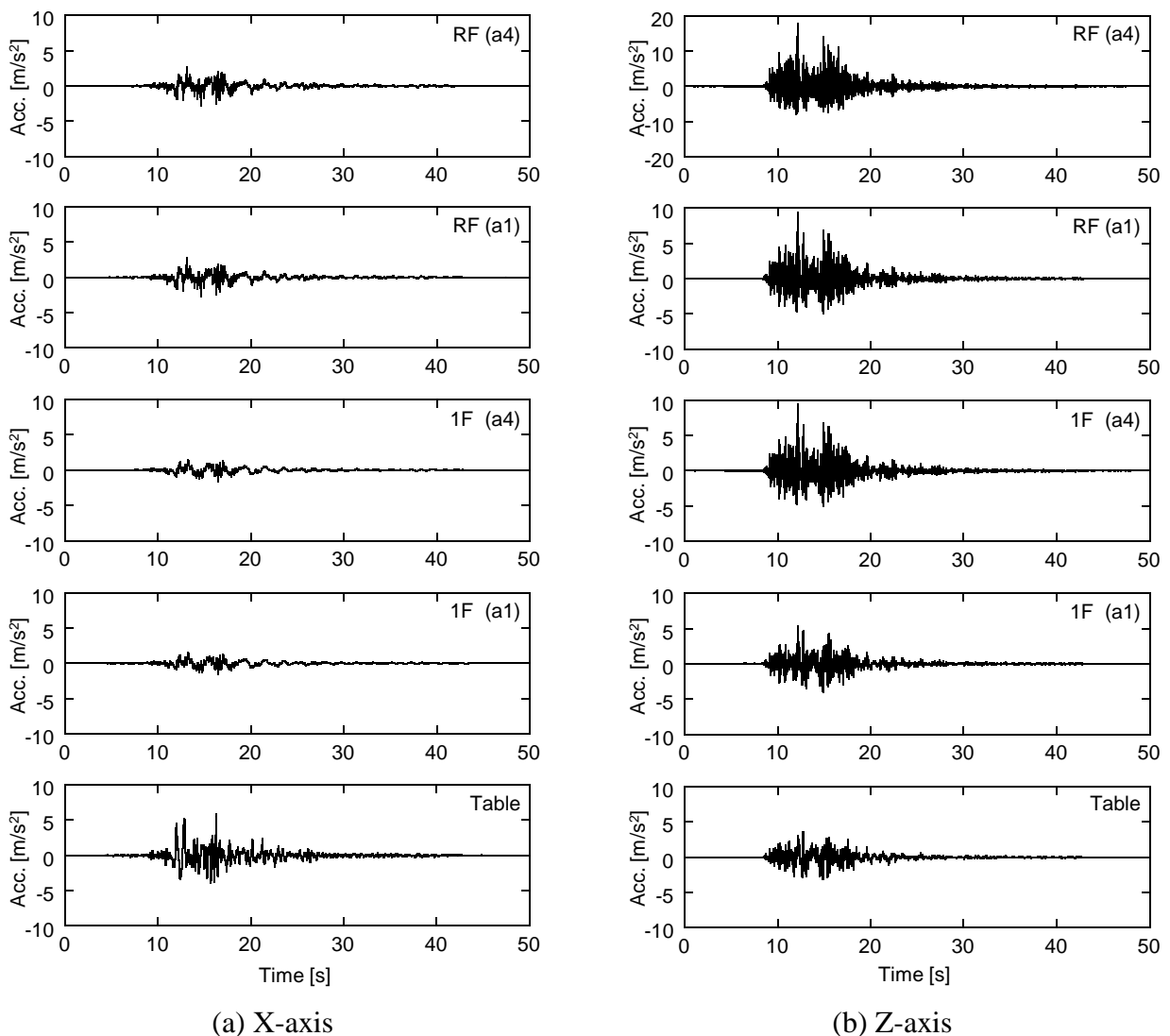
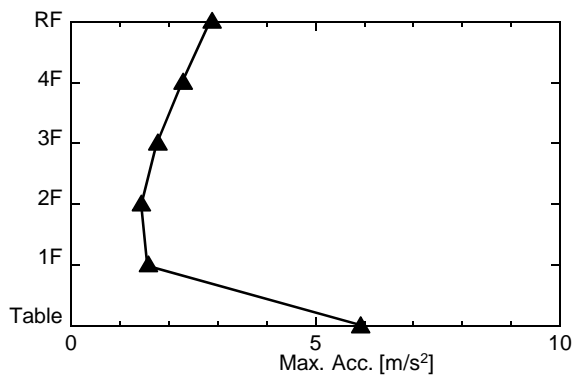
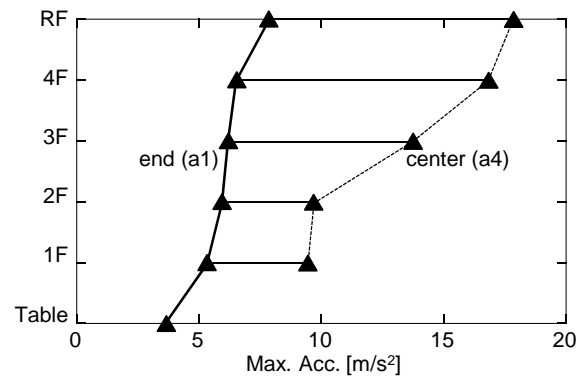


Figure 5-3 Floor acceleration time history of HDRB for JMA Kobe XYZ



(a) X-axis



(b) Z-axis

Figure 5-4 Maximum acceleration responses of HDRB for JMA Kobe XYZ

## 5.4 Dynamic response characteristics of base-isolated system

### 5.4.1 Response amplification

The shift of the vertical dynamic response characteristics of the fixed-base system (the superstructure) to that of the base-isolated systems by inserting the base isolation layer is observed in this subsection. Figures 5-5 to 5-7 shows the response amplification obtained by the transfer functions of the vertical accelerations recorded at **a1** (corner) and **a4** (center) of all five floors for a white noise wave. The transfer function of a white noise number (II-ii) and (II-iii) was shown for HDRB and for the fixed-base system, respectively. The amplitude of the white noise input to the fixed-base system was two times larger than that of the base-isolated system which was intended to obtain clearer response characteristics. The details of a white noise wave used in Test II and measurements are described in Chapter 3. The transfer functions were obtained as a quotient of the auto-spectral density of the output signal over the cross-spectral density of the input and output signals. In the signal processing, a digital filter was used to eliminate the measurement noise; a Hanning window was added to reduce the effects of leakage, and an averaging technique was adopted to reduce the relative standard deviation of the power spectra.

The response amplifications of the fixed-base system (Figure 5-5) had closely-spaced modes, and lost their consistency throughout the whole system, varying from a floor to floor, especially among the responses recorded at the center of the floor. Since the responses at the corners yielded relatively stable and consistent response amplifications with two peaks for all floors, the natural frequency of the fixed-base system was decided to be estimated by them, more concisely the corner of the fourth floor. The frequency domain curve-fitting algorithm [5-1] was used to estimate the damping ratio, which may not be accurate as a few modes were spaced too closely. The yielded fitted curves were also plotted in the figures. The natural frequency of mode I was estimated as 13.6 Hz with a damping ratio of 5 to 6%.

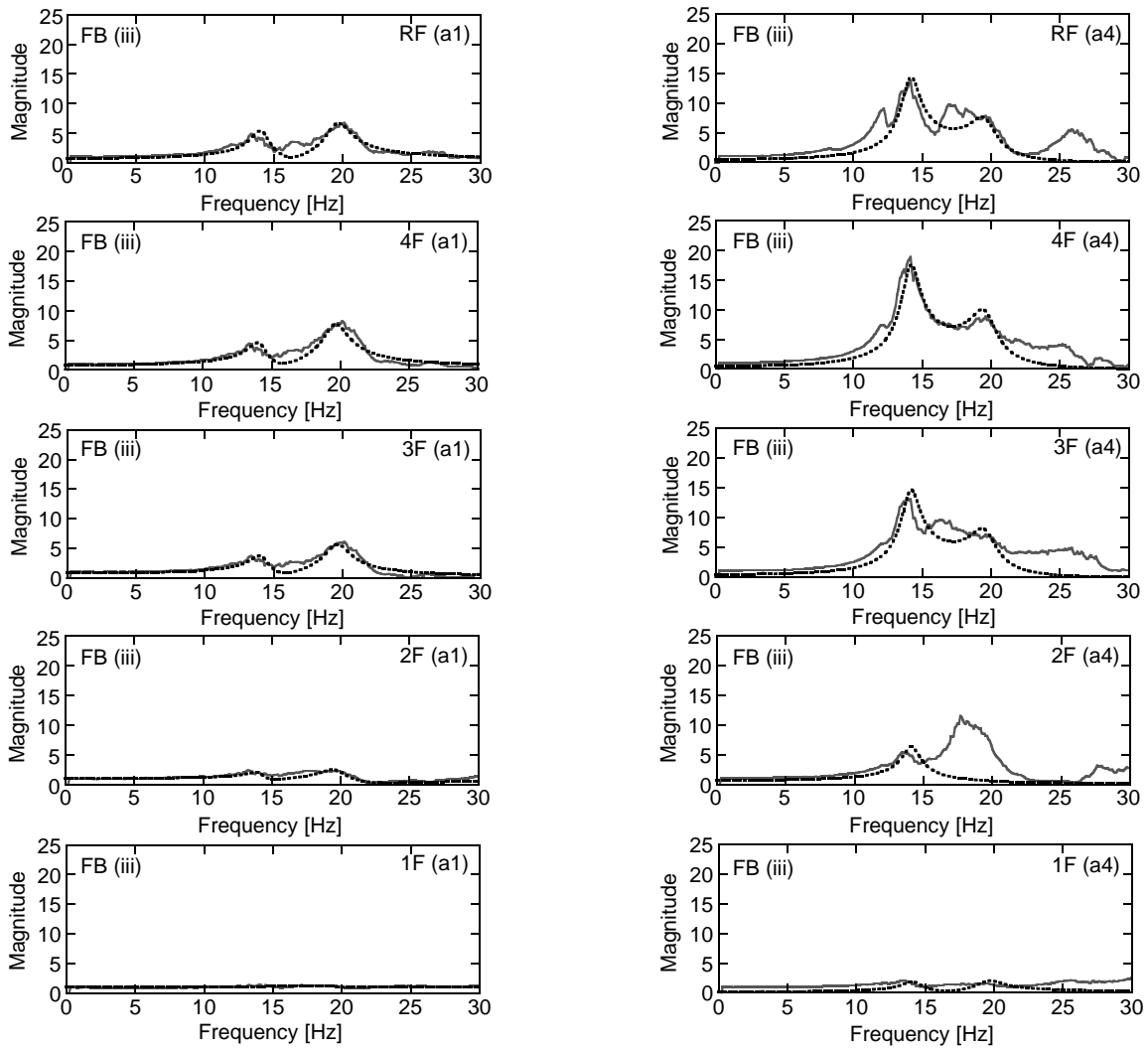


Figure 5-5 Transfer function of the vertical floor responses of the fixed-base system

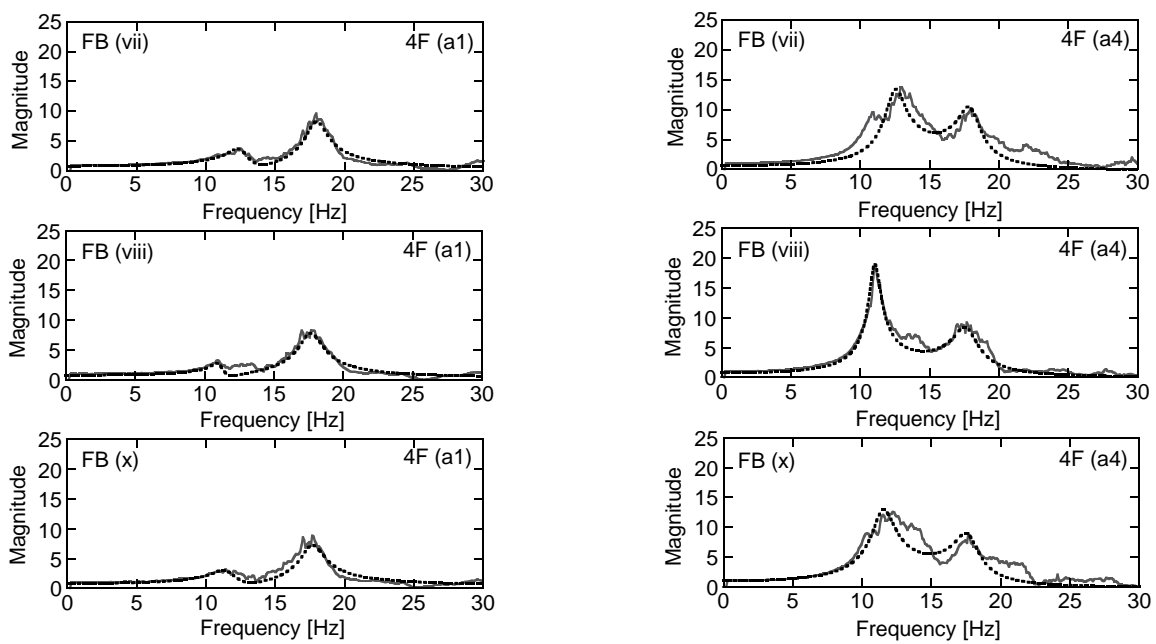


Figure 5-6 Transient of transfer functions of the fixed-base system for selected white noise numbers

These shapes were also changed after every shake, some examples of which are shown in Figure 5-6: white noise number (II-vii) before JMA Kobe XYZ was input, (II-viii) after JMA Kobe XYZ was input, and (II-x) after all shaking table tests were finished. Following the sequence of (II-ii)  $\rightarrow$  (II-vii)  $\rightarrow$  (II-viii)  $\rightarrow$  (II-x), the major lowest peak was reasonably shifted toward a lower frequency. But no trend can be observed from the transient of response amplifications with respect to the number of experienced shakings, or the accumulation of specimen damage due to consecutive shakings. The damping ratio related to the first mode was also varied every after shakings from 4 to 6%.

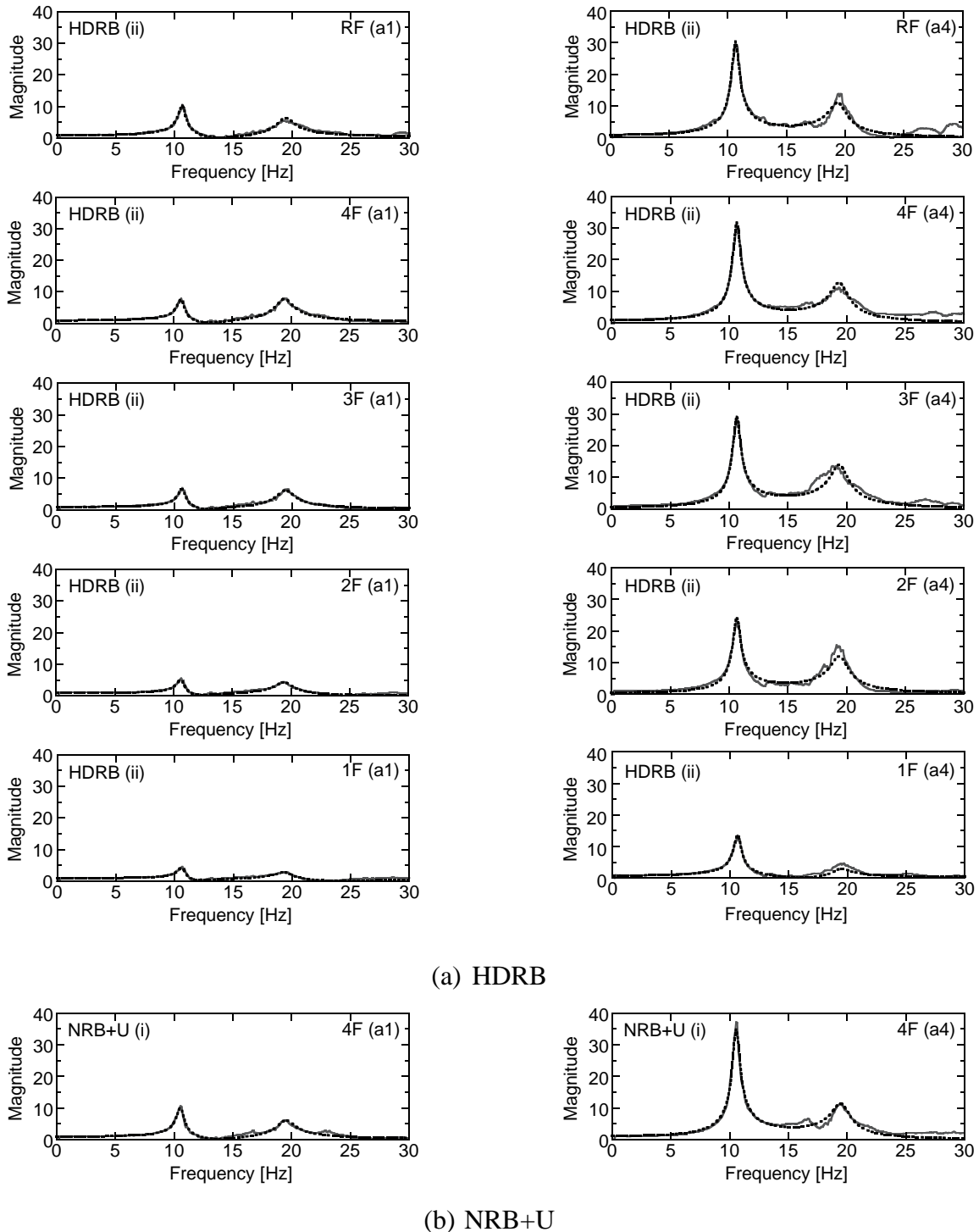


Figure 5-7 Transfer function of the vertical floor responses of the base-isolated system

Once the base isolation layer was inserted under the superstructure (the fixed-base system), the fundamental dynamic response characteristics in the vertical direction was completely changed. The response amplifications of the base-isolated system (HDRB) (Figure 5-7) show the clear independent first and second peaks, and had similar shape over frequency at any locations. The first mode natural frequency was estimated at the center of the fourth floor as 10.7 Hz and the second mode natural frequency as 19.4 Hz. Since the two modes were well separated and lightly damped to be considered as independent from each other, damping ratio and mode shapes were estimated with sufficient accuracy by employing a frequency domain curve-fitting algorithm. The details of the obtaining damping ratios and mode shapes are described in the following section. Those basic characteristics of transfer functions were shared by the two base-isolation systems of HDRB and NRB+U. Response amplifications at the fourth floor center (a4) for NRB+U are also shown in Figure 5-7(b).

The differences in the vertical dynamic response characteristics between the base-isolated system and the fixed-base system are discussed using a finite element model later in this chapter.

### ***5.4.2 Natural frequency and damping ratio***

The difference in vertical dynamic characteristics between the fixed-base and base-isolated systems based on the result of Test II are as follows:

- (1) The damping ratio in the vertical direction of the fixed-base system ranged 4~6 %, estimated by the white noise wave with PGA of  $0.6 \text{ m/s}^2$  and the maximum vertical floor acceleration of about  $2.0 \text{ m/s}^2$ . Since some modes were too closely spaced to obtain an independent damping ratio, those apparent damping ratios may be increased due to the adjacent modes.
- (2) The first vertical natural frequency was reduced by 10 ~ 20 % from 12 ~ 13 Hz (the superstructure) to 10.6 Hz for NRB+U and 10.7 Hz for HDRB, by inserting the base isolation layer of 17.1 Hz and 20.3 Hz, respectively. The first natural frequency of the superstructure must be smaller than that of the fixed-base system of 13.7 Hz, because the restrained conditions were more relaxed in the base-isolated system. The superstructure of the base-isolated system was supported at four points by the base isolators, while several points along the walls in the longitudinal direction were also anchored to the shaking table in the fixed-base system.
- (3) The first mode damping ratio in the vertical direction of both base isolation systems were 2.5 % for NRB+U and 2.9 % for HDRB, which were estimated by the white noise waves with PGA of less than  $0.3 \text{ m/s}^2$  and the maximum vertical floor acceleration of about  $1.0 \text{ m/s}^2$ . The estimated damping ratios were little bigger than those presented by Nobata et al. [5-2] of less than 1 to 2 % (which was estimated based on the earthquake records with PGA of less than  $0.5 \text{ m/s}^2$ ). This may be because the base-isolated buildings observed by Nobata et al. [5-2] were not damaged by the earthquakes, while the specimen (superstructure) had been already damaged due to the tests of the fixed-base system. The inserting the base isolation layer below the superstructure decrease the damping ratio as the total system since the damping ratio of the

superstructure range 4 ~ 6 %. This broad range is because the first mode was not clear as that of the base-isolated system, and because the damping ratio (and also the response amplitude) of the first mode was changed after every shaking (Figure 5-7). Three reasons for this reduction in the damping ratio can be considered; (a) The base isolation layer itself does not have any effective contribution to dissipate energy related to the vertical input, while the contribution of the superstructure was lessened because of the existence of the base isolation layer. (b) The higher modes contributed to the increase in the apparent damping ratio for the fixed-base system. (c) The amplitude of the white noise input to the fixed-base system was twice as large as that of the base-isolated system. Since the response of the superstructure may have some nonlinearity, the damping ratio may increase for larger responses. Those issues are discussed later more detail in this chapter.

- (4) The slightly larger damping ratio estimated for HDRB compared with that for NRB+U was not a constant relation since the measured damping ratio of HDRB was smaller than that of NRB+U in Test I; 4.2 % for HDRB while 3.0 % for NRB+U. Even though those values contain more errors, as these estimation provided was based on a six-axial random wave (Figure 3-15), at least those relative magnitudes were supported by the vertical floor acceleration responses at the roof of HDRB being larger than those of NRB+U in Test I;  $7.28 \text{ m/s}^2$  for HDRB while  $6.65 \text{ m/s}^2$  for NRB+U at the corner of the roof when JMA Kobe XYZ was input. This relationship reversed in Test II;  $7.85 \text{ m/s}^2$  for HDRB while  $8.05 \text{ m/s}^2$  for NRB+U. One of the reasons may be that Test I was conducted in the middle of winter while Test II was conducted from the early fall to winter, temperature may have affected the performance of the base isolators. Even though damping ratios were varied, they remained smaller than those of the fixed-base system.

### 5.4.3 Mode shape

The first and second dominant mode shapes in the vertical direction are shared among NRB+U, HDRB and the fixed-base systems with different amplitude distributions. The dominant first and second modes identified from the experiment results are designated modes I and II. Figure 5-8 compared the mode shapes of HDRB (obtained by white noise (II-ii)) with the fixed-base system (obtained by white noise (II-iii) before the test of the fixed-base system started). The hollow circles represent the plots of HDRB and the black circles represent the plots of the fixed-base system. Since the mode amplitude distributions were very close to each other between two base-isolated systems, that NRB+U was not represented in this figure. Two accelerometers per floor are chosen to plot the figure, which are **a1** at the corner and **a4** at the center. Figure 5-8(a) shows the locations of accelerometers used to plot the mode shape. The mode shapes are converted to generalized response amplitude distributions, as shown in Figure 5-9. In this figure, all plots related to the corner responses are connected by a line from the bottom, and the center responses are connected to the corresponding corner of the same floor. Note that the fixed-base system was anchored to the shaking table at the first floor level. By an unhappy accident, there was no accelerometer installed at **a1** when a white noise wave (II-i) was input to NRB+U. Table

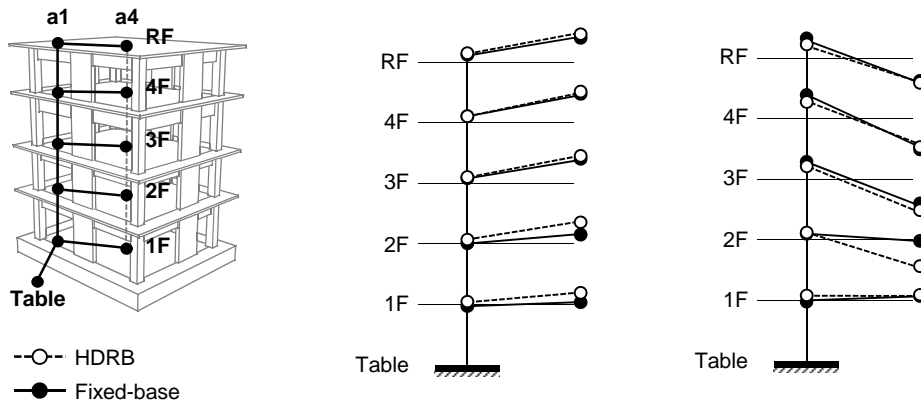


5-1 summarizes the major information obtained by mode shapes, which are the response amplifications by major components of the base isolation layer, columns and slabs, and their contribution percentage relative to the maximum response amplitude. The response amplitude distributions are compared between the base-isolated (HDRB) and fixed-base systems as follows:

- (1) All three structural systems present relatively similar mode shapes. The corner and center of each floor was in phase for mode I, while it became out of phase for mode II (Figure 5-8(b-1) and (b-2)).
- (2) The overall trends of mode shapes of two base-isolated systems (NRB+U and HDRB) were similar.
- (3) The inverted-triangle amplification characterized the fixed-base system as different from the base-isolated systems which had the relatively uniform in response amplitudes over the height. The response amplitude at the center of each floors was 0.35, 0.83, 1, and 0.82 for the fixed-base system while these were 0.76, 0.92, 1, and 0.95 for the base-isolated system (HDRB) from the second to roof floor for mode I, whose values were normalized by the maximum response amplitude. This is because the response of the base-isolated system was mildly concentrated to the base isolation layer while the superstructure was moderately amplified, compared with that of the fixed-base system. This phenomenon was obvious because the soft base isolation layer can be replaced by several stories of floors, which has the equivalent stiffness to that of the base isolation layer.
- (4) For the base-isolated system, the contribution of the floors to the response amplification was large compared to those of the base isolation layer and columns. For mode I of HDRB, the contribution ratio of the base isolation layer was 13 %, that of the columns which was 19 %, and those of the floors which were 61 %, 73 %, 77 %, and 64 % from the second floor to the roof for HDRB. The contribution of columns was obtained by the summation of all columns' contributions from the first to fourth stories (Table 5-1). For the fixed-base system, the contribution of the floors to the response amplification for the first mode was also large but these magnitudes increased from the lower floors to the upper floors. The contribution ratio of the columns was 28 %, and those of the floors became 28 %, 65 %, 77 %, and 53 % from the second floor to the roof for the fixed-base system. The contribution of the columns increased from the base-isolated systems, and the contributions of the slabs varied in broader ranges compared to those of the base-isolated system.
- (5) If the base-isolated system of HDRB vibrated in mode I, the response amplification from the corner to the center of the floors would become 5.0, 4.7, 4.3, and 3.0 from the second floor to the roof. Except the roof, the response amplification was similar for the second to fourth floors. This was also observed for NRB+U with different magnitude ranging from 3.5 to 3.6 with smaller amplification for the roof of 2.5. For the fixed-base system, the response amplification from the corner to the center of the floors would become 4.9, 4.5, 4.4, and 2.9 from the second floor to the roof (Table 5-1). The response amplifications by the slab were very close between HDRB and the fixed-base system but NRB+U. Since the response

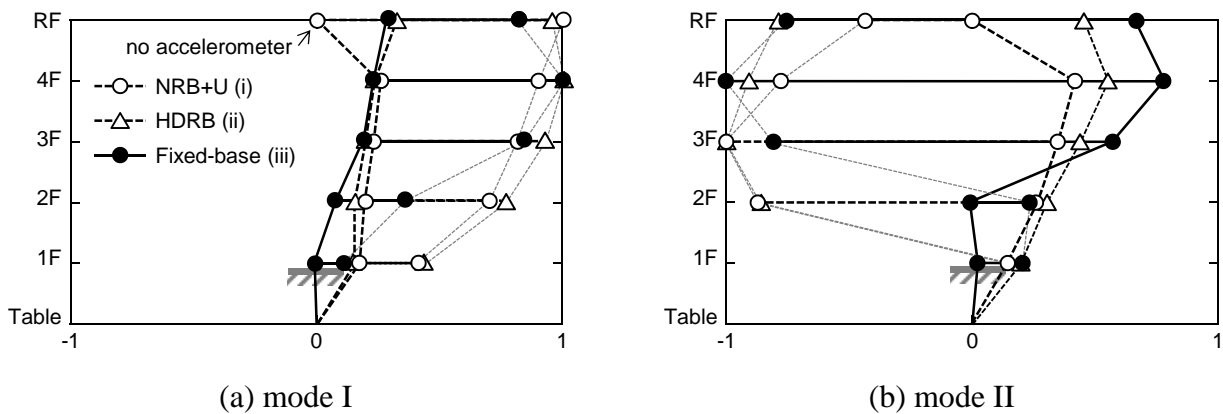
amplifications of respective floors are considered to be similar among different systems since they shared the same slab, no major reason for the different response amplifications of NRB+U from other two was found.

- (6) Smaller contribution of the base floor to the response amplification than those of the upper floors was observable for the base-isolated and the fixed-base systems. It was 30.0 % for HDRB and 10.0 % for the fixed-base system. This is because the floor mass and stiffness are significantly different from the upper floors so that mode I did not enhance the vibration of the base floor. Similarly, the contribution ratio to the response amplification became smaller for the roof because the restrained condition was different from the second to fourth floors. In addition, the additional penthouse anchored to the roof also caused the difference in dynamic characteristics from other lower floors for HDRB and the fixed-base system.
- (7) Overall characteristics of mode II follow mode I. The uniform response amplitude over the height at floor centers for the base-isolated system was observable, while it was increased toward the upper floors for the fixed-base system. The moderate concentration of response to the base isolation layer at mode I was also represented at mode II.



(a) Location of plots (b-1) mode I (b-2) mode II

Figure 5-8 Mode shapes of modes I and II for HDRB and the fixed-base system



(a) mode I (b) mode II

Figure 5-9 Generalized amplitude of the mode vector of NRB+U, HDRB, and fixed-base system

Table 5-1 Response amplifications by major components and their contributions

		NRB+U		HDRB		Fixed-base	
		percentage	amp.	percentage	amp.	percentage	amp.
	Roof	-	-	64%	3	53%	2.9
	4th	64%	3.5	77%	4.3	77%	4.4
slab	3rd	59%	3.5	73%	4.7	65%	4.5
	2nd	51%	3.6	61%	5	28%	4.9
	1st	25%	2.5	30%	3.4	10%	-
	column	-	-	19%	-	28%	-
	base isolation layer	17%	-	13%	-	-	-

(\*1) Since there was no accelerometer at a1 on the roof, the values related to this are omitted.

(\*2) Percentage was calculated with respect to the maximum amplitude of the mode vector, which was normalized as one in Figure 5-11.

## 5.5 Analytical study of vertical modes

In section 5.4, it was found that some modes spaced closely to the first mode for the fixed-base system while the well-separated modes can be observed for the base-isolated system. As both systems have exactly the same superstructure, this significant difference between the modes must be caused by the existence of the base isolation layer. Since it is hard to identify each mode from the transfer functions of the fixed-base system, the specimen was modeled using the finite element method software. The fixed-base system was compared with the base-isolated system of HDRB in this section.

### 5.5.1 Modeling description

Figure 5-10 shows the image and restrained conditions of the model. The proportions of all components were determined based on the actual section of the specimen. All beams (250 mm × 1,250 mm or 250 mm × 900 mm), girders (300 mm × 750 mm), base beams (1,250 mm × 2,000 mm, 1,250 mm × 1,250 mm) and columns (600 mm x 600 mm) were modeled by a bar element. Shear walls (300 mm x 2,100 mm) were also modeled by a bar element, which was located at the middle of the walls, and beams the width of which these walls were connected to were replaced by the rigid beam. The slabs with a thickness of 150 mm were modeled by plate element with a condition of a plane stress. The slabs surrounding beams of each floor with a width of 1 to 1.4 m were also included (Figure 5-10). If not modeling them, it was found that the model had difficulty in simulating mode II of both systems. The figure also shows the division number of the slab for meshing. The specified strength of concrete was  $F_C = 30 \text{ N/mm}^2$  for the base floor beams and  $F_C = 24 \text{ N/mm}^2$  for the rest of the specimen. Young's modulus of 24,000  $\text{N/mm}^2$  originally set to the components consists of the base floor where  $F_C$  was 30  $\text{N/mm}^2$ , and 23,000  $\text{N/mm}^2$  for the upper

structure where  $F_C$  was  $24 \text{ N/mm}^2$ , which is determined by the current Japanese design code [5-3]. The strength of concrete or reinforcement bars were ignored since analysis was conducted in an elastic range. Mass was sourced by self weight of each of the components with a mass density of  $24 \text{ kN/m}^3$ , and the additional mass of the penthouse (167 kN) were distributed over the top floors. The total weight became 7,510 kN, whose margin of error from the measured weight of 7,470 kN was less than 1%. For the base-isolated system, the bottoms of the four base isolators were fully restrained, while nodes along the walls of the longitudinal directions were also fully restrained, in addition to the bottoms of the four columns for the fixed-base system (Figure 5-10(b)). Analysis was conducted under the condition that X, Y axes and the rotation around Z axis were restrained. Modes up to forty were considered.

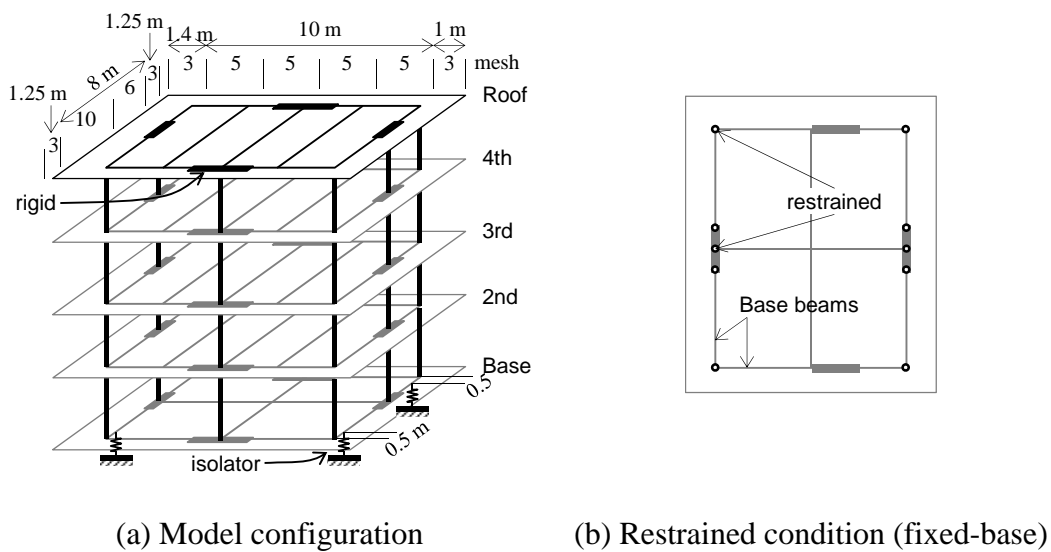


Figure 5-10 Analytical modeling

The stiffness of each component was adjusted so that the major natural frequencies of the models became close to those of the specimen obtained by a white noise input.

- (1) First, the vertical first natural frequency of the superstructure (fixed-base condition) was adjusted to be 13.6 Hz by proportioning Young's modulus.
- (2) Later, the stiffness of the base isolation layer was changed so that the vertical first natural frequency became 10.7 Hz.

Stiffness settings of considered models are summarized in Table 5-2. In the table, stiffness (the Young' modulus) are determined for each floors, in which included the slab, beams and girder, represented by the ratio to that of the roof floor's components. The stiffness ratio of the base isolation layer compared to the vertical stiffness of the high-damping rubber bearing is also shown. Table 5-3 shows major natural frequencies of considered models and those of the specimen measured by white noise. In the table,  $F_{BI}$ ,  $F_C$ , and  $F_S$  are the natural frequency related to the base isolation layer, the columns, and the slab, respectively. The natural frequency of the base isolation

layer  $F_{BI}$  can be obtained assuming the superstructure as a rigid body. The natural frequency of the column can be obtained regarding all slabs of the superstructure as rigid bodies. The natural frequency of the slab  $F_S$  was determined assuming the slab was simply supported at the points connected to the vertical components of columns and walls. This frequency is regarded as the lower band, considering some restriction can be obtained by the flexibility of columns and wall. The relations of these natural frequencies can be considered as major indicators in the prediction of the dynamic response characteristics as a whole system. Their definitions and relation with the vertical dynamic response characteristics can be found in Chapter 8.

Table 5-2 Model descriptions

	Young's modulus of Roof [N/mm <sup>2</sup> ]	Stiffness ratio (/ Roof) <sup>(*1)</sup>			base isolation layer <sup>(*3)</sup>
		Roof	other	Base <sup>(*2)</sup>	
Model 0	17,900	1.00	1.00	1.04	0.56
Model 1	27,400	1.00	0.48	0.50	0.85

(\*1) Stiffness ratio with respect to the roof floor components

(\*2) Stiffness of the base floor was proportioned by 1.04 times to other, which is determined by the original ratio of Young's modulus of 24,000 N/mm<sup>2</sup> to 23,000 N/mm<sup>2</sup>.

(\*3) Stiffness ratio with respect to the vertical stiffness of 3090,000 kN/m (HDRB)

Table 5-3 Summary of natural frequencies

	Fixed-base		Base-isolated		$F_S$					
	mode I	mode II	mode I	mode II	$F_{BI}$	$F_C$	base	2nd	3rd and 4th	roof
Experiment	13.6	19.6	10.65	19.4	-	-	-	-	-	-
Model 0	13.6	22.4	10.56	20.1	15.1	48.9	25.7	17.6	16.3	13.7
Model 1	13.6	22.8	10.65	18.3	18.6	33.9	22.0	15.1	13.9	16.8

The original model as the fixed-base condition yielded the first natural frequency in the vertical direction, 15.4 Hz. Since the first measured vertical natural frequency was 13.6 Hz, the stiffness of all components was reduced simultaneously by 0.78 times. The stiffnesses of the bearings were also reduced to 56 % so that the vertical first natural frequency of the base-isolated system (HDRB) became about 10.7 Hz. This model is designated as Model 0. Model 0 was found to have a vertical first mode response dominated by the roof response. This is shown in Figure 5-11(a-1), which shows the generalized response amplitude distribution of modes I for the fixed-base system. In the figure, Model 0 is represented by hollow circles with a dotted line, and the experiment result is represented in black circles with solid line. It is notable that the response amplitude of the roof center is significantly larger, while others remained small. This excessive contribution of the roof to the first mode is because of the lower natural frequency of the roof. The roof floors supporting condition is relaxed compared to other floors since there is no column or wall above this layer, and

more weight due to the penthouse also reduced the natural frequency. Table 5-3 shows that the natural frequency of the roof supported by pins was the smallest among all floors. On the other hand, the generalized response amplitude obtained by the experiment indicates that the roof had lower contribution than the fourth floor in the mode I. This may be attributed to damages at the lower stories due to consecutive shakings from Test I. Therefore, it was decided that the stiffness of components was to be adjusted disproportionately considering these findings.

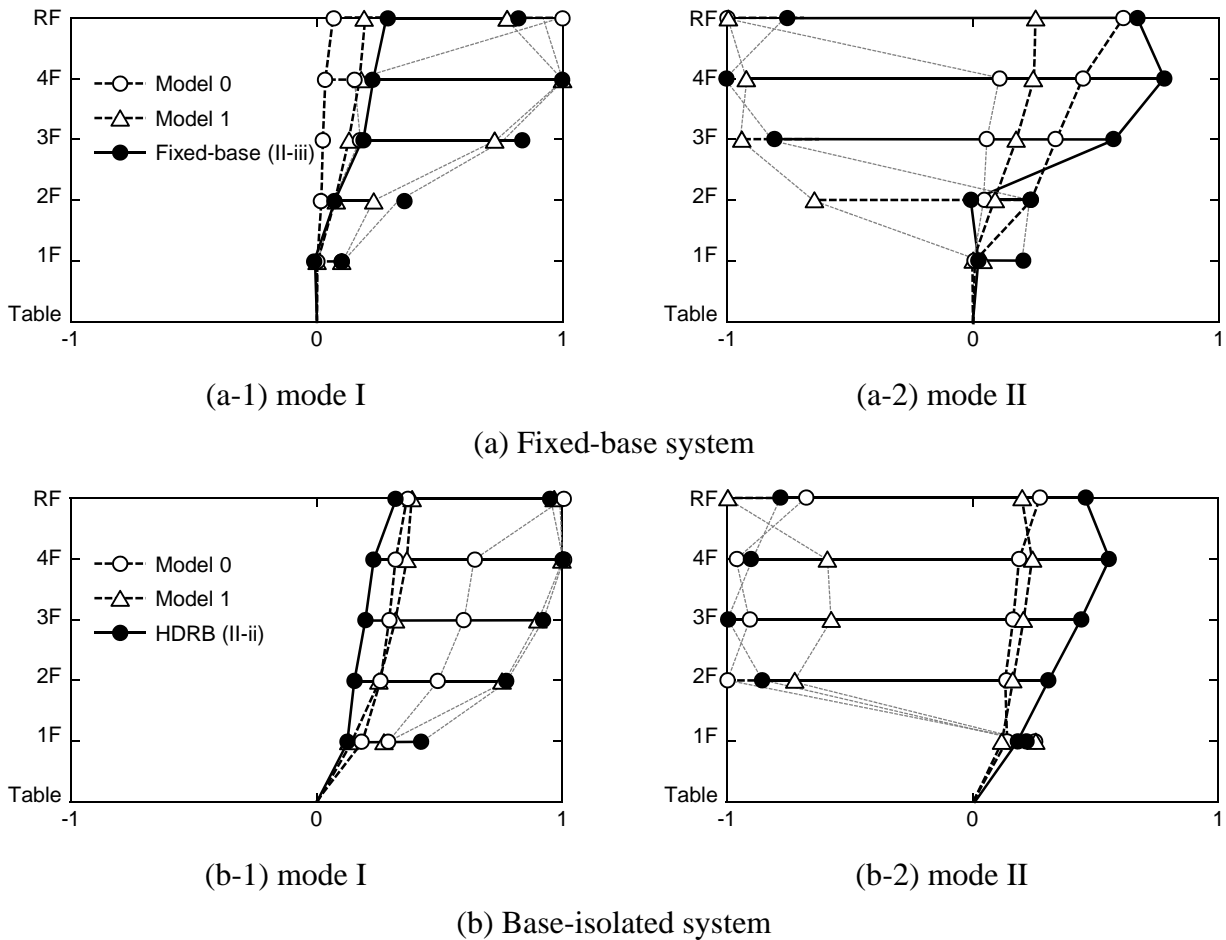


Figure 5-11 Vertical mode vectors of mode I and II

Since there was countless number of possible combinations in the stiffness among all components, the number of variables was reduced as much as possible for the purpose of simplification. In Model 1, it was decided that the stiffness for all components but the roof floor were to be simply reduced proportionally. The ratio of Young's modulus of the other components to the roof floor (including beams and girders) was fixed to 0.48, which yielded reasonably matched generalized response amplitude to that of the fixed-base specimen (Figure 5-11(a-1)). Model 1 is represented by a hollow triangle with dotted lines in the figure. The stiffness of the base isolation layer was reduced to 0.85 times that of the design value. Even with such a simple modification in stiffness proportions, it is notable that Model I simulates the response amplitude distributions fairly well for modes I and II of both systems (Figure 5-11). The natural frequency of mode II in simulation was also fair with an error margin of 16 % larger for the fixed-base system while it was

6 % smaller than the specimen for the base-isolated system. Some notable differences are that the amplification through columns tends to be larger than the specimen in mode I for the base-isolated model, even though that of the columns was underestimated in the fixed-base model. It also tends to underestimate the response amplitude at the corners in mode II for both systems. These observations indicate that the difficulty in identifying the most suitable stiffness combinations, ones which agree with the experiment results for both systems simultaneously. Further discussion is made using Model 1 since this model simulates the basic dynamic characteristics of the specimens well enough to observe the differences between the base-isolated and fixed-base systems.

### ***5.5.2 Estimation of vertical dynamic configurations***

Before look into the vertical response characteristics of analytical models, the configuration related to dynamic response in the vertical direction was discussed using Model 1. For the specific model discussed here (Model 1), the first natural frequency of the base isolation layer was found to be 18.6 Hz, that of the columns was 33.9 Hz, and those of the slabs with the condition of simply (fixedly) supported at the points connected to the vertical components of columns and walls were 22.0 (22.1), 15.1 (18.4), 13.9 (21.1), 13.9 (21.1), and 16.8 (23.2) Hz from the base to roof floor (Table 5-4). The ratio of the natural frequency of the slabs to the columns was 0.41 to 0.50 (except the base floor). As a total system, the first natural frequency of the superstructure became 12.1 Hz, and that of the base-isolated system became 10.7 Hz. The natural frequency of the superstructure was estimated under the condition that the superstructure was fixedly supported at the points where the base isolators were installed (Figure 5-10(b)). The ratio of the natural frequency of the base isolation layer to that of the superstructure was 1.54. This means that the first mode dominated the vertical response of the base-isolated systems even though the base isolation layer had a larger natural frequency than that of the superstructure.

### ***5.5.3 Identifications of modes and damping ratio***

Figure 5-12 shows the response amplification with various damping ratios at the center of the second, fourth and roof floors with respect to the input. In the figure, the corresponding response amplifications measured in the experiment are also shown. In analysis, the uniform damping ratios were applied to all considered modes.

From Figure 5-12, it is notable that the response amplifications of Model 1 fairly reproduced the major characteristics of the fixed-base and base-isolated systems, in which some modes spaced closely to mode I for the fixed-base system, while the well-separated modes can be observed in mode I for the base-isolated system. The damping ratio that matches the experiment result for mode I was clearly 3% for the base-isolated system (Figure 5-12(b)). This ratio agreed with the estimated damping ratio of 2.9% for the experiment by the white noise. For the fixed-base system, the response amplitude with the damping ratio of 5 to 7% became closer to those of the experiment (Figure 5-12(a)). That range was little larger than the experiment results of 4 to 6%, but it is still

similar. For mode II, the corresponding damping ratio may increase to more than 4% for the base-isolated system, which also matches the estimated damping ratio of 3.9%, which was estimated by the experiment.

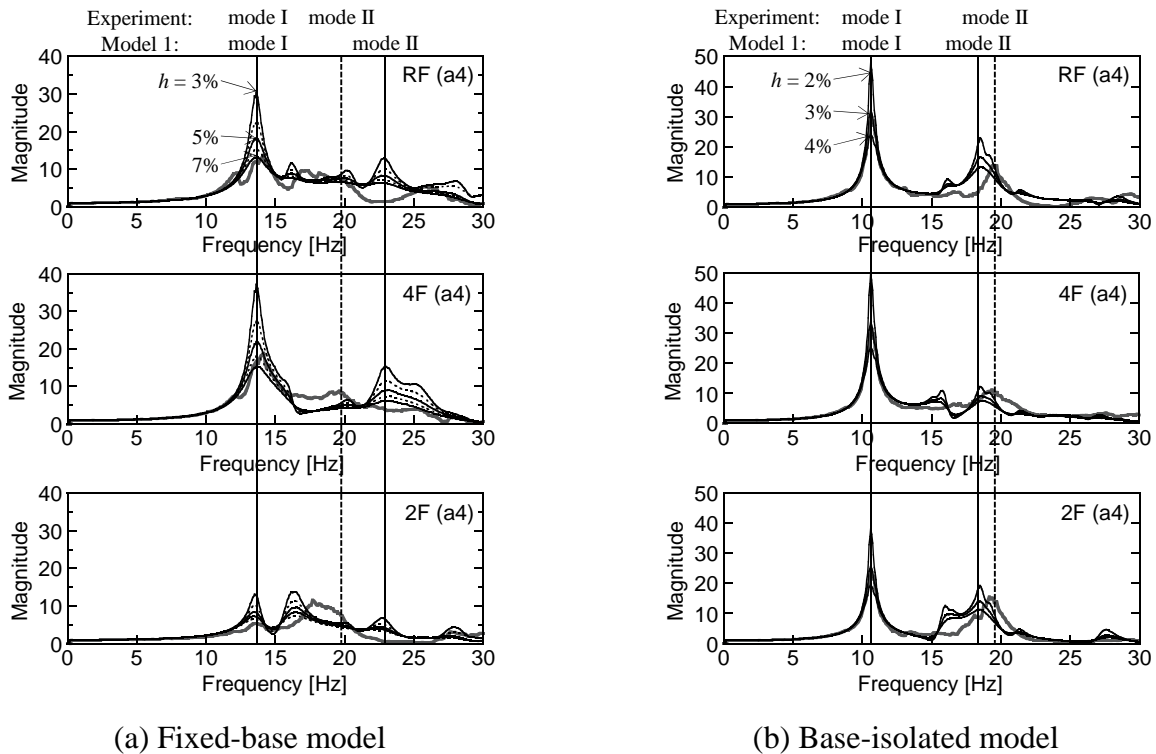


Figure 5-12 Vertical response amplification of Model 1

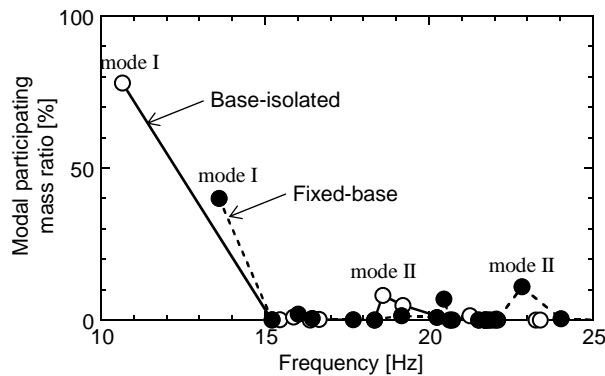


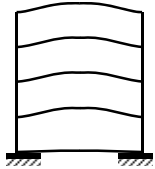
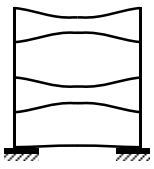
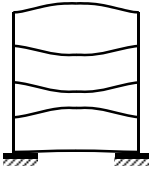
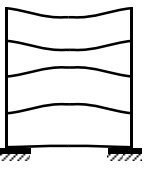
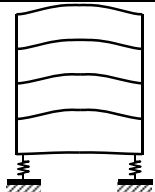
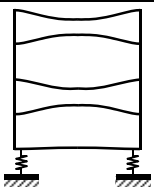
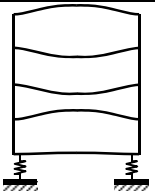
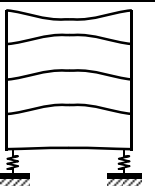
Figure 5-13 Modal participating mass ratio of the base-isolated and fixed-base models

Figure 5-13 shows the modal participating mass ratio of the base-isolated and fixed-base systems. It is notable that mode I dominates the vertical response of the base-isolated system, while it is mitigated for the fixed-base system. The modal participating mass ratio of mode I increases significantly from 40% to 78%, by inserting the base isolation layer. It is also notable that the modal participating mass ratios do not concentrate into a few modes but distributed over the large number of modes for the fixed-base system. Indeed, the accumulated modal participating mass ratio remains 63% for the first twenty modes, while it reaches to 88% for the only first eight modes for the



base-isolated system. It was confirmed that even the first eighty mode contributions (up to 42.4 Hz) remained still 77 % for the fixed-base model without any other conspicuous dominant modes. These findings indicate that the base isolation layer enhance the contribution of a few higher modes.

Table 5-4 Mode shape of the first to third modes

		mode	1	2	3	4
Fixed-base system	Mode shape					
	Natural frequency		13.6	15.2	16.0	16.4
	<hr/>					
Base-isolated system	Mode shape					
	Natural frequency		10.7	15.2	15.9	16.4
	<hr/>					

(\*1) The third mode of the base-isolated system is the rocking mode with respect to the x-axis.

Table 5-4 shows the mode shapes of the first four modes for the fixed-base system and the first five modes except the third mode for the base-isolated system. All modes in the table have the same slab mode, in which each floor vibrates in phase, respectively, but various phase combinations among different floors. The third mode of the base-isolated system is a rocking mode with respect to the x-axis, whose effect was not represented clearly in the shaking table test. Except the first mode of the base-isolated system, the modes with the first slab mode have relatively close natural frequencies among two systems. It is 13.6, 15.2, 16.0, and 16.4 Hz for the fixed-base system, while it is 15.2, 15.9, and 16.4 Hz for the base-isolated system (Table 5-4). These natural frequencies are also close to that of the first slab mode of each floor (13.9 to 16.9 Hz (Table 5-3)). Since the natural frequency of the slab is sufficiently lower than that of the columns of 33.9 Hz (Table 5-3), the natural frequencies of modes with the same slab mode are controlled by that of the slab mode in the superstructure. It is also notable that the base isolation layer helps the separation of only the first mode from higher modes. This is observed from the fact that not only the mode shape but also the corresponding natural frequency of the second mode for both systems remained exactly the same regardless of with and without the base isolation layer (Table 5-3). Those higher modes with the same slab mode are closely spaced to the first mode (mode I) of 13.6 Hz with a difference of 1.6 Hz for the fixed-base system, while the difference increases to 4.6 Hz for the base-isolated system. This means that the contribution of the base isolation layer was larger to the first mode, in which all

components vibrate in phase, than other higher modes.

In summary, the followings are notable:

- (1) The fundamental configuration of the base-isolated system was estimated by the ratio of the natural frequencies. The first natural frequency of the base isolation layer was found to be 18.6 Hz, that of the columns was 33.9 Hz, and those of the slabs were 22.0, 15.1, 13.9, 13.9, and 16.9 Hz from the base to roof floor. The resulting natural frequency of the superstructure was estimated as 12.1 Hz, and the natural frequency of the base-isolated system was 10.7 Hz with the base isolation layer of 18.6 Hz.
- (2) Higher modes closely spaced to the first mode for the fixed-base system were confirmed as modes with the same slab mode as the first mode (mode I). Because the natural frequency of the slab was sufficiently smaller than that of the column by less than half, those first few modes tend to be controlled by the slab mode, resulting in closely spaced modes to the first mode for the fixed-base system.
- (3) The base isolation layer helps with the independence of the first mode, resulting in the higher contribution of the first mode (mode I) from 40% to 78% as a modal participating mass ratio in the vertical responses.
- (4) The conditions of a dominant single mode for the base-isolated system has disadvantage compared to the fixed-base system since the distribution of the modal contributions lead the mitigation of the maximum response. Note that this independence of the first mode was realized even with the base isolation layer, whose natural frequency (18.6 Hz) was larger than that of the superstructure (estimated as 12.1 Hz with the superstructure restrained at the top of four isolators).

## **5.6 Comparison of vertical responses between the base-isolated and fixed-base systems against ground motion**

The vertical dynamic response characteristics obtained by a white noise input indicated the possibility that vertical acceleration responses of the base-isolated system become larger, especially at lower stories than with the fixed-base system. This phenomenon was examined by comparing both system responses for JMA Kobe Z (vertical PGA=3.4 m/s<sup>2</sup>), in which the reproduced waves recorded on the table were reasonably matched. When JMA Kobe Z was input, the dominant response frequencies of both systems were 9.6 Hz for HDRB and about 11 Hz for the fixed-base system. From Figure 5-2(a), it is notable that the pseudo acceleration response amplitudes were ideally close to each other for this frequency range. Figure 5-14 shows the maximum vertical floor acceleration responses recorded at the corner and the center of all floors (**a1** and **a4** in Figure 3-16).

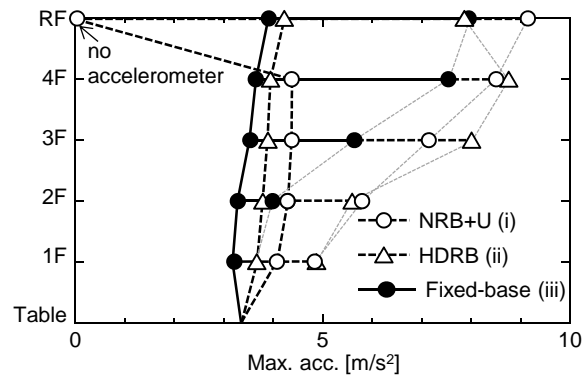


Figure 5-14 Maximum vertical floor acceleration responses for JMA Kobe Z

Since the dominant frequency range of the vertical motion of JMA Kobe is less than 13 Hz, the overall shape of the maximum acceleration response distribution well followed mode I for each system (Figure 5-9(a)). It is notable that the responses of the base-isolated system were larger for almost all recorded points than those of the fixed-base system. This means that the damping ratio of the base-isolated system tended to be smaller than that of the fixed-base system even for ground motion input, which was also observed from white noise waves (2.9 % for HDRB, while 4 to 6 % for the fixed-base system). Moreover, higher modes closely spaced to the first mode may also help distributing mode contributions, resulting in the mitigation the responses for the fixed-base systems. The disparities between the two systems became smaller for the upper floors. The maximum vertical floor responses were  $9.14 \text{ m/s}^2$  and  $8.77 \text{ m/s}^2$  for NRB+U and HDRB, while it was  $7.93 \text{ m/s}^2$  for the fixed-base system at the roof center, the disparity ratios being 1.2 and 1.1. On the other hand, the difference became larger for the lower floors. The maximum vertical floor responses were  $5.79 \text{ m/s}^2$  and  $5.59 \text{ m/s}^2$  for NRB+U and HDRB, while it was  $3.96 \text{ m/s}^2$  for the fixed-base system at the second floor's center. The disparity ratios between the base-isolated and fixed-base systems increased to 1.5 and 1.4 time.

The results show clearly that the vertical floor acceleration response of the base-isolated system tended to be larger than that of the fixed-base system because (1) it had less damping ratio for the first mode in the vertical direction, and (2) vertical response was dominated by a certain mode while it was distributed among a few modes for the fixed-base system.

## 5.7 Shift of vertical dynamic response characteristics for larger response amplitude

### 5.7.1 Vertical acceleration response amplifications

The vertical acceleration response amplifications by major components recorded for ground

motions with the vertical motion (JMA Kobe Z, JMA Kobe XYZ, and El Centro XYZ) are summarized in Figure 5-15. The increasing order of the amplitudes of the reproduced input waves at the first mode response was JMA Kobe Lv1, JMA Kobe Z, and JMA Kobe XYZ for the fixed-base system, and was JMA Kobe Z, JMA Kobe XYZ, and El Centro XYZ for the base-isolated systems (NRB+U and HDRB) (Figure 5-2). The figure plots the acceleration response amplifications by the base isolation layer, columns, and respective floors from the bottom of the figure. The values obtained by the first mode vectors of the experiment result (Figure 5-9) are also shown in the gray-colored squares with a dotted line. Some values are not available in NRB+U since an accelerometer was not installed to the corner of the roof in some cases. From the figures, the followings are notable:

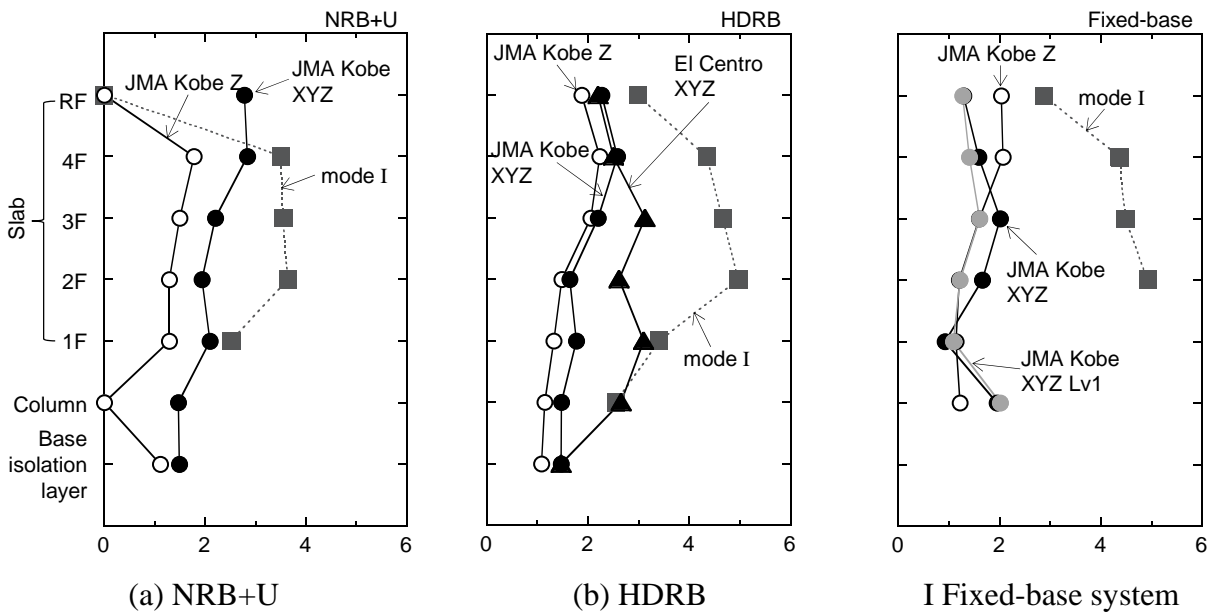


Figure 5-15 Vertical acceleration response amplifications by major components

- (1) The response amplifications by the base isolation layer and the columns ranged between 1.0 and 1.5 for the base-isolated systems, while the range of the column response amplifications increased to 1.0 to 2.0 for the fixed-base system. The response amplification range of the base isolation layer was fairly close to the range of 1.0 to 2.0 mentioned by Nobata et.al. [5-2], which was observed based on the earthquake records with PGA of less than  $0.5 \text{ m/s}^2$  for one to six-stories reinforced concrete base-isolated buildings. When the vertical response was resonated, the column response amplification may increase to 3 (HDRB for El Centro XYZ).
- (2) The response amplifications by the slabs ranged from 1.5 to 3.0 for the base-isolated system, while it decreased to 1.5 to 2.0 for the fixed-base system. For the base-isolated systems, the response amplifications increased as the amplitude of the input ground motion at the first mode response increases (JMA Kobe Z  $\rightarrow$  JMA Kobe XYZ  $\rightarrow$  El Centro XYZ). On the other hand, the response amplifications of the fixed-base system are relatively stable, and less dependency on the input amplitude (JMA Kobe XYZ Lv1  $\rightarrow$  JMA Kobe Z  $\rightarrow$  JMA Kobe XYZ) can be observed. This is because the responses of the base-isolated systems were dominated by the

first mode, and was sensitive to the input amplitude around the first natural frequency, while some higher modes also contributed to that of the fixed-base system.

- (3) Even the vertical response of HDRB was resonated with El Centro XYZ, the response amplifications was securely smaller than those obtained by the mode vector of mode I.

### 5.7.2 Shift of vertical natural frequencies and damping ratios

Damping ratio in the vertical direction, which was estimated about 2 to 3% by a white noise wave, was found to increase for larger acceleration response amplitudes. Figure 5-16 shows the shift of the response amplifications at the fourth floor center to the table of NRB+U and HDRB for ground motions with vertical components. Figure 5-17 shows the shift of the natural frequencies and the damping ratios for mode I with respect to the maximum vertical floor accelerations recorded for the respective ground motions. The natural frequencies are plotted by hollow marks, and the damping ratios are plotted by black marks. Input ground motions (and the recorded maximum vertical floor acceleration) were a white noise ( $1.03 \text{ m/s}^2$ ), JMA Kobe Z ( $9.14 \text{ m/s}^2$ ) and JMA Kobe XYZ ( $22.36 \text{ m/s}^2$ ) for NRB+U, and white noise ( $1.03 \text{ m/s}^2$ ), JMA Kobe Z ( $8.77 \text{ m/s}^2$ ), JMA Kobe XYZ ( $16.84 \text{ m/s}^2$ ), and El Centro XYZ ( $41.03 \text{ m/s}^2$ ) for HDRB.

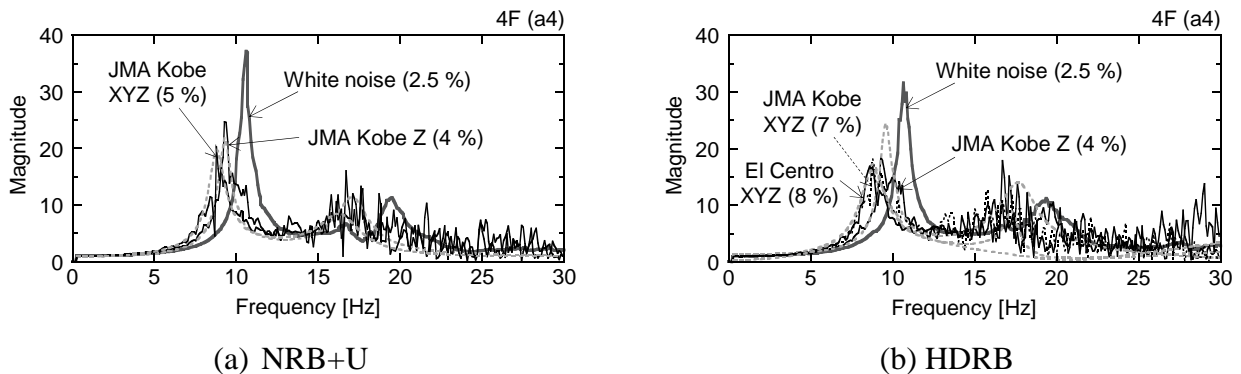


Figure 5-16 Shift of the response amplifications of the base-isolated systems for ground motion inputs

For NRB+U, it is notable that the vertical damping ratio increased from a damping ratio of 2.5 %, which was estimated by the white noise wave, to 4.0 % when the vertical floor accelerations reached about 1 g for JMA Kobe Z. It moderately increased to 5 % for JMA Kobe XYZ with the maximum vertical floor accelerations at  $22.36 \text{ m/s}^2$ . For HDRB, the damping ratio was also mildly increased to 4 % from 2.9 %, when the vertical floor accelerations reached about 1 g for JMA Kobe Z. It significantly increased to 7 % for JMA Kobe XYZ with the maximum floor acceleration at  $16.84 \text{ m/s}^2$ , and little increase to 8 % for El Centro XYZ with extreme maximum floor acceleration of  $41.03 \text{ m/s}^2$ . Simultaneously, the natural frequencies were reduced for larger ground motions. For JMA Kobe Z, the initial natural frequency was reduced to 90 %, and it reached 80 % for JMA Kobe XYZ and El Centro XYZ for both systems. The shift of the natural frequencies and damping ratio in the vertical direction may be caused by the nonlinear behavior of

the superstructure. If the response is dominated by the base isolation layer, the increase of the damping ratio may not be expected unless additional special device is installed to the base isolation layer to dissipate energy.

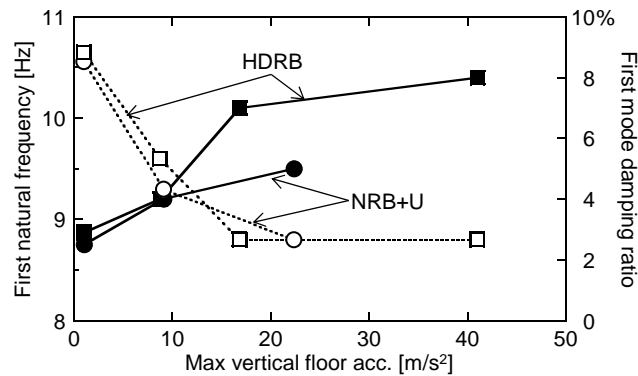


Figure 5-17 Shift of first natural frequency and damping ratio

## 5.8 Damping ratio in the vertical direction

In subsection 5.4.2, it is mentioned that three factors can be considered for why the first mode damping ratio of the fixed-base system was larger than that of the base-isolated system:

- (a) The base isolation layer itself does not have any effective contribution to dissipate energy related to the vertical input, while the contribution of the superstructure was lessened by the base isolation layer.
- (b) The higher modes contributed to an increase in the apparent damping ratio for the first mode for the fixed-base system.
- (c) The amplitude of the white noise input to the fixed-base system was twice as large as that of the base-isolated system, the disparity of which was also applicable to the floor acceleration responses. Since the response of the superstructure may have some nonlinearity, damping ratio may increase for larger input amplitude.

The above possibilities are reconsidered in more details.

From Figure 5-12, the response amplification obtained with the damping ratio of 3 %, which was similar to that of the base-isolated system, had to yield closer results to those obtained by the shaking table test, if (b) were to be applicable. However, response amplifications with a larger damping ratio of 5 to 7 % fitted better in Figure 5-12. Therefore, the factor (b) may not be a main reason. The factor (c) can be considered as one of the major reasons, because the damping ratio tended to increase for larger input even for the base-isolated systems (Figure 5-17) because of the nonlinearity of the superstructure. In addition, the factor (a) is also considered to be the major reason for the larger damping ratio for the fixed-base system than base-isolated system. Since the

deformation was mildly concentrated into the base isolation layer, the contribution of the superstructure to the damping, which was obtained from its nonlinearity, was lessened. This reasoning is the same as that the horizontal damping ratio of the base-isolated building is controlled by that of the base isolation layer rather than the superstructure because the superstructure behaves as a rigid body.

## 5.9 Axial force sustained by base isolators

Axial forces exerted into the base isolators under vertical excitation are also one of the concerns for the base-isolated buildings. Since axial forces of the base isolators were not directly measured in the experiments, it was estimated by the inertia forces of the superstructure. The concept of this procedure is explained in Figure 5-18. The total mass of 7,470 kN was distributed to all floors according to the mass distribution ratio estimated in the design (Figure 5-18). Each floor mass was divided into two; one was belonging to the column mass  $m_C$  and the other was belonging to the slab mass  $m_S$ . Since it was found that the lower modes of the base-isolated system had the same slab mode (Table 5-4), the slab was condensed into a single degree of freedom. The mass contributions of the slab mass to the floor mass were determined as 0.30 for the base floor, 0.54 for the second floor, and 0.59 for the third to the roof floors. The concepts for obtaining the mass contribution ratio of the slab mass to the floor mass are described in Chapter 8. The resulting mass distribution is listed in Figure 5-18. The accelerations recorded at the center of the floor,  $a_4$ , were regarded as representing the acceleration responses of the slab mass, and the accelerations recorded at the corners,  $a_1$  and  $a_3$ , were regarded as representing those of the column masses. Accelerations recorded at the two diagonal corners were averaged to eliminate the rocking effect. The force supported by the base isolation layer was obtained by the summation of inertia forces of those masses. In the following Equations (6-1) and (6-3),  $f_{Si}(s)$  stands for the inertia force of the slab mass and  $f_{Ci}(s)$  stands for that of the column mass located at the  $i$ -th floor at a certain time  $s$ .  $a_{Si}(s)$  and  $a_{Ci}(s)$  are the acceleration of the slab and column DOF of  $i$ -th floor.  $F_i(s)$  is the story axial force sustained by vertical components (including gravity load), which is obtained by the superposition of the inertia forces of every mass located floors upper than the current  $i$ -th story (Equation (6-3)).

$$f_{Si}(s) = ma_{Si}(s) \quad (6-1)$$

$$f_{Ci}(s) = ma_{Ci}(s) \quad (6-2)$$

$$F_i(s) = F_{(i+1)}(s) + f_{Si}(s) + f_{Ci}(s) \quad (6-3)$$

Figure 5-19 plots the maximum and minimum story axial forces  $F_i$  (time-domain superposition of inertia of each DOF) in solid lines. For comparison purposes, values obtained by the direct summation of the maximum or minimum inertia of each DOF are also plotted, and are represented by hollow circles. The plots of axial force due to gravity loads are also plotted in the dotted line.

In the figures, compression forces are represented by plus signs. Four shakings with the vertical ground motions for the base-isolated systems (NRB+U and HDRB in Test II) were shown, which are (a-1) JMA Kobe XYZ for NRB+U, and (b-1) JMA Kobe Z, (b-2) JMA Kobe XYZ and (b-3) El Centro XYZ for HDRB. Since the reproduced waves were quite different between JMA Kobe Z and JMA Kobe XYZ (Figure 5-2(a)), those three waves can be considered as motions with different levels of the amplitude. The followings are notable from the figures:

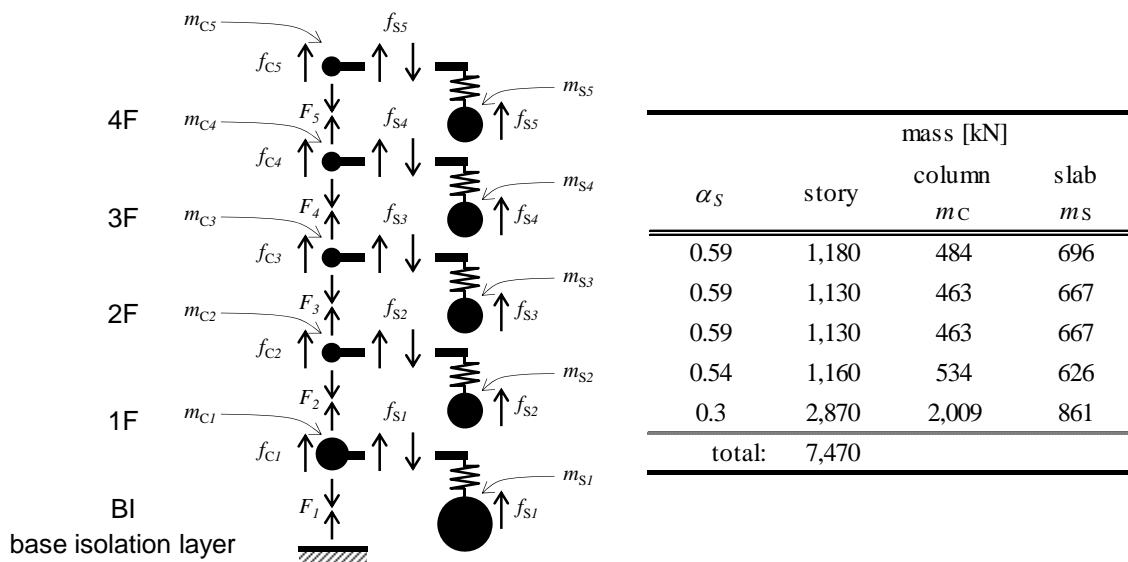
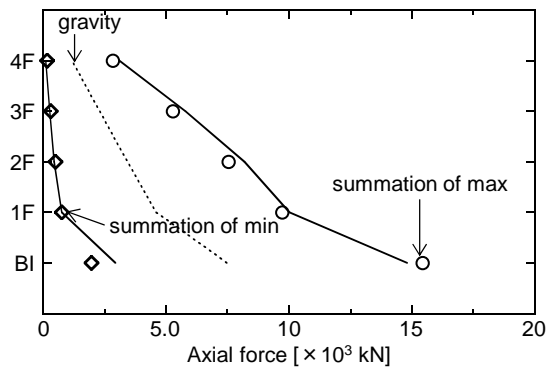


Figure 5-18 Lump mass model to calculated the axial force of the base isolators

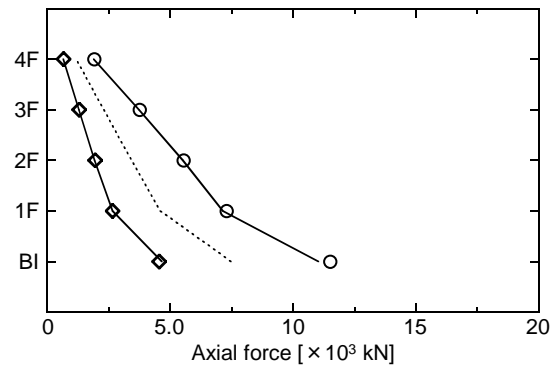
- (1) The compression force of the base isolation layer of HDRB was increased by 1.45 times for JMA Kobe Z, and 1.89 times for JMA Kobe XYZ, 2.63 times for El Centro XYZ from gravity loads alone. These forces were sufficiently below the critical load of the base isolators, which were originally 14 times larger than gravity load for NRB+U, and 15 times larger for HDRB.
- (2) For JMA Kobe Z and JMA XYZ, the base isolation layer did not experience the tension force. In the extreme case of El Centro XYZ, when the resonance occurred between the input wave and the natural frequency of the base-isolated system, the rubber isolators experienced tension force (Figure 5-19(b-3)). The maximum tension stress is estimated as  $0.65 \text{ N/mm}^2$ , which was less than the linear limit tension stress of the rubber isolators of  $1.0$  to  $1.5 \text{ N/mm}^2$ . The tension stress became  $0.79$  if rocking was considered, which was also less than the linear limit.
- (3) The contributions of rocking to the axial forces were less than 2% for the maximum forces. For the extreme case (El Centro XYZ), it increased to 26%.
- (4) The direct summation of the maximum or minimum forces generated by each DOF reasonably matches to the axial forces obtained by the time-domain superposition of inertia of each DOF. This means that the responses were dominated by the first mode, and that the axial force can be estimated sufficiently by considering the first mode only for this system.
- (5) Relatively larger errors in the axial force of the base isolation layer than those of upper stories were observed between the direct summation and the time-domain superposition. This is



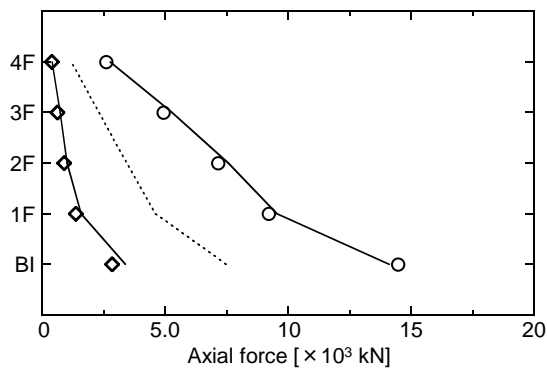
because the natural frequency of the base floor was larger than the upper floors making it so that the first mode did not dominated at the first floor.



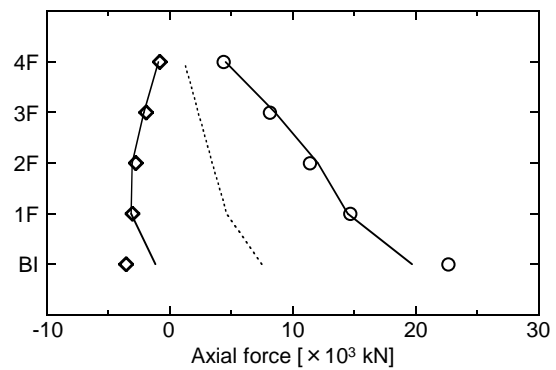
(a-1) NRB+U for JMA Kobe XYZ



(b-1) HDRB for JMA Kobe Z



(b-2) HDRB for JMA Kobe XYZ



(b-3) HDRB for El Centro XYZ

Figure 5-19 Axial forces sustained by each story

In summary, it is notable that the axial force exerted on the base isolation layer can be estimated only by considering the first mode contribution of the specimen (the natural frequency ratio of the base isolation layer to the superstructure was estimated as 1.54). Even when the base isolation layer experienced extreme loading, tension forces remained below the linear limit of the rubbers, and the contribution of rocking on the axial force exerted into the isolation layer was small.

## 5.10 Summary and conclusions of Chapter 5

This chapter discussed the dynamic response characteristics of the base-isolated system, compared with those of the fixed-base system based on the full-scaled shaking table test results. In addition, some supplemental analysis was also conducted to examine the mode contributions to the vertical response in detail. The major findings obtained in this chapter are as follows:

- (1) Significantly larger vertical floor acceleration responses were recorded compared to the horizontal acceleration responses when the full-scaled base-isolated system was tested for

three-directional ground motions. Input accelerations were amplified by almost 5 times for JMA Kobe XYZ, resulting in the disparity in floor acceleration responses at the roof center between vertical and horizontal directions of 6.5:1.

- (2) Some modes spaced closely for the fixed-base system, while the first mode was well separated by inserting the base isolation layer.
- (3) The first vertical natural frequency was reduced by 10 ~ 20 % from 12 ~ 13 Hz (the superstructure) to 10.6 Hz for NRB+U and 10.7 Hz for HDRB, by inserting the base isolation layer of 17.1 Hz and 20.3 Hz, respectively.
- (4) The damping ratio for the first mode of the base-isolated system was estimated as lower than 3 %, while that of the superstructure was 4 ~ 6%. The main factor which caused the smaller damping ratio of for base-isolated system may be less contribution from the base isolation layer to the damping in the vertical direction. The damping ratio increased up to 8 % when the acceleration response amplitude became larger.
- (5) The base-isolated system had relatively uniform response amplitudes from the bottom to the top floors, which characterized the response mode of the base-isolated system against the inverted-triangle response mode of the fixed-base system. This is because the response amplifications were concentrated into the soft base isolation layer as if there were additional several stories inserted below the superstructure. This characteristic was observed both for a white noise wave input and also for ground motion inputs.
- (6) The floor accelerations for JMA Kobe Z (only the vertical motion) recorded for the base-isolated system were larger at almost all measurement points than the fixed-base system. When JMA Kobe Z was input to both systems, the input amplitudes at the dominant response frequency for both systems were ideally close to each other. The results show clearly that the vertical floor acceleration response of the base-isolated system tended to be larger than that of the fixed-base system because (1) it had less damping ratio for the first mode in the vertical direction, and (2) vertical response was dominated by a certain mode while it was distributed among a few modes for the fixed-base system.
- (7) The response amplifications by the base isolation layer and the columns ranged between 1.0 and 1.5 for the base-isolated systems, while the range of the column response amplifications increased to 1.0 to 2.0 for the fixed-base system. The response amplification range of the base isolation layer was fairly close to the range of 1.0 to 2.0 mentioned by Nobata et.al. [5-2], which was observed based on the earthquake records with PGA of less than  $0.5 \text{ m/s}^2$  for one to six-stories reinforced concrete base-isolated buildings. When the vertical response was resonated, the column response amplification may increase to 3 (HDRB for El Centro XYZ).
- (8) The response amplifications by the slabs ranged from 1.5 to 3.0 for the base-isolated system, while it decreased to 1.5 to 2.0 for the fixed-base system. For the base-isolated systems, the response amplifications increased as the amplitude of the input ground motion at the first mode response increases. On the other hand, the response amplifications of the fixed-base system are relatively stable, and less dependency on the input amplitude can be observed.

This is because the responses of the base-isolated systems were dominated by the first mode, and was sensitive to the input amplitude around the first natural frequency, while some higher modes also contributed to that of the fixed-base system.

- (9) The axial force exerted onto the base isolator was found to be dominated by the first mode. Tension force occurred in the base isolators, when the maximum vertical floor acceleration of the superstructure reached 4 g. But the estimated maximum tension force was sufficiently below the linear limit tension stress of the rubbers. It was also notable that the contribution of the rocking on the axial force was less than 30% even in the extreme case when the resonance occurred.
- (10) With the finite element model of the specimen, the natural frequency of the superstructure was found to be about 12.1 Hz (estimated for the superstructure restrained at the top of four isolators), in which the natural frequency of the columns was 33.9 Hz, and those of the slabs were 13.9 to 15.1 Hz. On the other hand, the natural frequency of the base isolation layer is estimated as 18.6 Hz for HDRB, which is about 92 % of the natural frequency obtained by the design values of 20.3 Hz with the condition of the rigid-body superstructure.
- (11) Finite element analysis also showed that the upper few modes shared the same slab mode. Because the natural frequency of the slab was sufficiently smaller than that of the column by less than half, those first few modes tend to be controlled by the slab mode, resulting in closely spaced higher modes to the first mode for the fixed-base system. By inserting the base isolation layer, only the first mode was independent from others. The modal participating mass ratio of the first mode was increased significantly from 40 to 78 % by inserting the base isolation layer at the bottom of the superstructure.
- (12) The conditions of a dominant single mode for the base-isolated system has disadvantage compared to the fixed-base system because the distribution of the modal contributions lead the mitigation of the maximum response. Note that this independence of the first mode was realized even with the base isolation layer, whose natural frequency (18.6 Hz) was larger than that of the superstructure (estimated as 12.1 Hz).

## REFERENCES

- [5-1] Nagamatsu A., Introduction to Modal Analysis, Corona-sha
- [5-2] Nobata A., Teramura A., and Yasui Y., Vertical Resposne Characteristic of Base-Isolated Building Based on Observed Earthquake Records, Report of Obayashi Corporation Technical Research Institute, No.56, 1998, pp.23-28.
- [5-3] AIJ Standard for Structural Calculation of Reinforced Concrete Structures -Based on Allowable Stress Concept-, revised 2010, Architectural Institue of Japan
- [5-4] Chopra A. K., Dynamics of Structure, Third Edition, Pearson Education, Inc., 2007.

# **CHAPTER 6**

## **MEDICAL EQUIPMENT BEHAVIOR**

### **FOR HORIZONTAL MOTIONS**

#### **6.1 Introduction**

This chapter describes the interior performance of the base-isolated medical facility for horizontal ground motions obtained from the full-scale shaking table tests. Damages to the medical facility arranged according to the current practices are observed based on Test I, and the effectiveness of some measures applied in Test II is also discussed. The performance was also compared with that of the fixed-base system.

#### **6.2 Contents installed in the facility**

In Test I, each room of the specimen was furnished and equipped with medical equipments as realistically as possible according to current medical practices. The arrangement of each room, the installation of nonstructural components, and the layout of equipment and its setting conditions are described in Chapter 3.

The number of items installed in Test I is summarized in Table 6-1 with respect to the room. In the table, the CT scan, dialyzer, and surgical microscope are given as examples of ‘Medical equipment.’ Book shelves, an emergency cart, and overbed tables are given as examples of ‘Furniture.’ Doors, virus-proof walls, and raised floors are given as examples of ‘Nonstructural components.’ Sprinklers, air conditioners, and suction bins are given as example of ‘Utility.’ Fire-proof shutters, flexible joints, roof top tanks and servers are categorized into ‘Others.’ Among items categorized in medical equipment and furniture, the number of pieces of equipment that are used for laying a patient, such as a hyperbaric pressured oxygen capsule and a consultation bed, are also counted. Plumbing and lights are not counted in Table 6-1. One of the most significant characteristics of the interiors of medical facilities is that most of them are designed to be flexible and mobile. Most of furniture and equipment are supported by casters. Hanging-type sliding doors are usually adopted because these are very easy to open. The number of items

supported by casters, among which the number of items whose casters were locked is also counted in Table 6-1. It was found that 68 % of furniture and medical equipment were supported by casters, 85 % of which were left in the lock-free condition, following the advice of professionals at the National Institute of Public Health. The largest number of pieces of medical equipment was arranged in the third floor operating room. All of these were supported by casters, but none of them was locked except an operating table. To observe the effect of locking casters, half of the beds in the patient room were locked, and the other half were left lock-free.

Table 6-2 shows the properties of some representative equipment installed in the operating room and beds of the patient room. All of them were supported by casters. The friction coefficients for unlocked casters were mostly between 3 to 5 %, while the coefficients were increased to 20 to 50 % when these were locked. Except for the monitor rack, most of them had relatively lower heights of less than 1 m, those aspect ratios were about 2.0. Some mobile equipment weighted more than 1 kN such as the heart-lung bypass, the anesthesia machine, and patient beds. The friction coefficient of free-standing furniture and equipment, which did not have casters, such as a consultation table in the consultation room (2F), ranged from 30 ~ 60%.

Table 6-1 Medical equipment, furniture, and nonstructural components installed in the specimen for Test I

Item	Bed <sup>(*1)</sup>	Medical app.			Furniture			Ceiling pendant	Nonstructural			Utility <sup>(*4)</sup>	Others <sup>(*5)</sup>
		total	with caster	locked <sup>(*2)</sup>	total	with caster	locked <sup>(*2)</sup>		total	door	partition <sup>(*3)</sup>		
1F X-ray Room	2	9	3	2				1	1				
Server Room 1								3	1	2		6	
Consultation Room	1	1	1	1	9	6	0	1	1		3		
2F Dialysis Room	2	3	2	1	3	3	2	1	1				
Staff Station					15	9	1				1		
3F ICU	2	1	1	0	5	5	2	2	1	1	2		
Operating Room	1	10	10	0	1	1	0	4	5	1	4	2	
4F Patient Room	4	2	2	1	19	10	2		3	1	2	15	
Server Room 2									3	1	2		
Others									3	3		3	
SUM	12 7.6%	26 16.5%	19	5 (26%)	52 32.9%	34	7 (21%)	6 3.8%	21 13.3%	11	10	26 16.5%	27 17.1%

(\*1) Any pieces of furniture or medical equipment is counted as a bed if it is used for laying down a patient. A consultation bed, a high-pressured oxygen capsule and an operating table belongs in this category.

(\*2) Any pieces of furniture or medical equipment whose casters is locked or lifted from the floor by adjusters belongs in this category.

(\*3) The Category 'Partition' includes virus-proof walls installed to the operating room and raised floors in the server room.

(\*4) The category 'Utility' includes sprinklers, air conditioners, suction bins, fire hydrants, and console units for the patient room.

(\*5) All others belong to the category 'Others,' which includes flexible joints for the base isolation layer, nitrogen tanks, server systems, and roof-top tanks.

Table 6-2 Properties of furniture and equipment

	width	depth	height [mm]	aspect ratio		weight [kN]	unlocked	locked
	[mm]	[mm]		width	depth			
anesthesia machine	560	680				1.40	2.5%	10.5%
surgical microscopes	410	480	830	2.02	1.73	0.33	5.0%	
monitor rack	600	800	1380 <sup>(*1)</sup>	2.02	1.73	0.65	16.7%	22.7%
suction pump	500	500	700	2.02	1.40	0.08	8.0%	45.3%
hear-lung bypass	900	600	650 (1550 <sup>(*2)</sup> )	0.72	1.08	2.22	4.6%	
telemeter	370	600	900 (1170 <sup>(*3)</sup> )	2.43	1.50	0.33	3.2%	32.4%
cardioverter defibrillator	350	500	800 (1000 <sup>(*3)</sup> )	2.29	1.60	0.30	3.2%	38.5%
wagon	600	500	920	1.53	1.84	0.72	1.8%	20.3%
operation table	560	2100	830	1.48	0.40	2.56	6.0%	54.4%
patient beds	1100	2100	320 ~ 700			1.18 ~ 1.27	2 ~ 3%	40 ~ 60 %

(\*1) A TV monitor was placed on the top

(\*2) Height including bars.

(\*3) Height including a machine placed on the top

### 6.3 Performance of medical equipment for horizontal ground motions

The interior performance of the base-isolated system obtained from the full-scale shaking table test was examined with respect to the two types of ground motions; one was near-fault ground motion, the other was long-period and long-duration ground motion. JMA Kobe was chosen as a representative of the near-fault ground motion, and Sannomaru as the long-period and long-duration ground motion. Because only a few pieces of medical equipment were tested under operational condition, physical damages such as dislocation distance were mainly focused. The performance of medical equipment during shaking was observed by video, and the residual conditions and damages were observed based on the check sheets and dislocation plots, which were filled out by research members after every major shakings. These performances were compared with respect to the following corresponding floor responses: absolute acceleration, absolute velocity, and absolute displacement. The absolute acceleration of floors is believed to be one of most significant indicators to assess the performance of objects arranged inside a building, because it determines whether an object starts to move. The absolute velocity is also a commonly used indicator to predict the possibility of an object overturning. The absolute displacement of floors is an indicator that is related to the dislocation distance by sliding if the friction coefficient of the item is nearly zero.

The maximum absolute accelerations, velocities, and the radii of circles that enclose a trajectory of absolute displacements recorded for each system are summarized in Table 6-3 with respect to the types of structural system and ground motions. It is notable that except for the fixed-base system against the near-fault ground motion, accelerations for all other cases were not more than 3.00 m/s<sup>2</sup>. This relatively small acceleration amplitude, however, was enough to dislocate most of the furniture

and equipment supported by unlocked casters (Table 6-2). From Figures 6-1 to 6-4, the residual location of furniture, equipment, and ceiling pendants are plotted together with their initial positions. The plans of each figure are gridded at every 500 mm. The plots are for the third floor where the ICU and the operating rooms were located, and the fourth floor where a patient room was located. The plots for the fourth floor server room are not included in the figures. A small circle belonging to each piece of equipment was the reference point to record the dislocation distance, commonly the location of its supports. Hollow circles represent items with unlocked casters, and black circles represent those with locked casters or free-standing furniture without casters. In the figures, the corresponding acceleration and absolute displacement time histories are shown for the third floor. The trajectories of the absolute floor displacements are also shown with the concentric circles with the radius of 100, 200, and 300 mm. Table 6-3 also summaries the notable damages to medical equipment, furniture, and service equipment, in addition to their maximum residual displacement and sliding velocity relative to the floor. Performance of equipment supported by casters is categorized into two: with and without caster locks.

Table 6-3 Summary of damages to furniture item, medical equipment and service equipments

Furniture items and Medical Appliances	Friction Coefficient	JMA Kobe		Sannomaru		
		Fixed-base	Base-isolated	Fixed-base	Base-isolated	
Duration of major wave [s]		20		120		
Max. acc. [ $\text{m/s}^2$ ]		25.02 (3F)	2.68 (RF)	3.00 (RF)	2.58 (4F)	
Max. vel. [m/s]		1.27 (RF)	0.76 (4F)	0.55 (3F)	1.11 (4F)	
Radius enclosing absolute disp. [m]		0.2	0.3	0.2	0.4	
Patient beds	unlocked	0.02 – 0.03	1.0 m	1.0 m	0.5 to 1.0 m	1.5 m
	locked	0.4 – 0.6	0.5 m <sup>(*1)</sup>	No movement	No movement	No movement
Other item supported by casters	unlocked	0.03 – 0.05	0.5 to 1.0 m	0.5 to 1.0 m	0.5 to 1.0 m	1.0 to 3.0 m
	locked	0.2 - 0.45	~ 0.5 m	~ 0.5 m	~ 0.5 m	~ 0.5 m
Free-standing items		0.4 - 0.6	0.5 m	No movement	No movement	No movement
Other Notable Damage		Scatter of various articles; Damage to piping systems; Water leakage in tank pipes; Falling of objects; Dislocation of sliding doors	Minor collisions between moving items with casters	Overflow of water from tank on roof	Serious collisions between moving items with casters; Damage to plastic lid of water tank; Popping out of chest of drawers	
Relative vel. of item with casters [m/s] <sup>(*2)</sup>		0.4	0.3 (0.5 <sup>(*3)</sup> )	0.2	0.7	

(\*1) Brackage of locking devices

(\*2) Roughly estimated velocity with respect to the floor based on video

(\*3) Involving bumping against walls or other equipment

### ***6.3.1 Near-fault ground motions***

The near-fault ground motions had large acceleration components for lower periods. In the fixed-base system, very large floor accelerations of  $25.0 \text{ m/s}^2$  and absolute velocities of  $1.23 \text{ m/s}$  were recorded. Absolute displacements were relatively small compared to other cases whose trajectory was within the concentric circle with the radius of  $0.2 \text{ m}$ , most parts of which were smaller than  $0.1 \text{ m}$  in the radius. The corresponding figures are shown in Figure 6-1, and the notable findings are as follows:

- (1) No damage occurred in plumbing systems, sprinklers, or suspended ceilings, which are typical components where damages were reported after major earthquakes [6-1 to 5]. Some minor damage was observed to the pipes that were connected to the water tank on the roof. Minor water leakage was observed at the connection of the pipe to the tank.
- (2) No equipment that was tested in the operated condition had a problem in its function.
- (3) The floor acceleration of up to  $25.0 \text{ m/s}^2$  was strong enough to dislocate all free-standing items and those with locked casters. The distance of dislocation was about  $0.5 \text{ m}$ . Furniture was propelled little by little by major pulses, accumulating relatively larger residual dislocations.
- (4) Even though the absolute velocity was relatively large to  $1.23 \text{ m/s}$ , toppling of furniture or equipment was not observed, because most of slender items whose aspect ratio was more than two were supported by unlocked casters. One exception was a book shelf facing the wall on its back on the second floor,  $920 \text{ mm}$  height and with an aspect ratio of  $2.0$ , which fell down, scattering its contents.
- (5) Thanks to their low friction, no violent acceleration input was observed for items supported by unlocked casters. The dislocation distance increased to the maximum of  $1.0 \text{ m}$ . The reason for these relatively larger residual displacements in relation to the absolute floor displacement was caused by the characteristics of the casters. The axis of the casters tended to maintain its current directions, because stronger forces of sufficient duration are needed to change a direction of casters, which caused the drift of neutral location after every major pulses. Estimated by the video, the relative velocity to the floor of these equipment was about  $0.4 \text{ m/s}$ .
- (6) Patient beds with unlocked casters tended to slide a longer distance than others. Some patient beds slid more than  $1.0 \text{ m}$ . The primarily reason is because of friction coefficients. The coefficient was slightly smaller in patient beds ( $0.02$  to  $0.03$ ) than in other equipment ( $0.02$  to  $0.1$ ) supported by casters. This was because the casters supporting the patient beds were fabricated more delicately. Another reason is that the patient beds were arranged along the walls. Items facing the wall tended to dislocate further due to bumping against the wall if their casters were not locked.
- (7) Because of large accelerations, a mannequin that had been placed on the operating bed slipped off, as shown in Figure 6-1. In addition, contents of tables and inside shelves, such as a monitor placed on a ceiling pendant at ICU, were toppled.
- (8) Stable response of contents placed on furniture or equipment supported by unlocked casters, such



as monitors on the monitor rack, were observed.

Contrary to the fixed-base system, the base-isolated system exhibited significantly less movement in medical equipment because of the reduction of acceleration input. Note that the floor acceleration never exceeded  $2.68 \text{ m/s}^2$ , and the absolute floor velocity of  $0.76 \text{ m/s}$  remained lower than that of the fixed-base system (Table 6-3). Only the absolute displacement increased so that its trajectory reached  $0.3 \text{ m}$  in the radius. The corresponding figures are shown in Figure 6-2, and notable findings for the base-isolated system were as follows:

- (1) Because of the great reduction in floor acceleration, no violent response was observed inside the specimen. No free-standing equipment was moved.
- (2) No scattering of contents on tables or shelves was observed. Some drawers were open because of their low friction.
- (3) Items with unlocked casters slid about  $0.5$  to  $1.0 \text{ m}$ , but the sliding velocities of these items relative to the floor were small, not greater than  $0.3 \text{ m/s}$ .
- (4) Dislocation of patient beds reached  $1.0 \text{ m}$ . A number of bumping was observed against the wall and locker next to them, which caused an increase in the relative sliding velocity to  $0.5 \text{ m/s}$ , and dislocation distance larger than other items. The increase in dislocation distance due to pounding was also observed on the wagon located in the operating room next to the door.
- (5) When the patient bed was locked, no sliding movement was observed.

Overall, the base-isolated system exhibited great performance maintaining the condition of the facility inside for the near-fault ground motion. This was due to the great reduction of the acceleration input to the facility. Dislocation of items supported by casters may cause some problems to people inside the room, because the speed of movement sometimes reached  $0.5 \text{ m/s}$  especially when bumped against the wall. It is recommended to lock casters especially if the equipment is heavy and facing the wall.

### ***6.3.2 Long-period and long-duration ground motions***

The long-period and long-duration ground motion does not generate large accelerations, but lasts longer with dominant periods more than  $2 \text{ s}$ . Because of this, the damage of the fixed-base system was significantly reduced compared to that observed for the near-fault ground motion. As shown in Table 6-3, the floor responses in the fixed-base system for Sannomaru were small in the maximum acceleration ( $3.00 \text{ m/s}^2$ ), and the maximum velocity ( $0.53 \text{ m/s}$ ). The trajectory of the absolute floor displacement was  $0.2 \text{ m}$  in radius, which was similar to that for JMA Kobe. The corresponding figures are shown in Figure 6-3, and some notable observations are summarized as follows:

- (1) Little movement was observed except that of medical equipment and beds with unlocked casters.
- (2) The dislocation distance of casters was similar to that experienced in the near-fault ground motion.

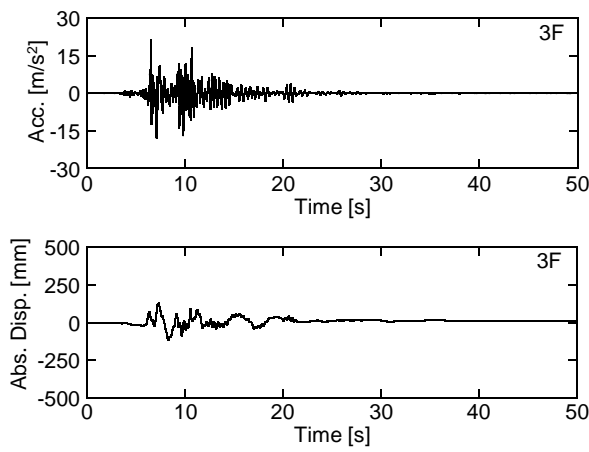
Items supported by unlocked casters, including the patient beds moved about 0.5 to 1.0 m, which was similar to the dislocation distance observed against the near-fault ground motion of 0.5 to 1.0 m for unlocked casters. This indicates that the acceleration amplitude has less effect on the residual dislocation amplitude of caster-supported items, once acceleration reaches the extent that the item starts to move.

- (3) The relative velocity of moving items reached 0.2 m/s, which was much smaller than 0.4 m/s for the near fault ground motion. This means that the intensity of sliding movement of equipment supported by casters was more moderate than that for the near-fault ground motion even though the dislocation distance was similar to each other.

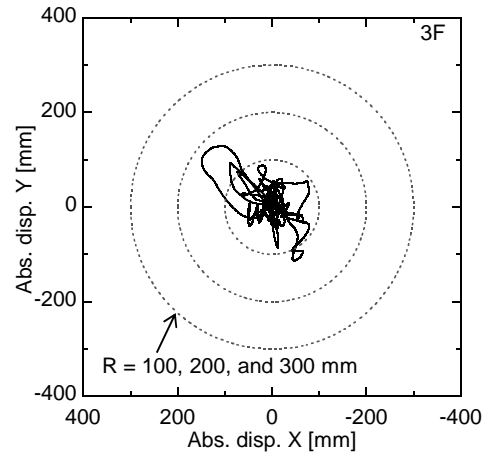
The long-period and long-duration ground motion is one of the serious concerns for the base-isolated system. The floor acceleration remained less than  $3.0 \text{ m/s}^2$ , while the absolute velocity reached more than 1.0 m/s, and the trajectory of the absolute displacement reached to about 0.4 m in radius. The performance of equipment was deteriorated mainly because of the large amplitudes in the floor displacement. Under JMA Kobe, most parts of the floor displacement trajectory were enclosed with the radius of 0.2 m, while several cycles reached further than 0.2 m (up to 0.4 m) for Sannomaru. The corresponding figures are shown in Figure 6-4, and major findings are as follows:

- (1) In the base-isolated system, most notable is the wild movement of medical equipment and patient beds with unlocked casters (Figure 6-4). The equipment moved back and forth many times with a displacement amplitude of about 0.7 m. Some equipment reached its residual displacement of more than 3.0 m (a heart-lung bypass machine in the operating room). The relative velocity to the floor was estimated about 0.7 m/s by the video, which was more than two times faster than that for the near-fault ground motion. This large movement caused not a few of them bumped to other equipment and wall panels and boards, which caused damage.
- (2) Other free-standing equipment and furniture items and those with locked casters showed no movement at all if no bumping by other moving items was present.
- (3) Hanging-type sliding doors were continuously opened and closed throughout the shaking. Some doors were damaged in the stoppers because of consecutive impacts.
- (4) No scattering of contents on tables or shelves was observed. Some drawers were open because of their low friction.

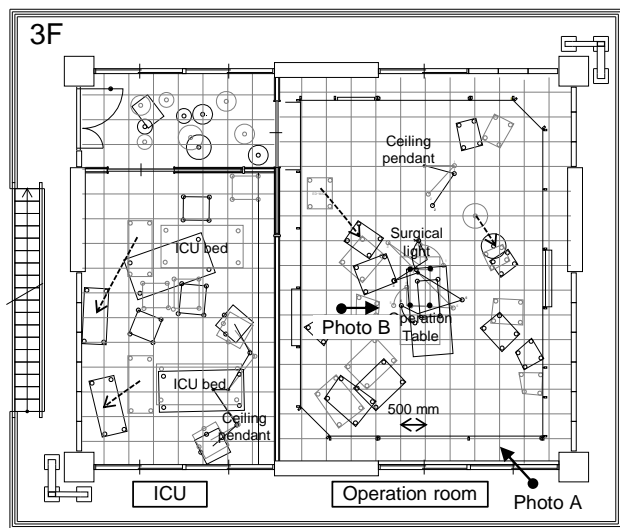
The results obtained from the long-period ground motion clearly indicate that the base-isolated system is not necessarily invincible against this type of ground motion. There was no structural damage, and, due to relatively smaller floor accelerations, no movement occurred in most of furniture items and other equipment. The only exceptions were item with mobile casters, which are the characteristic of furniture and equipment used in medical facilities. The items moved wildly for many cycles, which resulted in collisions among themselves and against partition walls. It was also notable that once the casters were locked there was no movement observed at all.



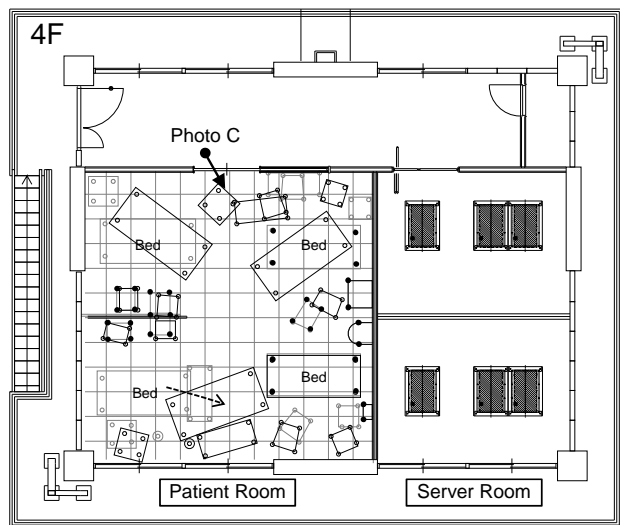
(a) Acceleration and absolute displacement time histories of the third floor



(b) Trajectory of absolute displacement of the third floor



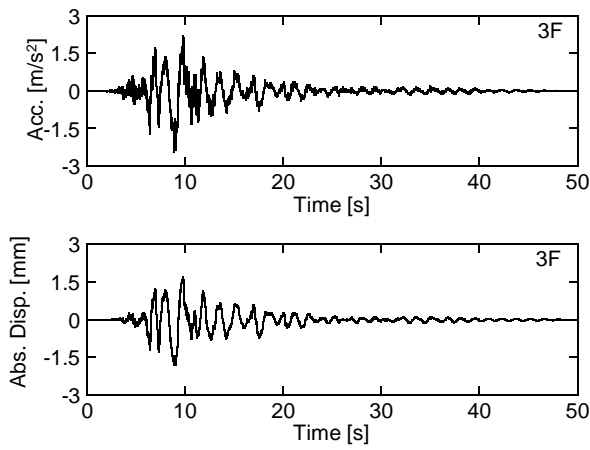
(c-1) Third floor



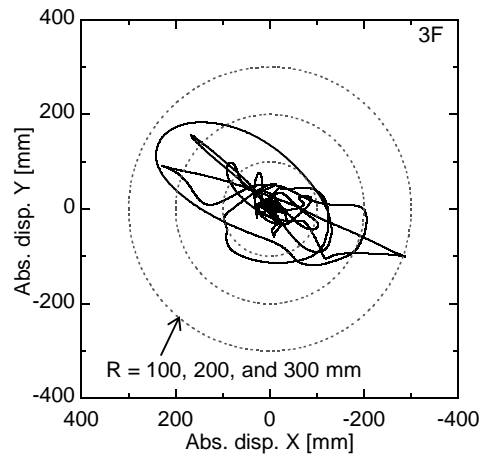
(c-2) Fourth floor

(c) Post-shake location of equipment, and related photos

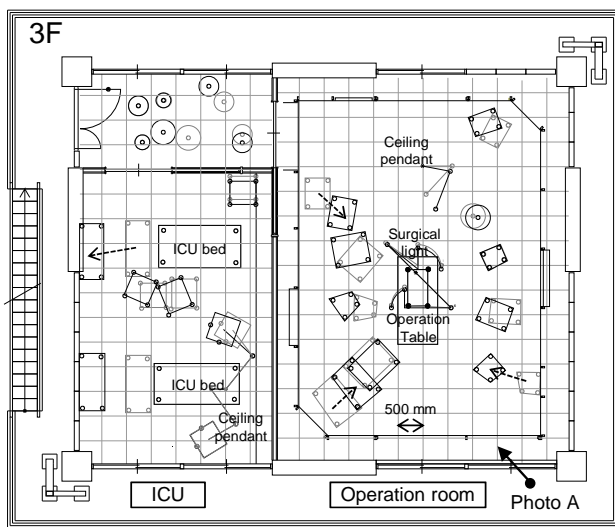
Figure 6-1 Post-shake location of equipment of the fixed-base system for JMA Kobe



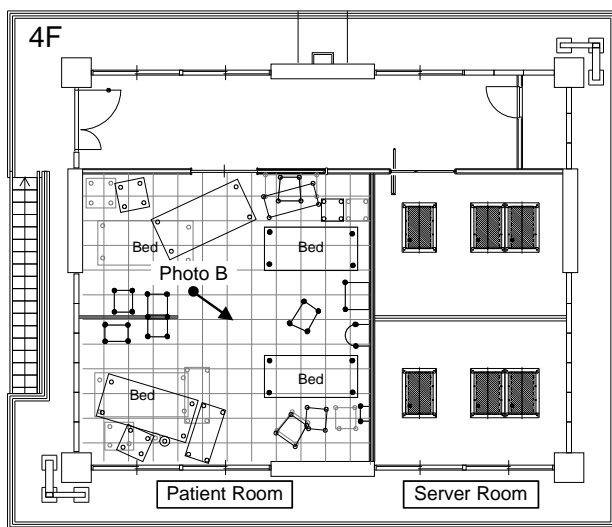
(a) Acceleration and absolute displacement time histories of the third floor



(b) Trajectory of absolute displacement of the third floor



(c-1) Third floor

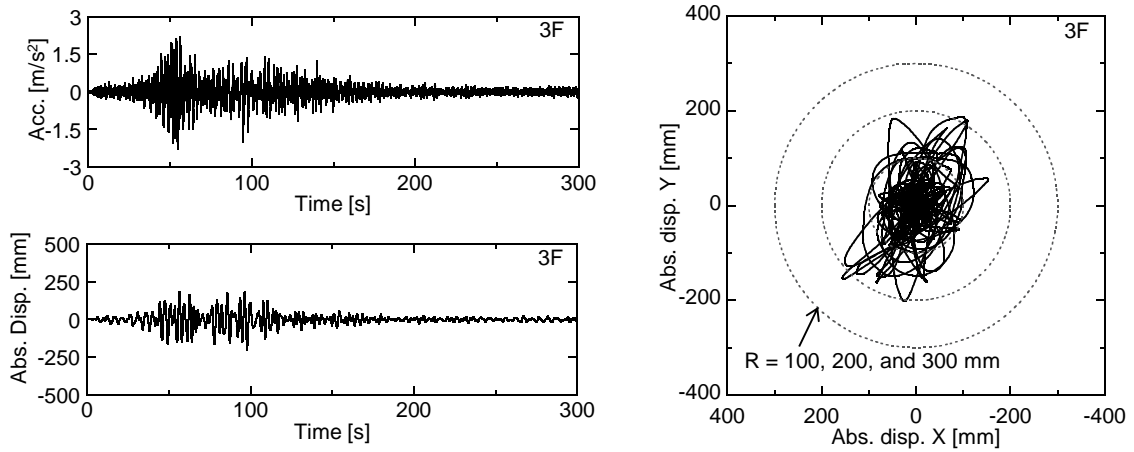


(c-2) Fourth floor



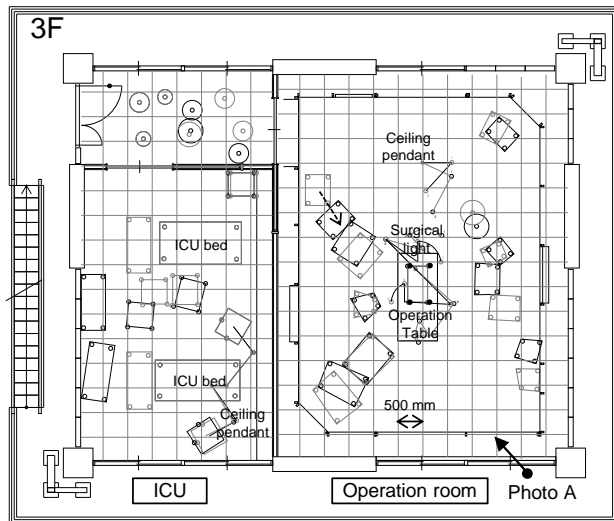
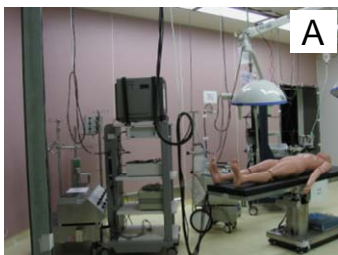
(c) Post-shake location of equipment, and related photos

Figure 6-2 Post-shake location of equipment of NRB+U for JMA Kobe

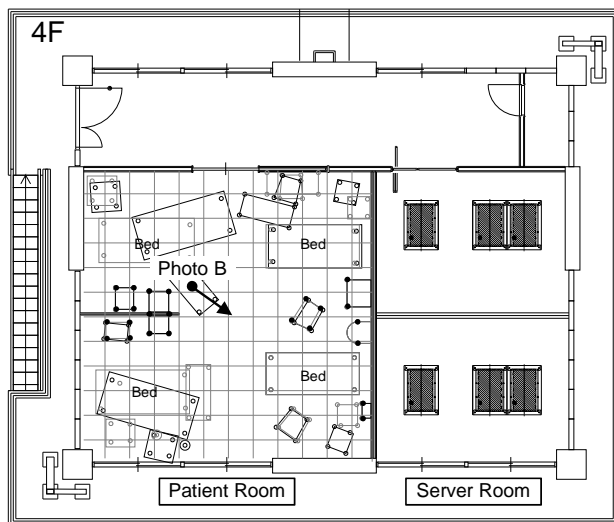


(a) Acceleration and absolute displacement time histories of the third floor

(b) Trajectory of absolute displacement of the third floor



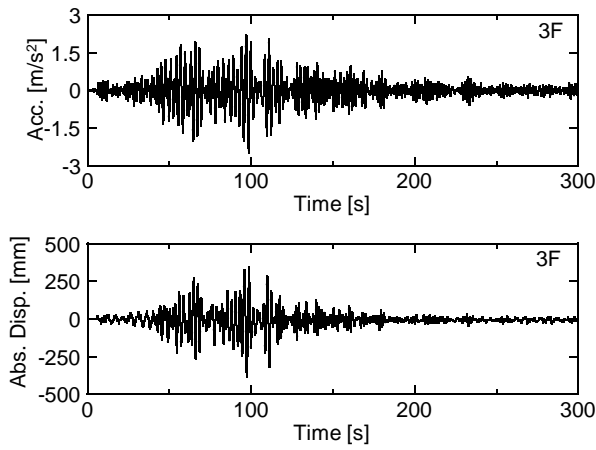
(c-1) Third floor



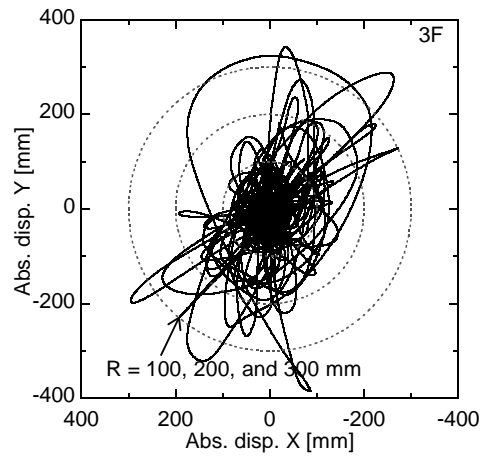
(c-2) Fourth floor

(c) Post-shake location of equipment, and related photos

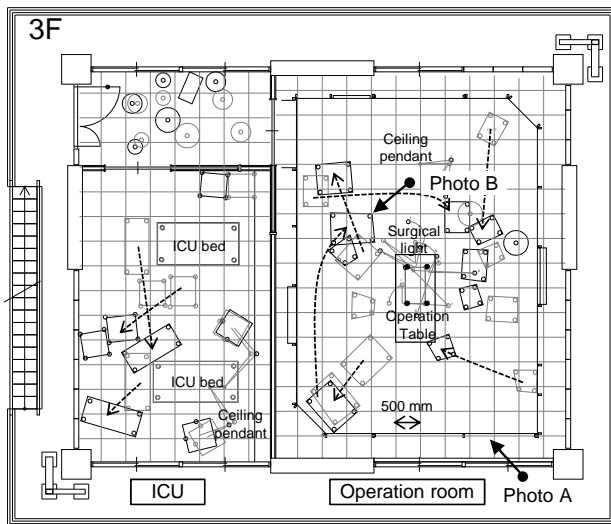
Figure 6-3 Post-shake location of equipment of the fixed-base system for Sannomaru



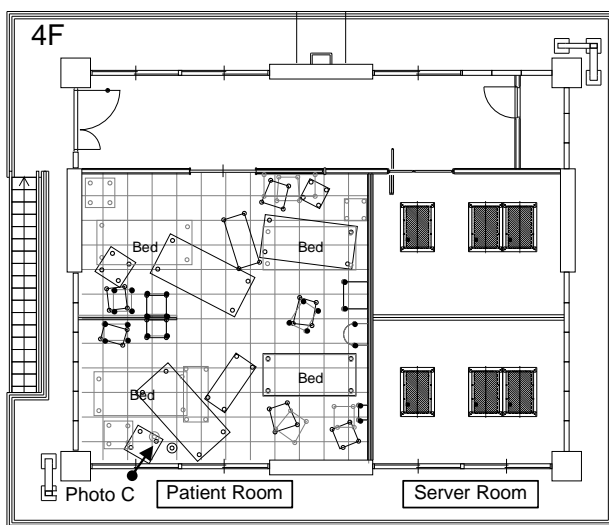
(a) Acceleration and absolute displacement time histories of the third floor



(b) Trajectory of absolute displacement of the third floor



(c-1) Third floor



(c-2) Fourth floor



(c) Post-shake location of equipment, and related photos

Figure 6-4 Post-shake location of equipment of NRB+U for Sannomaru

## 6.4 Effect of measures

Based on the observations obtained from Test I, some measures were applied in Test II to improve the performance as a medical facility. Most of the measures were intended to reduce displacements by means of locking all casters, attaching some additional devices to increase the friction, and/or fastening the object by belts to the wall. Some examples are shown in Figure 6-5. Their effectiveness is calibrated in this section.

### 6.4.1 Effect of measures

All measures were found to be effective for the base-isolated system; no violent acceleration amplification due to fixing the equipment was observed, and dislocation distance was significantly reduced regardless of the type of ground motions. Patient beds which had locks on all four casters did not move at all when they all were locked (the friction coefficient ranged from 0.4 to 0.6). Other equipment, however, still slid up to 0.5 m. This was because much of equipment had lock devices for only two casters (the front two in most cases), causing them to slide by swinging with respect to locked casters, even for floor accelerations of less than  $0.3 \text{ m/s}^2$ . 47% of casters with lock devices had their locks only in the front, which may have made it more convenient to lock them. To prevent them from even slight sliding, it is better to have locks all four casters when these are installed in the base-isolated facilities. Equipment fastened by belts to the walls also worked well (Figure 6-5 (a) and (b)). However, when long belts were used (Figure 6-5(b)), items slid back and forth within the range of the belts, causing bumping against the walls and threatening to exceed the allowable range with a large velocity. This phenomenon was observed when the base-isolated system encountered the long-period and long-duration ground motion. This suggests the possibility that plugs in equipment may be torn by excessive movement when they encounter the long-period and long-duration ground motion.

For the fixed-base system, locking casters was not effective in reducing the distance of dislocation when it encountered the near-fault ground motion. The dislocation of patient beds was reduced but still slid about 0.6 m because the friction coefficients (0.4 to 0.6) were not large enough to avoid sliding for floor accelerations of greater than  $15.0 \text{ m/s}^2$ . Bands fastened equipment to the wall prevented the equipment from excessive dislocation as long as they were not torn (this was observed when the belt bore consecutive shakings). These measures also yielded some countereffects. Fixing equipment increased acceleration responses, causing rocking for medical equipment in the operating room. This was because their aspect ratios were mostly more than two, and the mass of some equipment was concentrated on the top, because the main body of medical equipment was placed on the top. In addition, the increase in acceleration responses of equipment caused violent response of a monitor placed on the tall monitor rack with the height of 1.4 m. If the monitor had not been fastened by a belt to the monitor rack, it might have fallen down. Those responses were not observed when all casters were unlocked (Figure 6-5(d)). Even though responses became violent, no toppling was observed.



In summary, fixing items to the building components generally improved the order of the facility inside for the base-isolated system. To achieve no slight movement, it is better to adopt equipment with lock devices for all casters. For the fixed-base system, it was difficult to improve equipment performance by increasing the degree of fixating. With some equipment with high aspect ratios, which store heavy items or important items, it may be better to release the locks to avoid scattering and toppling the contents, unless they do not face the wall (there is a report sliding caster-supported equipment caused pounding on walls or other objects, causing damages to both the equipment and their contents). When casters were locked, it is better to fix any items stored on the equipment. Past research recommends that it is better to lock casters diagonally to reduce the possibility of toppling and to reduce the sliding distance [6-6]. For patient beds, whose aspect ratios are sufficiently low, it may be better to lock all casters because these tend to slide longer distances than the others.



(a) Equipment attached by belts to bars on the wall



(b) Equipment attached by longer belts to the wall



(c) Additional devices to increase friction



(d) Monitor rack with a larger aspect ratio

Figure 6-5 Example of measures

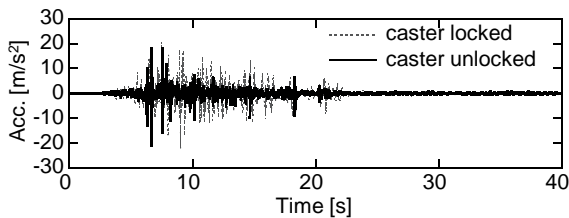
### 6.4.2 Effect of locking casters

Locking casters was the most effective measure to reduce damage caused by casters sliding at high speed. By locking casters, however, acceleration responses of equipment may increase, because the friction coefficient increased by 5 to 10 times (Table 6-2). The effects of locking casters were

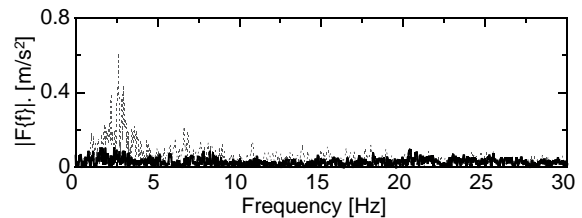


observed using the patient beds in the patient room.

Because some of patient beds in the patient room were locked and the others were unlocked, the effects of locking casters were examined by comparing their responses. One patient bed for each was selected. Figure 6-6 shows that acceleration time histories and the corresponding Fourier amplitude spectra for the transverse (width) direction when JMA Kobe was input. For the fixed-base system, the overall increase of the acceleration response can be observed from the acceleration time histories (Figure 6-6 (a-1)) when casters were locked. The maximum acceleration was similar between with and without locks, because bumping was observed when casters were not locked. The significantly increased response amplitude around 3 Hz indicated that the natural frequency of the patient beds in the transverse direction was about 3 Hz, which was close to the natural frequency of the fixed-base system of 3 to 4 Hz. On the other hand, the acceleration response of the patient bed placed on the base-isolated system did not change regardless of locks or unlocks if some pulsive accelerations due to bumping were ignored. Little increase in response amplitude around 3 Hz was observed, because the floor accelerations of the base-isolated system were dominated by the frequency of less than 0.5 Hz. It was found that the natural frequencies in the horizontal direction of the major medical equipment ranged between about 3 to 8 Hz. Therefore, locking casters has little possibility of having its countereffect for the base-isolated system. For the fixed-base system, however, the natural frequency of buildings becomes closer to those of equipment, causing increased acceleration responses of equipment. More detail examination about the natural frequency of equipment is described in Chapter 7.

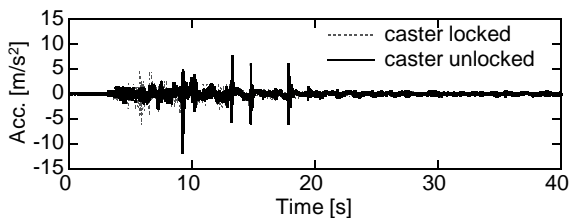


(a-1) Acceleration response time history

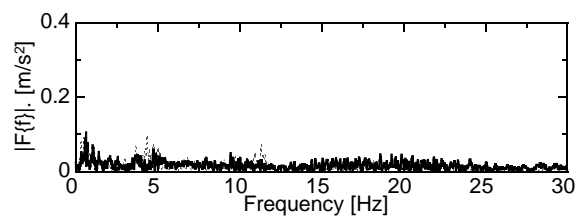


(a-2) Fourier amplitude spectra of (a-1)

(a) the fixed-base system



(b-1) Acceleration response time history



(b-2) Fourier amplitude spectra of (b-1)

(b) the base-isolated system

Figure 6-6 Effect of caster locks on response amplitude of patient beds (JMA Kobe)

## 6.5 Summary and conclusions of Chapter 6

This chapter described the performance of medical equipment installed in the base-isolated medical facility observed from the full-scaled shaking table tests. Notable findings are summarized as follows:

- (1) Even when the fixed-base system encountered JMA Kobe, almost no damage occurred in plumbing systems, sprinklers, and suspended ceilings, which had major damage reported after major earthquakes, which were installed following current practice.
- (2) It was reconfirmed that very many furniture items and medical equipment were mobile, meaning that they were supported by casters to make them as mobile as possible to travel between various places in the medical facility.
- (3) It is notable that serious movement of and according damage to the furniture items and medical equipment would occur in two distinctively different conditions, one in fixed-base systems when subjected to near fault ground motions, and the other in base-isolated systems when subjected to long-period ground motions. In the former case, the pulsive response of equipment and its contents due to large floor acceleration was the primary factor that caused damage, while the larger displacement and velocity of sliding equipment became the main reason that the function of the medical facility deteriorated, because most of items were supported by casters.
- (4) The mobility of items supported by casters caused large movement in such items and equipment for both the fixed-base and base-isolated systems and for both the near-fault and long-period ground motions. In the fixed-base system, they moved 0.5 to 1.0 m both in JMA Kobe and Sannomaru. In the base-isolated system, they moved 0.5 m to 1.0 m in JMA Kobe and most notably over 3 m in Sannomaru. Due to such large movement, many piece of equipment collided with each other or against the surrounding walls, causing damage and serious disorder.
- (5) Such wild movement was recognized as far beyond the expectations of medical doctors, people working in hospitals, and those involved in hospital design and operation. Since the test, they have been seriously discussing way to reduce such damage. Locking the casters is an easy solution, but nurses who work around the beds strongly complain about the difficulties of locking them all the time under extremely busy schedules.
- (6) Increasing the degree of fixation of equipment such as locking casters is the best solution to improve the performance of base-isolated medical facilities. On the other hand, such measurement has a countereffect especially for equipment with high aspect ratios and for contents stored in equipment for the fixed-base facilities. It is better to release lock to avoid toppling.

## REFERENCES

- [6-1] Kakehi A., Symposium (1) What Happened to Buildings and Equipment of Hospitals at The Great Hanshin-Awaji Earthquake: To Buildings-1, Journal of Medical Instrument,

Vol.38, June, 1996, pp.281-288 (Japanese).

- [6-2] Watanabe T., et.al, Symposium: Earthquake and Medical Equipment –How Experiences of Hanshin-Awaji earthquake changes Design–, Japanese Journal of Medical Instrumentation, Vol.67, No.2, 1197, pp.49-81 (Japanese).
- [6-3] Report of Investigation of Hospital Damages of Southern Hogo Prefecture earthquake, Japan Institute of Healthcare Architecture, March, 1996 (Japanese).
- [6-4] Report of Medical Damages due to Hanshin-Awaji earthquake, National Institute of Public Health, 1995 (Japanese).
- [6-5] Nakamura M., et al., Seismic Hazard Mitigation based on Social Engineering Approach: (part 8) Hospital Damages on Northridge Earthquake and Lessons Learned, Proceedings of the Annual Conference on Architectural Institute of Japan, August 1995, paper ID: 21009 (Japanese).
- [6-6] Report of Medical Function Maintenance for Earthquakes in Metropolitan Areas, National Institute of Public Health, 1984 (Japanese).

# **CHAPTER 7**

## **MEDICAL EQUIPMENT BEHAVIOR**

### **FOR VERTICAL MOTIONS**

#### **7.1 Introduction**

This chapter describes the effect of vertical floor accelerations on equipment installed to the base-isolated medical facility. The vertical ground motion is not reduced while the horizontal ground motion is significantly reduced by the base isolation system. Therefore, it is worthwhile to examine damage to building's contents with respect to the vertical floor responses. This chapter focuses on physical damages related to vertical input rather than the operational malfunction of equipment. The response of patients in beds is also of interest in this chapter. Some notable vertical responses observed in the full-scale shaking table tests are discussed for the first half, and the vertical dynamic properties of selected medical equipment are examined later, based on the supplemental shaking table tests.

#### **7.2 Notable vertical responses of equipment**

In the full-scale shaking table tests, many conspicuous responses were observed, because the floor accelerations exceeded 1 g in some shakings. Notable responses are summarized in this section.

Table 7-1 summarizes physical damages for equipment caused by the vertical floor vibrations, when waves with the vertical motion were input to the base-isolated system (HDRB). The mannequins placed on the operating table and incubator was also observed, which had mass distribution similar to a real human body. The mannequin placed on the incubator was a small-sized baby mannequin. It was found that the equipment with the vertical eccentricity tended to respond more severely than well-proportioned equipment, their response behavior is categorized in the table. The responses of some other items such as container stored in shelves, monitor on the ceiling pendant, and raised floor of the penthouse on the roof are also listed in the table. The performances were examined for three shakings with the vertical ground motions for the base-isolated system (HDRB in Test II), which are JMA Kobe Z, JMA Kobe XYZ, and El Centro XYZ. Because the

reproduced waves were quite different between JMA Kobe Z and JMA Kobe XYZ (Chapter 5), those three can be considered as waves with different levels of the amplitude. The maximum vertical floor accelerations recorded at the first to fourth floors' center (a4 in Figure 1(c)) were also listed in the table. The vertical acceleration amplitude ratio was about 1:1.9:4.5 for that of JMA Kobe Z, JMA Kobe XYZ and El Centro XYZ.

If the maximum vertical acceleration was smaller than 1 g (JMA Kobe Z), no major damage was observed. But once the maximum vertical acceleration exceeded 1 g and reached about 14 m/s<sup>2</sup> for JMA Kobe XYZ, some significant damages were observed: (1) The mannequin on the operating table and the incubator jumped, (2) Monitors on the ceiling pendant (ICU, third floor) jumped, and (3) Bottles stored by the shelves toppled and sometimes fell down, (4) Equipment with vertical eccentricity showed rocking or jumping, while no such severe damage was observed for well-proportioned equipment. Conspicuous responses were observed mainly for items placed on furniture or equipment, by which the vertical floor accelerations were further amplified, and items with vertical eccentricity for JMA Kobe XYZ with the maximum vertical acceleration of 14 m/s<sup>2</sup>. Even more severe damages were observed for El Centro XYZ, with the maximum vertical acceleration of about 30 m/s<sup>2</sup>. The vertical floor accelerations were large so that the equipment on the floor also jumped. The operating table itself jumped in addition to the mannequin, and most of well-proportioned equipment also jumped. Notable damages are examined in more detail later in this section. Some other responses are described later in this chapter. No malfunction of equipment tested in the operated condition was reported, and no notable damage in plumbing system was observed against the vertical floor accelerations of the base-isolated system.

If the maximum vertical acceleration ranged 5 to 9 m/s<sup>2</sup> (JMA Kobe Z), no major damage was observed. One exception was that the head part of the baby mannequin on the incubator lifted slightly, and hit by the thin mattress several times. When the maximum vertical acceleration ranged between 9 to 17 m/s<sup>2</sup> for JMA Kobe XYZ, some significant damages were observed: (1) The mannequin on the operating table and the incubator jumped (Figure 7-3 and 7-7), (2) Monitors on the ceiling pendant (ICU, third floor) jumped (Figure 7-1), and (3) Bottles stored by the shelves toppled and sometimes fell down (Figure 7-9(a)), (4) Equipment with vertical eccentricity showed rocking or jumping, while no such severe damage was observed for well-proportioned equipment (Figure 7-2). Conspicuous responses were observed mainly for items placed on other furniture or equipment. This may be because the vertical floor acceleration was further amplified by the equipment itself, and it reached acceleration amplitude enough for items stored on the furniture or equipment to jump. The equipment with the vertical eccentricity placed on the floor directly showed severe responses. The CT scan gantry (Figure 7-2(a)) located in the first floor and the autologous blood transfusion machine (Figure 7-2(b)) located in the third floor's operating room are given as examples, both of which had about 200 mm eccentricity between the mass center and the vertical supports. The autologous blood transfusion jumped, and the CT scan gantry dislocated by rocking, causing dislocation about 50 mm, when JMA Kobe XYZ was input. Even more severe damages were observed for El Centro XYZ, with the maximum vertical acceleration ranged between 22 to 39 m/s<sup>2</sup>. The vertical floor accelerations were large so that the equipment directly placed on the floor also jumped. The

operating table itself jumped in addition to the top mannequin, and most of well-proportioned equipment also jumped. The blocks of the heart-lung bypass machine were derailed by a jump (Figure 7-9(b)). Panels of the raised floor were also derailed and fell (Figure 7-9(c)) when the maximum acceleration input to the raised floor exceeded 2 g (recorded at the steel frame supporting the raised floor).

Table 7-1 Notable damages with respect to different amplitude levels of vertical floor responses for the base-isolated system

Ground motion		JMA Kobe Z	JMA Kobe XYZ	El Centro XYZ
Max. vertical floor acc. [m/s <sup>2</sup> ]	4F (center)	8.8	16.8	38.8
	3F (center)	8.0	13.7	29.0
	2F (center)	5.6	9.7	25.4
	1F (center)	4.9	9.4	21.9
Operating table (3F)			Body jumped	Body and table jumped
Incubator (3F)		Head part lifted	Body jumped	Body and incubator jumped
Well-proportioned other equipment (*1)		No damage	No damage	Jumped
With an eccentricity	CT scan (1F) (*2)	-	Rocking occurred	-
	ABT (3F) (*3)	No damage	Jumped	Jumped
Others	Containers on shelves	No damage	Fell down	Fell down
	Monitor on ceiling pendant (3F) (*2)	-	Jumped	-
	Raised floor (RF)	No damage	-	Panels derailed

(\*1) Desk, drawers, baby bed

(\*2) Observed in the test series of 2008 to 2009, in which the wave with the vertical motion input to HDRB was only JMA Kobe XYZ.

(\*3) ABT: Autologous blood transfusion machine

### 7.2.1 Suspended items

#### Surgical light

The surgical light hanging from the ceiling of the operating room fell about 200 to 300 mm when the vertical motion was input to the base-isolated system, although no significant change was observed when only horizontal motions were input. Because the surgical light has to have its position changed manually, it has universal joints. This falling, however, was not a major problem, because horizontal accelerations of the base-isolated system with the maximum floor acceleration of

2 to 3 m/s<sup>2</sup> already had enough to swing the light significantly, resulting in the dislocations of more than 0.5 m in the horizontal direction. Figure 7-1(a) shows the surgical light in the operating room.

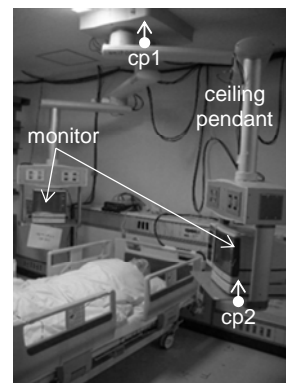
### Ceiling pendant

A monitor on the ceiling pendant slid with slight jumping, which did not occur when no vertical motion was input. Figure 7-1(b) shows the ceiling pendant with two monitors at each wing. In the figure, cp1 and 2 show the locations of the accelerometers. Even though the vertical maximum acceleration at the bottom of the ceiling pendant cp1 was 8.5 m/s<sup>2</sup>, the monitor jumped, because the acceleration was greatly increased by 2.6 times at cp2 of 22.3 m/s<sup>2</sup> for JMA Kobe XYZ. Once those monitors were fixed by adhesive sheets, no sliding was observed. The first vertical natural frequency of the ceiling pendant was estimated as about 6 to 7 Hz, which was lower than the natural frequency of the base-isolated systems of about 10 to 11 Hz.

Since the base-isolated buildings tend to have their first vertical natural frequencies between 5 to 15 Hz, there is a high possibility that the response of the pendants will be amplified. It is advisable to affix monitors to the pendants.



(a) Surgical light (Operating room)



(b) Ceiling pendant (ICU)

Figure 7-1 Suspended items

### 7.2.2 Equipment with eccentricity

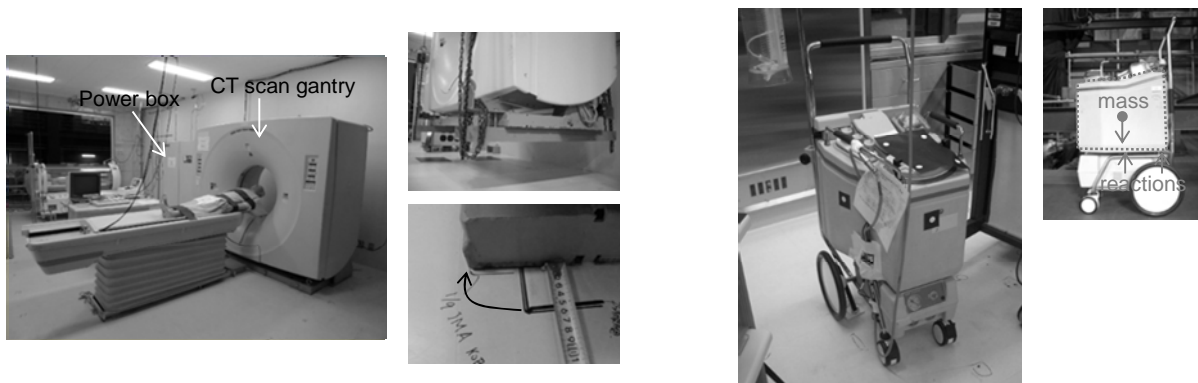
Some items with large eccentricity tended to respond more severely than well-proportioned items under the vertical motions. Two examples are shown in Figure 7-2; the CT scan gantry in the X-ray room and the autologous blood transfusion machine in the operating room. In the CT scan gantry, whose weight was 16.7 kN, the main upper part was supported on the back with an eccentricity of about 200 mm (Figure 7-2 (a)). The main upper part of the autologous blood transfusion machine installed in the operating room also had an eccentricity of about 180 mm (Figure 7-2 (b)).

The CT scan gantry was placed without an anchor in Test I, following actual practices, and was dislocated by about 50 mm during JMA Kobe XYZ, even though the friction coefficient of the CT scan gantry was 0.3 to 0.4, which was larger than the inertia generated by the horizontal floor

acceleration with the maximum of less than  $3.0 \text{ m/s}^2$ . This is because of severe rocking due to the eccentricity in the vertical direction. The acceleration response reached more than 6 g, while the accelerations recorded in the power box next to the CT scan gantry (Figure 7-2(a)) remained less than 1.5 g. In test II, the CT scan gantry was bolted to the floor. No dislocation was observed, and the acceleration responses were also significantly reduced to 1.5 g. The accelerometer was attached directly to the top of the main part of the machine (not plastic cover).

The autologous blood transfusion machine exhibited severe jumping during vertical ground motions. No jump was observed for JMA Kobe Z with the maximum floor acceleration of  $8.00 \text{ m/s}^2$ , while clear jumps occurred for JMA Kobe XYZ with the maximum floor acceleration of  $13.67 \text{ m/s}^2$ . The maximum acceleration became  $87 \text{ m/s}^2$  for JMA Kobe XYZ, which was significantly larger than the others which had with the maximum accelerations of less than  $50 \text{ m/s}^2$ . No clear jump was confirmed for other equipment in the operating room for JMA Kobe XYZ.

If an item is sensitive to the acceleration response, it is better to mitigate the eccentricity with respect to the vertical direction.



(a) CT scan gantry (X-ray room, 1F)

(b) autologous blood transfusion machine  
(Operating room, 3F)

Figure 7-2 Equipment with eccentricity

### 7.2.3 Operating table

The vibration of a patient being operated on is one of the most critical issues. Because horizontal motions were sufficiently reduced by the base isolation layer, dislocation due to horizontal sliding was not observed for the base-isolated system. However, serious vertical vibrations of the body, sometimes accompanied by jumping, were observed during shaking with vertical motions. Figure 7-3 shows the operating table with a mannequin on the top. The operating table was placed at the center of the third floor operating room (Figure 3-9(a)). The mannequin had mass distribution similar to a real human body, and had its weight of 45.5 kg. Three shakings with vertical ground motions for the base-isolated system (HDRB in Test II) were examined, which are JMA Kobe Z, JMA Kobe XYZ, and El Centro XYZ. Figure 7-3 shows the locations of accelerometers and these labels, and Figure 7-4 shows the vertical acceleration time histories recorded at the third floor center, ot1 and body (defined in Figure 7-3). In Figure 7-4, dotted lines represent the acceleration of



gravity ( $g = 9.8 \text{ m/s}^2$ ). Table 7-2 summarizes whether the operating table and body jumped, which was checked by video.

For JMA Kobe Z, the maximum vertical acceleration of  $7.61 \text{ m/s}^2$  recorded at the bottom (ot1) was amplified by 1.77, resulting in the maximum acceleration of  $13.4 \text{ m/s}^2$  for the mannequin (body). No clear jumping was observed for this input, because overall acceleration responses of the mannequin were less than 1 g (Figure 7-4(a)). For JMA Kobe XYZ, the overall acceleration amplitude at ot1 was less than 1 g, but it was doubly amplified to the body, causing jumping. It became more severe for El Centro XYZ with the maximum vertical floor acceleration of  $29.04 \text{ m/s}^2$ . Because the vertical floor accelerations had been already larger than 1 g, the operating table itself jumped. Severe jumping was also observed for the mannequin, with the maximum acceleration close to 5 g. The landing impacts, because of consecutive jumpings, are also clearly seen in the acceleration time history of the mannequin (body, Figure 7-4(c)), in which acceleration was amplified only on the upper side. Those results indicate that the floor acceleration tended to increase throughout the operating table. Figure 7-4 (d) shows the Fourier amplitude spectra of accelerations for JMA Kobe XYZ. It is notable that the dominant frequency of the vertical floor accelerations was maintained throughout the system from the floor up to the mannequin, but the amplitude of around 10 Hz was significantly amplified. Based on the supplemental tests, it was found that the natural frequency of the mannequin on the operating table was 10 Hz, which happened to be close to the natural frequency of the base-isolated system. The detailed examination of the vertical dynamic response characteristics of the operating table is described later in this chapter.

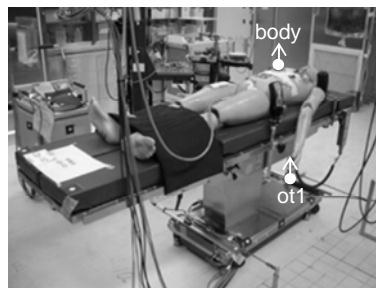


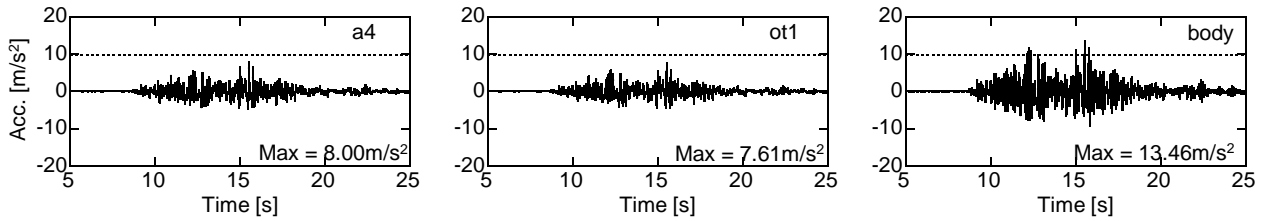
Figure 7-3 Operating table (Operating room, 3F)

Table 7-2 Phenomena observed for operating table and body

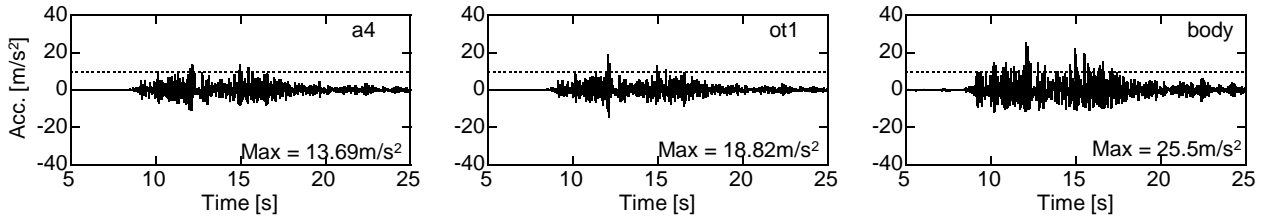
	Floor Acc.	Acc. of Body	Operation table	Body
JMA Kobe Z	8.00	13.46	no jumping	no clear jumping
JMA Kobe XYZ	13.69	25.50	not clear	obviously jumping
El Centro XYZ	29.04	47.05	obviously jumping	obviously jumping

In summary, it is notable in the response of the operating table that (1) jumps occurred not only for the mannequin but also the operating table itself when the acceleration responses exceeded more than 1 g, and (2) the operating table was not stiff enough to be considered as rigid body, because the

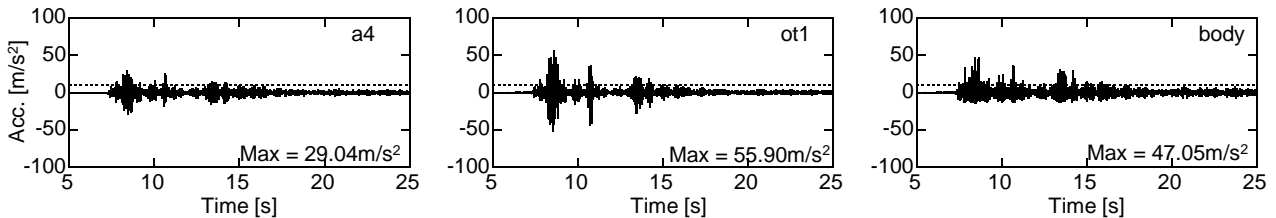
input acceleration was amplified to the mannequin.



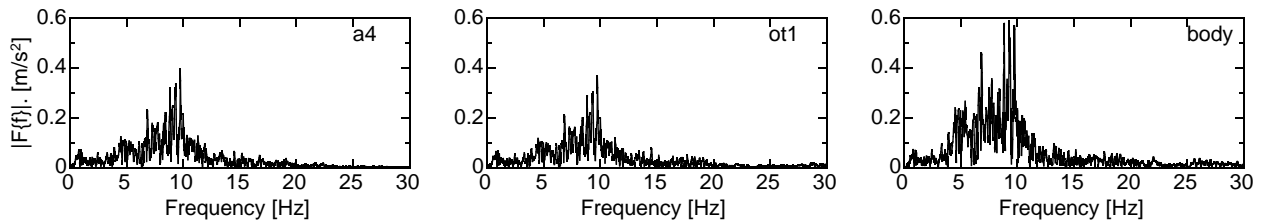
(a) Acceleration responses for JMA Kobe Z



(b) Acceleration responses for JMA Kobe XYZ



(c) Acceleration responses for El Centro XYZ;



(d) Fourier amplitude spectra for JMA Kobe XYZ

Figure 7-4 Vertical acceleration time histories and corresponding Fourier amplitude spectra of the third floor and operating tables

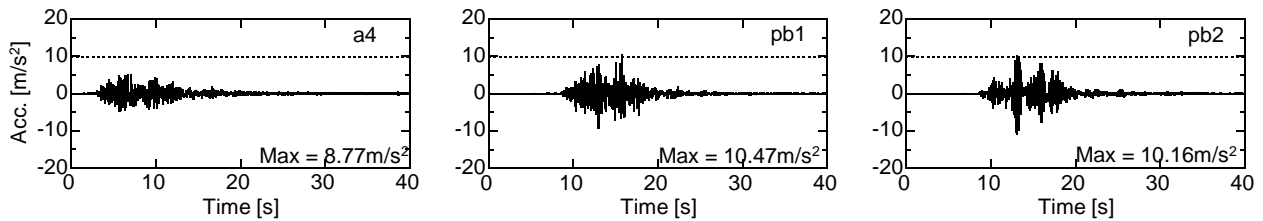
## 7.2.4 Patient bed

Patient beds are also one of the most important equipment in which the effect of vertical vibration on the patient is a concern. The same sets of input waves as used for the operating table were chosen to observe the performance of patient beds. One of the patient beds in the fourth floor patient room was chosen for detailed examination. The height of the chosen bed was fixed to 410 mm. A mannequin similar to that on the operating table was not placed on the bed, but additional masses (steel plates) adjusting to human weight of about 60 kg was placed. The mannequin shown in Figure 7-5 was a very light dummy. Figure 7-5 shows the locations of accelerometers. The patient bed had two layers: one was the main frame and the other was the upper layer consisted of a few plates that enable a patient to change the position. Some accelerometers were located in both layers, one of which per layer was chosen for examination. Figure 7-6 shows the vertical

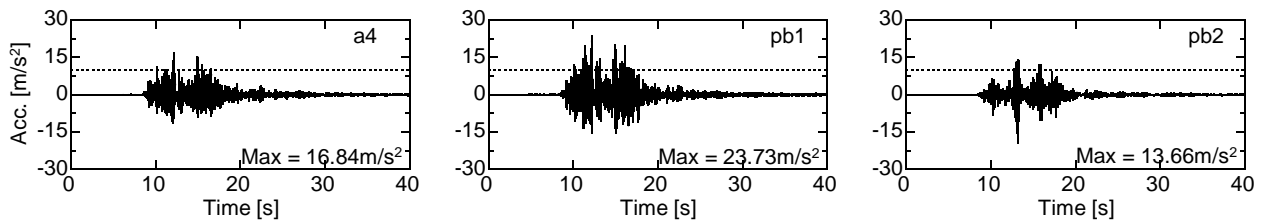
acceleration time histories and the corresponding Fourier amplitude spectra for the fourth floor center and the patient bed (pb1 and pb2).



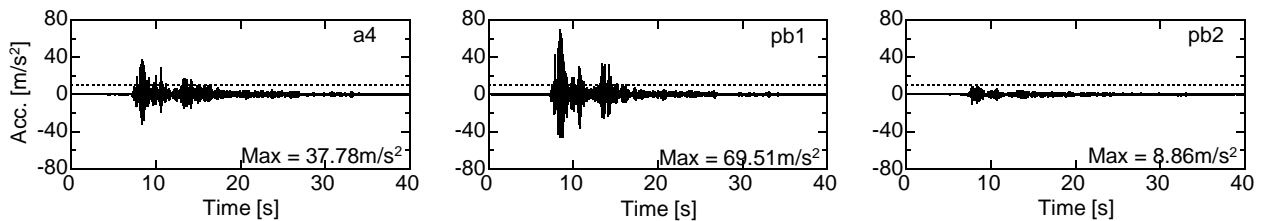
Figure 7-5 Patient bed (Patient room, 4F)



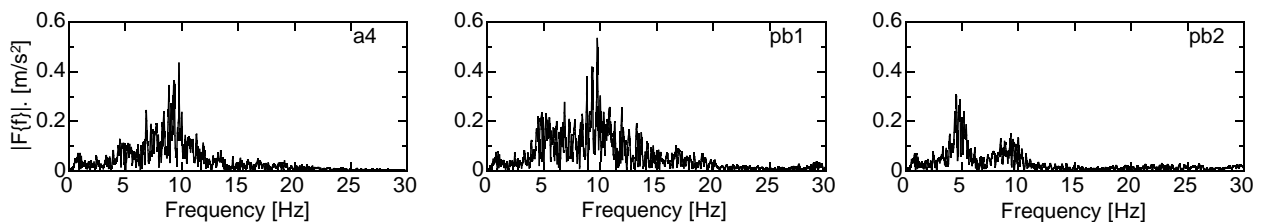
(a) Acceleration responses for JMA Kobe Z



(b) Acceleration responses for JMA Kobe XYZ



(c) Acceleration responses for El Centro XYZ



(d) Fourier amplitude spectra for JMA Kobe XYZ

Figure 7-6 Vertical acceleration time histories and corresponding Fourier amplitude spectra of the third floor and patient bed

From Figure 7-6, it is notable that the acceleration responses increased from the floor to the first layer of pb1 but reduced to pb2, whose tendency became more significant for larger floor

responses. The maximum acceleration was reduced from  $23.73 \text{ m/s}^2$  to  $13.66 \text{ m/s}^2$  for JMA Kobe XYZ, and  $69.51 \text{ m/s}^2$  to  $8.86 \text{ m/s}^2$  for El Centro XYZ. The Fourier amplitude spectra show that the amplitude distributions were relatively similar between the floor acceleration and pbl but were significantly changed for pb2. The patient bed obviously had the vertical first mode about 5 Hz, which was lower than the vertical first mode of the base-isolated system of about 10 to 11 Hz. It was confirmed that the other three patient beds in the fourth floor patient room also had the vertical first natural frequency at about 5 Hz, even though all four patient beds had different supporting frames. Adjusted heights of them were also varied between 330 and 700 mm. The patient bed was one of the softest equipment in the vertical direction since they had a number of mechanical joints to adjust the position including their heights. The smaller first mode frequency than the dominant frequency of the floor response, however, is not enough to explain the significant reduction to the upper layer. A separated shaking table test to the patient bed also did not have answer to this phenomenon. It was found that out that there was the vertical third mode at about 10 to 11 Hz, in which the response of the mannequin was mitigated. However, the difference in responses of the upper and lower frame of the patient bed was very small in the third mode.

In summary, it is notable in the response of the patient bed that (1) the natural frequency was 5 Hz, which can be considered as one of the most soft equipment in the vertical direction, (2) the acceleration responses were mitigated on the top layer of the bed which remained under question, and (3) no jump was observed for the patient bed even though the acceleration responses exceeded 1 g at the top frame thanks to the flexible joints supporting the bed.

### 7.2.5 Incubator

Vertical vibration has a possibility to cause problems for an infant lying in an incubator. An incubator placed at the third floor NICU was examined here for the same sets of input as examined in the previous equipment. Most of the mass of the incubator concentrated at the top and was supported by a column with slight eccentricity. A baby mannequin with the weight distribution similar to that of an infant was placed on a removable container inside the clear case, as shown in Figure 7-7. Accelerometers were attached to the bottom and the back side of the container. Figure 7-8 shows the acceleration time histories and the corresponding Fourier amplitude spectra for the third floor center and the incubator (inc1 and inc2).

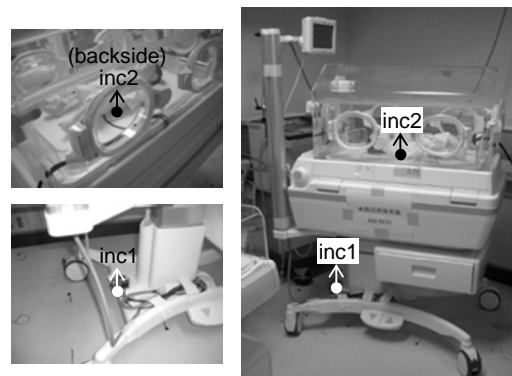
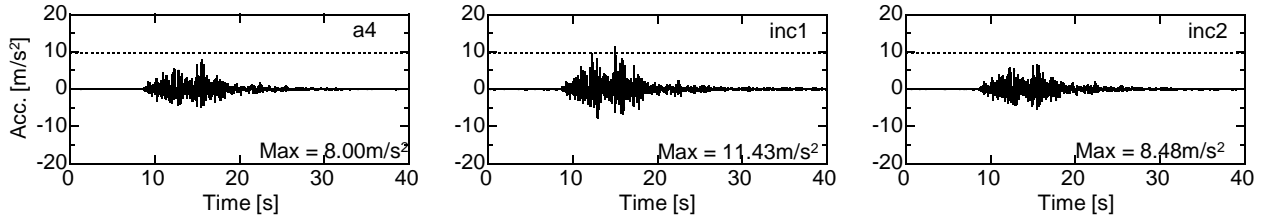
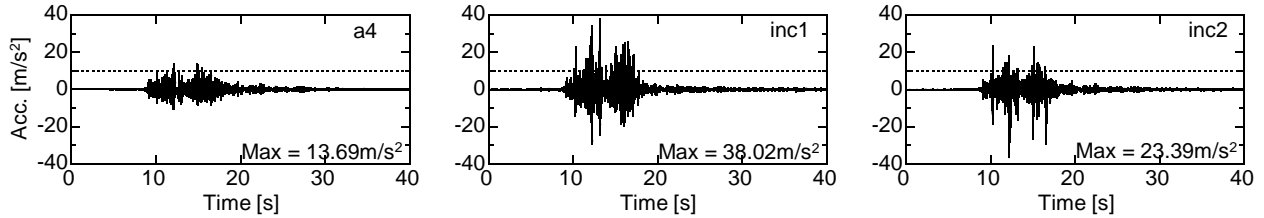


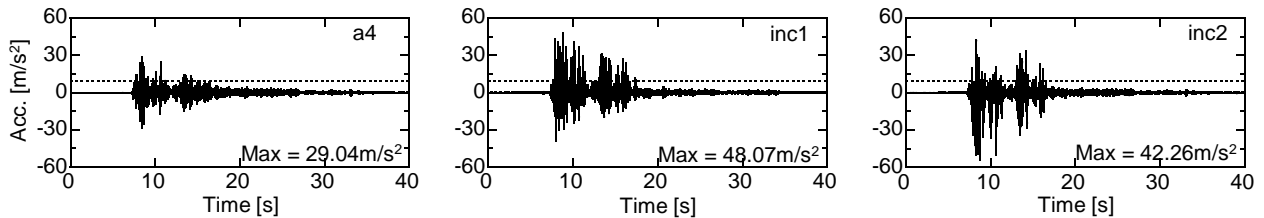
Figure 7-7 Incubator (NICU, 3F)



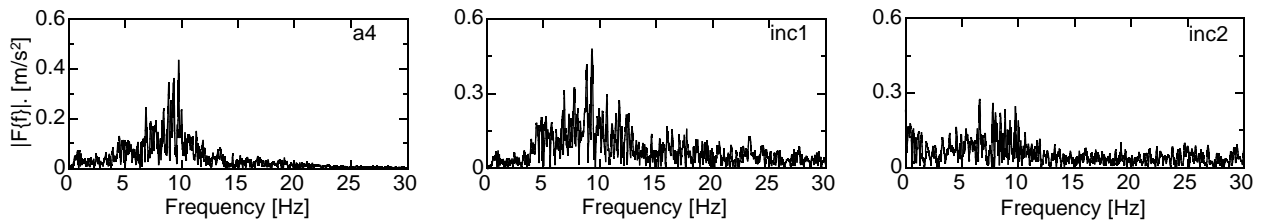
(a) Acceleration responses for JMA Kobe Z



(b) Acceleration responses for JMA Kobe XYZ



(c) Acceleration responses for El Centro XYZ



(d) Fourier amplitude spectra for JMA Kobe XYZ

Figure 7-8 Vertical acceleration time histories and corresponding Fourier amplitude spectra of the third floor and the incubator

It is notable from the Figure 7-8 that the maximum accelerations were mildly reduced from the bottom (inc1) to the container (inc2). It is also notable that the dominant frequency of the floor acceleration of about 10 to 11 Hz was unchanged at the bottom of inc1, but its contribution was reduced, while that of frequency lower than 2 Hz was increased for inc2 (Figure 7-8(d)). This decrease in the contribution of high-frequency ranges may be because the removable container (where a mannequin was laid) was flexibly jointed to the main body of the equipment. Some reduction of accelerations from inc1 to inc2 was observed for JMA Kobe Z but reductions for JMA Kobe XYZ and El Centro XYZ were not significant. This may be because the container bumped with the main body, because jumps occurred to the baby mannequin, causing impulsive acceleration responses. No clear jumping was observed for the incubator itself when JMA Kobe XYZ was input even though the acceleration response at the bottom (inc1) exceeded 3 g. This may be because the loose connection of casters had a capability to absorb the vertical response of the main

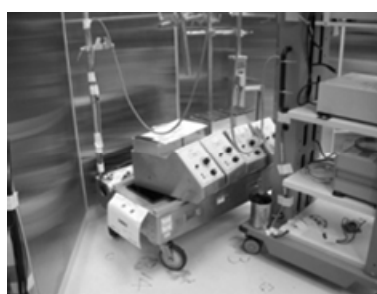
body. This kind of flexibility in the vertical direction was also observed for the patient bed. For El Centro XYZ, in which the maximum acceleration at the bottom (inc1) reached close to 5 g, a slight jump was observed. The baby mannequin, on the other hand, vibrated severely in all cases. Even with the maximum acceleration of 8.48 m/s<sup>2</sup> for the container (inc2), a head part of the mannequin lifted slightly and hit to a thin mattress for JMA Kobe Z. The whole body of the baby mannequin jumped for JMA Kobe XYZ with the maximum acceleration of 23.39 m/s<sup>2</sup> and became even more severe for El Centro XYZ with the maximum acceleration of 42.26 m/s<sup>2</sup>. Such behavior was obviously more severe than the mannequin on the operating table. This may be because the velocity responses of the baby mannequin were larger than those of the mannequin on the operating table. The input wave of the former had larger contribution of the lower frequency range, while the maximum accelerations were similar in both cases (Figure 7-4 (d) and Figure 7-8 (d)).

### 7.2.6 Others

Some items arranged on tables or shelves became disorganized and fell, as shown in Figure 7-9 (a), which had not occurred when no vertical motion was input to the base-isolated system. Containers filled with some dangerous liquid must be securely stored. In the extreme case that the vertical acceleration at the center of the floor exceeded 3 g, the blocks of the heart-lung bypass machine was derailed by a jump (Figure 7-9(b)). Panels of the raised floor were also derailed and fell (Figure 7-9(c)) when the maximum acceleration input to the floor exceeded 2 g (recorded at the steel frame right below the raised floor). The furniture on the raised floor also toppled. It is also notable that the sliding movement of items supported by casters was not significantly affected by the vertical motions as long as the item did not have eccentricity in the vertical direction. No vertical motions caused malfunction of the equipment tested in the operating condition (dialyzers, and servers).



(a) Containers stored in shelves



(b) heart-lung bypass



(c) raised floor panels

Figure 7-9 Example of notable equipment responses

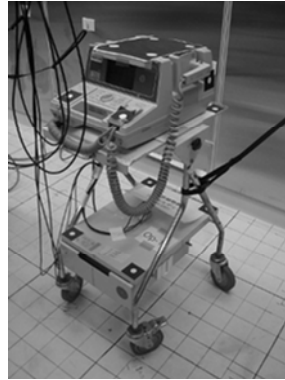
## 7.3 Supplemental shaking table test of equipment

Dynamic response characteristics of some equipment were examined further by supplemental shaking table tests. Tests were conducted by the tri-axial shaking table of Disaster Prevention

Research Institute at Kyoto University. The dimensions of the table are 5 m by 3 m. The surface was covered by panels, which had smooth surface. Seven equipment were tested, i.e., a wagon (Figure 7-10 (a)), a cardioverter defibrillator (Figure 7-10 (b)), an autologous blood transfusion (Figure 7-2 (b)), operating table (Figure 7-3), a patient bed (Figure 7-5), a baby bed (Figure 7-10(c)), and an incubator (Figure 7-7). All of them were supported by casters.



(a) Wagon



(b) Cardioverter defibrillator



(c) Baby bed

Figure 7-10 Equipment tested by supplemental shaking table test

### 7.3.1 *Dynamic properties of equipment*

A Gaussian white noise with a pass band of 0.2 to 30 Hz, a root mean square (RMS) amplitude of 0.10 m/s<sup>2</sup> and the duration of 250 s was used for all seven items. For the operating table and the patient bed, difference setting of a Gaussian white noise was also used, whose pass band range became broader to 0.2 to 50 Hz and the duration was 200 s to observe higher modes effect. All equipment was tested in caster-locked condition. Table 7-3 shows the estimated first natural frequencies and the corresponding damping ratios in the three directions. For the operating table, the dynamic characteristics were estimated based on the acceleration response of the mannequin on the top. It is notable that the natural frequencies of equipment in the vertical direction were much higher and had the broader range than those in the horizontal direction. Damping ratios in the horizontal direction ranged between 4 to 10 %. A damping ratio of 5 % may be sufficient to adopt for the horizontal response of the equipment.

From Table 7-3, it is found that the range of natural frequencies in the horizontal direction (3 to 7.5 Hz) happened to be close to the range of natural frequencies of low-rise fixed-base buildings. This indicates that the response amplitude of equipment tends to increase for fixed-base buildings if they are fixed to the floor, while their response amplifications are expected to become smaller for base-isolated buildings. Damping ratios in the horizontal direction ranged between 4 to 10 %. A damping ratio of 5 % may be sufficient to adopt for the horizontal response of the equipment. The natural frequencies in the vertical direction of 5 to 28 Hz were also overlapped with those estimated for existing buildings of 4 to 25 Hz (6 to 15 Hz for base-isolated buildings) [7-1, 2]. For well-proportional equipment in the vertical direction (the wagon, cardioverter defibrillator) had the natural frequency of larger than 20 Hz, and the damping ratio of at least 5 %. If the appliance has

vertical eccentricity (autologous blood transfusion, incubator), the first natural frequencies became a rocking mode and decreased to 13 and 17 Hz. The corresponding damping ratio was also reduced to 3 %. Beds with mattress had even lower natural frequency, which was 10 Hz for the operating table and 5 Hz for the patient bed, while the damping ratio tended to increase for beds. Detail examination is conducted later in this section.

Table 7-3 Dynamic properties of equipment

Item	Wagon	Cardioverter difibrilator	Autologous blood transfusion	Patient bed <sup>(*1)</sup>	Operation table <sup>(*2)</sup>	Baby bed	Incubator	
Weight [kg]	34.7	31.1	62.6	178.9	261.6	13.1	139	
F <sub>1</sub>	X	6	6	4	4	6	7.5	3.5
	Y	3.5	3	4.5	3	4.5	4	3.5
	Z	28	23	16.5	5	10	16.5	13
			rocking mode				rocking mode	
h <sub>1</sub>	X	4%	5%	6%	5%	8%	5%	10%
	Y		5%	5%	5%	10%	9%	7%
	Z	7%	5%	3%	6%	25%	12%	3%

(\*1) height = 310 mm. weight with a mannequin of 45.5 kg.

(\*2) height = 850 mm. weight with a mannequin of 45.5 kg; Dynamic properties were estimated based on the accelerations recorded on the mannequin

(note) X = longitudinal direction, Y = transverse direction, Z = vertical direction

### 7.3.2 Operating table and patient bed

It was found that equipment used as a bed tended to have relatively smaller vertical natural frequencies than others as shown in Table 7-3. The supplemental shaking table test revealed that the mattress played an important role. In this subsection, the operating table and a patient bed are chosen to be examined further.

Figure 7-11 shows photos of the two equipment on the shaking table. In addition to the equipment tests, the effects to the mattresses were also examined, as shown in Figures 7-11(a-2) and (b-2). The operating table was covered by mattress with a thickness of 50 mm, which consisted of three layers of urethane foam. The upper and lower layer was made of low resilient material and the middle layer was high resilient material. The patient bed had a thicker mattress of 100 mm, the upper layer of which was low resilient urethane foam, and the lower layer of which was high resilient urethane foam. A mannequin was laid on the top in all cases, which was the same as that used in the full-scale shaking table test on the operating table. It had the weight of 45.5 kg and the similar mass distribution to the human body. The figures also show the acceleration recording locations. The upper table of the operating table consisted of three parts: the center part, two other plates for feet, and the other plate for the upper body (Figure 7-11(a-1)). Two accelerations recorded in each part were averaged to obtain the accelerations of the center, feet,



and head portions (denoted by *otc*, *otf*, and *oth*, respectively in Figure 7-11(a-1)). As mentioned in the previous subsection, the patient bed had two layers: the main frame and the upper position-adjustable layer. Four accelerometers were attached to both layers, and they were averaged per layer (denoted by *pbl*, and *pbu* in Figure 7-11(b-1)). One accelerometer in the vertical direction was attached to the chest of the mannequin.

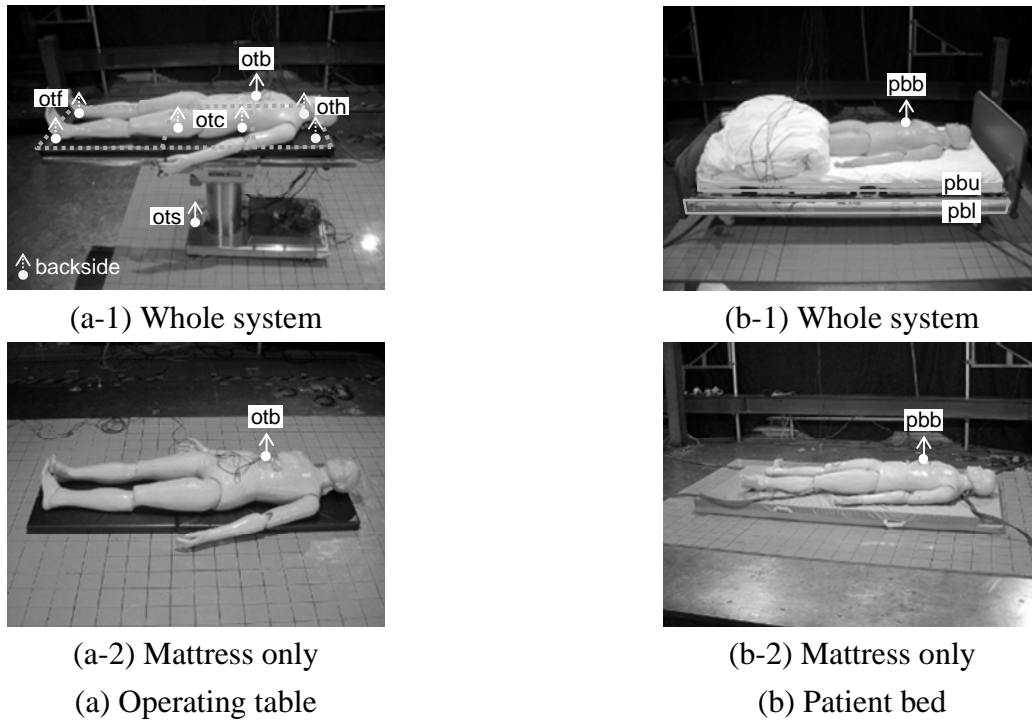


Figure 7-11 Supplemental shaking table tests of operating table and patient bed

### Effect of Mattress

The dynamic response characteristics in the vertical direction of the mattress were examined by a white noise. A Gaussian white noise with a pass band of 0.2 to 50, a root mean square (RMS) amplitude of  $0.10 \text{ m/s}^2$  with the maximum acceleration of  $0.5 \text{ m/s}^2$  and the duration of 200 s was used. The vertical response amplitudes of the acceleration recorded on the chest of the mannequin over the input are shown in Figure 7-12. It is notable that the each mattress has a clear single mode. Those natural frequencies were relatively small of 8 Hz for the patient bed mattress and 9 to 10 Hz for the operating table mattress. The contribution of the mattress was very significant, since the natural frequency of the operating table mattress was similar to that estimated for equipment (10 Hz for the operating table). It is also notable that the corresponding damping ratios in the vertical direction were relatively large. The estimated damping ratios were 12% for the patient bed mattress and 22% for the operating table mattress.

Figures 7-13 show the maximum vertical acceleration response at a steady state of the mannequin (a) on the panel, (b) on the patient bed mattress, and (c) on the operating table mattress, when sinusoidal waves with various frequencies were input in the vertical direction. For each frequency, four levels of amplitudes were adopted, which were 2.5, 5.0, 7.5, 10.0  $\text{m/s}^2$ . The reproduced amplitudes on the table had errors ranging between  $-0.5 \text{ m/s}^2$  and  $+1.5 \text{ m/s}^2$  from these target values.

In the figures, filled marks represent cases when the mannequin jumped. Jump intensity were categorized into three levels according to their heights observed by videos: the darkest mark are the cases that clear jumping was observed, the milder marks are the cases that slight jumping was observed, and the lightest marks are the cases that no clear jump but dislocation was occurred. Values adjacent to filled marks show the maximum relative velocity of the mannequin to the table, which may become an indicator related to the jumping height. Since there was no accelerometer on the mattress, the maximum relative velocities for the cases with mattresses may not be related directly to jumping height. From the figures, the followings are notable:

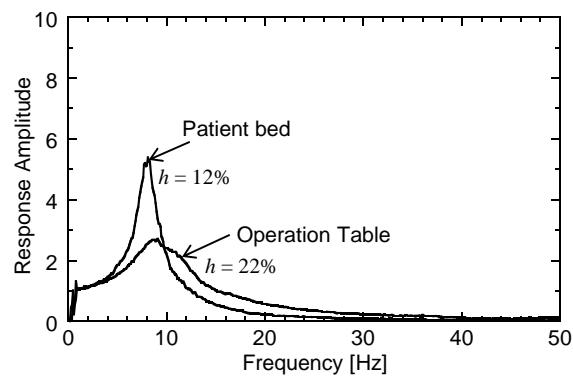
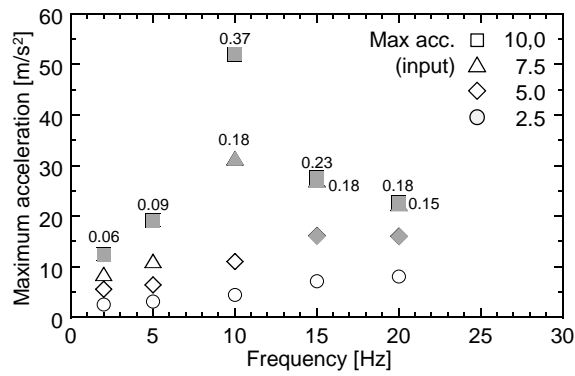
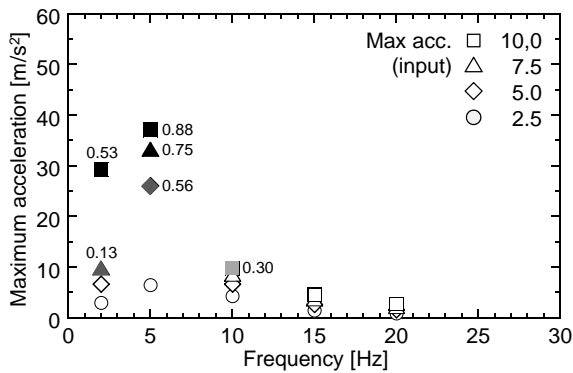


Figure 7-12 Response amplitude of manequin on mattresses

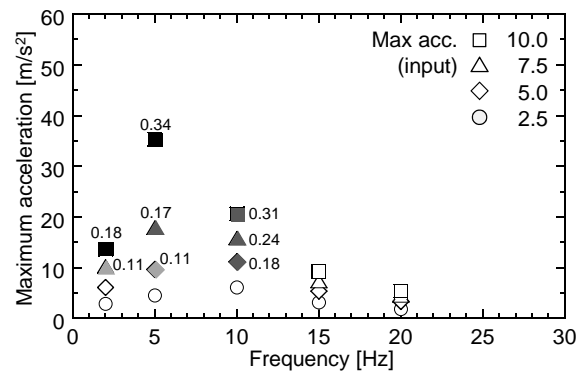
- (1) Acceleration response distributions in the case without jumping sufficiently follow the response amplitudes which are shown in Figure 7-12.
- (2) When the maximum acceleration responses became larger than 1 g ( $9.8 \text{ m/s}^2$ ), jump occurred in all cases.
- (3) Once jump occurred, the landing impact acceleration amplitude or jump intensity depends not only on the relation between the natural frequency and the dominant frequency of input waves (Figure 7-12) but also the velocity amplitude of input wave. It was notable that the largest acceleration amplitude of the mannequin on the operating table mattress was shifted toward 5 Hz from 10 Hz, which was the natural frequency of the mattress. This is because the impact acceleration due to landing was affected by the jumping height or the relative velocity.
- (4) The patient bed mattress effectively mitigated impact accelerations due to landing, which was notable when the cases with similar relative velocities were compared between before and after the insertion of a mattress. It reached more than 3 g with the maximum relative velocity of 0.18 m/s for the case without the mattress, while the reaction acceleration was reduced to less than 1 g for the maximum relative velocity of 0.30 m/s when the patient bed mattress was inserted. On the other hand, the soft mattress tended to increase the relative velocity input to the mannequin, or jumping height. Consequently, no significant reduction (30%) was observed for the maximum accelerations recorded in the series of shakings. The impact acceleration remained greater than 3 g with mattress.



(a) Panels



(b) Patient bed mattress



(c) Operating table mattress

(Note) values in tables represent the relative velocity with respect to the table [m/s]

Figure 7-13 Maximum acceleration of the mannequin on the mattress

- (5) Similar tendency related to impact acceleration with respect to the relative velocity was observed for the operating table mattress.
- (6) The operating table mattress did not increase the maximum relative velocity as much as the patient bed mattress did thanks to larger damping ratio (22% for the operating table mattress) and higher natural frequency (10 Hz). The recorded maximum relative velocity of the mannequin on the former mattress was 0.88 m/s, while it was 0.34 m/s for the mannequin on the latter mattress, both of which were recorded when the sinusoidal wave with the frequency of 5 Hz was input with the amplitude of 10.0 m/s<sup>2</sup>.
- (7) Even though the relative velocity did not increase for the operating table mattress, the impact acceleration due to landing tended to be larger than that of the patient bed with respect to similar relative velocity. This may be due to the mattress with larger stiffness and damping ratio.
- (8) Increase in jumping height also increase the dislocation distance of the mannequin. In the severe case, mannequin slid off from the mattress.

In summary, insertion of the mattress successfully mitigated the impact acceleration due to landing after jump. However, height of jump tended to become higher with the mattress, resulting in increase in the reaction acceleration. Higher jump caused dislocation of patient, which may become serious problem. Jump intensity has close relationship with the velocity input to the mannequin, which tended to increase for the input wave with lower frequency.

## Patient Bed

Figures 7-14(a) show the response amplification of the patient bed for pbl, pbu, and pbb (mannequin) obtained by the white noise with the maximum acceleration of  $0.5 \text{ m/s}^2$ . The patient bed was set to be the lowest-adjustable height of 310 mm. The notable findings are as follows:

- (1) There are three conspicuous modes at about 5, 6 and 11 Hz. In the lower two modes, all points vibrated in phase. No significant difference in mode shapes in lower two modes was observed by the limited recording locations. In the third modes, the lower two parts (pbl and pbu) vibrate in phase but the mannequin (pbb). The corresponding damping ratios ranges between 8% and 5% for lower two modes and 10% for the third modes.
- (2) The natural frequency of the main frame of the patient bed was estimated as about 7.5 Hz. It is measured by a white noise input to the patient bed whose mannequin on the mattress was tightened by belts to the main frame of the patient bed. This indicated that the main frame of the patient bed and the mattress had very close natural frequencies. It was 7.5 Hz for the former while 8 Hz for the latter, resulted in 5 Hz as the whole system.
- (3) The accelerations on the mannequin became smaller than the input acceleration for the frequency range higher than 10 to 11 Hz. This was also confirmed by the acceleration responses of the series of shaking table test using the sinusoidal wave (Figure 7-15 (a)).
- (4) The natural frequencies were reduced to 80 to 90%, and the damping ratio increased to 10% for all modes when the maximum acceleration of the white noise increased by 10 times to  $5.0 \text{ m/s}^2$  (Figure 7-14(a-2)). Since the dependence of damping ratio on the input amplitude was not confirmed for the patient bed mattress, this increase majorly attribute to the main body of the patient bed assembled by a number of flexible joints. Damping ratio of 10% is applicable to large earthquakes.
- (5) No significant difference in the dynamic properties was observed with respect to difference in the height of the bed. There was 20 % increase in the first natural frequency was observed while the damping ratio remained unchanged when the height of the patient bed was increased to the upper limit of 710 mm.
- (6) In the full-scale shaking table test for the base-isolated system, it was observed that the response amplitudes of the upper frame became smaller than those of the lower frames (Figure 7-6). The supplemental shaking table test failed to find the reason for this phenomenon since the acceleration response of the upper frame was always similar to that of the lower frame for all frequency range.
- (7) The same sets of sinusoidal waves as the mattresses were also input to the patient bed. Among four levels of acceleration amplitudes used in the mattress test ( $2.5$ ,  $5.0$ ,  $7.5$ , and  $10.0 \text{ m/s}^2$ ),  $2.5 \text{ m/s}^2$  was not used. The maximum acceleration responses on the mannequin at the steady state were plotted in Figure 7-15(a). The results show the acceleration responses in the cases without jumping generally followed the response amplitude obtained by a white noise (Figure 7-14(a)). Very clear jumping was observed for the lower frequency of 2 and 5 Hz, once the acceleration response exceeded 1 g.

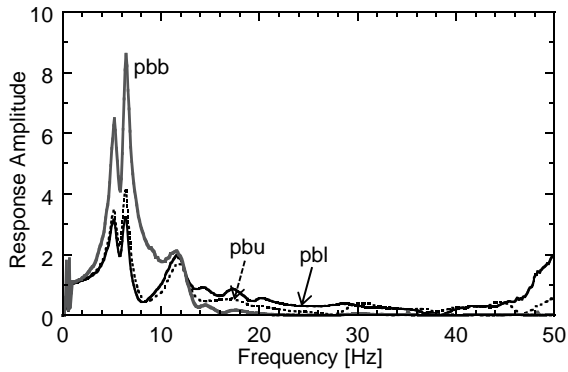
## Operating Table

Figures 7-14(b) show the response amplitude of the operating table for *otc*, *otf*, *oth*, and *otb* (mannequin). The height of the operating table was fixed to be 850 mm. The operating table has the dominant mode of the whole system at about 24 to 27 Hz (damping ratio of 5 to 10%) with some other local modes in the lower frequency range. It is notable that the response amplitude of *otb* (mannequin) was significantly affected only by the dynamic response characteristics of the mattress, because it had very similar response amplitude distribution to that of the mattress only (Figure 7-12). The dominant frequency of *otb* was about 10 Hz with the damping ratios of 25%. These dynamic properties were similar to that of the mannequin on the operating table mattress of 10 Hz for the natural frequency and 22 % for the damping ratio. This coincidence in dynamic properties of the mannequin laid on the operating table may be because the mattress had much smaller the natural frequency (9 Hz) than that of the main body of the operating table (more than 24 Hz). Other local modes had little influence on the responses of the mannequin at least on the location of the chest (Figure 7-11(a)). This indicated that the dynamic response characteristics of the human on the operating table were mainly controlled by that of the operating table mattress. The only difference was that the response amplitude of *otb* (mannequin) did not decrease to zero for the higher frequency range but remained as one up to 30 to 40 Hz (Figure 7-14(b)) because of the existence of higher modes of the operating table itself. It is also notable that the response amplitude of the mannequin on the operating table did not affected by the input amplitude. This can be confirmed by comparing the response amplitudes for the white noises with two different maximum accelerations of 0.5 and 5.0 m/s<sup>2</sup> (Figure 7-14 (b-1) and (b-2)).

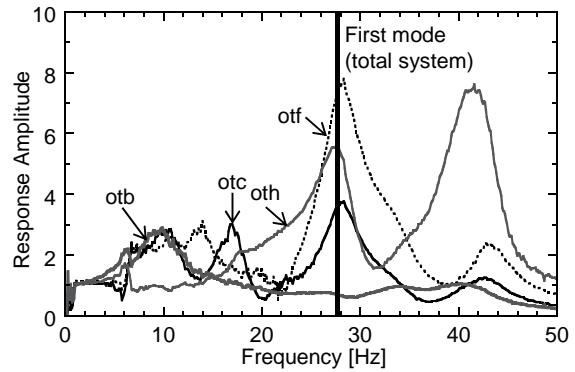
The same sets of sinusoidal waves as the patient bed were also input to the operating table. The results showed in Figure 7-15(b). The acceleration responses generally follow the response amplification of the mannequin on the patient bed (Figure 7-14(b)). For higher frequency range, it was observed that the acceleration response remained similar to the input acceleration. It is also notable that the jumping height was affected by the dominant frequency of the input wave than the natural frequency of the item itself. For the sinusoidal wave with the frequencies of 2 and 5 Hz, the mannequin tended to jump higher than that with 10 Hz even though the natural frequency was 10 Hz. These jumping heights were large enough to cause the mannequin falling down from the operating table. Since the width of the operating table is design to be smaller (500 mm for this operating table), it is better to reduce the possibility of jump for the patient.

Figure 7-16 compares the acceleration time history of the mannequin on the operating table recorded for the full-scale shaking table test with the corresponding SDOF model considering the mattress as a spring. The natural frequency was fixed to 9 Hz. Two motions used by the full-scale shaking table test (HDRB) were examined, which were JMA Kobe with the maximum accelerations of 8.00 m/s<sup>2</sup> and JMA Kobe XYZ with the maximum accelerations of 13.69 m/s<sup>2</sup> at the third floor center. For JMA Kobe Z, no jump occurred to the mannequin. A damping ratio was adjusted to 19% in which a reasonable agreement to the recorded acceleration of the full-scale shaking table test was obtained (Figure 7-16(a)). 19% as the damping ratio was slightly smaller than those estimated by a white noise (22 to 25%), but it still indicated that it is reasonable to use

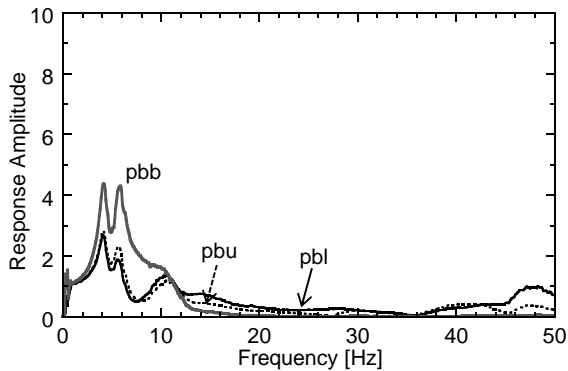
the damping ratio of about 20% for the operating table mattress. Once jump of the mannequin occurred for JMA Kobe XYZ, overestimation was observed for this SDOF model. Jump of the mannequin for JMA Kobe XYZ seems to mitigate the amplification responses smaller than those of SDOF results. However, the possibility of jump is better to be reduced since it causes the dislocation of the mannequin, or fall off in the worst case.



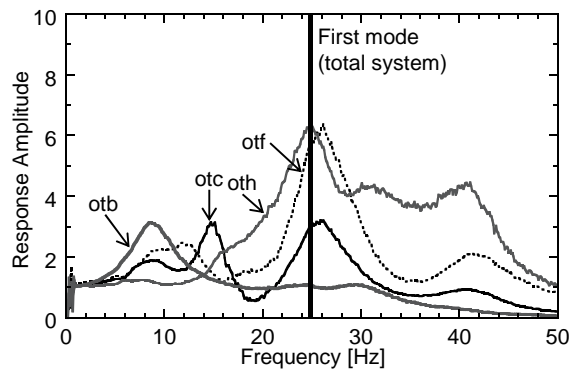
(a-1) Input Max Acc. = 0.5 m/s<sup>2</sup>



(b-1) Input Max Acc. = 0.5 m/s<sup>2</sup>



(a-2) Input Max Acc. = 5 m/s<sup>2</sup>

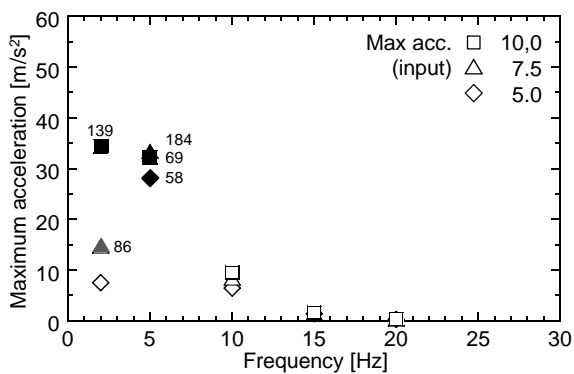


(b-2) Input Max Acc. = 5 m/s<sup>2</sup>

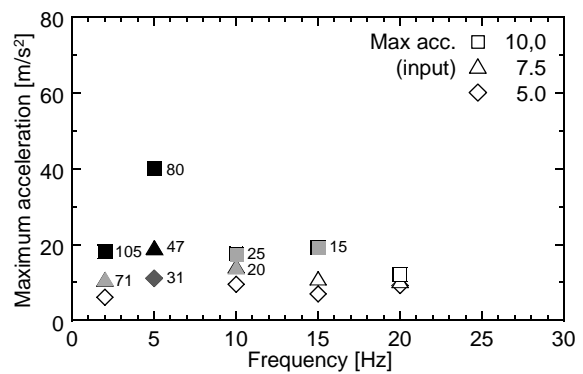
(a) Patient bed

(b) Operating table

Figure 7-14 Response amplitude of patient bed and operating table



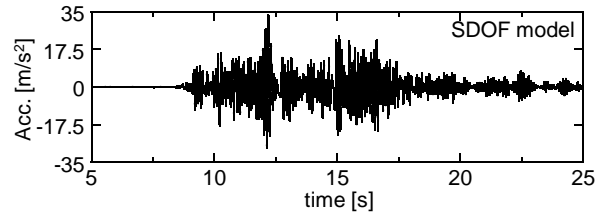
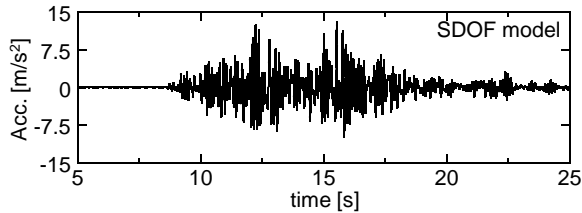
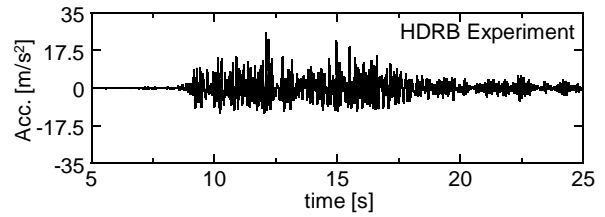
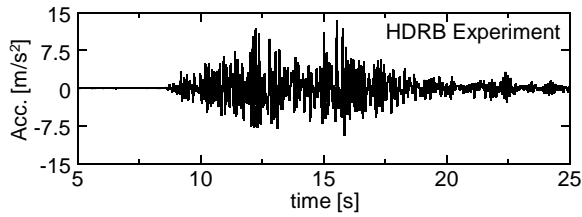
(a) Patient bed



(b) Operating table

(Note) values in tables represent the relative velocity with respect to the table

Figure 7-15 Maximum acceleration of the mannequin on the appliances



(a) JMA Kobe Z

(b) JMA Kobe XYZ

Figure 7-16 Reproduced acceleration responses of the mannequin on the operating table by SDOF lump mass model (natural frequency = 9 Hz, damping ratio of 19%)

## 7.4 Summary and conclusions of Chapter 7

This chapter described the performance of medical equipment installed on the base-isolated medical facility for ground motions with the vertical components based on the full-scale shaking table tests. The dynamic response characteristics of some equipment in the vertical direction are examined by a supplemental shaking table test. Notable findings obtained in this chapter are summarized as follows:

- (1) Vertical floor accelerations were amplified further within the appliance. Up to about 1 g as the vertical floor acceleration, no clear damage was observed. Once it exceeded 1 g, some notable damaged were observed: intensive responses occurred mainly for items placed on furniture or equipment, such as the monitor on the ceiling pendant, the mannequin on the operating table, and bottles on the shelves. For the vertical floor acceleration of 3 g, most of equipment themselves jumped.
- (2) Items with eccentricity in the vertical direction responded more severely than other well-proportioned items.
- (3) Any vertical motions did not cause malfunction of the equipment tested in the operated condition (dialyzers, and servers).
- (4) It is found that the range of natural frequencies in the horizontal direction (3 to 7.5 Hz) happened to be close to the range of natural frequencies of low-rise fixed-base buildings. This indicates that the response amplitude of equipment tends to increase for fixed-base buildings if they are fixed to the floor, while their response amplifications are expected to become smaller for base-isolated buildings. A damping ratio of 5 % may be sufficient to

adopt for the horizontal response of the equipment.

- (5) Equipment has the broad vertical natural frequencies of 5 to 28 Hz. If equipment (except beds) was well proportional, the vertical natural frequency became larger than 20 Hz. The natural frequency became lower for equipment with the vertical eccentricity (the autologous blood transfusion machine of 17 Hz, and the incubator of 13 Hz). Beds with mattress tended to have even lower vertical natural frequencies, 10 Hz for the operating table and 5 Hz for the patient bed. The damping ratio in the vertical direction of equipment was at least 5 %. Equipment with eccentricity had smaller of about 3 %. Beds tended to have larger damping ratio.
- (6) Since the main body of the operating table is much stiffer than the mattress, the response of the mannequin on the top is controlled by a SDOF of the mattress as a spring. A minor change is that the response amplitude remains one for higher frequency range instead of converging to zero. A damping ratio of 20 % is sufficient to the vertical response of the mannequin on the operating table. The dependency on the intensity of the input wave was little.
- (7) Since the main frame of the patient bed has a lower natural frequency, flexibility of the bed is to be considered in addition to the flexibility of the mattress. For the frequency range higher than its dominant natural frequencies up to 11 Hz, the input acceleration to the patient was mitigated through the patient bed. A first mode damping ratio of 10 % is sufficient for larger earthquakes, and first natural frequency may be varied about 20 % not only due to the intensity of the input wave but also due to the height of the bed.
- (8) Once the acceleration response of an item exceeded 1g, jump occurred accompanied by dislocation or falling off in a severe case. Because the jumping height of the item is related to the relative velocity, the height tended to increase when an input motion to the item was dominated by a lower frequency range with a larger velocity. Increasing in jumping height also increases the dislocation distance, and the possibility to fall down from the bed.

To mitigate the physical damage due to the vertical responses, the following measures are recommended:

- (1) Free items placed on other equipment or furniture are recommended to be fixed, especially when it is placed on the ceiling pendant, which tends to have a lower natural frequency.
- (2) It is recommended to mitigate eccentricity with respect to the vertical direction.
- (3) To mitigate the physical damage, the acceleration and velocity have to be reduced. The first natural frequency of base-isolated buildings is better to avoid the peak range of the vertical motions of 5 to 10 Hz. In addition, because the increase in the floor velocity lead to increase the jumping height, the first natural frequency is better to set to be higher than at least 10 Hz. The vertical first natural frequency of larger than 10 Hz is considered as a realistic target since the natural frequency of base-isolated buildings ranged from 11 to 16 Hz if the superstructure was normal-sized reinforced concrete structure (not steel structure or building with longer



spans) (Chapter 2). Lower vertical natural frequency is also effective as long as it ensure vertical floor acceleration responses to remained securely less than 1 g. This condition can be realized by adopting the vertical isolation system.

## **REFERENCES**

- [7-1] A. J. Papazoglow and A. S. Elnashai, Analytical and Field Evidence of the Damaging Effect of Vertical Earthquake Ground Motion, *Earthquake Engineering and Structural Dynamics*, Vol.25, pp.1109-1137, 1996.
- [7-2] C. Papaleontious and J. M. Roesset, Effect of vertical accelefrations on seismic response of frames, in T. Moan et al., (eds), *Structural Dynamics – EURODYN '93*, Balkema, Rotterdam, 1993, pp. 19 – 26.

# **CHAPTER 8**

## **VERTICAL DYNAMIC RESPONSE CHARACTERISTICS OF BASE-ISOLATED BUILDINGS**

### **8.1 Introduction**

Not a few records of vertical floor accelerations of buildings have been accumulated for past earthquakes, including base-isolated buildings (Chapter 2). Some studies tried to obtain acceleration amplifications by the base isolation layer, the dominant frequency of responses of base-isolated buildings, and the corresponding damping ratios [8-1 to 8-8]. In those records, however, the number of sensors per building was limited and details of their arrangements were sometimes not available. Therefore, it is difficult to comprehensively observe fundamental vertical dynamic response characteristics of base-isolated buildings, especially considering the slab vibration effect. In most cases, no sensor was applied to the mid span, which made it difficult to observe its contribution. The series of the full-scale shaking table tests of the base-isolated systems yielded sufficient data that showed (1) contribution of floors to amplification in acceleration responses (about 50 ~ 60%), (2) difference in the first mode contributions and (3) differences in mode shapes between the base-isolated and fixed-base systems (Chapter 5). Those data are significantly important but it remain limited to specimen with specific configurations; the natural frequency of the superstructure = 12.1 Hz with that of the base isolation layer = 18.6 Hz for HDRB (Chapter 5).

So far, there has been no research that comprehensively captures the relationship between the vertical dynamic response characteristics and the combination of major components of the base-isolated building. Therefore, this chapter aims at examining the following two issues with respect to the various combination of the mass allocation and stiffness distribution among structural components:

- (1) The vertical floor response amplitude of base-isolated buildings, considering the contribution of the floors
- (2) The first mode contribution to the vertical response

Issue (1) is primarily for observing the vertical floor acceleration amplitude, and issue (2) is to examine the demand of axial force exerted on base isolators. If the first mode contribution increases, it causes the higher demand on base isolators.

In their simplification of the model for the vertical response of the building, Nobata et al. [8-6] used a hanging lump mass model to represent the floor contribution to the vertical response characteristics of a base-isolated building. The yielded response amplitude showed reasonable agreement with that of the earthquake record. Pan [8-7] also examined a hanging lump mass model to represent the floor vibration. He concluded that the model sufficiently represented the floor responses, comparing their responses with the corresponding full model. In this chapter, a simple lumped mass model that consists of three degrees of freedom is proposed to represent the vertical first mode of the base-isolated building. The model consists of a DOF that represents the vibration of the base-isolation layer, with the superstructure as a rigid body, another DOF that expresses the first mode vibration of the columns along the height, and the last DOF that represents the first mode floor vibration of the slabs in all floors. The proposed model is examined for accuracy by comparison with the corresponding full model, and the limitation of the proposed model is discussed. Then, by conducting parametric analysis, examination is given to which types of base-isolated buildings are subject to larger vertical floor response and when it is mitigated. In addition, the modal participating mass ratio of the first mode is examined by the same parametric analysis.

## **8.2 Development of generic lump mass model for vertical vibration examination of base-isolated buildings**

A single-degree-of-freedom lump mass model is the most widely-used model for examining the horizontal response of base-isolated buildings. This simplification is reasonable because these buildings are designed so that base isolators control the whole system response. For the vertical response, however, such condensation into an SDOF is no longer valid, primarily for the following reasons:

- (1) The vertical stiffness of commonly used base isolators is not small enough in the vertical direction to regard the superstructure as a rigid body.
- (2) In this condition, the vertical response induced by the flexibility of columns cannot be ignored.
- (3) In modeling the superstructure, flexibility of slabs in the out-of-plane direction plays a significant role.

If the base isolated building has its horizontal frequency between 0.2 Hz to 0.5 Hz (2 to 5 s) [8-9], the vertical natural frequency of the base isolation falls commonly between 6.3 Hz and 27.4 Hz

(0.04s to 0.16s) based on the condition that the superstructure is assumed to behave as a rigid body, and that the vertical to horizontal stiffness ratio of the base isolators ranges between 1,000 and 3,000 when ordinal rubber bearings are adopted. Papadopoulou [8-10] suggests that the vertical frequencies of one to eight story RC frames would be in a range of 8.3 to 25.0 Hz. Bozorgnia [8-11] analyzed the recorded floor accelerations for earthquakes of seven fixed-base buildings (RC, braced steel frame, etc.), and estimated the vertical natural frequency within a range of 3.9 to 13.3 Hz. These observations support the conclusion that the base isolation and the superstructure have similar natural frequencies so that the superstructure cannot be regarded as a rigid body.

### 8.2.1 Three representative modes of base-isolated buildings

The vertical motion is amplified by three components of the base-isolated building: (1) base isolation layer, (2) columns, and (3) slabs. It is convenient to decouple each components contribution to the vertical amplification. Here, three modes are defined: the modes of the base isolation layer are defined as the modes obtained when the superstructure is set to be rigid (Figure 8-1 (b-1)), which has, therefore, only a single mode. The modes of columns are defined as the modes obtained when all floors of the superstructure are set to be rigid (Figure 8-1 (b-2)). The modes associated with the columns have a number equal to the number of the stories. The modes of slabs are determined under the condition that each slab is supported at the points where it connects with the vertical components or the columns (Figure 8-1 (b-3)).

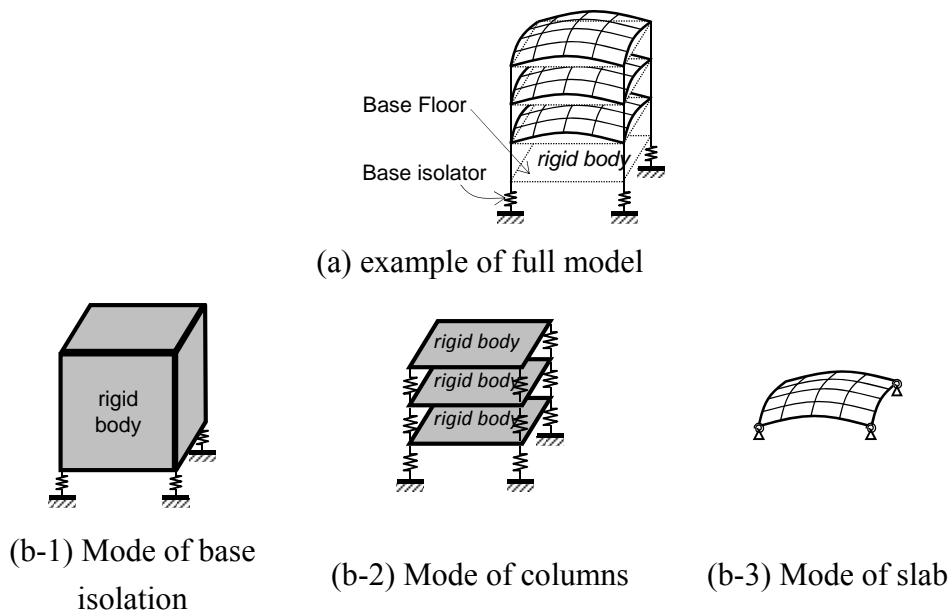


Figure 8-1 Decomposition of vertical mode of base-isolated building

Table 8-1 shows the possible ranges of natural frequencies of the respective modes. It is notable that these ranges overlap. The natural frequency of the base isolation layer  $F_{BI}$  ranges from about 6 to 28, as described above, when ordinal rubber bearings are adopted (Table 8-1(a)). The range of natural frequency of the columns is approximately estimated to be from 5 to 30 Hz for

RC buildings when the same section properties are adopted for all stories and other parameters are set as shown in Table 8-1(b). This table includes: the number of stories; story height; the specific design strength of concrete,  $F_c$ ; which determines Young's modulus,  $E$  [8-12]; axial force ratio to allowable strength of concrete in design,  $\sigma_0 / \sigma_y$ ; and dead load with surface loads,  $w$ . The natural frequency of the slab ranges from about 2 ~ 50 Hz, as shown in Table 8-1(c). The parameters shown in the table are thickness  $d$ , spans  $L_x$  and  $L_y$ , mass density  $\rho$ , and Young's modulus  $E$ . The natural frequency of the slab is affected most significantly by its supporting conditions (simply supported, fixedly supported, and four-edge pin supported, are considered) [8-13, 14]. For example, if a 5 m square slab with a thickness of 200 mm is adopted with the concrete of  $F_c = 24 \text{ N/mm}^2$ , the first natural frequencies of the slab supported by beams fall in between that of the slab supported by no beam (24.5 Hz) and that of the fixed-supported slab (8.9 Hz) at the surrounding edges.

Table 8-1 Possible ranges of the first natural frequencies of three modes

(a) Base isolation layer

parameter
$T_H = 2 \sim 5 \text{ s}$
$V/H = 1,000 \sim 3,000$
$F_{BI} = 6.3 \sim 27.4 \text{ Hz}$

V/H = vertical stiffness ratio to horizontal

(b) Column

set	parameter
story height = 3.5 m	$F_c = 24 \sim 40 \text{ N/mm}^2$
span = 6 m	$\sigma_0 / \sigma_y = 0.1 \sim 0.3$
$w = 11.8 \text{ kN/m}^2$	# of stories = 1 ~ 50
$F_c = 5 \sim 30 \text{ Hz}$	

(c) Slab

set	parameter
$F_c = 24 \text{ N/mm}^2$	$L_x / L_y = 1$
$\nu = 0.2$	$L_x = L_y = 5 \sim 10 \text{ m}$
$\rho = 2,450 \text{ kg/m}^3$	$d = 0.15 \sim 0.25 \text{ m}$
simply supported	$F_s = 4.3 \sim 28.3 \text{ Hz}$
fixedly supported	$F_s = 7.8 \sim 51.7 \text{ Hz}$
four-edge supported	$F_s = 1.9 \sim 12.5 \text{ Hz}$

### 8.2.2 3DOF lump mass model

To obtain a simplest model to assess the vertical floor responses of base-isolated buildings subjected to the first mode vibration, three major components are condensed further based on the following conditions and assumptions,

Assumptions:

- (1) The first mode dominates in the respective components, i.e., the base isolation, the columns and the slabs.
- (2) The building is assumed to have the same floor plan for all floors, the same story height, and the same section columns for all stories.

- (3) The columns sustain only the axial force.
- (4) The difference in supported conditions can be neglected between the mid-story floors and the top floor, where no column is present above.
- (5) The floor right above the base isolation layer is stiff enough to be regarded as a rigid body.

With the assumptions from (1) to (5), the following conditions are available:

- (1) The floor deflection shape is assumed to be the same throughout the floors.
- (2) The floor deflection amplitudes are proportional to the response amplitude at the connecting point with the columns.

With the above assumptions, a three-degrees-of-freedom lump mass model, ‘3DOF lump mass model,’ called 3DOF model hereinafter, is proposed, as shown in Figure 8-2. In Figure 8-2, each lump mass represents a floor mass right above the base isolation layer, a column mass, and a slab mass from the bottom. They are defined as  $m_{BF}$ ,  $m_C$  and  $m_S$ , and the equivalent stiffnesses are defined as  $k_{BI}$  (base isolation),  $k_C$  (column) and  $k_S$  (slab), respectively.  $m_{BF}$  is set to be the same as the base floor mass of the corresponding full model, and the sum of  $m_C$  and  $m_S$  is equal to the mass of the superstructure excluding the base floor. The concept of mass allocations of the superstructure to three DOFs is shown in Figure 8-3. The distribution of the mass between the slab DOF and the column DOF is determined in the next section.

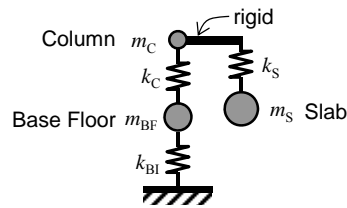


Figure 8-2 3DOF model

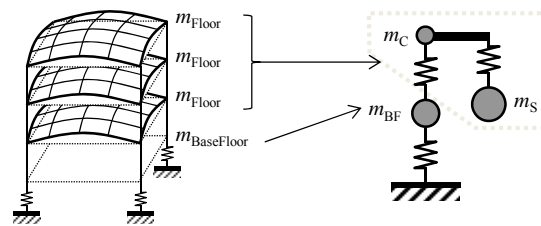


Figure 8-3 Mass allocations among 3DOF

The natural frequency of each mode is determined as follows:

$$F_{BI} = \frac{1}{2\pi} \sqrt{\frac{k_{BI}}{m_{BF} + m_C + m_S}} \quad (8-1)$$

$$F_C = \frac{1}{2\pi} \sqrt{\frac{k_C}{m_C + m_S}} \quad (8-2)$$

$$F_S = \frac{1}{2\pi} \sqrt{\frac{k_S}{m_S}} \quad (8-3)$$

Where  $F_{BI}$  is the natural frequency of the mode of the base isolation (Figure 8-1 (b-1)),  $F_C$  is the first natural frequency of the mode associated with columns (Figure 8-1 (b-2)), and  $F_S$  is the first natural frequency of the mode associated with a slab (Figure 8-1 (b-3)).

The response relative to the ground yielded by 3DOF model is amplified using two factors that consider the effect of shape functions to obtain the actual responses of the corresponding full model. The column amplification factor  $\alpha_C$  represents the response amplification from the equivalent SDOF to the top of the column at the target floor, and the slab amplification factor  $\alpha_S$  represents the response amplification from the equivalent SDOF to the target point of the slab. Finally, the relative response for the first mode of the corresponding full model is obtained as follows:

$$\phi_{BF}' = \phi_{BF} \quad (8-4)$$

$$\phi_C' = (\phi_C - \phi_{BF})\alpha_C + \phi_{BF}' \quad (8-5)$$

$$\phi_S' = \left( \phi_S \frac{\phi_C'}{\phi_C} - \phi_C' \right) \alpha_S + \phi_C' \quad (8-6)$$

Where  $\phi_{BF}$ ,  $\phi_C$ , and  $\phi_S$  are the components of the first vertical mode vector at the base floor, the column, and the slab DOF of the 3DOF model, and  $\phi_{BF}'$ ,  $\phi_C'$ , and  $\phi_S'$  are the corresponding components of the first vertical mode vector of the full model. In Eq. (8-5), the difference between  $\phi_C$  and  $\phi_{BF}$  is amplified by  $\alpha_C$  and summed up with  $\phi_{BF}'$  to obtain the vertical response of the target floor's column,  $\phi_C'$ . Since  $\phi_S$  is always proportional to  $\phi_C$ ,  $\phi_S$  is magnified by the ratio of  $\phi_C'$  to  $\phi_C$ . Again, the difference between this magnified  $\phi_S$  by  $(\phi_C' / \phi_C)$  and  $\phi_C'$  is amplified further by  $\alpha_S$  and added by  $\phi_C'$  to obtain the vertical response of the target point on the slab,  $\phi_S'$ , via the procedure shown in Eq. (8-6).

## 8.3 Supporting factors for 3DOF model

Three factors of response amplifications and mass allocations have to be determined to condense the multi-degrees of freedom of the full model to the 3DOF model. They are the column amplification factor of  $\alpha_C$ , slab amplification factor of  $\alpha_S$ , and mass contribution factor of the slab to the floor of  $\gamma_S$ .

### 8.3.1 Supporting factor for column

As mentioned above, the building is assumed to have the same story height and the same column section for all stories. All masses are concentrated at the floors, and no mass is distributed along the height of columns. Therefore,  $\alpha_C$  becomes only the function of the number of stories. The column amplification factors are calculated as response amplification numerically. Figure 8-4 shows  $\alpha_C$  with respect to the number of stories (up to twenty stories). The first floor and the roof are set to be

the target floors.  $\alpha_C$  for the roof increases rapidly from one to five stories from 1.0 to 1.26. For stories above five, the increment becomes more moderate and converges to 1.28. For more than ten stories,  $\alpha_C$  can be approximated as 1.28 with errors not greater than 0.1%.  $\alpha_C$  for the first floor decreases rapidly from one to five stories from 1.0 to 0.38 and keeps decreasing for taller buildings but its declining rate becomes more moderate as the number of stories increases.

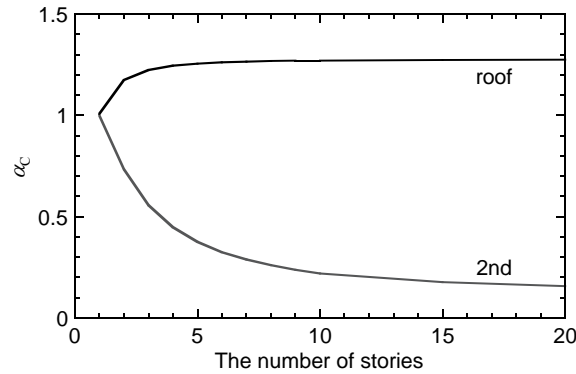


Figure 8-4 Column acceleration amplification factors  $\alpha_C$

### 8.3.2 Supporting factors for slab

Two supporting factors for slabs,  $\alpha_S$  and  $\gamma_S$  are determined based on the following assumptions:

- (1) The supporting factors for the slab,  $\alpha_S$  and  $\gamma_S$ , are determined independent of the columns.
- (2) The first mode effective mass of the independent slab (Figure 8-1 (b-3)) is adopted as the slab mass contribution factor to the floor mass,  $\gamma_S$ .

The above assumptions are examined using a simple model whose deformations can be easily formulated: a single-span and single-story frame model.

#### Formulation example using a frame model

Table 8-2 shows two types of single-span single-story frame model: one has a pin-supported beam, and the other has a fixed-supported beam. The corresponding  $\alpha_S$  and  $\gamma_S$  are calculated based on assumptions (1) and (2) above. Rayleigh's method [8-15, 16] is adopted. If the shape function,  $\phi(x)$ , is given, the response amplification,  $\alpha$ , is defined in Eq. (8-7), and the first mode effective mass,  $M_{eq}$ , is defined as follows:

$$\alpha(x) = \Gamma_n \phi(x) \tag{8-7}$$

$$\text{where } \Gamma_n = \frac{L_n}{M_n} \tag{8-8}$$

$$L_n = \int_0^L m(x) \phi(x) dx \tag{8-9}$$



$$M_n = \int_0^L m(x)\phi(x)^2 dx \quad (8-10)$$

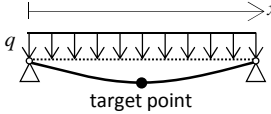
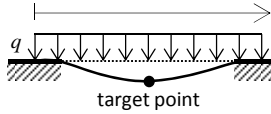
$$M_{eq} = \Gamma_n^2 M_n \quad (8-11)$$

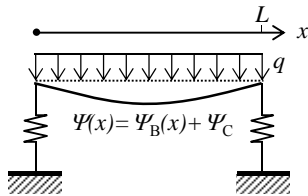
The slab mass contribution factor to the floor mass  $\gamma_s$  is assigned as:

$$\gamma_s = \frac{M_{eq}}{\int_0^L m(x)dx} \quad (8-12)$$

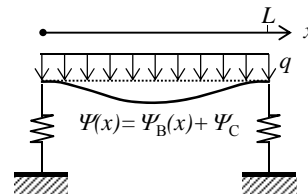
Where  $m(x)$  is mass distribution per unit length.

Table 8-2 Supporting factors for beam model examples

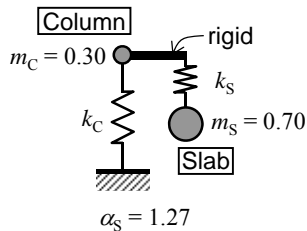
	(a) Pin-supported beam	(b) Fixed-supported beam
		
$\phi_B(x)$	$\frac{q}{24EI}(-L^3x + 2Lx^3 - x^4)$	$\frac{q}{24EI}(-L^2x^2 + 2Lx^3 - x^4)$
$\gamma_s$	0.81	0.70
$\alpha_s (x=L/2)$	1.27	1.31



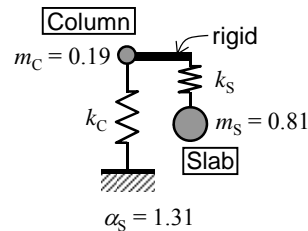
(a-1) frame model



(b-1) frame model



(a-2) 2DOF model



(b-2) 2DOF model

(a) Pin-supported beam

(b) Fixed-supported beam

Figure 8-5 Frame models and equivalent 2DOF lump mass model for the verification of supporting factors

The deflected shape of the beam,  $\phi_B$ , generated under the distributed load with its magnitude of  $q$ , is given for the pin-supported and fixed-supported beams with the beam theory, as shown in Table 8-2. In the table,  $E$  and  $I$  are Young's modulus and the moment of inertia of the beam, respectively.  $q$  is equivalent to a unit-length mass multiplied by gravity.  $\alpha_S$ , calculated by Eq. (8-7), and  $\gamma_S$ , calculated by Eq. (8-12) are also listed in the table. The target point for  $\alpha_S$  is set as the center of the beam where  $x = L/2$ .

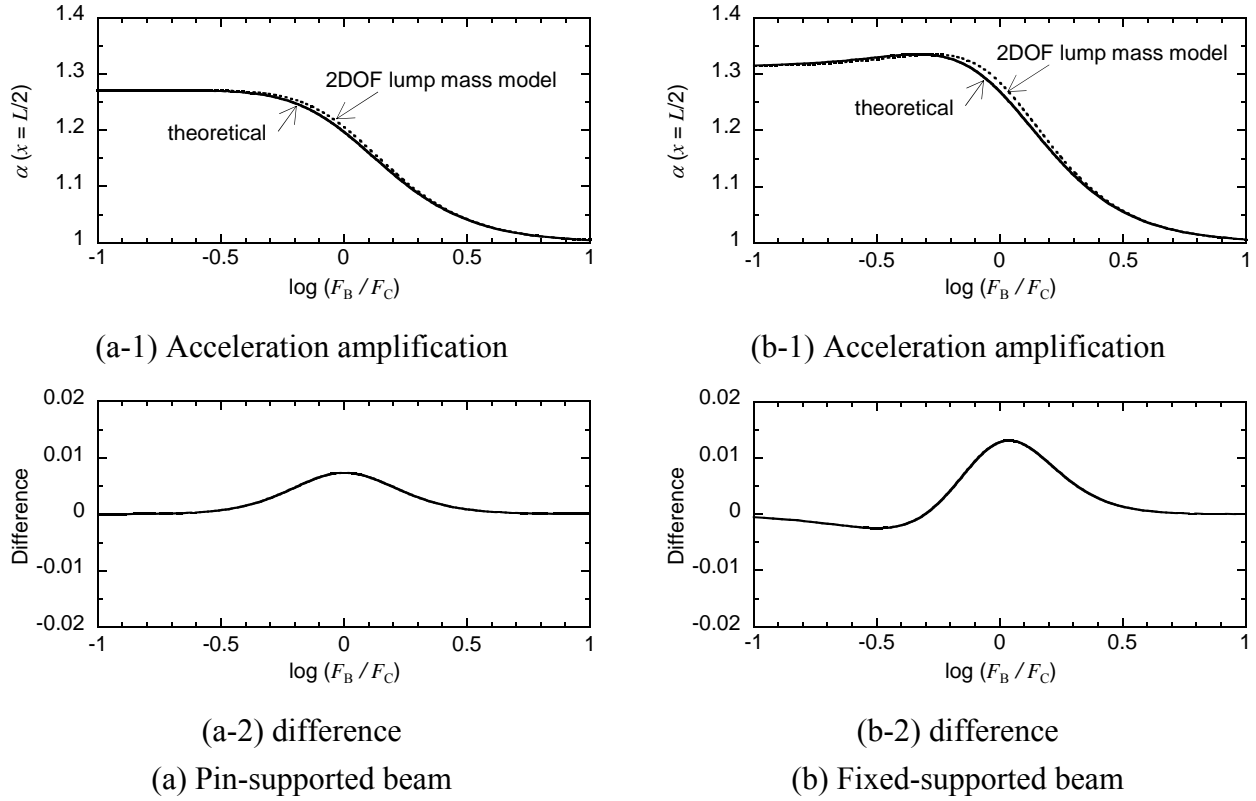


Figure 8-6 Comparison in response amplification at beam center between theoretical formula and 2DOF lump mass model analysis

The first mode response amplifications  $\alpha$  (Eq. (8-7)) obtained by the 2DOF model with variables listed in Table 8-2 are verified by comparison with the theoretical results of the frame model, models of which are shown in Figure 8-5. The columns are modeled to sustain only axial force. With the column deflection, the deflected shape functions of the beam,  $\phi(x)$ , are given by the summation of the deflection of the beam,  $\phi_B(x)$ , and that of the columns,  $\phi_C(x)$ , which is given in the form of:

$$\phi(x) = \phi_B(x) + \phi_C \quad (8-13)$$

$$\phi_C = -\frac{qL}{k_C} \quad (8-14)$$

Where  $k_C$  is the axial stiffness of the two columns on both sides. The first mode response amplification at  $x = L/2$  is calculated with respect to the ratio of the first natural frequency of the slab  $F_S$  to that of the column  $F_C$ , as shown in Figures 8-6 (a-1) and (b-1). In the 2DOF model, the first

mode response amplification is obtained numerically by calculating the response amplification at the first natural frequency. Figures 8-6 (a-2) and (b-2) show the difference between the two results. From these figures, the results of the 2DOF model show reasonable agreement with the theoretical results. The maximum error occurs when  $F_S$  equals  $F_C$ , but it is not greater than 0.02%. The difference becomes least at both ends, where each mode of the slab or columns controls the entire response.

According to the results, it is reasonable to adopt the assumptions (1) and (2), in which the slab supporting factors,  $\alpha_S$  and  $\gamma_S$ , are calculated independently of the column stiffness, and the first mode effective mass of the slab is adopted as  $\gamma_S$ .

### Numerical determination of slab supporting factors

The supporting factors for the slab are calculated numerically using FEM software.  $\alpha_S$  is obtained by calculating the ratio of the acceleration response at the target point of the slab under sinusoidal excitation with its frequency equal to the first mode to the resonance acceleration response of the equivalent SDOF, which is  $1/2h$ , where  $h$  is the first mode damping ratio. This procedure is equivalent to extracting values of a participation factor ( $\Gamma_n$  in Eq. (8-7)) multiplied by the corresponding component of the mode vector ( $\phi$  in Eq. (8-7)). The slab mass contribution to the floor mass,  $\gamma_S$ , is determined as the first mode effective mass of the slab.

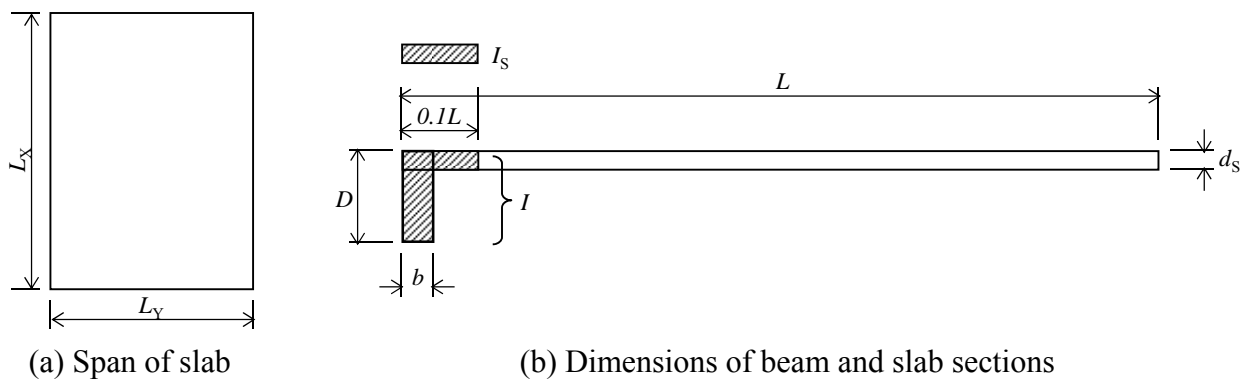


Figure 8-7 Definition of dimension and sections of slab and beams

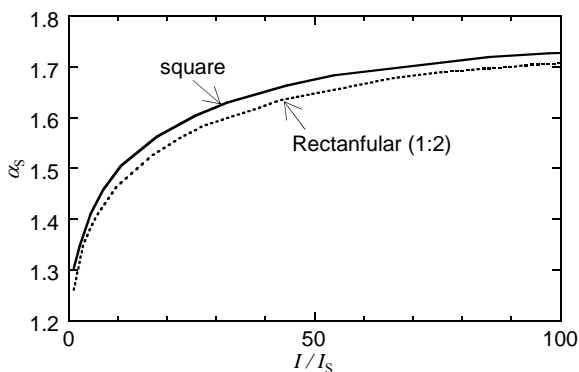
A floor supported at four corners by columns is considered, with the connections modeled as pins. Two parameters are chosen: one is the slab shape and the other is the slab stiffened ratio as affected by beams. Two slab shapes are considered:

- 1) Square:  $L_X = L_Y$
- 2) Rectangular:  $L_X = 2L_Y$

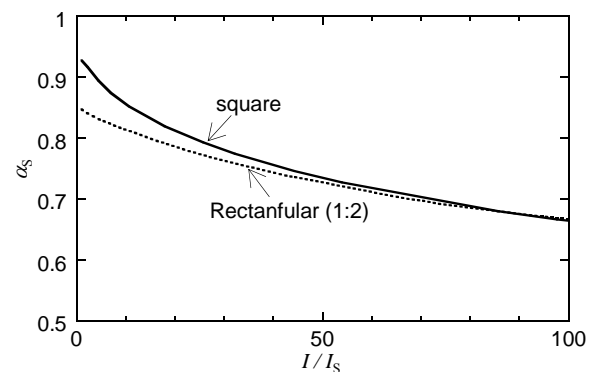
Where  $L_X$  and  $L_Y$  are the span lengths of the longitudinal and transverse directions of the slab, as shown in Figure 8-7. The slab stiffened ratio is defined as the ratio of the moment of inertia of the composite beam  $I$  to that of the slab without the beam  $I_S$ . The width of the slab considered in calculating  $I$  and  $I_S$  are set to be one-tenth of the beam span [8-12], as shown in Figure 8-7 (b). For

the rectangular beam, the beam having the shorter span  $L_Y$  is adopted as the variable. The beam section of the longer beam is determined according to the condition that the ratio of moment inertia of the longer beam ( $x$  direction) to the shorter beam ( $y$  direction) is equal to  $L_X/L_Y$ . This treatment is made so that the rotational stiffness of beams is proportional to its length. The ratio of the depth  $D$  to the width of beam sections  $b$  is fixed to two. Note that the difference between the resulting supporting factors for the ratio  $D/b$  of two and three is confirmed to be not greater than 1% for the square slab. Mass is assumed to be distributed uniformly throughout the floor. The self weight of beams is neglected. All beams are located on the slab edges and no additional girder is considered.

Figure 8-8 (a) and (b) show  $\alpha_S$  and  $\gamma_S$  with respect to  $I/I_S$  for a range of 1 to 100.  $I/I_S$  equals one means a slab without the beam. As  $I/I_S$  becomes larger, the supporting condition of the slab becomes closer to the fixed-supported slab. Therefore,  $\alpha_S$  and  $\gamma_S$  have its lower and upper bounds;  $\alpha_S$  has its value between 1.3 and 1.72, and  $\gamma_S$  between 0.93 and 0.56 for the square slab, and  $\alpha_S$  has its value between 1.26 and 1.71, and  $\gamma_S$  has the range between 0.85 and 0.55 for the rectangular slab. The square slab always has larger supporting factors than the rectangular slab, and the difference becomes smaller as  $I/I_S$  becomes larger.  $\alpha_S$  increases drastically from  $I/I_S$  equal 1 to 10 but increases moderately for larger  $I/I_S$ , and converges to 1.72 for a square or 1.71 for a rectangular slab. Generally, the slab supported by the ordinal sized beam has  $I/I_S$  smaller than 40. When a 5 m square slab with a thickness of 200 mm is supported 260 mm by 520 mm beams, the corresponding  $I/I_S$  is 10.7. This results in  $\alpha_S$  equal to 1.51 and  $\gamma_S$  equal to 0.85.



(a) slab acceleration amplification factor,  $\alpha_S$



(b) mass contribution ratio of slab mass to the floor mass,  $\gamma_S$

Figure 8-8 Supporting factors of slab obtained by numerical analysis

## 8.4. Verification of 3DOF model

To verify the proposing model, the responses of the 3DOF model are compared with those of the corresponding full mode for the first mode.

### 8.4.1 Model description

Comparison is made for several cases in which the conditions that the number of stories, mass distribution, the floor shape and its stiffened ratio by beams are set as fixed values for all cases. The combination of natural frequencies of the base isolation  $F_{BI}$ , columns  $F_C$ , and slab  $F_S$  are considered as variables. The selected models to verify the 3DOF model have one, four and ten stories with one bay in each direction. The floor has dimensions of 5 m by 5 m, and 150 mm thickness slab supported by 250 by 600 mm beams, resulting in beam stiffened ratio of  $I / I_S$  equal to 34.80. These setting yield  $\alpha_S$  and  $\gamma_S$  equal 1.24 and 1.63, respectively. The full model and the corresponding 3DOF model are shown in Figure 8-9 for the four-story model. Table 8-4 shows response amplification factors and mass distribution ratios among three DOFs applied to 3DOF model. Mass is distributed so that the ratio of the mass of the upper floors to the base floor becomes 1 to 1.5. Floor masses are divided into the column and slab DOFs following  $\gamma_S$  of 0.75. The columns sustain only axial force, and the columns and beams are connected by pins.

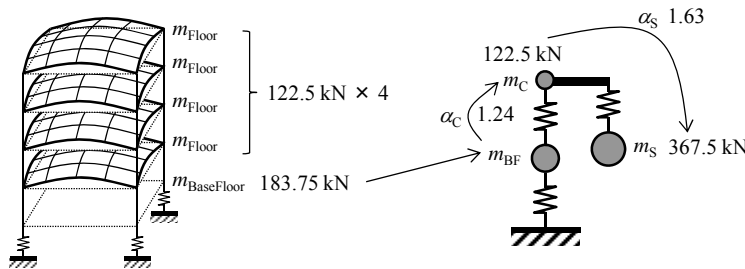


Figure 8-9 Model description of the full model and 3DOF model (4 story model)

Table 8-4 Model setting for 3DOF

	1story	4 story	10 story
$\alpha_s$	1.63	1.63	1.63
$\gamma_s$	0.75	0.75	0.75
$\alpha_c$	1	1.24	1.28
base floor	1.5	1.5	1.5
mass			
column	0.25	1	2.5
slab	0.75	3	7.5

Table 8-5 Combination of the natural frequencies of  $F_{BI}$ ,  $F_C$ , and  $F_S$

		$F_S / F_C$				
		0.1	0.5	1	2	10
$F_{BI} / F_C$	10	(1)		(2)		(3)
	2		(4)	(5)	(6)	
	1	(7)	(8)	(9)	(10)	(11)
	0.5		(12)	(13)	(14)	
	0.1	(15)		(16)		(17)

Table 8-6 shows all 17 combinations of  $F_S / F_C$  and  $F_{BI} / F_C$  for which these responses were verified. The stiffnesses of the full model and the corresponding 3DOF model are adjusted proportionally so that the first natural frequency is set to 5 Hz. The response amplification at the center of the roof slab is examined.

### ***8.4.2 Verification of 3DOF model***

The first mode response amplification with the damping ratio of 5% is compared between the 3DOF model and the corresponding full model, whose errors are shown in Table 8-6. The tables also show the differences between two models in modal participating mass ratios of the first mode. In the full model, the response amplification at the first natural frequency is yielded numerically by inputting the sinusoidal excitation having the frequency equal to the first mode. Table 8-7 shows the natural frequencies and the modal participating mass ratios for the first four modes of the full model for the four-story model.

For response amplification, good agreement is found for all cases for the one-story model with the error of not greater than 3%. For the four- and ten-story models, almost all cases have errors of not greater than 5%, but some overestimation was observed for two cases, (1) and (7): the combination of  $F_S/F_C$  equal to 0.1 and  $F_{BI}/F_C$  equal to 10 yields greater than 20% difference (Case (1)), and the combination of  $F_S/F_C$  equal to 0.1 and  $F_{BI}/F_C$  equal to 1 yields greater than 10% difference (Case (7)). In Cases (1) and (7), both of which have an extremely soft slab, the natural frequencies from the first to fourth modes fall in a range of 0.4% difference, as shown in Table 8-7 (a). This concentration of modal frequencies causes inputting sinusoidal excitation having its frequency adjusted to the first natural frequency also triggers the second to fourth modes in the full model, whose effects cannot be eliminated in this numerical calculation. Figure 8-10 (c-1) to (c-4) shows the first to fourth modes of the full model with extremely soft slab that is applicable to Cases (1) and (7), which show combined modes of the first slab mode (Figure 8-10 (a)) accompanied by the first to fourth column modes (Figure 8-10 (b-1) to (b-4)). In Figure 8-10(b), the magnitudes of the column vertical mode vector are projected in the horizontal direction. With an extremely soft slab or natural frequency of  $F_S/F_C$  equal to 0.1, the slab natural frequency controls the combined natural frequency so that the resulting first four natural frequencies distribute very close to the first natural frequency of the slab only. Especially due to the contribution of the column second mode, the apparent response amplification at the top floor for the first mode is reduced in the full model, resulting in overestimation of the 3DOF model results. The same reason for the larger differences in response amplification in the case with extremely soft slab is applicable to the ten-story model.

For the modal participating mass ratio, good agreement is notable for the one-story model in all cases and also for the four- and ten-story models the cases, in which the natural frequency of the base isolation layer is the smallest. This difference increases as  $F_{BI}/F_C$  becomes larger, in which the system becomes close to the fixed-base system. However, it remained less than 15% in difference for an extreme case of  $F_{BI}/F_C$  equal to 10.

Table 8-6 Errors in the first mode response characteristics between 3DOF model and the corresponding full model

(a) 1 story						(b) 4 story							
(a-1) Response amplification						(b-1) Response amplification							
		$F_s/F_c$							$F_s/F_c$				
		0.1	0.5	1	2	10			0.1	0.5	1	2	10
$F_{BI}/F_C$	10	-3%		1%		0%	$F_{BI}/F_C$	10	23%		2%		1%
	2		-1%	0%	0%			2		2%	-1%	-1%	
	1	-1%	-1%	1%	0%	0%		1	13%	-1%	-1%	-2%	-2%
	0.5		0%	0%	0%			0.5		-1%	0%	-1%	
	0.1	1%		0%		0%		0.1	1%		1%		1%
(a-2) Modal participating mass ratio						(b-2) Modal participating mass ratio							
		$F_s/F_c$							$F_s/F_c$				
		0.1	0.5	1	2	10			0.1	0.5	1	2	10
$F_{BI}/F_C$	10	0%		0%		0%	$F_{BI}/F_C$	10	6%		7%		8%
	2		0%	0%	0%			2		5%	5%	6%	
	1	0%	0%	0%	0%	0%		1	3%	2%	2%	2%	2%
	0.5		0%	0%	0%			0.5		0%	0%	0%	
	0.1	0%		0%		0%		0.1	0%		0%		0%
(c) 10 story													
(c-1) Response amplification													
		$F_s/F_c$											
		0.1	0.5	1	2	10							
$F_{BI}/F_C$	10	27%		2%		1%							
	2		3%	-2%	-2%								
	1	13%	-2%	-4%	-4%	-3%							
	0.5		-3%	-3%	-2%								
	0.1	-1%		0%		0%							
(c-2) Modal participating mass ratio													
		$F_s/F_c$											
		0.1	0.5	1	2	10							
$F_{BI}/F_C$	10	12%		12%		13%							
	2		9%	9%	9%								
	1	7%	4%	4%	4%	3%							
	0.5		1%	1%	0%								
	0.1	0%		0%		0%							

In summary, it is verified that the 3DOF model reasonably represents the first mode response amplification of the full model. In the case that the slab has the smallest natural frequency among three modes, the 3DOF model tends to overestimate the response amplitude because of the contribution of higher modes to cancel the first mode response amplitude. In the extreme case, when the ratios of the natural frequency of the slab to other two are more than 10, the first mode response amplitude may be reduced to less than 80%. In addition, the 3DOF model has a sufficient capacity to predict the modal participating mass ratio of the first mode especially when

the natural frequency of the base isolation layer  $F_{BI}$  is the smallest. It also yields reasonable mass ratios with the difference of less than 15% even for the cases in which the base isolation layer is stiff enough to be considered as a fixed-base system.

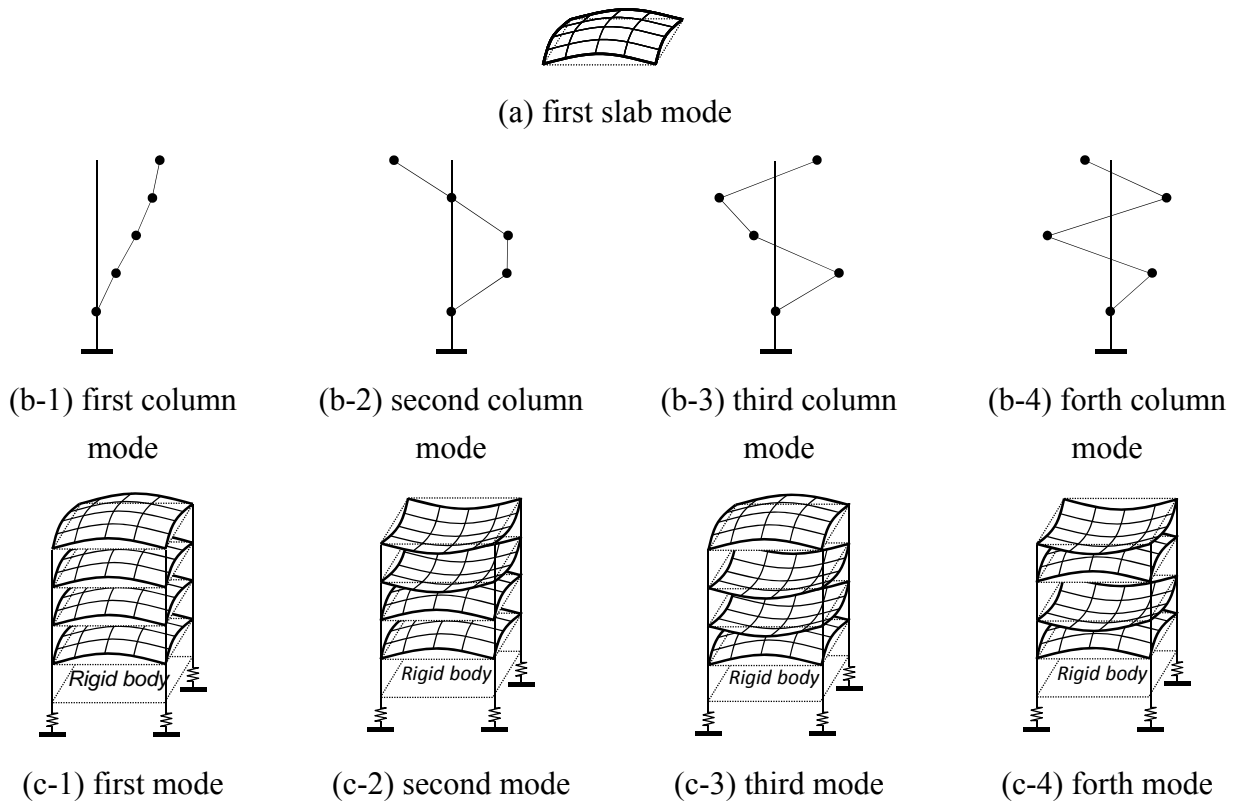


Figure 8-10 Mode shapes for the extremely small  $F_S/F_C$  of 0.1 with  $F_{BI}/F_C$  larger than 1

This study also indicates that the contribution of higher modes tends to decrease the vertical response amplification and also the axial force exerted on the base isolation layer, when the natural frequency of the slab is the smallest among three or equal to others. This condition is applicable to Case (1), (2), (4), (5), (7), (8) and (9). In those cases, the modal participating mass ratio of the first mode is relatively smaller than other cases, and effective higher modes are close to the first mode (Table 8-8). The cases with the smallest natural frequency of the column (Case (3), (6), (10), and (11)) also resulted in smaller modal participating mass ratio, but the natural frequency of the second effective mode is spaced further from the first natural frequency, and, therefore, there is lower possibility that the higher modes cancel the first mode.



Table 8-7 Modal information of the first mode for four-story model

(a) Natural frequencies of first five modes

	$F_1$	$F_2$	$F_3$	$F_4$
(1)	5.00	5.02	5.02	5.02
(2)	5.00	6.54	6.71	6.76
(3)	5.00	8.54	8.54	14.02
(4)	5.00	5.48	5.52	5.53
(5)	5.00	6.78	6.98	7.03
(6)	5.00	8.75	8.75	9.72
(7)	5.00	5.03	5.03	5.03
(8)	5.00	5.72	5.78	5.79
(9)	5.00	7.59	7.89	7.96
(10)	5.00	8.13	8.13	11.10
(11)	5.00	7.90	7.90	13.94
(12)	5.00	6.84	6.92	6.94
(13)	5.00	7.57	7.57	10.76
(14)	5.00	7.31	7.31	15.72
(15)	5.00	6.60	6.60	6.60
(16)	5.00	6.94	6.94	32.48
(17)	5.00	6.93	6.93	82.17

(b) Modal participating mass ratio

	$m_{eq1}$	$m_{eq2}$	$m_{eq3}$	$m_{eq4}$
(1)	0.48	0.04	0.01	0.00
(2)	0.61	0.05	0.01	0.00
(3)	0.65	0.00	0.00	0.06
(4)	0.58	0.04	0.01	0.00
(5)	0.68	0.04	0.01	0.00
(6)	0.74	0.00	0.00	0.06
(7)	0.53	0.02	0.00	0.00
(8)	0.67	0.02	0.00	0.00
(9)	0.82	0.02	0.00	0.00
(10)	0.89	0.00	0.00	0.05
(11)	0.90	0.00	0.00	0.08
(12)	0.86	0.00	0.00	0.00
(13)	0.97	0.00	0.00	0.00
(14)	0.98	0.00	0.00	0.00
(15)	0.87	0.00	0.00	0.00
(16)	1.00	0.00	0.00	0.00
(17)	1.00	0.00	0.00	0.00

## 8.5 First vertical floor response amplification of base-isolated buildings

Dynamic response characteristics in the vertical direction in base-isolated buildings are examined for the first mode using the proposed 3DOF model. The main points of interests are which combination of mass and stiffness distribution among the base isolator, columns and slab would lead to the maximum floor responses, and when these responses are mitigated. In addition, which combinations would result in the first mode dominated response is also examined.

### 8.5.1 Model description

In addition to the combination of  $F_{BI}$ ,  $F_C$ , and  $F_S$ , the following variables are chosen as analysis parameters: the number of stories, which determines the column amplification factor  $\alpha_C$ , the slab stiffened ratio of  $I / I_S$ , which determines the slab amplification factor  $\alpha_S$  and the slab mass contribution to the floor mass  $\gamma_S$ ; and the ratio of the base floor's mass to the mass of the superstructure except the base floor  $\gamma_{BF} = m_{BF} / m_C + m_S$ . All combinations considered are summarized in Table 8-3. The center of the roof and the base floor (rigid body) are set to be the target point to qualify the response amplification. Three values are selected for  $\alpha_C$ : 1.0, 1.24 and 1.28, representing the column amplification factor of one, four, and more than ten stories obtained from Figure 8-4.  $\gamma_{BF}$  is chosen according to the number of stories:  $\gamma_{BF} = 1.5$  for a one-story

building,  $\gamma_{BF} = 1.0$  and  $0.3$  for a four-story building, and  $\gamma_{BF} = 0.15$  for a building higher than ten stories. For each combination,  $I / I_S$  is set as 1.0, 18.0, infinity, representing the slab supported by no beam, that supported by a common-sized beam, 600x300 with 200 mm thick slab as an example, and that supported fixedly at the surrounding edges. Once  $I / I_S$  is set, the corresponding  $\alpha_S$  and  $\gamma_S$  are determined when the slab shape is set to be square from Figure 8-8.

Table 8-8 Combination of factors for 3DOF model

Number of story	$\alpha_C$	$\gamma_{BF}$	$I / I_S$	$\alpha_S$	$\gamma_S$	
(a-1)			1	1.30	0.93	No beam
(a-2)	1	1	18	1.56	0.82	Reasonable sized beam
(a-3)			Infinity	1.72	0.56	Very stiff beam
(b-1)			1	1.30	0.93	No beam
(b-2)	4	1.24	18	1.56	0.82	Reasonable sized beam
(b-3)			Infinity	1.72	0.56	Very stiff beam
(c-1)			1	1.30	0.93	No beam
(c-2)	4	1.24	18	1.56	0.82	Reasonable sized beam
(c-3)			Infinity	1.72	0.56	Very stiff beam
(d-1)			1	1.30	0.93	No beam
(d-2)	10	1.28	18	1.56	0.82	Reasonable sized beam
(d-3)			infinity	1.72	0.56	Very stiff beam

### 8.5.2 Vertical floor response amplification of base-isolated buildings

#### Explanation on contour figure

The vertical response amplification distribution with damping ratio of 5% is plotted as contours with respect to the combinations of  $F_S$ ,  $F_C$  and  $F_{BI}$ , one example of which is shown in Figure 8-11. In the figure, the horizontal axis is the natural frequency of the slab normalized by that of the column,  $F_S / F_C$ , and the vertical axis is the natural frequency of the base isolation normalized by that of the column,  $F_{BI} / F_C$ . Log scales are adopted so that the frequency ratio of  $F_S = 0.5F_C$  and  $F_S = 2F_C$  is located at the same distance from  $F_S = F_C$ , which is 0 in log scale.  $F_S / F_C$  and  $F_{BI} / F_C$  are chosen in a range of 0.1 to 10. Four edges in Figure 8-11 are captioned as A to D from left to right, and from top to bottom. A few comments on characteristics of the figures are as follows:

- (1) The central horizontal line labeled 0 represents  $F_{BI} = F_C$ , and the central vertical line labeled 0 represents  $F_S = F_C$ . The diagonal line from top right to bottom left is the line of  $F_{BI} = F_S$ .
- (2)  $F_S$  is the smallest among the three for Area I,  $F_{BI}$  is the smallest for Area II, and  $F_C$  is the smallest for Area III.
- (3) The closer to the upper end (line A-B), the closer to the condition of the fixed-base system since a base isolation layer becomes stiffer relative to columns as  $F_{BI} / F_C$  becomes larger.

- (4) Being closer to the top left end (point A), the slab mode dominates the response.
- (5) Being closer to the top right end (point B), the column mode dominates the response. The response amplitude becomes close to the values obtained by the multiplication of that of the SDOF resonant response amplification and the column amplification factor  $\alpha_C$  (12.4 for the damping ratio  $h$  of 5% and  $\alpha_C$  of 1.24).
- (6) The closer to the bottom right end (point D), the closer to the complete base-isolated system in the vertical direction since the base isolation is so soft that all vertical response concentrate into the base isolation layer, resulting in a response amplification of 10, which is equal to the SDOF response of  $1/2h$  for  $h = 5\%$ .

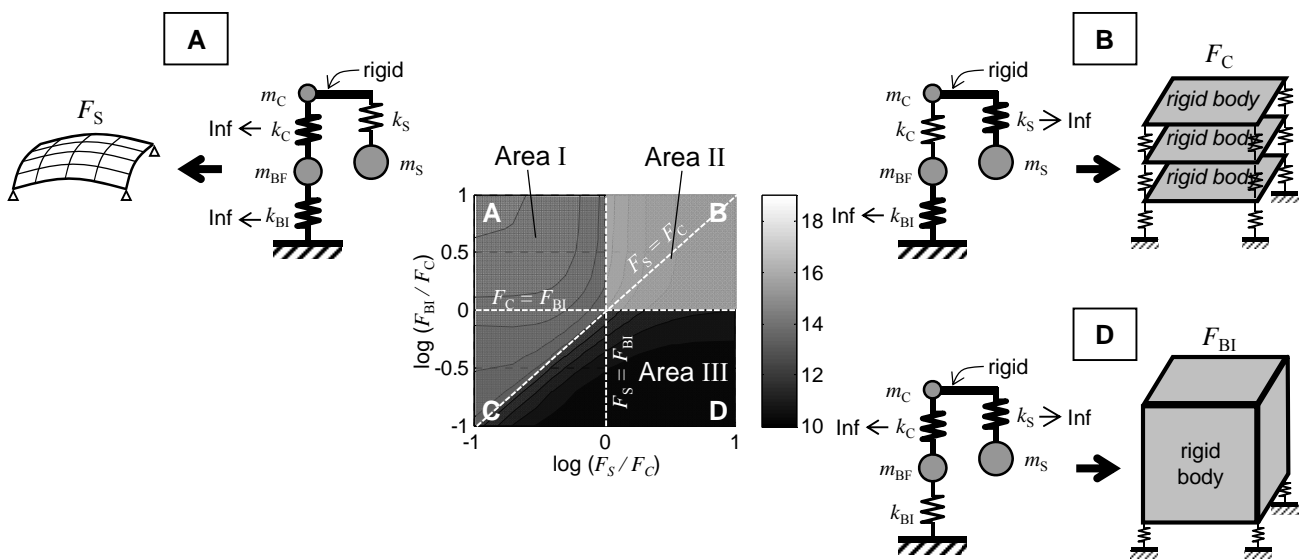


Figure 8-11 Condition description of 3DOF model results

### Categorized patterns of response amplification contours at the top center

Figures 8-11 show the vertical response amplifications for the top center for all analyzed cases. For all cases, the minimum vertical floor acceleration amplification response at the top center is recorded in the area around D, where the base isolation successfully isolates the superstructure in the vertical direction. The maximum responses, however, are recorded at different locations, which can be categorized into three patterns.

- (i) One is that the peak appears on the line of  $F_{BI} = F_S < F_C$ , which is applied to Figure 8-11 (a-1), (a-2) and (a-3).
- (ii) Another is that the closer to the upper left (point A), the larger the response amplification, which is applied to Figure 8-11 (c-1), (c-2), (d-1) and (d-2).
- (iii) The last is that the peak of (ii) is shifted right-downward along  $F_S = F_C$ , which is applied to Figure 8-11(c-3) and (d-3).

These differences are determined by the relationship between the initial response amplitude generated by the 3DOF model, which is a function of mass allocation among three DOFs, and the

magnitude of response amplification factors of  $\alpha_C$  and  $\alpha_S$ . Figure 8-12 shows the vertical response amplification at the slab DOF of the 3DOF model before and after amplification measures ( $\phi_S$  for before amplification measures, and  $\phi_S'$  for after amplification measures in Eqs. (8-4) to (8-6)). Figure 8-12 (a-2) for Pattern (i), (c-2) for Pattern (ii), and (c-3) for Pattern (iii) are selected for examination. The mass allocation ratios are also shown in the figures.

If a larger mass is present at the upper DOF, the response amplification at the slab DOF is reduced because the upper heavy mass works as if more restriction were added to the lower DOF, which can be seen for Pattern (ii) (Figure 8-12(c-2-2)) with the lowest vertical full scale response among the three examples. It shows the peaks along  $F_{BI} = F_S < F_C$ ,  $F_{BI} = F_C < F_S$  and  $F_C = F_S < F_{BI}$ , where two out of the three mode frequencies are the same and the other is larger than the two. Among the three peak lines,  $F_{BI} = F_S < F_C$  shows the largest amplification. Through the amplification process by  $\alpha_C$  and  $\alpha_S$ , however, Point A, where the slab has the smallest frequency, undergoes the largest response amplification, as shown in Figure 8-12 (c-2). This is because, among the three components, which are the base isolation layer, the columns, and the slab, the slab has the largest contribution to the response amplification magnification because  $\alpha_S$  is significantly large in a range of 1.3 and 1.72 compared to a range of 1.0 to 1.28 for assigned  $\alpha_C$ . In addition, the original response amplitudes of the peaks yielded by the 3DOF model are not large enough to remain as peaks after response amplification measures. This Pattern (ii) can be considered the most common case for conventional base-isolated buildings since the setting conditions are applicable for mid-rise and the slab is supported by reasonable sized beams.

On the other hand, if relatively large mass is allocated on the lower DOF, the response amplitude at the upper DOF is enhanced, which can be seen as the vertical full scale response is the largest for Pattern (i) (Figure 8-12(a-2-2)). When the base floor's mass is heavy, which is applicable to Pattern (i), the response amplitudes of the lines of  $F_{BI} = F_S < F_C$  and  $F_{BI} = F_C < F_S$  on the slab DOF become larger, as shown in Figure 8-12 (a-2-2). Between two lines,  $F_{BI} = F_S < F_C$  shows the larger peak of 13.0 to 13.5. The resulting pattern after response amplification measures continues to peak on line  $F_{BI} = F_S < F_C$ , as shown in Figure 8-12 (a-2). For Pattern (iii) of Figure 8-12 (c-3), it does not have a heavy base floor mass but a relatively large column mass of  $\gamma_S = 0.53$  for  $I / I_S = \text{infinity}$  compared to  $\gamma_S = 0.82$  for  $I / I_S = 18.0$  in Pattern (ii). Note that since  $\gamma_S$  represents the slab mass contribution ratio to the floor mass, column mass contribution becomes larger as  $\gamma_S$  becomes smaller. This also results in the moderate increase in the magnitude of the line  $F_C = F_S < F_{BI}$ . As a result, Figure 8-12 (c-3) shows that the peak has shifted toward along the line of  $F_C = F_S < F_{BI}$ .

Therefore, each pattern is applicable to the following conditions:

- Pattern (i): The mass of the base floor is larger than that of the superstructure ( $\gamma_{BF} \geq 1.0$ )
- Pattern (ii): The mass of the slab is the largest among three, which can be considered as the most common case.
- Pattern (iii): The mass of the column is relatively larger compared to that of the slab ( $\alpha_S$  is smaller, or the slab support is close to the fixed-supported condition.)

### Observation of vertical response amplification at top center

From Figure 8-13, the following observations are notable for the vertical response amplification at the top center.

- (1) As  $I / I_S$  increases from 1.0 to infinity, the maximum vertical floor response amplification also increases from 16 to 22 regardless of other conditions. This means that as the slab edge supporting condition approaches fixed support, the vertical floor response tends to be larger, because the slab response amplification factor  $\alpha_S$  becomes larger as the supporting condition approaches the fixed condition from 1.3 to 1.72.
- (2) Pattern (i) is applicable when  $\gamma_{BF}$  increases to larger than one. This indicates that a building with a heavy base floor relative to the superstructure, such as a steel building with a concrete base or low-rise buildings, is subject to a larger vertical floor response if the natural frequencies of a base isolation and a slab are close enough to each other in addition to which the slab is softer than columns. If a building has stiffer slabs than columns, the vertical floor response becomes smaller. However, such types of low-rise buildings have a high possibility to have softer slabs than columns.
- (3) Pattern (ii) is applicable when  $\gamma_{BF}$  decreases, and the slab is supported lightly or by common-sized beams ( $I / I_S = 1.0$  and 18.0). When the slab is supported tightly ( $I / I_S$  large enough to be considered as fixed supports), Pattern (iii) is applicable. This indicates that a building with a lighter base floor relative to the superstructure, which is commonly applicable to middle- to high-rise buildings, has the maximum vertical floor response when the building has very soft slabs relative to columns, and base isolation layer is stiff enough to be considered as a fixed-base. When the restrained condition of the slab approaches the fixed condition, a building with stiffer base isolation layer and slab relatively softer than columns, whose natural frequency ratio is between 0.3 and 0.8, is subject to a larger maximum vertical floor response, compared with a building with an extremely soft slab. But those differences are small (20 and 22 for maximum response amplifications for respective cases).
- (4) The vertical floor response amplification tends to be mitigated for  $F_S > F_{BI}$  or  $F_S > F_C$ . If the base isolation layer is softer than the slab, or if the columns are softer than the slab, the vertical floor response is mitigated. In other words, when the slab is the softest among three components or the same as the other two, the building is subject to a larger vertical floor response.
- (5) The vertical floor response amplification decreases rapidly across the line of  $F_C = F_S < F_{BI}$  and  $F_{BI} = F_S > F_C$ . Because the contour lines on  $F_{BI} = F_S > F_C$  are more dense, the vertical floor response amplification is more sensitive to the condition of relative magnitude between  $F_{BI}$  and  $F_S$ . The response amplification is significantly changed for the range of  $0.5F_{BI} < F_S < 2.0F_{BI}$  for any conditions, which lines are drawn in Figure 8-13.
- (6) If the slab is lightly supported and the building has a heavier base floor (Figure 8-13(a-1) and (b-1)), the relation between the natural frequency of the slab and the columns becomes sensitive for the range of  $0.5F_C < F_S < 2.0F_C$ .

- (7) Because there is a high possibility that the response amplification is mitigated by the existence of higher modes when the natural frequency of the slab is the smallest (Area I), Pattern (i) may become more serious condition compared to Patterns (ii) and (iii).
- (8) The vertical floor response amplification is minimized when  $F_{BI}$  is the smallest among the three.

Basically, the softer a base isolation layer, the less the vertical floor acceleration response. This rule, however, cannot be applied to buildings with a heavy base floor relative to the superstructure. When the base isolation layer becomes the softest among three, the vertical floor amplification response becomes the smallest because the system performs as SDOF.

### **Observation of vertical response amplification at the base floor**

Figure 8-14 shows almost the same contours for all cases. This means that the response amplification at the base floor is determined only by the combinations of the natural frequencies, regardless of other conditions. The following findings are notable:

- (1) The maximum response amplification is recorded at the bottom right end, where the base isolation layer has the smallest natural frequency among three modes.
- (2) The minimum response amplification is recorded at the top side, where the natural frequency of the base isolation layer is maximized compared with that of the columns.
- (3) The relation between the natural frequency of the base isolation layer and the other two is sensitive in determining the response amplitude at the base floor as shown by the significantly dense contour lines of  $F_{BI} = F_S < F_C$  and  $F_{BI} = F_C < F_S$ .

Tendencies (1) and (2) are opposite to the response amplification at the top center, in which the minimum is recorded at the bottom right end while the maximum tends to be recorded at the top left end. This means that the response amplification at the base floor tends to become larger when the superstructure behaves as a rigid body (SDOF) with the soft base isolation layer, while it is mitigated when the system behaves as a fixed-base system with the stiff base isolation layer.

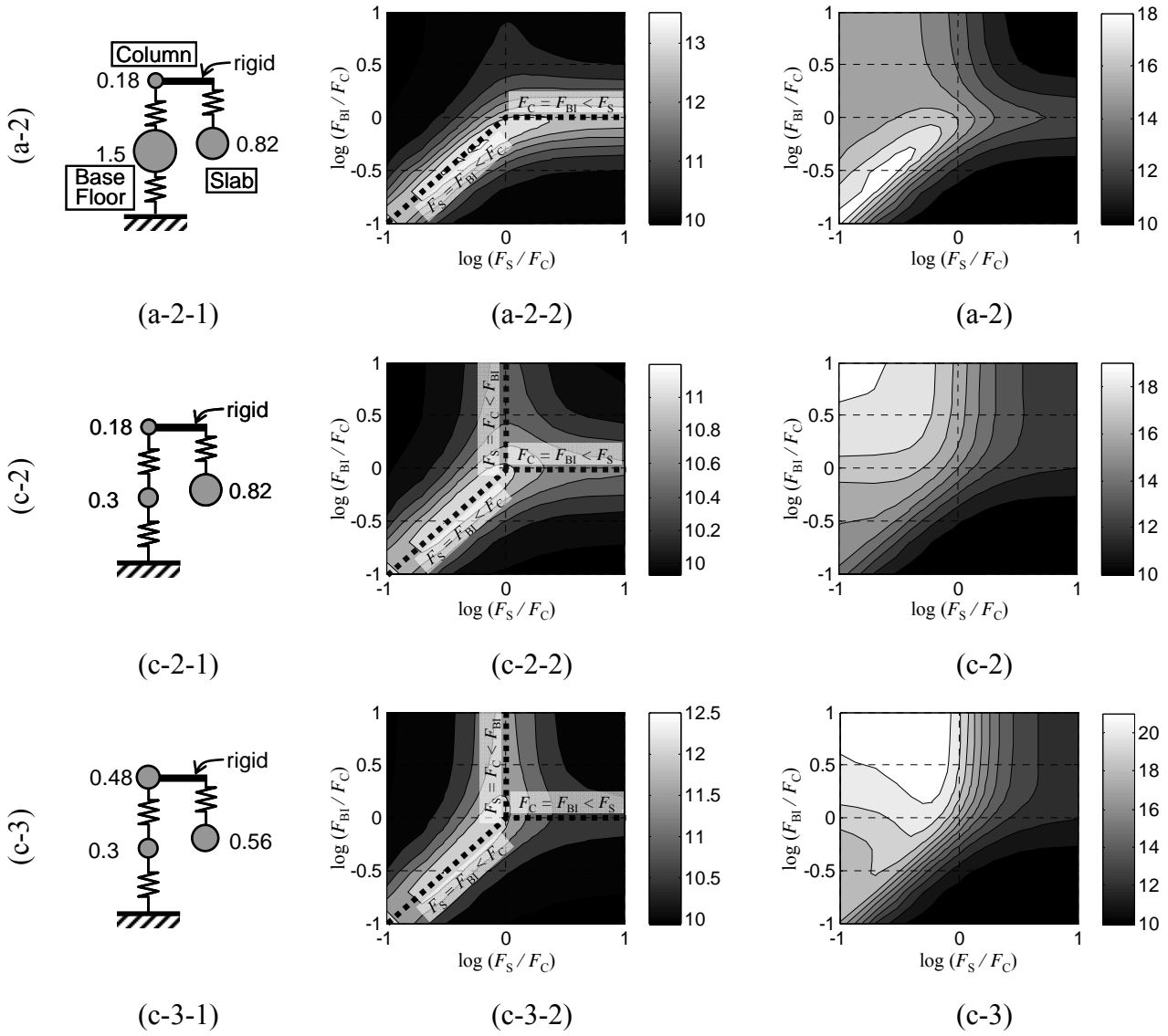
It is found that the magnitude of the natural frequency of the slab relative to other two (especially the base isolation layer) is a critical factor in determining the vertical floor response amplitude at the top center. For the base floor, the vertical response amplitude is not affected by the mass allocation ratios among DOFs nor slab supporting conditions but depends on the combinations of the natural frequencies. In summary,

The vertical floor response amplitude at the top floor tends to be larger when:

- (1) The natural frequencies of the slab and the base isolation layer are close to each other, which is applicable to a building with a relatively heavy base floor.
- (2) The natural frequency of the slab is the smallest among three, which is applicable to a building with a relatively light base floor. (This condition has high possibility that the response is

canceled by the higher modes effect.)

- (3) The vertical floor response amplitude at the top floor tends to be mitigated, when the natural frequency of the slab is not the smallest among three.
- (4) The vertical floor response amplitude at the base floor tends to become larger, when when the base isolation layer becomes softer, while it is mitigated when the base isolation layer becomes larger compared to the other two.



Mass distribution      Response amplitude at slab DOF      Slab response amplitude

Figure 8-12 Response amplification of a slab DOF before and after amplifications

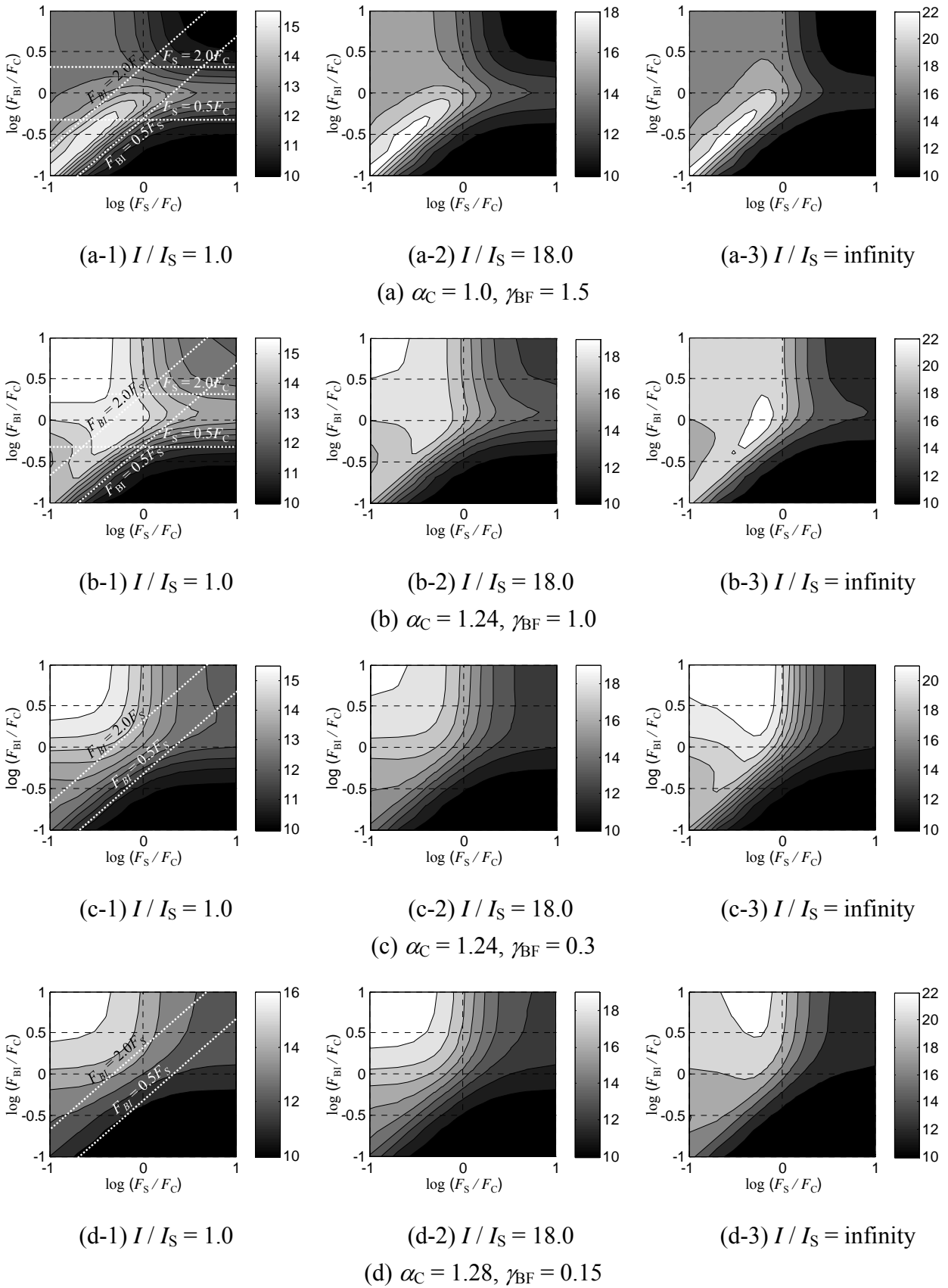


Figure 8-13 Vertical response amplification at the top center with respect to  $F_{BI} / F_C$  and  $F_S / F_C$



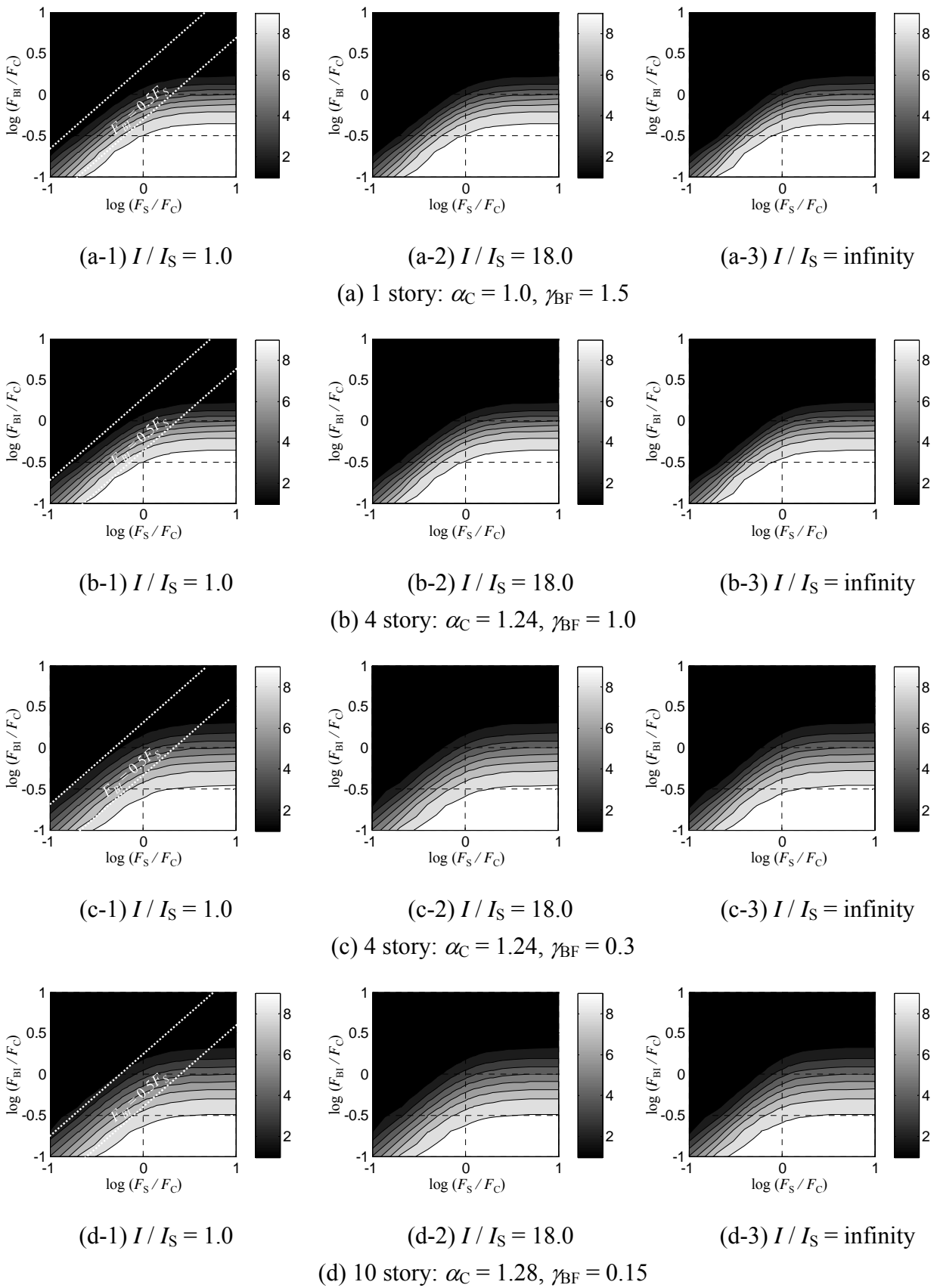


Figure 8-14 Vertical response amplification at the base floor with respect to  $F_{BI} / F_C$  and  $F_S / F_C$

### 8.5.3 First mode contribution

The contribution of the vertical first mode is examined in this subsection. In Chapter 2, it was found that the first mode may dominate for some base-isolated buildings while multiple modes may control other base-isolated buildings' responses in the vertical direction. Because it increases the demand on the axial force exerted on the base isolators, the first mode dominated response in the vertical direction is not preferable. This section examines which combination of natural frequencies of three modes (base isolation layer, columns, and slab) causes the increase in the axial force demand. Modal participating mass ratios of the first mode estimated by 3DOF model are calculated for several cases selected from Table 8-8, and are shown in Figure 8-15. Note that the response amplification factors do not affect the first mode contribution, while mass distribution among three DOFs influences the first mode contribution.

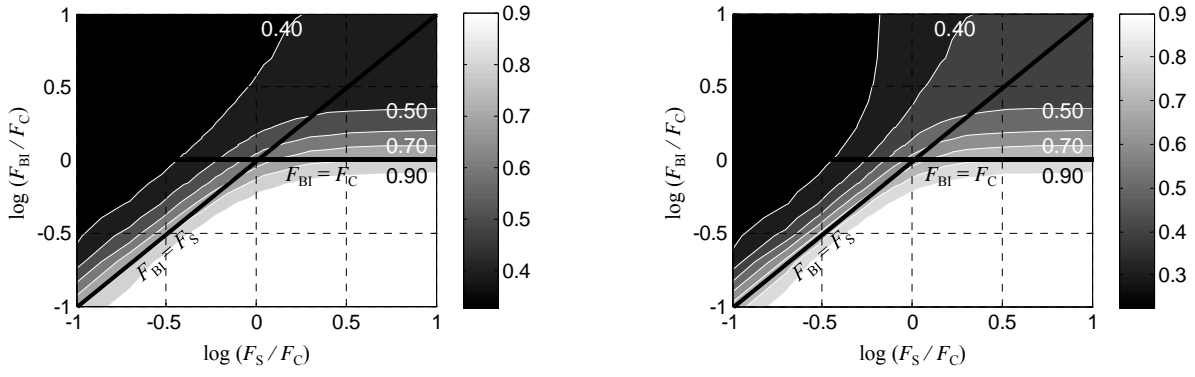
From the figures, the following findings are notable:

- (1) Basic contour distributions are similar in all cases. If the natural frequency of the slab,  $F_S$ , becomes smaller relative to the others, the modal participating mass ratio of the first mode becomes smaller (toward the top left end). On the other hand, the ratio increases as the the natural frequency of the base isolation layer,  $F_{BI}$ , becomes smaller (toward the bottom right end).
- (2) The first mode tends to dominate for larger ranges of  $F_S / F_C$  and  $F_{BI} / F_C$  as the number of stories increases (or the base floor mass ratio to the superstructure decreases). This is because the larger mass at the upper DOF enhances the first mode contribution. In other words, the existence of a larger mass at the base floor increases the contribution of higher modes when the natural frequency of the base isolation layer is not the smallest (Area I and II).
- (3) The difference in the supporting condition does not affect any change in contour in Area III. In other Areas (especially in Area I), however, the declining rate of the modal participating mass ratio becomes larger when the supporting condition becomes close to fixed-supported. Its declining ratio becomes steeper especially through the line of  $F_{BI} = F_S < F_C$ . This is also because of the existence of a relatively larger mass at the column DOF for the fixed-supported condition for the slab. This condition also enhances higher mode contribution, if the natural frequency of the column is not smaller than that of slab, which is applicable to Area I.
- (4) The modal participating mass ratio of the first mode becomes at least 0.80 in Area III for all cases in which the natural frequency of the base isolation layer is the smallest among three.
- (5) The modal participating mass ratio for  $\gamma_{BF} = 0.3$  (4 story, Figure 8-15(c)) remains 0.80 for  $F_{BI} < 1.5F_S$  and also  $F_{BI} < 1.5F_C$  for the slab supported by common-sized beams. It shifts to  $F_{BI} < 1.2F_S$  and also  $F_{BI} < 2.0F_C$  for fixed-supported slab.
- (6) For taller buildings and other cases in which the base floor mass is significantly smaller than the superstructure mass, the modal participating mass ratio remains at least 0.80 for  $F_{BI} < 1.5F_S$  and imposes no limitation on the relation of  $F_{BI}$  and  $F_C$  (Figure 8-15(d)). This means the vertical responses of taller buildings tends to be dominated by the first mode except when the building

has very soft slab.

- (7) The contour lines are more dense along the  $F_{BI} = F_S$  (especially  $1.0 < F_{BI} / F_S < 2.0$ ) so that the relation between the natural frequency of the slab and the base isolation layer is sensitive to the magnitude of the modal participating mass ratio of the first mode. Large shifts may be observed especially when the slab is tightly supported so as to be regarded as fixed supported. The reduction of the ratio of  $F_S$  to  $F_{BI}$  from 1.0 to 0.5 may result in 30% reduction in the mass ratio even for models with smaller base floor mass, (d-3) in Figure 8-15 as an example.
- (8) The four-story full-scale base-isolated specimen (HDRB), whose response characteristics were described in Chapters 5 had  $\gamma_{BF}$  of 0.63 and  $F_{BI} / F_S = 1.11$  to 1.33, and  $F_{BI} / F_C = 0.55$  (where the natural frequency of the base isolation layer  $F_{BI}$  is 18.6 Hz, that of the columns  $F_C$  is 33.9 Hz and that of the slab  $F_S$  is 13.9 to 16.8 Hz (Chapter 5)). Since the slabs are supported by four-edge columns and shear walls in the middle spans, the slab can be considered as simply supported. Therefore, the specimen condition falls between Figure 8-15 (a-3) and (c-3). From figures, the modal participating mass ratio of the first mode is estimated about 0.8, which indicates that the response is dominated by the first mode. The analytical model in Chapter 5 yielded 0.78 as the modal participating mass ratio of the first mode, and its response was actually dominated by the first mode when the vertical ground motions were input.

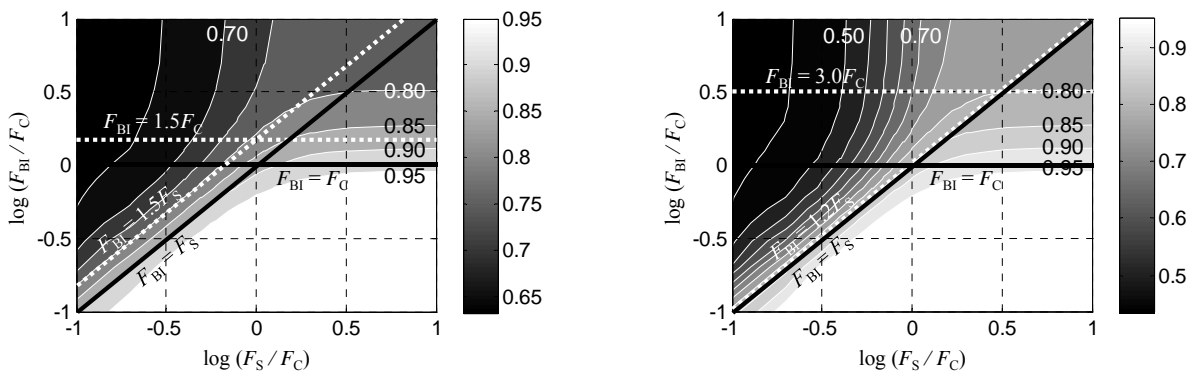
In summary, the modal participating mass ratio becomes at least 0.80 if the natural frequency of the base isolation layer is the smallest or equal to one of the other two. For mid- to high-rise buildings, this condition tends to be relaxed so that the vertical response of the building with the base isolation layer of the higher natural frequency than that of the superstructure may be dominated by the first mode. It is also found that the relation between the natural frequency of the slab and the base isolation layer is sensitive in determining the magnitude of the modal participating mass ratio of the first mode, which is the same as the floor response amplification.



(a-2)  $I / I_S = 18.0$

(a-3)  $I / I_S = \text{infinity}$

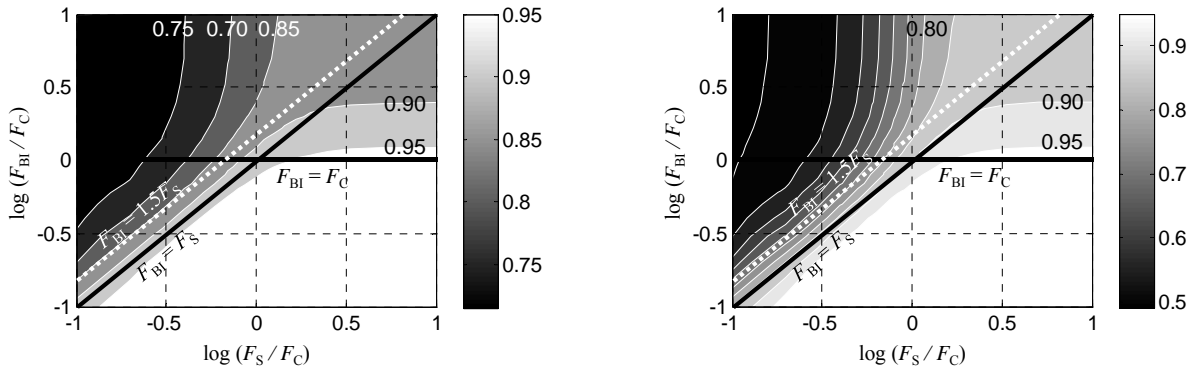
(a) 1 story:  $\alpha_C = 1.0, \gamma_{BF} = 1.5$



(c-2)  $I / I_S = 18.0$

(c-3)  $I / I_S = \text{infinity}$

(c) 4 story:  $\alpha_C = 1.24, \gamma_{BF} = 0.3$



(d-2)  $I / I_S = 18.0$

(d-3)  $I / I_S = \text{infinity}$

(d) 10 story:  $\alpha_C = 1.28, \gamma_{BF} = 0.15$

Figure 8-15 Modal participating mass ratios of the first mode (following the same captions as Figure 8-10)

## 8.6. Summary and conclusions of Chapter 8

This chapter examines how major components of the base-isolated building would control the vertical dynamic response characteristics of the entire system. The 3DOF lump mass model is proposed, as a convenient mode for examining the relationship between the combinations of natural frequencies of the three major modes in the vertical direction (the base isolation layer, the columns and the slab) and the vertical response amplification. Parametric studies are conducted to observe the first mode response amplifications and its modal participation mass ratio for base-isolated buildings. Major findings obtained in this chapter are summarized as follows:

- (1) Proposed 3DOF lump mass model can sufficiently represent the vertical floor responses of base-isolated buildings for the first mode, except for the case with extremely soft slabs. If the model has the softer slab, the higher modes' contribution becomes larger and tends to be closer to the first mode, resulting in cancel the first mode response amplitude. The modal participating mass ratio of the first mode is also represented sufficiently by 3DOF model.
- (2) When the slab supporting condition becomes closer to fixed support, the vertical floor response at the top floor center tends to be larger because the slab response amplification factor  $\alpha_S$  becomes larger as the supporting condition becomes closer to the fixed from 1.3 to 1.72.
- (3) The vertical floor response at the top floor center tends to be larger for two distinctive conditions: when the slab is softest among three major components for the buildings with relatively light base floor, and when the natural frequencies of the slab and the base isolation layer are close to each other for buildings with heavy base floors, or for the low-rise buildings. The condition for the former case, however, has high possibility that the floor response will be lessened because higher mode effect increases.
- (4) It is found the magnitude of the natural frequency of the slab relative to other two is a key factor in determining the vertical floor response amplitude at the top floor center, and that the relation between the natural frequencies of the slab and the base isolation layer is sensitive in determining the response amplitude, especially for the range of  $0.5F_{BI} < F_S < 2.0F_{BI}$ . If the slab is lightly supported and the building has a heavier base floor, the relation between the natural frequency of the slab and the column also becomes sensitive in the range of  $0.5F_C < F_S < 2.0F_C$ . In other words, the response amplitude can be controlled by a moderate change in the relative magnitude of the natural frequencies of three modes in these ranges.
- (5) The vertical response amplitude at the base floor is independent of the mass allocation ratios among DOFs and slab supporting conditions but depends on the combinations of the natural frequencies; it becomes larger when the base isolation layer becomes softer, and it is mitigated when the base isolation layer becomes larger compared to other two.
- (6) The modal participating mass ratio becomes at least 0.8 if the natural frequency of the base isolation layer is the smallest or equal to one of other two. For the mid- to high-rise building, the first mode dominates the vertical response except for the case with a very soft slab ( $F_S < 1.5F_{BI}$ ). This means that the first mode may dominate the vertical response even though the

natural frequency of the base isolation layer is larger than that of the superstructure.

- (7) The relation between the natural frequencies of the slab and the base isolation layer is sensitive to the modal participating mass ratio of the first mode, especially for the range of  $0.5F_{BI} < F_S < 2.0F_{BI}$ . In other words, the first mode contribution ratio can be controlled by a moderate change in the relative magnitude of the natural frequencies of three modes in this range.

## REFERENCES

- [8-1] Masahiko Higashino and Shin Okamoto, Response Control and Seismic Isolation of Buildings, Taylor & Francis, 2006.
- [8-2] Morishita T., Sito Y., Yoshida T., and Ryujin H., Properties of Vibration through Earthquake Observation on a Base Isolated Building, Summaries of Technical Papers of Annual Meeting, AIJ, Hokkaido, paper ID: 21147, 2004 (Japanese).
- [8-3] Shinohara T., Uru M., Nakayama K., and Kondo T., Study on the Response Characteristics of Base-Isolated Structures for Vertical Earthquake Motion Part-1 and 2, Proceedings of the Annual Conference on Architectural Institute of Japan, September 1998, paper ID:21320 – 21321 (Japanese).
- [8-4] Kondo T., Uru M., Nakayama K., and Hashimura H., Study on the Response Characteristics of Base-Isolated Structures for Vertical Earthquake Motion Part-3 to 5, Proceedings of the Annual Conference on Architectural Institute of Japan, September 1999, paper ID:21322 – 21324 (Japanese).
- [8-5] Kondo T., Uru M., and Hashimura H., Study on the Response Characteristics of Base-Isolated Structures for Vertical Earthquake Motion Part-6 and 8, Proceedings of the Annual Conference on Architectural Institute of Japan, September 2000, paper ID:21267 – 21269 (Japanese).
- [8-6] Nobata A., Teramura A., and Yasui Y., Vertical Resposne Characteristic of Base-Isolated Building Based on Observed Earthquake Records, Report of Obayashi Corporation Technical Research Institute, No.56, 1998, pp.23-28.
- [8-7] Peng Pan, Safety and Functionality of Base-isolated Building Structures Subjected to Vertical Ground Motions, Ph.D. dissertation, Kyoto University, 2004
- [8-8] Yamanaka Reiko, Hisano M., and Tanaka K., Vertical Response Property of High-rise Buildings Based on Observed Earthquake Response Records (Part 1 and 2), Proceedings of the Annual Conference on Architectural Institute of Japan, September 1994, paper ID:2329 and 2330 (Japanese).
- [8-9] Yuji Tanaka, Nobuo Fukuwa, Jun Tobita, and Masafumi Mori, Present Situation of Isolation Buildings in Japan Based on Establishing a Database on Technical Evaluation Sheet, 13th symposium of Japan Earthquake Institute, Tsukuba, 2010.11.
- [8-10] A. J. Papazoglou and A. S. Elnashai, Analytical and field evidence of the damaging effect of vertical earthquake ground motion, Earthquake Engineering and Structural Dynamics, Vol. 25, pp.1109-1137, 1996.

- [8-11] Bozorgnia Yousef, Stephen A. Mahin, and Gerald Brady, Vertical Response of Twelve Structures Recorded during the Northridge Earthquake, *Earthquake Spectra*, Vol. 14, No. 3, August 1998, pp. 411-432.
- [8-12] AIJ Standard for Structural Calculation of Reinforced Concrete Structures -Based on Allowable Stress Concept-, revised 2010, AIJ
- [8-13] Handbook for mechanical Engineering, Japan Society of Mechanical Engineers, 12.1998
- [8-14] Osami Kawakami, Free Vibration of Square Plate with Multiple Fixed-Points on Edges, Vol.58, No.553, Paper No.92-0038, 9.1992.
- [8-15] Chopra AK, *Dynamics of Structures: Theory and Applications to Earthquake Engineering*; 3<sup>rd</sup> edn, Prentice Hall: New Jersey, 2007.
- [8-16] Clough RW and Penzien J., *Dynamics of Structures*; McGraw-Hill, Inc., 1975.

## CHAPTER 9

### SUMMARY AND CONCLUSIONS

In Japan, the seismic isolation system has been flourished especially after Kobe earthquake, 1995. More than 100 isolated buildings has been newly constructed every year, and the number has reached 2,500 by 2010 [9-1]. This prevalence is conspicuous since the number of the application has remained only about 100 in the U.S. [9-2]. This popularity of the isolation system in Japan has well represented that high motivation of Japanese people to invest money on their assets to ensure not only the structural safety but also the buissness continuity during and after earthquakes, and also that the system has been well recognized by people as the effective method to realize their high-level demands. The medical facility is one of the facilities that are mostly required to maintain their service during and after earthquakes. Based on the past experiences in which function as a medical facility were disturbed not only because the structural damages but also the iterior damages, many newly-constructed hospitals has been adopted the isolation system. Currently, about 300 hospitals in Japan are isolated [9-1]. Consequently, the society expectation on the performance of the isolated building has been significantly grown. However, the isolation system has some concerns about the performance against some types of ground motions, which are the long-period pulse, the long-period and long-duration ground motion, and the vertical ground motion generated by the near-fault ground motions. Since major metropolitan areas, where the large number of isolated buildings are concentrated, has high possibility to encounter these types of ground motion, it is urgent task to find the intrinsic factors to deteriorate their performance before they are revealed by actual damages.

This dissertation provides quantitative damage observations of the base-isolated medical facility about the structural and interior performance against the long-period and long-duration ground motion and the vertical ground motion. The full-scale shaking table test of the base-isolated medical facility was conducted, and some supplemental shaking table test was also conducted separately for some medical appliances. In addition, the vertical dynamic response characteristics of the base-isolated building were generalized with respect to the structural configurations, which help to capture with which combinations of stiffness and mass distribution among major structural components result in larger floor responses. The dissertation consists of nine chapters. Except Chapter 1 for introduction, Chapter 2 for reviewing the previous research and Chapter 9 for summary and conclusion, five out of the remaining six chapters deal with the full-scale shaking table test of the base-isolated medical facility. Chapter 3 explains the setting of shaking table test,



Chapter 4 and 5 discusses the structural responses in the horizontal and vertical direction, respectively, and Chapter 6 and 7 discusses the interior performance of the medical facility for the horizontal and vertical motions. Chapter 8 generalizes the vertical dynamic response characteristics of the base-isolated buildings with respect to various combinations of major components. The major contents and discussions made in each chapter are as follows:

## **Review of previous research**

The present state of the base isolation application and past research related to this dissertation topics were summarized for (1) design practices and application of isolation systems in Japan; (2) the characteristics of two types of ground motions that may degrade the performance of base-isolated buildings, that is the long-period and long-duration ground motion and the vertical ground motion, (3) recorded responses of base-isolated buildings from past earthquakes, (4) vertical response characteristics of base-isolated buildings estimated based on past earthquake records, and (5) reported damages of hospitals observed from past earthquakes.

- (1) Earthquake records of base-isolated buildings show their effectiveness at reducing horizontal acceleration responses. However, their efficiency may deteriorate for the long-period and long-duration ground motion and for the vertical ground motion.
- (2) The vertical first natural frequencies ranged from 5 to 16 Hz for low- to mid-rise buildings including the reinforced concrete and steel braced frame as the superstructure. It ranges from 11 to 16 Hz for the common reinforced buildings with rubber bearings, while it is reduced to 5 to 10 Hz when the superstructure had longer spans, was constructed using the steel frame, or had a softer base isolation layer. Their range is overlapped by the plateau range (5 to 10 Hz) of the vertical response spectrum.
- (3) Damping ratios of the first mode in the vertical direction were estimated as 1% to 2%, if the soil effect was not considered. It increased to 20% once the soil contribution was considered.
- (4) Vertical response of base-isolated buildings may be dominated by a single mode while multiple modes may dominate if the building has longer spans.
- (5) There is little research on the contribution to vertical response amplification by floors and vertical floor accelerations, factors which is thought to be related to functionality.
- (6) No significant damage has been reported for base-isolated buildings from the past earthquakes.

## **Full-scale shaking table test of base-isolated medical facility**

Full-scale shaking table tests were conducted on the E-Defense shaking table to examine a base-isolated system not only for the structural performance but also for the operability and functionality during strong earthquakes. A specimen was designed as a medical facility, in which major nonstructural components and plumbing system were installed, and rooms were furnished and equipped with medical equipment to simulate an actual medical facility. The series of shaking

table tests were divided into two parts: one was the series of shaking conducted from December 2008 to January 2009, and the other was the series of shaking in the fall of 2010. The purpose of the first series of test (designated Test I) was to observe the performance of a base-isolated medical facility against large earthquakes. Equipment inside the specimen was arranged based on the current medical practices. The second series of tests (designated Test II) aimed at the verification of the capability of various countermeasures to improve the performance. The performance of a base-isolated system against vertical motions was also tested in Test II. The same superstructure and base isolation systems were used for both Tests I and II. The room arrangement of medical facilities and the layout of furniture and medical appliances in each room were also basically the same as Tests I and II. A fixed-base system was also tested using the same superstructure to facilitate the comparison between the base-isolated and fixed-base systems.

### **Structural responses of the base-isolated system for horizontal motions**

Horizontal structural responses of the base-isolated system were observed from the full-scaled shaking table tests. The responses of two types of structural systems (the base-isolated system and the base-fixed system) for two types of ground motions (near-fault ground motion and long-period and long-duration ground motion) are compared. In addition, the performance of two different base-isolation systems (NRB+U and HDRB) are also compared. Major findings are summarized as follows:

- (1) The performance of the base isolation systems was satisfactory for both the near-fault and long-period and long-duration ground motions. The maximum horizontal displacements of the base isolation layer were twice as large in the long-period and long-duration ground motion (486 mm in the long-period ground motion named Sannomaru and 230 mm in the near fault ground motion named JMA Kobe). Also notable was a significant difference in cumulative horizontal displacement, i.e., 46 m in Sannomaru and less than 5 m in JMA Kobe. This large difference (by a factor of ten) was due to a combined effect of resonance of the base-isolated system with Sannomaru and the long duration of 300 s in Sannomaru. Despite such large displacements, the base-isolated system remained stable, and the U-shaped steel damper eventually sustained 81 m of cumulative displacement without any significant stiffness degradation.
- (2) In the base-isolated system (NRB+U) when subjected to JMA Kobe, the floor accelerations were significantly reduced; the maximum floor acceleration ( $2.61 \text{ m/s}^2$ ) was 0.38 times the input maximum acceleration ( $6.80 \text{ m/s}^2$ ), and 0.13 times the maximum floor acceleration recorded in the counterpart fixed-base system ( $19.7 \text{ m/s}^2$ ). The maximum floor velocity was also smaller in the base-isolated system (0.62 m/s) than was in the fixed-base system (1.00 m/s), but the difference was not as large as the difference of the maximum floor acceleration.
- (3) In the base-isolated system when subjected to Sannomaru, the maximum floor acceleration was not reduced; instead, it ( $2.30 \text{ m/s}^2$ ) increased to 1.1 times the input maximum acceleration ( $2.10$

m/s<sup>2</sup>). The corresponding fixed-base system sustained the roof maximum acceleration of 2.52 m/s<sup>2</sup>, which was still larger than that obtained from the base-isolated system, but the disparity (1.1) was much smaller than the case for JMA Kobe (a disparity of 7.5). Notable was the large floor velocity observed in the base-isolated system, i.e., 1.0 m/s in the maximum floor velocity, which was twice the maximum floor velocity observed in the fixed-base system (0.5 m/s).

- (4) The maximum displacements of the base isolation layer were similar between NRB+U (223 mm) and HDRB (201 mm) for JMA Kobe, even though the estimated horizontal secant stiffnesses and damping ratios of HDRB were larger than NRB+U. Their differences in response characteristics were clearly represented in the long-period and long-duration ground motion; the maximum became 409 mm for NRB+U and 319 mm for HDRB for Sannomaru.
- (5) When two base-isolated systems with the different isolation systems but with the relatively close natural periods (2.56 s for NRB+U and 2.41 s for HDRB with respect to the secant stiffness estimated for the bearing displacement of 300 mm) are compared, the acceleration responses and story displacements of the superstructure were stable regardless of the differences in the displacement amplitude and the way of dissipating energy by the base isolation layer, while the velocity responses were affected by the displacement amplitude of the base isolation layer.
- (6) The stiffness reduction by one quarter of the superstructure had little effect on the performance stability of the base-isolated systems. Floor accelerations and velocities remained unchanged while story displacements were increased by four times from Test I to Test II. For the fixed-base system, the significant increases in velocities by 1.3 and 1.6 times for the X and Y-axis from Test I were observed because of the elongation of the natural period by more than 1.5 in the superstructure. Floor accelerations of the fixed-base system remained relatively unchanged because the major components had been already yielded in the test of the fixed-base system of Test I.

### **Structural responses of the base-isolated system for vertical motions**

The vertical dynamic response characteristics of the base-isolated system were observed, comparing with those of the base-fixed system based on the full-scaled shaking table test results. While the natural frequency ratio of the superstructure to the base isolation layer, which is calculated with the rigid-body superstructure assumption, was more than 7 in the horizontal direction, it was 0.7 ~ 0.8 in the vertical direction. Therefore, the structural response of the base-isolated system was quite difference in the vertical direction. The major findings obtained in this chapter are as follows:

- (1) Significantly larger vertical floor acceleration responses were recorded compared to the horizontal acceleration responses when the full-scaled base-isolated system was tested for three-directional ground motions. Input accelerations were amplified by almost 5 times for JMA Kobe XYZ, resulting in the disparity in floor acceleration responses at the roof center between vertical and horizontal directions of 6.5:1.

- (2) Some modes spaced closely for the fixed-base system, while the first mode was well separated by inserting the base isolation layer.
- (3) The damping ratio for the first mode of the base-isolated system was estimated as lower than 3 %, while that of the superstructure was 4 ~ 6%. The main factor which caused the smaller damping ratio of for base-isolated system may be less contribution from the base isolation layer to the damping in the vertical direction. The damping ratio increased up to 8 % when the acceleration response amplitude became larger.
- (4) The base-isolated system had relatively uniform response amplitudes from the bottom to the top floors, which characterized the response mode of the base-isolated system against the inverted-triangle response mode of the fixed-base system. This is because the response amplifications were concentrated into the soft base isolation layer as if there were additional several stories inserted below the superstructure. This characteristic was observed both for a white noise wave input and also for ground motion inputs.
- (5) The floor accelerations for JMA Kobe Z (only the vertical motion) recorded for the base-isolated system were larger at almost all measurement points than the fixed-base system. When JMA Kobe Z was input to both systems, the input amplitudes at the dominant response frequency for both systems were ideally close to each other. The results show clearly that the vertical floor acceleration response of the base-isolated system tended to be larger than that of the fixed-base system because (1) it had less damping ratio for the first mode in the vertical direction, and (2) vertical response was dominated by a certain mode while it was distributed among a few modes for the fixed-base system.
- (6) The response amplifications by the base isolation layer and the columns ranged between 1.0 and 1.5 for the base-isolated systems, while the range of the column response amplifications increased to 1.0 to 2.0 for the fixed-base system. The response amplification range of the base isolation layer was fairly close to the range of 1.0 to 2.0 mentioned by Nobata et.al. [9-3], which was observed based on the earthquake records with PGA of less than  $0.5 \text{ m/s}^2$  for one to six-stories reinforced concrete base-isolated buildings. When the vertical response was resonated, the column response amplification may increase to 3 (HDRB for El Centro XYZ).
- (7) The response amplifications by the slabs ranged from 1.5 to 3.0 for the base-isolated system, while it decreased to 1.5 to 2.0 for the fixed-base system. For the base-isolated systems, the response amplifications increased as the amplitude of the input ground motion at the first mode response increases. On the other hand, the response amplifications of the fixed-base system are relatively stable, and less dependency on the input amplitude can be observed. This is because the responses of the base-isolated systems were dominated by the first mode, and was sensitive to the input amplitude around the first natural frequency, while some higher modes also contributed to that of the fixed-base system.
- (8) The axial force exerted onto the base isolator was found to be dominated by the first mode. Tension force occurred in the base isolators, when the maximum vertical floor acceleration of the superstructure reached 4 g. But the estimated maximum tension force was sufficiently below the linear limit tension stress of the rubbers. It was also notable that the contribution of

the rocking on the axial force was less than 30% even in the extreme case when the resonance occurred.

- (9) With the finite element model of the specimen, the natural frequency of the superstructure was found to be about 12.1 Hz (estimated for the superstructure restrained at the top of four isolators), in which the natural frequency of the columns was 33.9 Hz, and those of the slabs were 13.9 to 15.1 Hz. On the other hand, the natural frequency of the base isolation layer is estimated as 18.6 Hz for HDRB, which is about 92 % of the natural frequency obtained by the design values of 20.3 Hz with the condition of the rigid-body superstructure.
- (10) Finite element analysis showed that the upper few modes shared the same slab mode. Because the natural frequency of the slab was sufficiently smaller than that of the column by less than half, those first few modes tend to be controlled by the slab mode, resulting in closely spaced higher modes to the first mode for the fixed-base system. By inserting the base isolation layer, only the first mode was independent from others. The modal participating mass ratio of the first mode was increased significantly from 40 to 78 % by inserting the base isolation layer at the bottom of the superstructure.
- (11) The conditions of a dominant single mode for the base-isolated system has disadvantage compared to the fixed-base system because the distribution of the modal contributions lead the mitigation of the maximum response. Note that this independence of the first mode was realized even with the base isolation layer, whose natural frequency (18.6 Hz) was larger than that of the superstructure (estimated as 12.1 Hz).

## **Medical equipment behavior for horizontal motions**

The effect of horizontal floor responses on equipment installed to the base-isolated medical facility was observed from the full-scaled shaking table tests. Notable findings are summarized as follows:

- (1) Even when the fixed-base system encountered JMA Kobe, almost no damage occurred in plumbing systems, sprinklers, and suspended ceilings, which had major damage reported after major earthquakes, which were installed following current practice.
- (2) It was reconfirmed that very many furniture items and medical equipment were mobile, meaning that they were supported by casters to make them as mobile as possible to travel between various places in the medical facility.
- (3) It is notable that serious movement of and according damage to the furniture items and medical equipment would occur in two distinctively different conditions, one in fixed-base systems when subjected to near fault ground motions, and the other in base-isolated systems when subjected to long-period ground motions. In the former case, the pulsive response of equipment and its contents due to large floor acceleration was the primary factor that caused damage, while the larger displacement and velocity of sliding equipment became the main reason that the function of the medical facility deteriorated, because most of items were supported by casters.

- (4) The mobility of items supported by casters caused large movement in such items and equipment for both the fixed-base and base-isolated systems and for both the near-fault and long-period ground motions. In the fixed-base system, they moved 0.5 to 1.0 m both in JMA Kobe and Sannomaru. In the base-isolated system, they moved 0.5 m to 1.0 m in JMA Kobe and most notably over 3 m in Sannomaru. Due to such large movement, many piece of equipment collided with each other or against the surrounding walls, causing damage and serious disorder.
- (5) Such wild movement was recognized as far beyond the expectations of medical doctors, people working in hospitals, and those involved in hospital design and operation. Since the test, they have been seriously discussing way to reduce such damage. Locking the casters is an easy solution, but nurses who work around the beds strongly complain about the difficulties of locking them all the time under extremely busy schedules.
- (6) Increasing the degree of fixation of equipment such as locking casters is the best solution to improve the performance of base-isolated medical facilities. On the other hand, such measurement has a countereffect especially for equipment with high aspect ratios and for contents stored in equipment for the fixed-base facilities. It is better to release lock to avoid toppling.

### **Medical equipment behavior for vertical motions**

The effect of vertical floor accelerations on equipment installed to the base-isolated medical facility was observed from the full-scaled shaking table tests. The dynamic response characteristics of some appliances in the vertical direction are examined by a supplemental shaking table test. Notable findings obtained in this chapter are summarized as follows:

- (1) Vertical floor accelerations were amplified further within the appliance. Up to about 1 g as the vertical floor acceleration, no clear damage was observed. Once it exceeded 1 g, some notable damaged were observed: intensive responses occurred mainly for items placed on furniture or equipment, such as the monitor on the ceiling pendant, the mannequin on the operating table, and bottles on the shelves. For the vertical floor acceleration of 3 g, most of equipment themselves jumped.
- (2) Items with eccentricity in the vertical direction responded more severely than other well-proportioned items.
- (3) Any vertical motions did not cause malfunction of the equipment tested in the operated condition (dialyzers, and servers).
- (4) It is found that the range of natural frequencies in the horizontal direction (3 to 7.5 Hz) happened to be close to the range of natural frequencies of low-rise fixed-base buildings. This indicates that the response amplitude of equipment tends to increase for fixed-base buildings if they are fixed to the floor, while their response amplifications are expected to become smaller for base-isolated buildings. A damping ratio of 5 % may be sufficient to adopt for the horizontal response of the equipment.
- (5) Equipment has the broad vertical natural frequencies of 5 to 28 Hz. If equipment (except beds)

was well proportional, the vertical natural frequency became larger than 20 Hz. The natural frequency became lower for equipment with the vertical eccentricity (the autologous blood transfusion machine of 17 Hz, and the incubator of 13 Hz). Beds with mattress tended to have even lower vertical natural frequencies, 10 Hz for the operating table and 5 Hz for the patient bed. The damping ratio in the vertical direction of equipment was at least 5 %. Equipment with eccentricity had smaller of about 3 %. Beds tended to have larger damping ratio.

- (6) Since the main body of the operating table is much stiffer than the mattress, the response of the mannequin on the top is controlled by a SDOF of the mattress as a spring. A minor change is that the response amplitude remains one for higher frequency range instead of converging to zero. A damping ratio of 20 % is sufficient to the vertical response of the mannequin on the operating table. The dependency on the intensity of the input wave was little.
- (7) Since the main frame of the patient bed has a lower natural frequency, flexibility of the bed is to be considered in addition to the flexibility of the mattress. For the frequency range higher than its dominant natural frequencies up to 11 Hz, the input acceleration to the patient was mitigated through the patient bed. A first mode damping ratio of 10 % is sufficient for larger earthquakes, and first natural frequency may be varied about 20 % not only due to the intensity of the input wave but also due to the height of the bed.
- (8) Once the acceleration response of an item exceeded 1g, jump occurred accompanied by dislocation or falling off in a severe case. Because the jumping height of the item is related to the relative velocity, the height tended to increase when an input motion to the item was dominated by a lower frequency range with a larger velocity. Increasing in jumping height also increases the dislocation distance, and the possibility to fall down from the bed.

To mitigate the physical damage due to the vertical responses, the following measures are recommended:

- (1) Free items placed on other equipment or furniture are recommended to be fixed, especially when it is placed on the ceiling pendant, which tends to have a lower natural frequency.
- (2) It is recommended to mitigate eccentricity with respect to the vertical direction.
- (3) To mitigate the physical damage, the acceleration and velocity have to be reduced. The first natural frequency of base-isolated buildings is better to avoid the peak range of the vertical motions of 5 to 10 Hz. In addition, because the increase in the floor velocity lead to increase the jumping height, the first natural frequency is better to set to be higher than at least 10 Hz. The vertical first natural frequency of larger than 10 Hz is considered as a realistic target since the natural frequency of base-isolated buildings ranged from 11 to 16 Hz if the superstructure was normal-sized reinforced concrete structure (not steel structure or building with longer spans) (Chapter 2). Lower vertical natural frequency is also effective as long as it ensure vertical floor acceleration responses to remained securely less than 1 g. This condition can be realized by adopting the vertical isolation system.

## Vertical Dynamic dynamic response characteristics of base-isolated buildings

The vertical floor responses of base-isolated buildings are examined for various combinations of mass and stiffness distributions among major structural components, and examining how those major components would control the vertical response characteristics of the entire system. The 3DOF lump mass model is proposed, whose model is convenient to examine the relationship between the combinations of natural frequencies of the three major modes in the vertical direction (the base isolation layer, the columns and the slab) and the corresponding vertical dynamic responses. The contributions of three modes were expressed by the natural frequency of the base isolation layer  $F_{BI}$ , columns  $F_C$ , and slab  $F_S$ . Parametric studies are conducted to observe the first mode response amplifications and its modal participation mass ratio for base-isolated buildings. Major findings obtained in this chapter are summarized as follows:

- (1) Proposed 3DOF lump mass model can sufficiently represent the vertical floor responses of base-isolated buildings for the first mode, except for the case with extremely soft slabs. If the model has the softer slab, the higher modes' contribution becomes larger and tends to be closer to the first mode, resulting in cancel the first mode response amplitude. The modal participating mass ratio of the first mode is also represented sufficiently by 3DOF model.
- (2) When the slab supporting condition becomes closer to fixed support, the vertical floor response at the top floor center tends to be larger because the slab response amplification factor  $\alpha_s$  becomes larger as the supporting condition becomes closer to the fixed from 1.3 to 1.72.
- (3) The vertical floor response at the top floor center tends to be larger for two distinctive conditions: when the slab is softest among three major components for the buildings with relatively light base floor, and when the natural frequencies of the slab and the base isolation layer are close to each other for buildings with heavy base floors, or for the low-rise buildings. The condition for the former case, however, has high possibility that the floor response will be lessened because higher mode effect increases.
- (4) It is found the magnitude of the natural frequency of the slab relative to other two is a key factor in determining the vertical floor response amplitude at the top floor center, and that the relation between the natural frequencies of the slab and the base isolation layer is sensitive in determining the response amplitude, especially for the range of  $0.5F_{BI} < F_S < 2.0F_{BI}$ . If the slab is lightly supported and the building has a heavier base floor, the relation between the natural frequency of the slab and the column also becomes sensitive in the range of  $0.5F_C < F_S < 2.0F_C$ . In other words, the response amplitude can be controlled by a moderate change in the relative magnitude of the natural frequencies of three modes in these ranges.
- (5) The vertical response amplitude at the base floor is independent of the mass allocation ratios among DOFs and slab supporting conditions but depends on the combinations of the natural frequencies; it becomes larger when the base isolation layer becomes softer, and it is mitigated when the base isolation layer becomes larger compared to other two.
- (6) The modal participating mass ratio becomes at least 0.8 if the natural frequency of the base



isolation layer is the smallest or equal to one of other two. For the mid- to high-rise building, the first mode dominates the vertical response except for the case with a very soft slab ( $F_S < 1.5F_{BI}$ ). This means that the first mode may dominate the vertical response even though the natural frequency of the base isolation layer is larger than that of the superstructure.

- (7) The relation between the natural frequencies of the slab and the base isolation layer is sensitive to the modal participating mass ratio of the first mode, especially for the range of  $0.5F_{BI} < F_S < 2.0F_{BI}$ . In other words, the first mode contribution ratio can be controlled by a moderate change in the relative magnitude of the natural frequencies of three modes in this range.

## REFERENCES

- [9-1] Tanaka Y., Fukuwa N., Tobita, J., and Mori M., Present Situation of Isolation Building in Japan Base on Establishing a Database on Technical Evaluation Sheet, The 13<sup>th</sup> Japan Earthquake Engineering Symposium, Japan Association for Earthquake Engineering, 2010, pp.569 – 576 (Japanese).
- [9-2] Becker T.C., Furukawa S., Mahin S.A. and Nakashima M., Comparison of US and Japanese Codes and Practices for Seismically Isolated Buildings, Structures Congress, Structural Engineering Institute of ASCE, 2010.
- [9-3] Nobata A., Teramura A., and Yasui Y., Vertical Resposne Characteristic of Base-Isolated Building Based on Observed Earthquake Records, Report of Obayashi Corporation Technical Research Institute, No.56, 1998, pp.23-28.



## ACKNOWLEDGMENT

私は、東北大学では卒業論文、修士論文ともに故山田大彦先生のご指導の下、弾性関節接合に関する研究に携わりました。2007年初夏からは、アメリカ合衆国ミシガン大学で約1年Goel先生のご指導の下、Performance-Based Plastic Design (PBPD)で設計された偏心K型ブレース架構の大地震下における性能信頼度に関する研究に従事しました。そして、2008年秋には、ミシガン大学に助教として赴任してこられたJason McCormick先生の紹介を通して中島先生を頼り、京都大学大学院博士後期課程に編入いたしました。本論文は、博士後期課程3年間で携わらせて頂きました、平成20年から22年にかけてE-ディフェンスで行われた免震病院の実大実験によって得られた知見をまとめたものであり、稚拙ではありますが、冗長性甚だしい私の学生生活の集大成となります。博士研究に没頭した最後の3年間のみならず、大学に進学してからこの11年間、多くの方のご指導、ご助力をいただきました。こんなところではありますが、心より感謝を述べさせていただきます。

中島正愛先生には、2度も修士を取っていたにも関わらず、研究事を何も深く理解できていなかった私を広い心で拾っていただき、お忙しい中にもかかわらず常に私を気にかけて、辛抱強くご指導くださったこと、心より深く感謝いたします。にもかかわらず、先生にご助言をいただこうとも自分で納得できないとてこでも動かず、先生には多くのご迷惑とご心配をおかけしたにも関わらず、最初から最後までわがままを通した私に我慢強く付き合ってくださいましたこと、感謝の念に堪えません。学生に対して真正面からとことん付き合う中島先生のその姿勢は、私が最も感銘を受けたことの一つです。どうかお体を大切に、これからも後輩達もエネルギーに指導し続けてください。

最初の指導者である故山田大彦先生は多くは語られませんでしたでしたが、要所要所で今でも心に残る、厳しく優しいお言葉をくださいました。中でも私が留学を決めた際、「若いうちに何かに没頭したという事実は、それが直接実らなくとも、後になっていつか大きな財産となる」と私の背を押してくださった山田先生の言葉は、今でも大きな支えです。いまだに五里霧中の亀の歩みですが、少しずつ成長している私をどこかで見ていてくださると、嬉しいです。

また、博士研究を進めるにあたり、多大なるご支援、ご指導を賜りました(独)防災科学技術研究所の佐藤栄児氏に、心より感謝いたします。実験中の2度にわたるE-ディフェンス生活は、私の博士学生生活の1番の思い出です。実験後もお忙しい中、折々貴重な時間を快く割いてご指導していただき、本当にありがとうございました。

その他、私の最初の研究生活でお世話になった小幡さん、秘書の桂島さん、植松先生をはじめとする東北大学の皆様、ミシガンでご指導いただいたGoel先生、Simon先生をはじめとするPBPD研究グループの皆様、実験時にお世話になった(独)防災科学技術研究所の皆様、私の博士論文に貴重なご意見をくださった京都大学の竹脇先生、河井先生、宇治振動台実験時にサポートしていただいた山崎さんをはじめとする技術職員の皆様、毎回何かしらポカをする私へ心強いサポートをくださった蒲生さんをはじめとする秘書の皆様、女性研究者の先輩として様々な相談に乗って下さった故日高桃子先生には、ここに記して、心

よりの感謝を述べさせていただきます。

また、研究室の皆さんのおかげでこの3年間本当に楽しい日々を過ごさせていただきました。研究に飽きたときに雑談したり、毎日ご飯を一緒に食べたり、何かしら理由をつけて飲み会を開いたり、充実した研究室生活でした。また私の足りない点をサポートし続けてくれた榎田君、伊藤さんをはじめ諸先輩、後輩の皆さんには、心から感謝しています。この3年は、とても大事な思い出です。みんなありがとう。

最後に、学部のところから留学中も博士論文執筆中も変わらず私を支え、応援し続けてくださった山口総香氏をはじめとする友人たち、わがままを通す私を全面的にサポートし続けてくれた両親に対して、最大級の感謝をここに述べさせていただきます。少しでも恩返しができるよう努力いたします。広い心で、お待ちいただければ、と思います。

古川 幸